UNIVERSITÀ
DEGLI STUDI
DI PADOVA

Head Office: Università degli Studi di Padova

Department of Geosciences

Ph.D. COURSE IN: EARTH SCIENCES
SERIES XXXII

STRATAL PATTERNS AND SEDIMENTARY FACIES IN TIDAL POINT BARS

Coordinator: Prof. Claudia Agnini
Supervisor: Prof. Massimiliano Ghinassi
Co-Supervisor: Prof. Andrea D'Alpaos
                    Prof. Nigel P. Mountney

Ph.D. student : Marta Cosma

To my family, friends, and mentors

I am strengthened by your endless love and support

ABSTRACT

Tidal channels play a key role in the evolution of coastal environments and commonly dominate tidal landscapes. These channels commonly show a clear meandering pattern which shapes the architectural geometries of sedimentary successions accumulated in tidal coastal realms. Nevertheless, a limited number of studies analysed the morphodynamic evolution of tidal meanders and the related point bar sedimentary bodies, whose internal architecture and sedimentary facies distribution remain still poorly explored, as highlighted by their scarce documentation in the rock record. The capability of reading the signature of tidal processes in sedimentary successions represents a powerful tool for paleo-environmental reconstructions. Detecting tidal channel deposits will contribute to studies on Holocene deposits and ancient rocks, with implications spanning from adaptation of natural systems to anthropic pressure to subsurface exploration for georesources. The present work aims at improving our understanding of the relationship between the evolution of tidal meander bends and the related sedimentary products, through the investigation of different research issues (RI), including: i) the influence of vertical aggradation and substrate compaction in shaping geometries of tidal point bars (RI1); ii) the reconstruction of three-dimensional architecture of tidal point bars, through a numerical modelling approach, developed under different aggradational conditions and planform transformation styles (RI2); iii) the relationship between mechanisms of bar growth and internal facies arrangements (RI3); and iv) the analysis of piracy-controlled geometries of point bar bodies (RI4). These research issues have been carried out in different tidal settings, including microtidal (Venice Lagoon, Italy – RI1, 2, and 4) and macrotidal (Bay of Mont Saint Michel, France – RI3) environments; both in modern (RI1, 2, 3, and 4) and ancient record

(Eocene deposits of the Tremp-Graus Basin, Spain – RI4). A multidisciplinary approach has been adopted for modern examples, with different methodologies encompassing remote sensing techniques (i.e. historical aerial photos and LiDAR topographic time-series analysis), geomorphological field observations, sedimentary core analysis, and 3D forward stratigraphic modelling. The analysis of the ancient case study examples relies on classical outcrop sedimentology approach, which included line-drawing of photomosaics, bed-by-bed logging, and collection of paleo-flow measurements.

The main results from this work highlighted that:

I) geometries of tidal point bars can vary following aggradational conditions of surrounding overbank areas, along with changes in local accommodation space and channel discharge. These are, in turn, influenced by differential substrate compaction and channel network evolution;

II) 3D geometries of point bars developed by slowly migrating tidal channels under aggradational conditions, differ from tabular bodies envisaged by traditional point bar models. Indeed, their geometries are shaped by the planform and vertical shift of channel bends;

III) tidal meanders can expand alternating accretionary stages along seaward and landward side of point bars. In this contest, large amounts of mud-rich deposits are stored in their axial zone, where rhythmic tidal deposition is better recorded;

IV) occurrence of densely-drained tidal networks prevents channel bends to freely meander and causes interaction with adjacent channels triggering piracies. These piracies cause premature deactivation of sinuous channels and hinder the development of laterally extensive point bar bodies.

RIASSUNTO

I meandri tidali costituiscono una delle principali componenti dei sistemi a marea presenti nelle aree costiere, e giocano un ruolo di fondamentale importanza nell'evoluzione di tali sistemi, determinando le architetture deposizionali delle relative successioni sedimentarie. Tuttavia, solo un limitato numero di studi scientifici ha analizzato l'evoluzione morfodinamica di questi meandri e i relativi prodotti sedimentari: le barre di meandro tidali. I modelli deposizionali per questi tipi di barre mancano ancora di chiare caratteristiche che ne permettano il riconoscimento, come evidenziato dalla loro scarsa documentazione in successioni sedimentarie. La capacità di riconoscere la firma tidale in depositi sia recenti che antichi è di fondamentale importanza, ed ha implicazioni che spaziano dal capire come i sistemi naturali si adattano alle pressioni antropiche, all'esplorazione del sottosuolo per lo sfruttamento di geo-risorse. Il presente lavoro, nell'intento di comprendere più approfonditamente le relazioni esistenti tra l'evoluzione morfodinamica dei meandri tidali e i relativi prodotti sedimentari, si focalizza su quattro differenti argomenti, che includono: i) l'analisi del ruolo di aggradazione verticale e compattazione del substrato nel determinare le architetture deposizionali delle barre di meandro tidali (A1); ii) la ricostruzione in tre dimensioni delle loro geometrie, analizzando il ruolo che diversi contesti aggradazionali e diverse trasformazioni in pianta ricoprono nel determinarne le geometrie (A2); iii) l'analisi delle relazioni esistenti tra meccanismi di crescita dei meandri tidali e distribuzione delle relative facies sedimentarie (A3); e iv) lo studio delle architetture deposizionali di barre tidali i cui canali hanno subito eventi di cattura (A4). Questi argomenti sono stati trattati in diversi contesti tidali, spaziando da ambienti micro- (Laguna di Venezia, Italia – A1, 2, and 4) a macro-tidali (Baia di Mont Saint Michel,

Francia – A3); e da depositi attuali (A1, 2, 3, and 4) ad antiche successioni sedimentarie (Bacino di Tremp, Spagna – A4). Per l'analisi dei casi studio moderni è stato utilizzato un approccio di tipo multidisciplinare, combinando metodologie quali *remote-sensing*, osservazioni *in situ*, analisi sedimentologiche su carote sedimentarie e modellazione numerica tridimensionale. L'analisi di casi nel record fossile, si è basta sulle classiche tecniche della sedimentologia di campagna che includono la misurazione di log stratigrafici, paleo-correnti e la redazione di *line-drawing* degli affioramenti.

I principali risultati ottenuti evidenziano che: I) le architetture deposizionali delle barre risentono delle diverse condizioni aggradazionali dell'ambiente a loro circostante, della disponibilità di spazio di accomodamento, e delle variazioni della portata dei relativi canali. Questi fattori sono a loro volta influenzati dalla compattazione differenziale del substrato e dall'evoluzione delle reti di canali; II) le geometrie tridimensionali di barre sviluppate da canali che migrano lateralmente piano rispetto ai tassi di aggradazione verticale dell'ambiente circostante, possono differire in modo sostanziale dalle geometrie predette dai classici modelli deposizionali. Queste sono infatti fortemente influenzate dalla trasformazione in pianta e dalla dislocazione verticale del relativo canale; III) i meandri tidali possono espandere in modo peculiare, alternando la deposizione di sedimenti nella porzione verso mare o verso terra della barra, e accumulando la maggior quantità di sedimento nelle aree apicali, dove meglio si registra nei sedimenti il segnale ritmico prodotto dalla marea; e IV) l'alta densità di drenaggio delle reti di canali tidali non permette ai canali stessi di migrare liberamente, causando l'interazione tra meandri adiacenti tramite eventi di cattura. Gli eventi di cattura causano la disattivazione prematura dei canali che pertanto presentano barre immature, cioè poco sviluppate lateralmente.

ACKNOWLEDGEMENTS

Firstly, I would like to thank my advisors: prof. Massimiliano Ghinassi for the continuous support and encouragement he gave me, for his guidance and great knowledge and for the passion he transmit doing his job; prof. Andrea D'Alpaos for his experience, support and presence when an advice was needed; and, last but not least, prof. Nigel P. Mountney for the great opportunity he gave me to join the FRG in Leeds as a visiting student, for his immense knowledge and for the time that he was always able to dedicate me despite all his commitments.

A sincere gratitude goes to my colleagues and co-authors in Padova: Alvise Finotello, Elena Bellizia, Marcella Roner, Laura Tommasini and Lara Brivio, who helped me during these three years and particularly in the last challenging period. They sustained me while I was writing and revising the thesis, providing suggestions with accurate observations. I certainly couldn't have done it without you and it would definitely have been a lot less fun. I also want to thank my friends from the Department: Luca Collanega, Maria Soppelsa, Giorgia Stasi, Arianna Vettorello, Enrico Marzotto, Samuele Boccardo, and Arianna Marcolla, who have helped me in so many ways, that if I were to list them, I would never end up these acknowledgements.

Another special thanks goes to prof. Dimitri Lague, for the opportunity he gave me to join his research group in Rennes, for the extended knowledge he has of the Mont Saint Michel Bay and for allowing me to use his exceptional high resolution LiDAR dataset. A particular thanks goes to Baptiste Feldmann, whose assistance and technical expertise with LiDAR data processing and python have been essential to obtain part of the results of my thesis. I want to express my gratitude also to all the great people I met in Rennes,

TABLE OF CONTENTS

CHAPTER 1

INTRODUCTION

1. OVERVIEW

This study deals with tidal meandering channels and aims at investigating both their morphodynamic evolution and the stratal architecture of related sedimentary bodies from a three-dimensional perspective. Sedimentary products deriving from migration of microtidal and macrotidal meanders were analysed through a multidisciplinary approach, which included remote sensing, sedimentological analyses, numerical modelling and comparison with ancient deposits.

2. STATE OF THE ART

In shallow intertidal environments, the landscape is dominated by unvegetated tidal flats or bars, vegetated marsh platforms, and tidal channels, which cut through and connect the other two components (D'Alpaos et al., 2005; Fagherazzi et al., 2006; Hughes, 2012). Tidal channel evolution depends on a number of factors, related to both the physical and biological features of the landscapes they dissect (e.g., bank erodibility, presence and type of vegetation, bioturbation), as well as to local hydrodynamics (e.g., water and solid discharges). At the same time, tidal channels exert a strong control on the coastal landscapes, providing the conduit for tide propagation, influencing local

tidal conditions, and driving the exchange of nutrients, sediments and biota in these areas (Rinaldo et al., 1999a; Hughes, 2012; Coco et al., 2013).

Tidal channels are commonly organized in networks, which exhibit a wide range of planform morphologies (Rinaldo et al., 1999b; Kearney and Fagherazzi, 2016) and a high drainage density (*sensu* Marani et al., 2003, i.e., defined as the mean unchanneled path length ℓ; see also Rinaldo et al., 1999b) with respect to the fluvial counterpart (Pallard et al., 2009; Trigg et al., 2012). The high spatial density of tidal channels ensures the regular intersection of adjacent migrating bends, leading to piracy events which cause local reorganization of the channel network (e.g., Letzsch and Frey, 1980; Rizzetto and Tosi, 2012; Litwin et al., 2013). This peculiar process can trigger remarkable changes in the evolution of tidal channel reaches. In consequence of these piracies, water discharge flowing through a single channel can dramatically increase, leading to a progressive deepening and widening of the channel in order to re-equilibrate its cross-sectional area with the local discharge. Vice-versa, if the water discharge decreases, the channel progressively shallows (i.e. channel floor aggradation), possibly until its final deactivation.

Tidal channels commonly show a clear meandering pattern, nevertheless only few studies analyse planimetric shape, morphometric characteristics, and morphodynamic evolution of tidal meanders (Finotello, 2017). The lateral migration of channels has the potential to produce significant depositional bodies, which, in turn, are important to determine the stratigraphy of intertidal regions (Hughes, 2012). Although lateral shift of tidal meanders is the most noticeable morphodynamic process, tidal channels can also be strongly shaped by processes occurring in the vertical domain, since they can be affected by: i) deepening through erosion and suspension of sediment, through compaction, or due to sea-level rise; ii) shallowing through inorganic sediment deposition; iii) or relative change due to the erosion or accretion of the surrounding platform or tidal flat. The interaction between these processes might have a relevant

impact on the formation of tidal-channel deposits, especially where vertical aggradation rates are high in comparison with rates of lateral channel migration.

Evolution of tidal meanders is influenced by the peculiar flow configuration (Fenies and Faugères, 1998; Fagherazzi et al., 2004; Dalrymple and Choi, 2007; Li et al., 2008 – Fig 1)
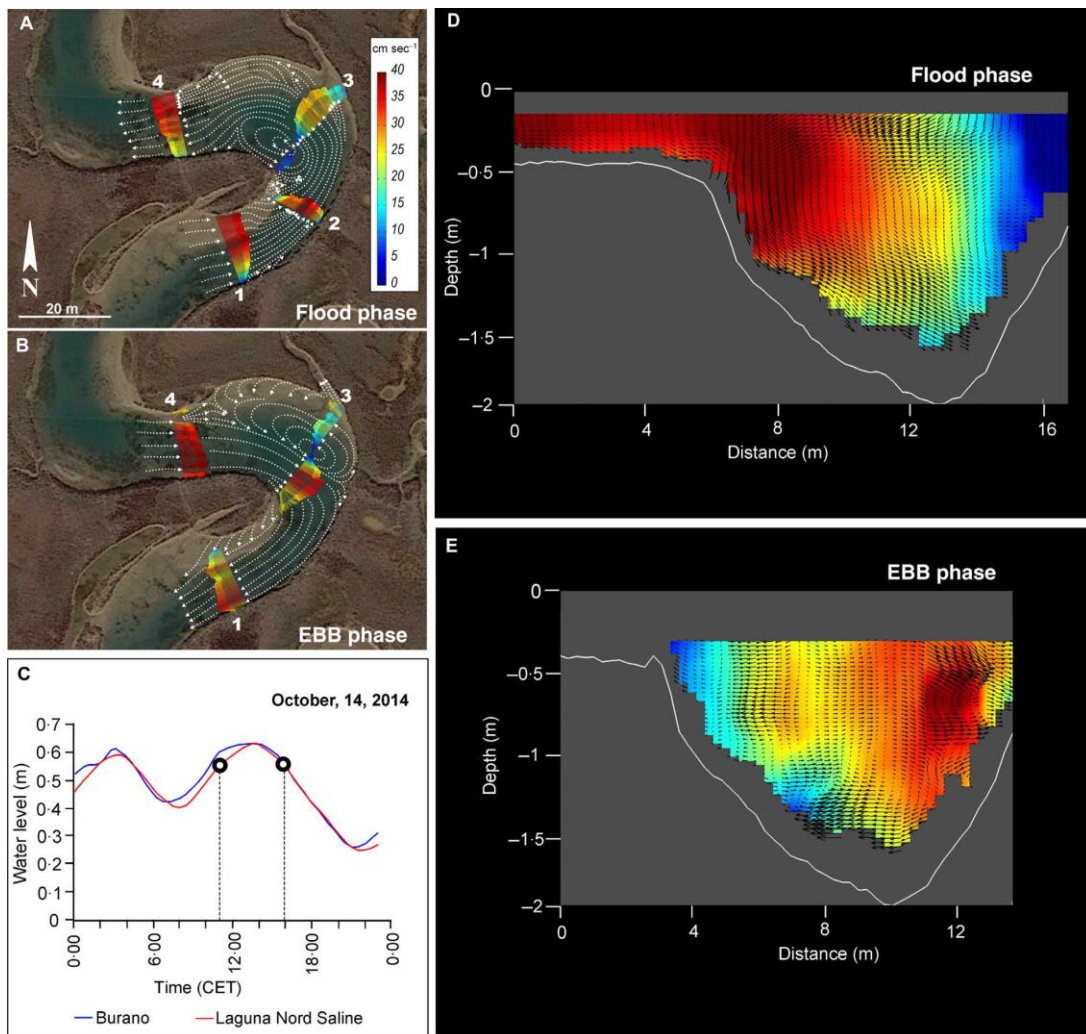
Figure 1 Peculiar flow configuration along a microtidal bend of the Venice Lagoon. (A) and (B): Plan view of depth-averaged velocities for the surveyed sections. Velocity magnitude is represented by both colour scale and vector lengths. Dotted lines stand for possible depth-averaged flow trajectories. (C) Water level recorded from two gauge stations ('Burano' and 'Laguna Nord Saline') close to the study site indicating the two times when the ADCP measurements were collected. (D) and (E) Cross-sectional view of Section 1 during ebb and flood phases. Colours indicate Rozovskii primary velocity magnitude, whereas vectors stand for both direction and intensity of Rozovskii secondary velocity (from Ghinassi et al., 2018b).

arising from the occurrence of: i) bidirectional flows, which causes a high variability of channel discharge and velocity over a relatively short time scale (i.e. hours); ii) asymmetry and hysteresis of tidal flows, which causes inequalities between flood and ebb magnitude velocities and flow periods; and iii) the mutually evasive nature of the ebb and flood currents (i.e. the two tides follow different path within the meander), which causes the offset of both the highest velocity and the secondary recirculation, which act in different directions and at different magnitudes in the meander. All these features have relevant impacts on the distribution of erosional and depositional processes along tidal meander bends (Hughes, 2012; Ghinassi et al., 2018b), and, therefore, on the sedimentary products of tidal bend migration.

A limited number of studies linked morphodynamic evolution of tidal meanders with related point bar sedimentary bodies, whose internal architecture and sedimentary facies distribution remain still poorly explored, as highlighted by their scarce documentation in the rock record. In the ancient record, tidal point bars are usually recognized on the basis of architectural model developed for fluvial point bars (e.g. Díez-Canseco et al., 2014), by assuming that the abundance of mud, high degree of bioturbation and occurrence of sedimentary structures bearing tidal signatures are the key-distinctive features for their identification (Gingras et al., 1999; Choi et al., 2004; Pearson and Gingras, 2006; Johnson and Dashtgard, 2014). Although the basic principles of tidal point bar sedimentology were highlighted before the 80's (van Straaten, 1954; Bridges and Leeder, 1976; Barwis, 1978), a key contribution to discriminate tidal point bars came by Allen (1982), who summarize geometries and facies-sequence of river and tidal point bars (Fig 2). Tidal point-bar deposits overlie a sub-horizontal erosional surface formed during expansion of the bend, and shows an upward-fining grain size sequence. Point-bar deposits were described as interbedded sigmoidal layers of sand and mud (Inclined Heterolithic Stratification; Thomas et al., 1987), in which bioturbation

is pervasive. Sandy layers became thicker and more common toward the bar base, and show sedimentary structures produced by ebb- and flood-directed bedforms.
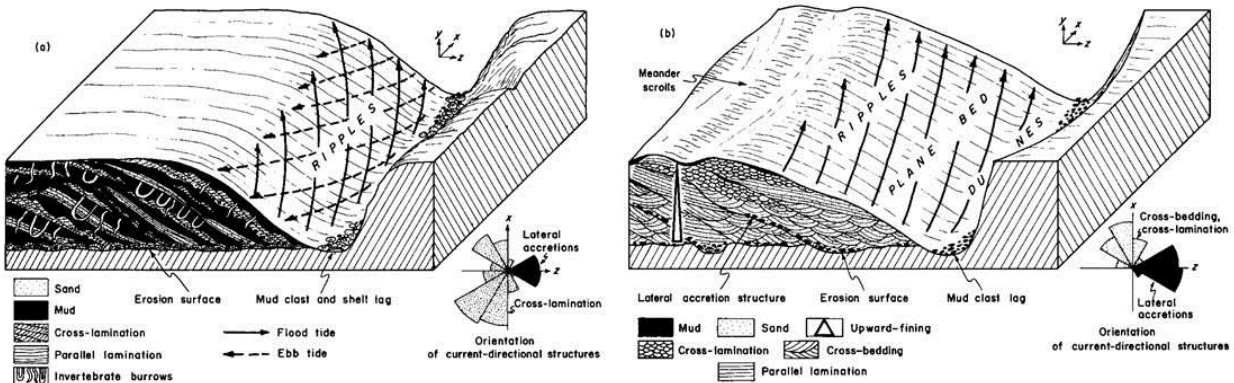
Figure 2 Example of a depositional model, developed by Allen (1982), highlighting lithologies and sedimentary structures in point bars. (a) Mixed mud-sand tidal gully.(b) Sand-bed river. The orientation of the master bedding (lateral accretions) is in each case compared with that of the smaller scale directional structures (form Allen, 1982).

A number of studies analysed point-bar deposits in modern coastal settings (De Mowbray, 1983; Choi et al., 2004; Pearson and Gingras, 2006; Choi, 2010; Fruergaard et al., 2011; K. S. Choi, 2011; Choi and Jo, 2015; Brivio et al., 2016; D'Alpaos et al., 2017; Ghinassi et al., 2018a, 2018b) providing further insights to the model proposed by Allen (1982). For example, in intertidal channels, the thalweg zone is often identifiable as a lag of coarse sediment or shells, although in mud-rich systems this may be more difficult to develop (Terwindt, 1988; Rieu et al., 2005; Pearson and Gingras, 2006). Lag deposits range in thickness from few decimetres (Brivio et al., 2016) in small salt-marsh creek, to a few meters in larger channels (Choi et al., 2004), and mud blocks from bank slumping can form large part of the lag (Terwindt, 1988; Musial et al., 2011; Broughton, 2018). Under certain conditions, tidal systems are dominated by fine-grained sediments resulting in predominantly muddy point bar bodies (Pearson and Gingras, 2006), while in others, muddy deposits are almost missing (Fenies and Faugères, 1998). Some studies also highlight the complexity of the planform morphology of tidal point bars, which tend to be stretched out in the direction of the dominant current (Barwis, 1978; De Mowbray, 1983; Fenies and Faugères, 1998; Choi, 2010), and can create a tidal barb in the

direction of the subordinate currents (Barwis, 1978). More recently, strongly asymmetric point bars have been described in association with a marked tidal asymmetry (Ghinassi et al., 2018b), which caused the bar to be eroded on one side, and depositional on the other one.

A large number of sedimentary structures are associated with the occurrence of tidal currents, including reactivation surfaces, mud drapes in cross-sets, and low angle dipping cross-sets with alternating thicker and thinner packages of sand and mud (Santos and Rossetti, 2006). Nevertheless tidal bundles, rhythmites and herringbone cross-stratification are the most reliable evidence for documenting occurrence of tidal processes (Choi and Park, 2000; Choi and Dalrymple, 2004). Occurrence of these diagnostic features in point-bar deposits is considered to be strongly influenced by the relative elevation of the point bar with respect to Mean Sea Level (Fig 3B). In intertidal conditions, rhythmites are commonly documented in the middle part of point bar deposits (Fig 3A), where major number of submergence events can be recorded (Tessier, 1993; Archer, 1998; Choi, 2010; K. Choi, 2011). In contrast, the dominance of subaerial exposure (Dalrymple et al., 1991) and high-energy conditions (Choi et al., 2004) prevents preservation of rhythmic deposition in upper and lower bar deposits, respectively. Furthermore, tidal point bars occurring in starved micro-tidal systems, can also fully lack any clear tidal signature (e.g. point bars of the Venice Lagoon – Brivio et al., 2016; D'Alpaos et al., 2017; Ghinassi et al., 2018). With the exception of some uniquely preserved examples (Pelletier et al., 2016), distribution and preservation of tidal sedimentary structures in the rock record are not ubiquitous, also considering that the abundance of bioturbation in tidal point bar bodies often prevents their identification. Furthermore, isolated occurrences of bundling and herringbone-cross stratification in the rock record has to be considered carefully because similar structures can occur in fully fluvial environments, such as the case for the tributary mouth bar sediments described by Alam et al. (1985).
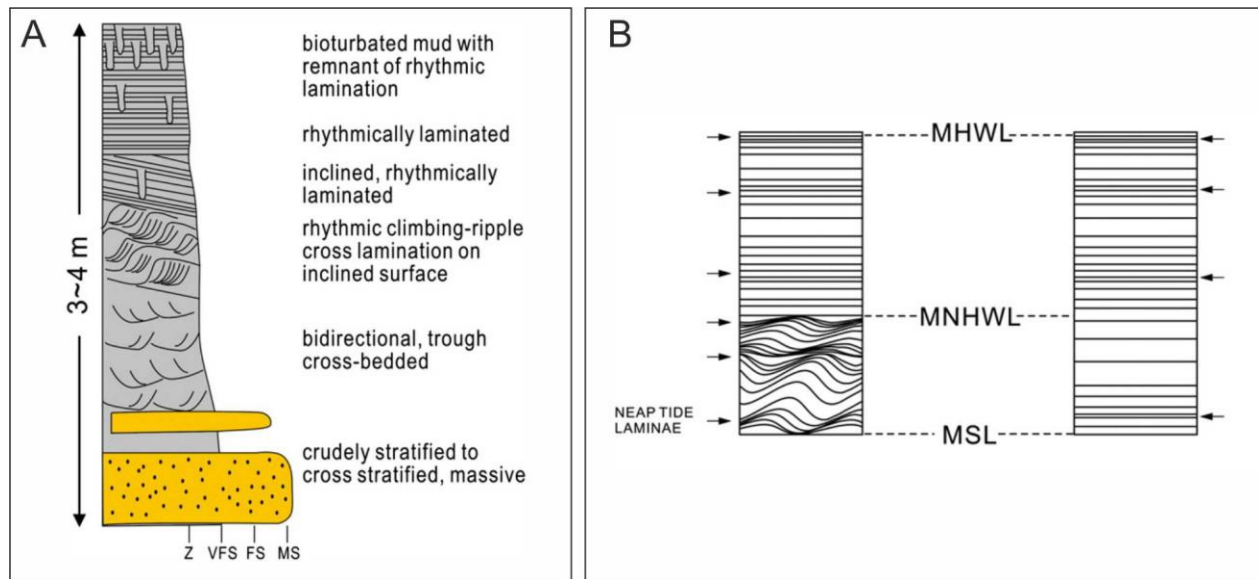
Figure 3 Example of the distribution of tidal rhythmites within a channel sequence (A) and within the tidal frame. (B) of a mixed-energy, macrotidal estuarine channel, Gomso Bay, west coast of Korea (Choi, 2011). (A) Schematic columnar section of Jujin Channel deposits whose upper part is dominated by rhythmically laminated silt (tidal rhythmites). Note either planar or inclined, rhythmically laminated silt facies is underlain by rhythmically climbing-ripple cross laminated silt facies (RCRL). Z, VFS, FS, and MS denote silt, very fine sand, fine sand, and medium sand, respectively. (B) Tidal rhythmites are preferentially formed above mean sea level (MSL) and below mean high water level (MHWL). In place, rhythmic climbing ripples occur below mean neap high water level (MNHWL). Note inferred neap–spring tidal cycles decrease in thickness with elevation (modified after Choi, 2011).

It arises that, although progression has been made in understanding some morphodynamic and sedimentological processes acting in tidal meander bends, they still need to be integrated in order to depict an integrated model, as stated by Hughes (2012):

'While both the planform morphology and vertical facies in tidal point bars have been described in the literature, a full three-dimensional description is still missing to fully document the internal structure and horizontal variations, which result from the heterogeneity of the physical (and biological) processes both across and along the forms.'

3. GOALS OF THE STUDY

Toward the goal of improving our understanding of the relationship between evolution of tidal meander bends and their related sedimentary products, the present work investigates the stratal architecture and sedimentary facies distribution of tidal point bars, focusing on four main subjects and related research questions:

SUBJECT 1: In salt marsh setting, rates of vertical bed aggradation can be relatively (i.e. mm-cm/yr) high with respect to lateral migration rates of tidal channels (i.e. cm-dm/yr).

Research question: can the vertical bed aggradation influence geometries of tidal point-bar bodies?

SUBJECT 2: Planform transformation styles of tidal meanders can differ from the classical model depicting an increase of bend sinuosity in a low aggradational setting.

Research question: Can the interplay between different planform transformation styles and vertical aggradation influence the three dimensional architecture of tidal point bar bodies?

SUBJECT 3: The progressive lateral shift of tidal channels produces laterally accreting strata which tend to preserve the signature of tidal processes in the mid-to-upper part of the bar, whereas these upper and lower bar deposits show scarce evidence of tidal processes.

Research question: how is the tidal signature recorded along a tidal meander bend?

SUBJECT 4: Tidal networks display a high drainage density, which prevents channels from freely migrating laterally without interacting with adjacent channels.

Research question: can this drainage network influence development of tidal point bar bodies?

4. THESIS OUTLINE

This thesis consists of five chapters in addition to this introduction:

THE SECOND CHAPTER reconstructs the two-dimensional, cross-sectional geometries of eight micro-tidal point bars of the Venice Lagoon, by means of detailed analyses of sedimentary cores collected along the point bar axes. Meaning of key surfaces defined during lateral shift of the channels (i.e. bar brink and channel thalweg trajectories) is discussed in relation with the relationship between the rate of vertical overbank aggradation and rate of lateral migration of channels.

This chapter is organized as a journal paper already published in 'Geomorphology' (https://doi.org/10.1016/j.geomorph.2019.06.009).

THE THIRD CHAPTER combines remote sensing and core analysis from micro-tidal point bars of the Venice Lagoon with a 3D forward stratigraphic model. This study aims to reconstruct and predict geometries of point bar bodies developed by slowly-migrating channels evolving under aggradational conditions. Particular attention has been paid to the interaction between different aggradational conditions and planform transformation styles of channel bends.

This chapter is organized as a journal paper, which was submitted to 'Sedimentology' (SED-2019-OM-183).

THE FOURTH CHAPTER integrates the analysis of multi-temporal LiDAR topographic surveys with sedimentary core data from a tidal bend of the Mont Saint Michel Bay (France). This work aims at understanding the stratal architecture and the sedimentology of the studied bar, mainly focusing on mechanisms of bar growth and along-bend variability of sedimentary features.

This chapter is organized as a journal paper to be submitted to 'Sedimentology'.

THE FIFTH CHAPTER describes the cross sectional architecture of two ancient tidal point bars occurring in the Eocene Castigaleu Fm (Tremp – Graus Basin, Spain), characterized by a relatively low lateral extent in comparison to their thickness. The architecture of these bars is compared with the one arising from the evolution of a tidal meander bend of the Venice Lagoon (Italy) after a piracy event. The work analyses the control of tidal network density on point bar geometries.

This chapter is organized as a journal paper in preparation for 'Frontiers in Earth Science. Sedimentology, Stratigraphy and Diagenesis'.

THE SIXTH CHAPTER summarizes the main results obtained from this thesis.

5. REFEERENCES

Alam, M.M., Crook, K.A.W., Taylto, G., 1985. Fluvial herring-bone cross-stratification in a modern tributary mouth bar, Coonamble, New South Wales, Australia. Sedimentology 32, 235–244. https://doi.org/10.1111/j.1365-3091.1985.tb00506.x

Archer, A.W., 1998. Hierarchy of Controls on Cyclic Rhythmite Deposition: Carboniferous Basins of Eastern and Mid-Continental U.S.A., in: Tidalites: Processes and Products. SEPM Society for Sedimentary Geology, pp. 59–68. https://doi.org/10.2110/pec.98.61.0059

Barwis, J.H., 1978. Sedimentology of some South Carolina tidal-creek point bars, and a comparison with their fluvial counterparts, in: Miall, A.D. (Ed.), Fluvial Sedimentology. Dallas Geological Society, Calgary, Alberta, Canada, pp. 487–510.

Bridges, P.H., Leeder, M.R., 1976. Sedimentary model for intertidal mudflat channels, with examples from the Solway Firth, Scotland. Sedimentology 23, 533–552. https://doi.org/10.1111/j.1365-3091.1976.tb00066.x

Brivio, L., Ghinassi, M., D'Alpaos, A., Finotello, A., Fontana, A., Roner, M., Howes, N., 2016. Aggradation and lateral migration shaping geometry of a tidal point bar: An example from salt marshes of the Northern Venice Lagoon (Italy). Sediment. Geol. 343, 141–155. https://doi.org/10.1016/j.sedgeo.2016.08.005

Broughton, P.L., 2018. Mudstone Clast Breccia in the Cretaceous Athabasca Oil Sands, Western Canada: Fluvial Debris-Flow Transitions into Traction Carpets. J. Geol. 126, 63–97. https://doi.org/10.1086/694747

Choi, K., 2011. Tidal rhythmites in a mixed-energy, macrotidal estuarine channel, Gomso Bay, west coast of Korea. Mar. Geol. 280, 105–115. https://doi.org/10.1016/j.margeo.2010.12.004

Choi, K., 2010. Rhythmic Climbing-Ripple Cross-Lamination in Inclined Heterolithic Stratification (IHS) of a Macrotidal Estuarine Channel, Gomso Bay, West Coast of Korea. J. Sediment. Res. 80, 550–561. https://doi.org/10.2110/jsr.2010.054

Choi, K.S., 2011. External controls on the architecture of inclined heterolithic stratification (IHS) of macrotidal Sukmo Channel: Wave versus rainfall. Mar. Geol. 285, 17–28. https://doi.org/10.1016/j.margeo.2011.05.002

Choi, K.S., Dalrymple, R.W., 2004. Recurring tide-dominated sedimentation in Kyonggi Bay (west coast of Korea): similarity of tidal deposits in late Pleistocene and Holocene sequences. Mar. Geol. 212, 81–96. https://doi.org/https://doi.org/10.1016/j.margeo.2004.07.008

Choi, K.S., Dalrymple, R.W., Chun, S.S., Kim, S.-P.S.-P., 2004. Sedimentology of modern, Inclined Heterolithic Stratification (IHS) in the macrotidal Han River Delta, Korea. J. Sediment. Res. 74, 677–689. https://doi.org/10.1306/030804740677

Choi, K.S., Jo, J.H., 2015. Morphodynamics of Tidal Channels in the Open Coast Macrotidal Flat, Southern Ganghwa Island in Gyeonggi Bay, West Coast of Korea. J. Sediment. Res. 85, 582–595. https://doi.org/10.2110/jsr.2015.44

Choi, K.S., Park, Y.A., 2000. Late Pleistocene silty tidal rhythmites in the macrotidal flat between Youngjong and Yongyou Islands, west coast of Korea. Mar. Geol. 167, 231–241. https://doi.org/https://doi.org/10.1016/S0025-3227(00)00037-2

Coco, G., Zhou, Z., van Maanen, B., Olabarrieta, M., Tinoco, R., Townend, I.H., 2013. Morphodynamics of tidal networks: Advances and challenges. Mar. Geol. 346, 1–16. https://doi.org/10.1016/j.margeo.2013.08.005

Cosma, M., Ghinassi, M., D'Alpaos, A., Roner, M., Finotello, A., Tommasini, L., Gatto, R., 2019. Point-bar brink and channel thalweg trajectories depicting interaction between vertical and lateral shifts of microtidal channels in the Venice Lagoon (Italy). Geomorphology 342, 37–50. https://doi.org/10.1016/j.geomorph.2019.06.009

D'Alpaos, A., Ghinassi, M., Finotello, A., Brivio, L., Bellucci, L.G., Marani, M., 2017. Tidal meander migration and dynamics: A case study from the Venice Lagoon. Mar. Pet. Geol. 87, 80–90. https://doi.org/10.1016/j.marpetgeo.2017.04.012

D'Alpaos, A., Lanzoni, S., Marani, M., Fagherazzi, S., Rinaldo, A., 2005. Tidal network ontogeny: Channel initiation and early development. J. Geophys. Res. Earth Surf. 110, 1–14. https://doi.org/10.1029/2004JF000182

Dalrymple, R.W., Choi, K.S., 2007. Morphologic and facies trends through the fluvial-marine transition in tide-dominated depositional systems: A schematic framework for environmental and sequence-stratigraphic interpretation. Earth-Science Rev. 81, 135–174. https://doi.org/10.1016/j.earscirev.2006.10.002

Dalrymple, R.W.R.W., Makino, Y., Zaitlin, B.B.A., 1991. Temporal and spatial patterns of rhythmite deposition on mud flats in the macrotidal Cobequid Bay-Salmon River Estuary, Bay of Fundy, Canada. Clastic tidal Sedimentol. 16, 137–160.

Dashtgard, S.E., Gingras, M.K., 2005. Facies Architecture and Ichnology of Recent Salt-Marsh Deposits: Waterside Marsh, New Brunswick, Canada. J. Sediment. Res. 75, 596–607. https://doi.org/10.2110/jsr.2005.049

De Mowbray, T., 1983. The genesis of lateral accretion deposits in recent intertidal mudflat channels, Solway Firth, Scotland. Sedimentology 30, 425–435. https://doi.org/10.1111/j.1365-3091.1983.tb00681.x

Díez-Canseco, D., Arz, J.A., Benito, J.I., Díaz-Molina, M., Arenillas, I., 2014. Tidal influence in redbeds: A palaeoenvironmental and biochronostratigraphic reconstruction of the Lower Tremp Formation (South-Central Pyrenees, Spain) around the Cretaceous/Paleogene boundary. Sediment. Geol. 312, 31–49. https://doi.org/http://dx.doi.org/10.1016/j.sedgeo.2014.06.008

Fagherazzi, S., Carniello, L., D'Alpaos, L., Defina, A., 2006. Critical bifurcation of shallow microtidal landforms in tidal flats and salt marshes. Proc. Natl. Acad. Sci. U. S. A. 103, 8337–8341. https://doi.org/10.1073/pnas.0508379103

Fagherazzi, S., Gabet, E.J., Furbish, D.J., 2004. The effect of bidirectional flow on tidal channel planforms. Earth Surf. Process. Landforms 29, 295–309. https://doi.org/10.1002/esp.1016

Fenies, H., Faugères, J.C., 1998. Facies and geometry of tidal channel-fill deposits (Arcachon Lagoon, SW France). Mar. Geol. 150, 131–148. https://doi.org/10.1016/S0025-3227(98)00049-8

Finotello, A., 2017. Tidal channel patterns: field investigations, numerical modelling and laboratory experiments. University of Padova.

Fruergaard, M., Andersen, T.J., Nielsen, L.H., Madsen, A.T., Johannessen, P.N., Murray, A.S., Kirkegaard, L., Pejrup, M., 2011. Punctuated sediment record resulting from channel migration in a shallow sand-dominated micro-tidal lagoon, Northern Wadden Sea, Denmark. Mar. Geol. 280, 91–104. https://doi.org/10.1016/j.margeo.2010.12.003

Ghinassi, M., Brivio, L., D'Alpaos, A., Finotello, A., Carniello, L., Marani, M., Cantelli, A., 2018a. Morphodynamic evolution and sedimentology of a microtidal meander bend of the Venice Lagoon (Italy). Mar. Pet. Geol. 96, 391–404. https://doi.org/10.1016/j.marpetgeo.2018.06.011

Ghinassi, M., D'alpaos, A., Gasparotto, A., Carniello, L., Brivio, L., Finotello, A., Roner, M., Franceschinis, E., Realdon, N., Howes, N., Cantelli, A., 2018b. Morphodynamic evolution and stratal architecture of translating tidal point bars: Inferences from the northern Venice Lagoon (Italy). Sedimentology 65, 1354–1377. https://doi.org/10.1111/sed.12425

Gingras, M.K., Pemberton, S.G., Saunders, T., Clifton, H.E., 1999. The Ichnology of Modern and Pleistocene Brackish-Water Deposits at Willapa Bay, Washington: Variability in Estuarine Settings. Palaios 14, 352–374. https://doi.org/10.2307/3515462

Hughes, Z.J., 2012. Tidal Channles on Tidal Flats and Marshes, in: Davis, R.A., Dalrymple, R.W. (Eds.), Principles of Tidal Sedimentology. Springer, pp. 269–300. https://doi.org/10.1007/978-94-007-0123-6_11

Johnson, S.M., Dashtgard, S.E., 2014. Inclined heterolithic stratification in a mixed tidal-fluvial channel: Differentiating tidal versus fluvial controls on sedimentation. Sediment. Geol. 301, 41–53. https://doi.org/10.1016/j.sedgeo.2013.12.004

Kearney, W.S., Fagherazzi, S., 2016. Salt marsh vegetation promotes efficient tidal channel networks. Nat. Commun. 7, 1–7. https://doi.org/10.1038/ncomms12287

Letzsch, W.S., Frey, R.W., 1980. Deposition and erosion in a Holocene salt marsh, Sapelo Island, Georgia. J. Sediment. Petrol. 50, 529–542. https://doi.org/10.1306/212F7A45-2B24-11D7-8648000102C1865D

Li, C., Chen, C., Guadagnoli, D., Georgiou, I.Y., 2008. Geometry-induced residual eddies in estuaries with curved channels: Observations and modeling studies. J. Geophys. Res. Ocean. 113, 1–14. https://doi.org/10.1029/2006JC004031

Litwin, R.J., Smoot, J.P., Pavich, M.J., Oberg, E., Steury, B., Helwig, B., Markewich, H.W., Santucci, V.L., Sanders, G., 2013. Rates and probable causes of freshwater tidal marsh failure, Potomac River estuary, Northern Virginia, USA. Wetlands 33, 1037–1061. https://doi.org/10.1007/s13157-013-0461-6

Marani, M., Belluco, E., D'Alpaos, A., Defina, A., Lanzoni, S., Rinaldo, A., 2003. On the drainage density of tidal networks. Water Resour. Res. 39, 1–11. https://doi.org/10.1029/2001WR001051

Musial, G., Reynaud, J.-Y., Gingras, M.K., Féniès, H., K.Labourdette, R., Parize, O., 2011. Subsurface and outcrop characterization of large tidally influenced point bars of the Cretaceous McMurray Formation (Alberta, Canada). Sediment. Geol. 279, 156–172. https://doi.org/10.1016/j.sedgeo.2011.04.020

Pallard, B., Castellarin, A., Montanari, A., 2009. A look at the links between drainage density and flood statistics. Hydrol. Earth Syst. Sci. 13, 1019–1029. https://doi.org/10.5194/hess-13-1019-2009

Pearson, N.J., Gingras, M.K., 2006. An Ichnological and Sedimentological Facies Model for Muddy Point-Bar Deposits. J. Sediment. Res. 76, 771–782. https://doi.org/10.2110/jsr.2006.070

Pelletier, J., Abouessa, A., Schuster, M., 2016. Hierarchy of tidal rhythmites from semidiurnal to solstitial cycles : Origin of inclined heterolithic stratifications (IHS) in tidal channels from the Dur At Talah Formation (upper Eocene , Sirte Basin , Libya) and a facies comparison with modern Mont. Contrib. to Mod. Anc. Tidal Sedimentol. Proc. Tidalites 2012 Conf. 203–216.

Rieu, R., van Heteren, S., van der Spek, A.J.F., De Boer, P.L., 2005. Development and preservation of a Mid-Holocene tidal-channel network offshore the Western Netherlands. J. Sediment. Res. 75, 409–419. https://doi.org/10.21110/jsr.2005.032

Rinaldo, A., Fagherazzi, S., Lanzoni, S., Marani, M., Dietrich, W.E., 1999a. Tidal networks 3. Landscape-forming discharges and studies in empirical geomorphic relationships. Water Resour. Res. 35, 3919–3929. https://doi.org/10.1029/1999WR900238

Rinaldo, A., Fagherazzi, S., Lanzoni, S., Marani, M., Dietrich, W.E., 1999b. Tidal networks 2. Watershed delineation and comparative network morphology. Water Resour. Res. 35, 3905–3917. https://doi.org/10.1029/1999WR900237

Rizzetto, F., Tosi, L., 2012. Rapid response of tidal channel networks to sea-level variations (Venice Lagoon, Italy). Glob. Planet. Change 92–93, 191–197. https://doi.org/10.1016/j.gloplacha.2012.05.022

Santos, A.E.D.A., Rossetti, D.D.F., 2006. Depositional model of the Ipixuna Formation (late cretaceous-?early tertiary), Rio Capim Area, northern Brazil. Lat. Am. J. Sedimentol. Basin Anal. 13, 101–117.

Smith, D.G., 1987. Meandering river point bar lithofacies models: modern and ancient examples compared, in: Ethridge, F.G., Flores, R.M., Harvey, M.D. (Eds.), Recent Developments in Fluvial Sedimentology: Contributions from the Third International Fluvial Sedimentology Conference. SEPM Society for Sedimentary Geology, pp. 83–91.

Terwindt, J.H.J., 1988. Palaeotidal reconstructions of inshore tidal depositional environments, in: De Boer, P.L., van Gelder, A., Nio, S.-D. (Eds.), Tide-Influenced Sedimentary Environments. pp. 233–263.

Tessier, B., 1993. Upper intertidal rhythmites in the Mont-Saint-Michel Bay (NW France): Perspectives for paleoreconstruction. Mar. Geol. 110, 355–367. https://doi.org/10.1016/0025-3227(93)90093-B

Trigg, M.A., Bates, P.D., Wilson, M.D., Schumann, G., Baugh, C., 2012. Floodplain channel morphology and networks of the middle Amazon River. Water Resour. Res. 48, 1–17. https://doi.org/10.1029/2012WR011888

van Straaten, L.M.J.U., 1954. Composition marine recent sediments the Netherlands formation. Leidse Geol. Meded. 19, 1–108. https://doi.org/10.5254/1.3538615

POINT-BAR BRINK AND CHANNEL THALWEG TRAJECTORIES DEPICTING INTERACTION BETWEEN VERTICAL AND LATERAL SHIFTS OF MICROTIDAL CHANNELS IN THE VENICE LAGOON (ITALY)

PAPER

Marta Cosma[a], Massimiliano Ghinassi[a], Andrea D'Alpaos[a], Marcella Roner[a], Alvise Finotello[a], Laura Tommasini[a], Roberto Gatto[a]

[a] Department of Geosciences, University of Padova, Padova, Italy

1. ABSTRACT

Although in tidal point bars, the point-bar brink (i.e. the break-in-slope between bar top and bar slope) and the channel thalweg (i.e. the deepest part of the channel) are thought to shift horizontally toward the outer bank, the occurrence of stable to slow-migrating channels in high-aggradational settings, e.g. salt marshes, is likely to promote a mixed, latero-vertical shift of meandering channel systems. The present study focuses on the trajectories of point-bar brink and channel thalweg of eight point bars located in the salt marshes of the Venice Lagoon, in order to understand how vertical aggradation can interact with lateral migration to shape their stratal geometries. High resolution facies-analysis carried out on closely-spaced sediment cores, collected along the bar axis, allowed us to define specific trajectories, which were classified either as ascending or descending, and linear or non-linear. All the analysed brink trajectories are ascending, and show evidence of lateral shift of the bar brink under aggradational conditions of surrounding marshes. Development of non-linear brink trajectories is linked with changes in the ratio between vertical and lateral shift rates of the brink, which is in turn dictated by changes in local base level due to substrate compaction. Conversely, thalweg trajectories can be either ascending or descending, reflecting an interaction between rates of lateral shift and aggradation/degradation of the channel floor. The brink and thalweg can either shift consistently (e.g., both trajectories are ascending) or incongruously (e.g., ascending brink vs. descending thalweg trajectory), reflecting different attitudes of the channel to maintain or increase its cross-sectional area. Results from this work have relevant implications on the accumulated bars geometries, which can differ substantially from published and widely accepted models of point-bar sedimentary architecture.

Keywords: tidal meander, salt-marsh aggradation, trajectory analysis, substrate compaction

2. INTRODUCTION

Trajectory analysis focuses on the migration pattern of easily recognizable geomorphological features (e.g., breaks-in-slope) and associated sedimentary environments through time (cf. Helland-Hansen and Hampson, 2009). This approach is suitable to be applied to a large variety of scales, which can range from bedforms (cf. "climb angle" by Larue and Martinez, 1989) to continental margins (Henriksen et al., 2011). However, little attention has been paid at the scale of depositional elements, like deltas (Gobo et al., 2015) or fluvial bars (Ghinassi et al., 2014).

Point bars generated by fluvial and tidal meandering channels are mostly described as laterally accreting bodies (Fisk, 1944; McGowen and Garner, 1970; Bridges and Leeder, 1976; Jackson, 1976; Miall, 1985; Smith, 1987; Durkin et al., 2015; Colombera et al., 2017; D'Alpaos et al., 2017) with a tabular geometry. This geometry is generated by lateral shift of the inner channel bank, which implies a synchronous horizontal shift (Fig 1A) of both the bar brink (i.e. the morphological break between bar top and bar slope) and the channel thalweg (i.e. the deepest part of the channel), which, in a cross section parallel to the bend axis, defines two parallel and horizontal trajectories (Fig 1A). Although the common occurrence of tabular point-bar bodies in the stratigraphic record (Puigdefabregas, 1973; Puigdefabregas and Van Vliet, 1977; Pranter et al., 2007) supports this model, documentation of stable to slow-migrating channels in high-aggradational settings (Nanson and Croke, 1992; Makaske, 2001; Ielpi et al., 2015; Candel et al., 2017) suggest that a high ratio between vertical aggradation and lateral accretion rate is likely to promote a mixed, latero-vertical shift of meandering channel systems. This work aims to investigate this very issue, focusing on the role of aggradation in shaping point-bar geometries.

The interaction between rates of vertical and lateral shift of fluvial meanders has rarely been documented in the stratigraphic record (Wightman and Pemberton, 1997; Rajchl

and Uličný, 2005; Ghinassi et al., 2014; Ielpi et al., 2015). Furthermore, numerical models (Willis and Tang, 2010; van de Lageweg et al., 2016), which usually consider mean rates of lateral migration on the order of meters per year (Bridge et al., 1995; Hudson and Kesel, 2000; Lagasse et al., 2004; Ghinassi et al., 2019), show that only high overbank aggradation rates (i.e. cm/yr to dm/yr) might possibly affect geometries of point bar bodies. Fluvial meanders developed by high sinuosity, slow-migrating, low-energy streams in peatlands of the Netherlands (Candel et al., 2017) represent an end-member of interaction between rates of vertical and lateral shifts of meandering channels. In this setting, geometries of bar bodies are prominently shaped by vertical displacement through processes of oblique aggradation (cf. Candel et al., 2017), which cause the bar brink and channel thalweg to shift synchronously following steep to vertical trajectories. Rajchl and Uličný (2005) analysed the influence of substrate compaction on geometries of point bar bodies recorded in the Neogene Hrabák fluvial system in the Most Basin (Czech Republic). They showed that syndepositional compaction of peat deposits, due to sediment loading of the overlying growing point bars, leads to a local increase in subsidence, which causes development of steep brink and channel thalweg trajectories (Fig 1B).

Similarly to their fluvial counterparts, tidal point bars were commonly described (Bridges and Leeder, 1976; Barwis, 1978) as tabular sedimentary bodies generated by horizontal and synchronous shift of bar brink and channel thalweg. Nevertheless, as demonstrated for fluvial systems, lateral migration of tidal meanders can follow different styles, and the trajectories defined by both point-bar brink and channel thalweg are not necessarily horizontal and parallel. As a matter of example, De Mowbray (1983) showed that the channel thalweg of a tidal meander bend in Drum Bay (Scotland) did not merely shift horizontally, but migrated under gradual aggradation (Fig 1C) in order to keep pace with the build-up of the adjacent tidal flats.
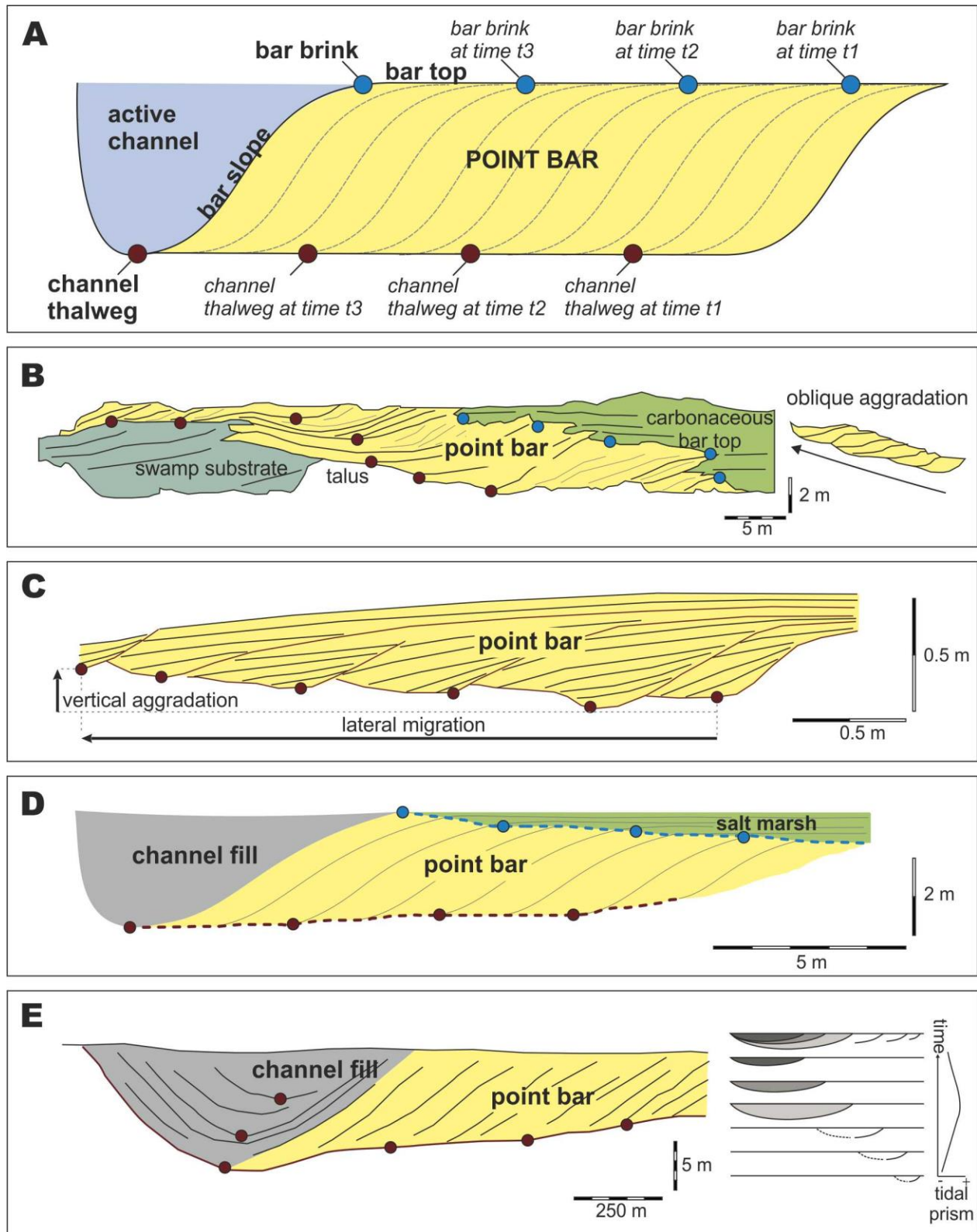
Figure 1. Models for point bar geometries. (A) Idealized model showing stratal geometries generated by lateral shift of the point bar brink and channel thalweg. (B) Lateral and vertical shift of a fluvial point bar of the Neogene Hrabák system, Czech Republic (modified after Rajchl and Uličný, 2005). (C) Channel thalweg migration under aggradational conditions in a modern tidal meander bend of the Drum Bay, Scotland (modified after De Mowbray, 1983). (D) Brink and thalweg trajectories of a modern tidal point bar in the Venice Lagoon (modified from Brivio et al., (2016). (E) Channel thalweg trajectory under the effect of a changing tidal prism in a Mid-Holocene channel, Netherlands (modified from Rieu et al., (2005).

A similar behaviour was also documented by Brivio et al. (2016) for the brink of a modern tidal point bar in the Venice Lagoon (Italy), where a combination between channel lateral shift and aggradation of the surrounding saltmarshes caused the bar brink to rise during the channel lateral shift (Fig 1D). Finally, using high-resolution seismic data from western Netherlands, Rieu et al. (2005) described a lateral shift of a mid-Holocene tidal channel under the effect of varying tidal prism. In this case, the shift of the channel thalweg defined a descending and ascending trajectory during phases of increase and decrease in the tidal prism, respectively (Fig 1E).

It emerges that, during lateral migration of tidal channels, the shift of the bar brink and the channel thalweg may not be horizontal and in phase, being that their behaviour is dictated by the interaction between different factors, including the rate of channel lateral shift (e.g. Fagherazzi et al., 2004; D'Alpaos et al., 2017; Finotello et al., 2018), rate of vertical aggradation of adjacent unchanneled areas (e.g. D'Alpaos et al., 2007), local variations of relative sea level and the related increase/decrease in tidal prism (e.g. D'Alpaos et al., 2010). The combinations between different types of bar brink and channel thalweg trajectories, along with the related changes of point bar thickness and geometry, can provide relevant insight in the identification of the depositional boundary conditions under which bend migration occurred. Therefore, describing different bar brink and thalweg trajectories, as well as their possible combinations, is a critical step towards an improved understanding of the morphodynamic evolution of tidal meanders and related sedimentary products. These issues are mostly relevant in tidal landscapes, where highly aggradational (i.e. cm/yr) marshes host a complex network of

slowly-migrating (i.e. cm to dm/yr) meandering channels (Garofalo, 1980; Gabet, 1998; Allen, 2000; Marani et al., 2002; Fagherazzi et al., 2004; Hughes, 2012), whose sedimentary and architectural features are still relatively unexplored (D'Alpaos et al., 2017; Boaga et al., 2018; Ghinassi et al., 2018). The present work focuses on meander bends of the Venice Lagoon providing the first description of different styles of bar brink and channel thalweg trajectories in order to improve our understanding of tidal point-bar evolution and architecture. Specifically, this study aims at i) illustrating geometries of tidal point bars along 2D axial cross sections; and ii) defining the behaviour of the bar brink and channel thalweg where point bar bodies accrete under aggradational conditions.

3. THE VENICE LAGOON AND THE STUDY SITES

The Venice Lagoon is located along the Northeastern coast of Italy, it has a total surface of about 550 km^2 and represents the largest brackish water body of the Mediterranean Basin (Fig 2A). The Lagoon is characterized by an elongated shape trending NE-SW and by a mean water depth of tidal flat and subtidal platform of about 1.5 m. It is connected to the Adriatic Sea through three inlets: Lido, Malamocco, and Chioggia (Fig 2A). The tidal regime is semidiurnal with an average range of about 1.0 m. The maximum water excursion at the inlets is ±0.75 m around Mean Sea Level (MSL) (D'Alpaos et al., 2013) which can be increased by meteorological forcing (Carniello et al., 2016).

The Venice Lagoon is part of a wider foreland basin located between the Apennine and the South Alpine chains (Massari et al., 2009). The Quaternary infill of the basin, in the Venice area, consists of a shallowing upward trend from deep marine hemipelagic mud and turbiditic succession to deltaic and shoreface deposits (Massari et al., 2004), which is followed by a cyclic alternation of continental to shallow marine facies deposited under

glacio-eustatic control in the uppermost succession (Kent et al., 2002). The last recorded cycle consists of the alluvial sediments of the Brenta River Megafan, developed in the area during the Last Glacial Maximum (Fontana et al., 2014), and of the lagoonal deposits related to the Holocene transgression, which prompted paralic deposition and the development of the Venice Lagoon (Amorosi et al., 2008; Zecchin et al., 2008, 2014). During the last five centuries, human interventions have strongly altered the natural evolution of the Lagoon, preventing its siltation (Gatto and Carbognin, 1981; D'Alpaos, 2010), and causing a human-induced transgressive phase (Zecchin et al., 2008, 2009, 2014), which is associated with a significant reduction in salt marsh surface (Day et al., 1998; Marani et al., 2007; D'Alpaos, 2010; Roner et al., 2016).
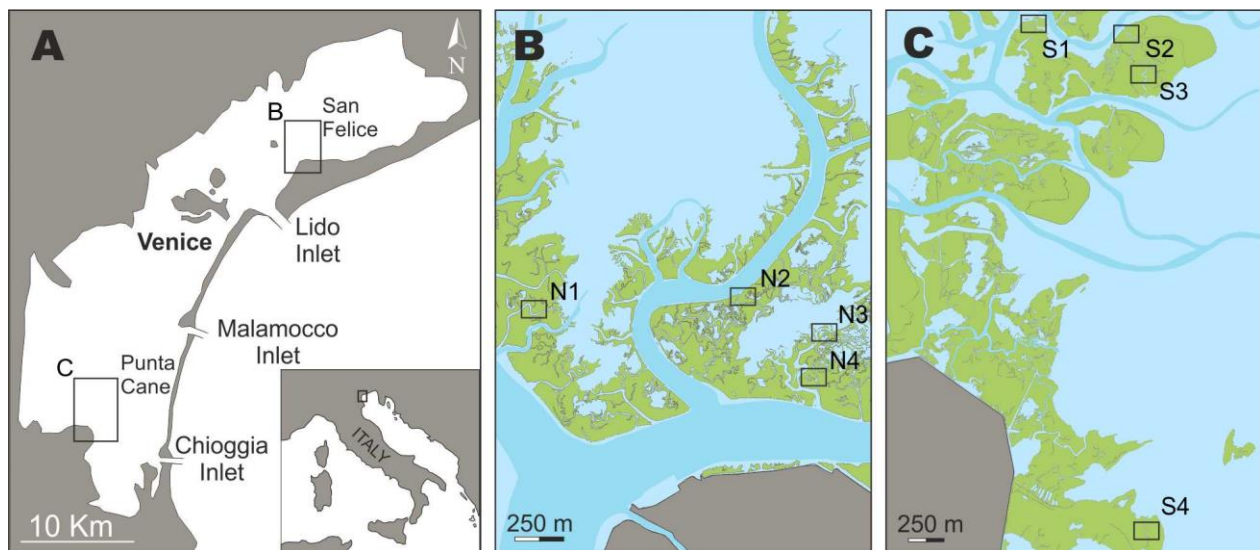
Figure 2. Study sites. (A) Location of the Venice Lagoon along the Northeastern coast of Italy. (B and C) Location of the study sites in the Northern (N1, N2, N3, and N4) and Southern (S1, S2, S3, and S4) Venice Lagoon, respectively.

Nowadays, the great majority of salt marshes are found in the Southwestern and Northwestern areas of the Lagoon. Salt marshes located in the Northern Venice Lagoon have been characterized by accretion rates ranging between 0.1 and 0.5 cm/yr during the last century, with the highest values observed after the 1960s (Bellucci et al., 2007). Conversely, the accretion rates of salt marshes located in the Southern Venice Lagoon

ranged between 0.1 and 1.2 cm/yr since the 14th century, when palustrine sedimentation ceased and salt marshes colonization began (Roner et al., 2017).
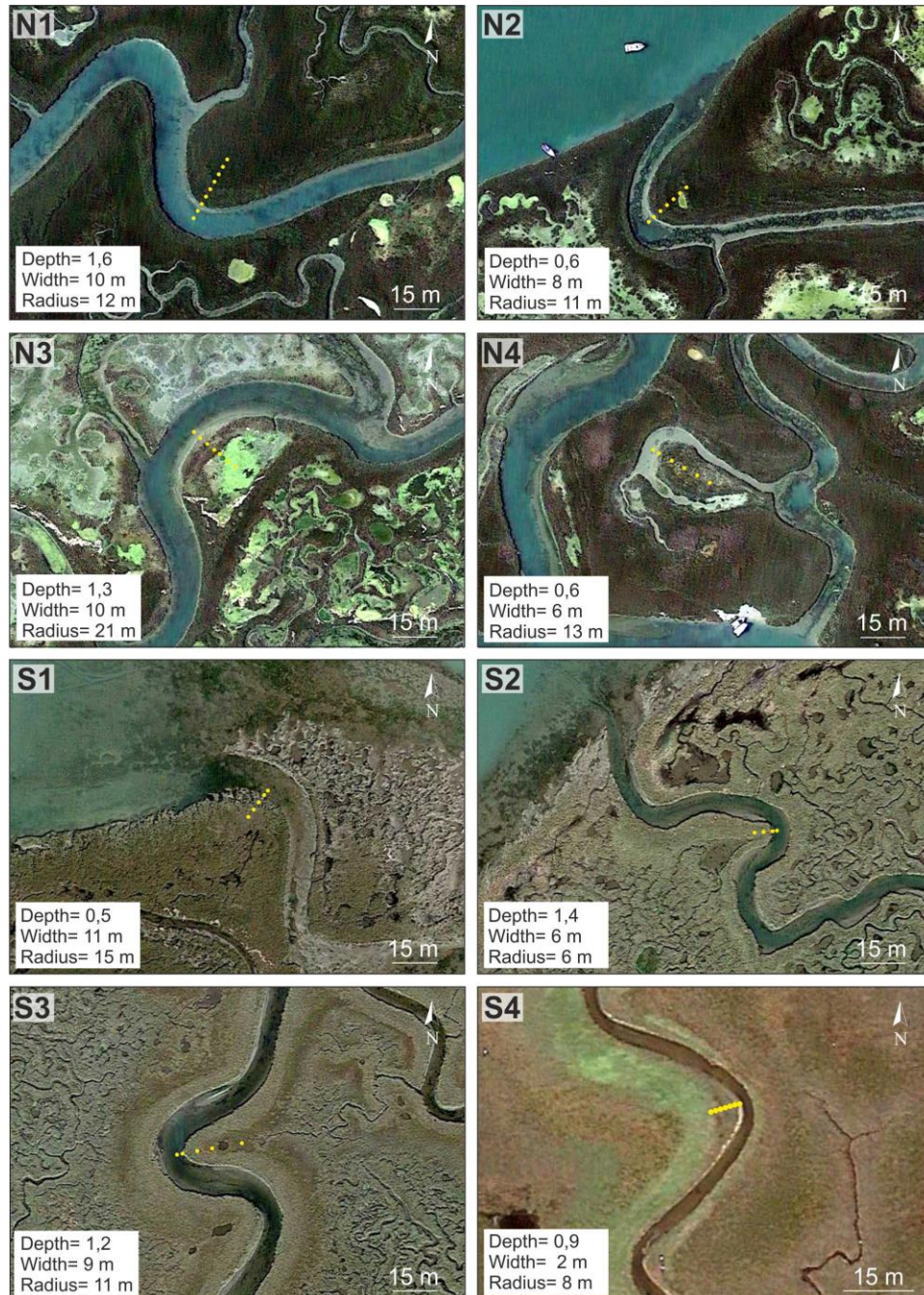
Figure 3. Satellite images (from Google™Earth) showing the study meander bends in the Northern (N1, N2, N3, and N4) and Southern (S1, S2, S3, and S4) Lagoon. Yellow dots indicate the position of the recovered cores in each meander.

The present study focuses on eight different meander bends, four of which (N1 –N4, Fig 2B) cut through the San Felice salt marshes in the Northern Lagoon, and the other four are located in the Southwestern marshes of Punta Cane (S1 – S4, Fig 2C). The study case bends are 2 – 11 m wide and 0.5 –1.6 m deep (Fig 3), and cut through salt marshes colonized by a dense halophytic vegetation species such as *Limonium narbonense, Spartina maritima, Sarcocornia fruticosa, Juncus maritimus*, and *Salicornia veneta*. All the study channel bends are still active, except at site N4 (Fig 3), which is now completely filled following a cut off that occurred during the 1950s (D'Alpaos et al., 2017). None of the active channels completely dry out at the lowest tides, and point bar tops can be covered by few decimetres of water at the highest tides. Meanders at sites N2 and S2 show a "simple asymmetric" (*sensu* Brice, 1974) planform geometry, whereas all the other channels can be labelled as "simple symmetric" (*sensu* Brice, 1974). The radius of curvature of the bends ranges between 6 and 21 m (Fig 3).

4. METHODS AND TERMINOLOGY

A total of 50 cores were recovered along axial transects of the study bends. Each transect extended from the channel thalweg to the line connecting inflection points of the bend (Fig 3). The position and elevation of the cores were determined using differential GPS TOPCON GR-3 receivers - dual frequency (L1/L2) and dual-constellation (NavStar/Glonass) with integrated Tx/Rx UHF radio. Cores were up to 3 m deep and were recovered using an Eijkelkamp hand auger, through a gouge sampler with a length of 1 m and a diameter of 30 mm, which prevented sediment compaction. PVC liners were used to keep the cores humid, which were successively cut longitudinally, photographed and logged. Sedimentological analyses were carried out on the study cores following the basic principles of facies analyses. Identification of different types of

deposits was based on the integration between core location and related sedimentary features, including sediment grain size and colour, presence of sedimentary structures, vertical grain-size trends, degree of bioturbation and occurrence of plant and/or shell remains. Correlation among cores allowed to disclose 2D point bar sections along the bend axis.

Terminology used in the present work is reported in Figure 4, and follows that used for fluvial point bars (cf. Ielpi and Ghinassi, 2014), although some modifications have been introduced due to the bidirectional nature of tidal currents (e.g. seaward/landward instead of downstream/upstream). The point bar brink is defined here as the bar rim (Fig 1A and 4C), and is characterized by a break in the angle of deposition from the flat bar top deposits to the inclined bar slope. Accordingly, in cores, the point bar brink was pointed out where lamination changed from horizontal (i.e. bar top deposits) to inclined (i.e. bar slope deposits). This change in inclination occurs within an interval spanning between 5 and 10 cm in thickness (Fig 4B), which represents the uncertainty for detecting the brink position in the study deposits. The channel thalweg is defined as the deepest part of the active channel (Figs 1A and 4C). In cores, it corresponds to the surface flooring channel lag deposits and can be precisely located (Fig 4B).

The study transects are considered parallel to the local vector of bar migration. Minimum and maximum lateral migration rates (ζ_{min}, ζ_{max}, respectively) of each bend have been approximately estimated on the basis of the ratio between the distance covered by the lateral shift of the channel (d in Figure 4C) and the minimum and maximum estimated time span over which migration occurred (Δt_{min} and Δt_{max}). The latter have been determined as $\Delta t_{min}=s_t/s_{a,min}$ and $\Delta t_{max}=s_t/s_{a,max}$, where s_t is the maximum thickness of bar top salt-marsh deposits accumulated during bar migration (Fig 4C) and $s_{a,min}$ and $s_{a,max}$ are the minimum and maximum vertical accretion rates of salt marshes reported in literature for the study area (Bellucci et al., 2007; Roner et al., 2017).
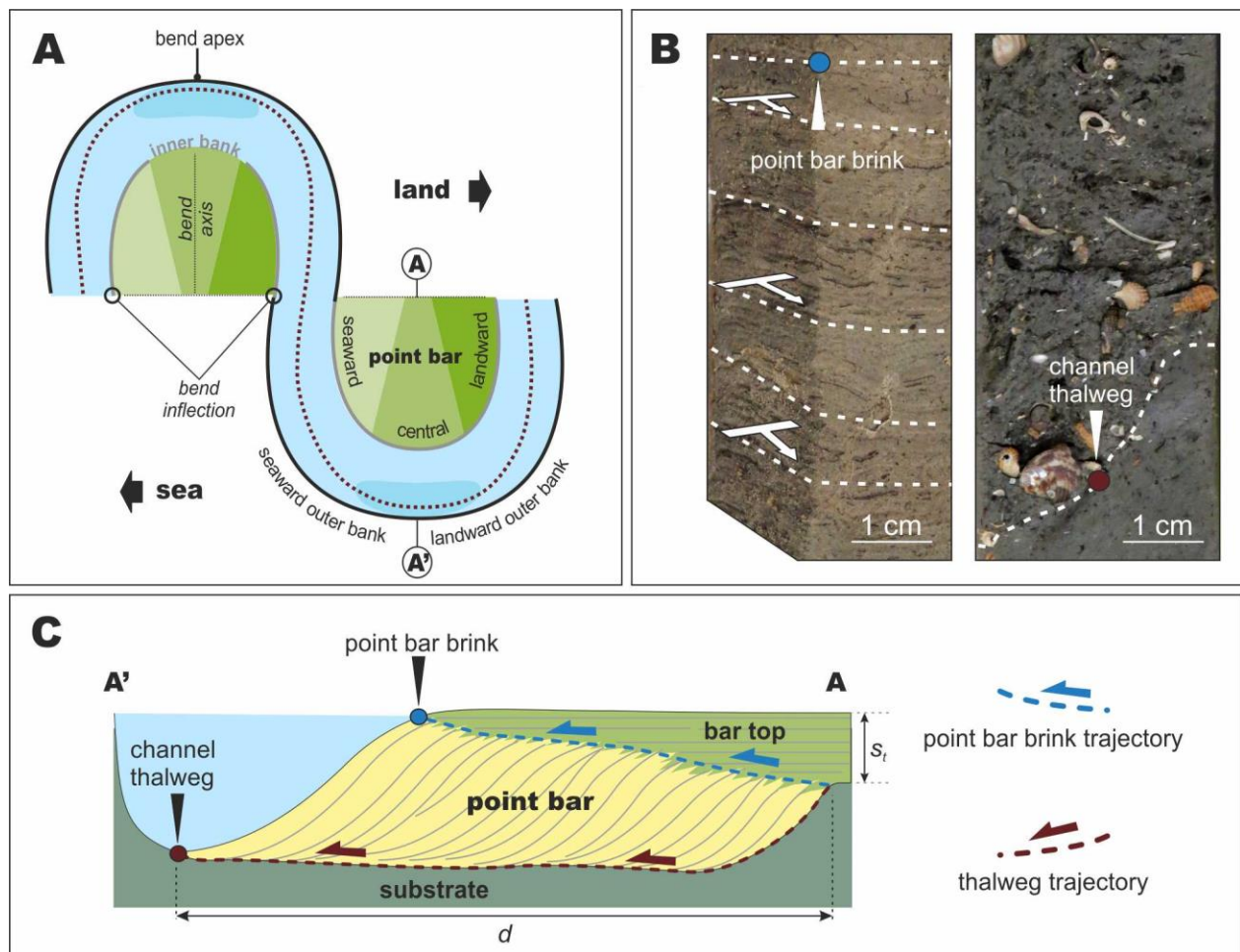
Figure 4. Terminology used in the present work. (A) Key terms used to define different elements of tidal meander bends. (B) Examples of point bar brink (left) and channel thalweg (right) deposits in sedimentary cores. (C) Tidal point bar architecture and definition of point bar brink and thalweg trajectories. s_t: maximum thickness of bar top, salt-marsh deposits accumulated during bar migration. d: distance covered by the lateral shift of the channel.

5. RESULTS

5.1. Study deposits

Four types of deposits have been recognized, namely: bar substrate, point-bar and channel-lag, salt-marsh and channel-fill deposits. In the following paragraphs, each of them is briefly described and interpreted.

5.1.1. Substrate deposits

These deposits represent the lowermost stratigraphic unit of each study case and are radically different in the Northern and Southern Venice Lagoon.

In the Northern Lagoon, they consist of an alternation between sandy and muddy layers. The sandy layers, that can locally exceed 1 m in thickness, consist of well-sorted dark grey sand, medium to very fine in grain size, with abundant shells, shell fragments and plant debris (Fig 5B). Sandy deposits can locally contain millimetric muddy laminae. The muddy layers consist of dark, organic-rich mud with scattered shells and plant fragments, and are up to 10 cm thick (Fig 5A). Bioturbation is common in both the sandy and muddy layers, and prevents detection of sedimentary structures. Substrate deposits of the Northern Lagoon are interpreted to be formed in a tidal flat/subtidal platform environment. Sandy deposits likely originated during wind-induced storm events, when wave winnowing entrained fine-grained sediments and sand concentrated on the lagoon floor (Carniello et al., 2009). Muddy deposits settled down from suspension or by flocculation processes during the waning stage of storm events. The presence of thick mud layers could suggest the occurrence of fluid mud (Dalrymple and Choi, 2007; Chen et al., 2015). However, maximum fine-grained suspended- sediment concentration in the Venice Lagoon is known to be much lower (Carniello et al., 2016) than the one required for developing fluid mud layers (Faas, 1991).

In the Southern Lagoon, substrate deposits consist of peat with abundant fragments of reeds (Fig 5D). In some of the cores from sites S2 and S3, a dark-grey mud interval with sparse reed fragments (Fig 5C) occurs on top of peat deposits. Peat consists of comminute dark brown to black plant debris with a minimum amount of dispersed mud. The presence of peat deposits and abundant reeds is consistent with a wetland setting with freshwater input (Bondesan and Meneghel, 2004; Tosi et al., 2007). The mud on top of peat deposits accumulated in local protected ponds, where vegetation cannot

grow and mud can settle down (Silvestri et al., 2005; Roner et al., 2016). Although peat is widespread in the Southern Lagoon (Roner et al., 2017), substrate deposits at site S4 (Fig 2) consist of an alternation between mud and sand similar to that occurring in the Northern Lagoon.
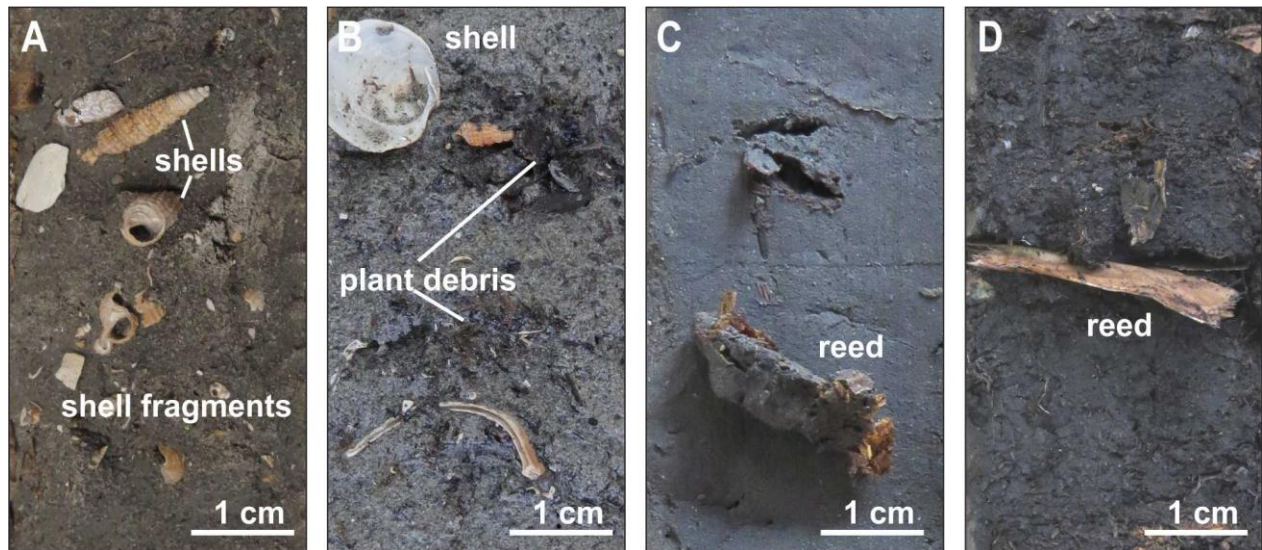
Figure 5. Substrate deposits of the Northern (A and B) and Southern (C and D) Lagoon. (A) Organic-rich mud with shells and plant fragments; (B) Dark-gray sand, medium to very fine in grain size, with abundant shells, shell fragments and plant debris. (C) dark-gray mud with scattered reed fragments; (D) Peat with abundant fragments of reeds.

5.1.2. Point-bar and channel-lag deposits

These deposits are up to 2.25 m thick and show a lateral extent of 10 – 20 m, and 3 – 15 m for the Northern and Southern sites, respectively (Table 1). These deposits pinch out toward the terminations of all the study transects (Fig 8). They are erosively-based and grade upward into salt-marsh or channel-fill deposits. The basal erosional surface is draped by a shell-rich, 5-20 cm thick massive layer (Fig 6 A.7 and B.5), which consists of fine to medium sand and of silt to fine sand in the Northern and Southern sites, respectively. Shells are commonly fragmented and include both gastropods (e.g. *Bittium scabrum, Tritia neritea, Gibbula* sp.) and bivalves (e.g. *Loripes orbiculatus, Acanthocardia*

tuberculata, Scrobicularia plana). Plant debris and pebble-sized, rounded mud clasts are also common (Fig 6 A.6).
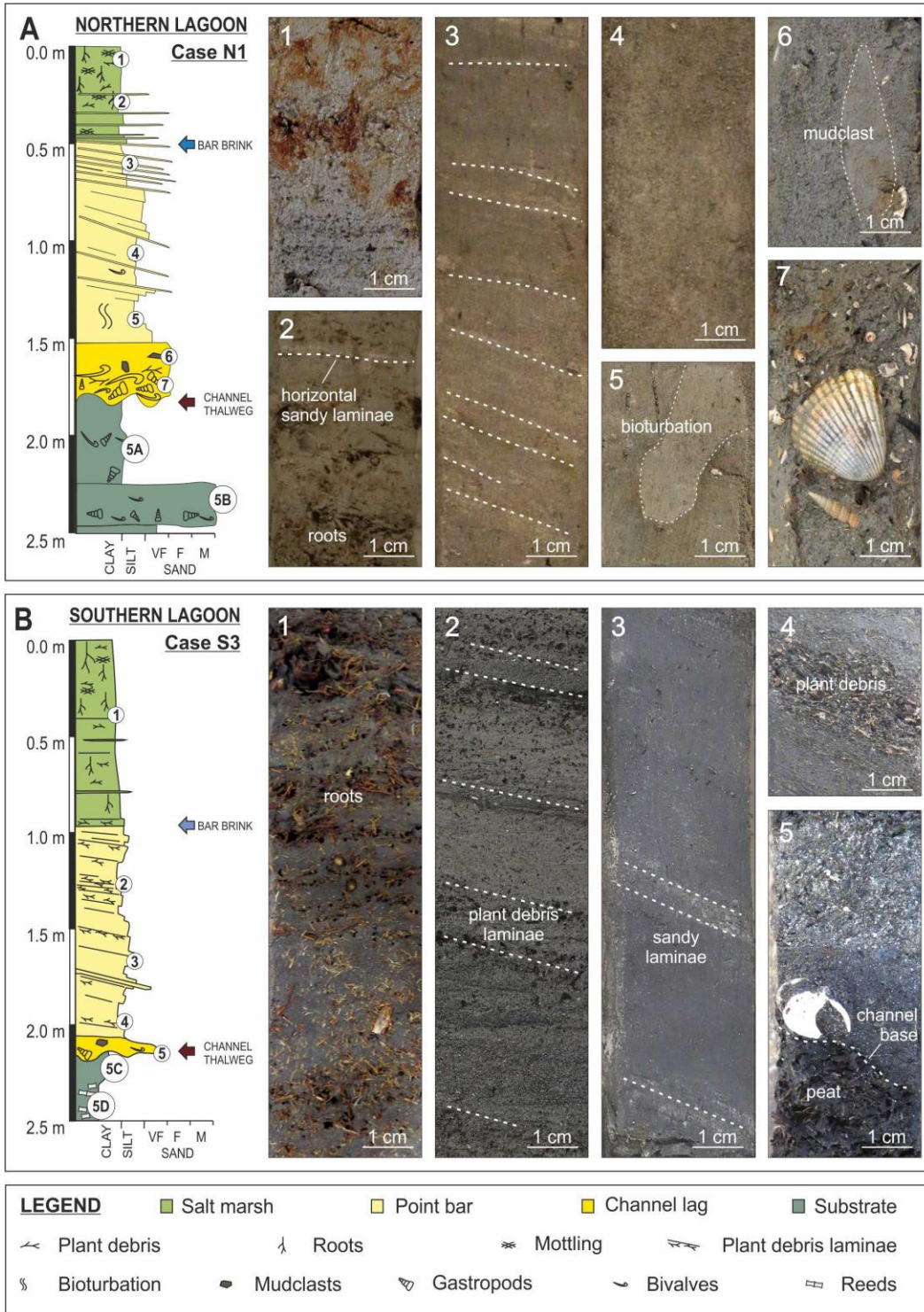
Figure 6. Point bar deposits from Northern and Southern study sites. (A) Northern Case. Example from site N1; (A.1) Oxidized salt-marsh mud; (A.2) Salt-marsh mud with horizontal sandy laminae and roots; (A.3) Bar deposits consisting of silt with inclined sandy laminae. Note the upward decrease in dip angle of sandy laminae; (A.4) and (A.5) Structureless sand and bioturbation in the lower part of the point bar; (A.6) Pebble-sized mud clast in massive channel-lag sand; (A.7) Shell-rich channel-lag sand; (B) Southern Case. Example from site S3; (B.1) Salt-marsh mud deposits with roots; (B.2), (B.3) and (B.4) Silty to muddy bar deposits with a variable amount of inclined plant debris and sandy laminae; (B.5) Massive channel-lag sand with shells and shells fragments, flooring the channel base.

The shell-rich layer is covered by clinostratified deposits, which are up to 2.2 m thick. Locally they show an overall fining-upward grain size trend (Fig 6A and B), and consist of two intervals. The lower interval is made of fine sand to silt-rich mud with scattered shell fragments and mud clasts. These deposits are mainly massive (Fig 6 A.4), although a local inclined lamination may be visible (Fig 6 B.3). Bioturbation is really common and often prevents the identification of primary bedding (Fig 6 A.5). The upper interval ranges in grain size between sandy silt and mud, with laminae dipping channelward between 5° to 25° (Fig 6A, A.3, B and B.2). Laminae consist of well-sorted very-fine to fine sand (Fig 6 A.3) or comminute plant debris (Fig 6 B.2), which are more common in the Northern and Southern sites, respectively. Inclination of laminae decreases moving upward in the clinostratified deposits, and becomes insignificant at the boundary with the overlying salt-marsh deposits (Fig 6A, A.3 and B).

The shell-rich basal layer and the overlying clinostratified silty sand are interpreted as channel lag and point bar deposits, respectively. Channel lag deposits accumulated in the deepest part of the channel, where the coarser sediments and shell fragments concentrate, as finer grains are entrained by currents (Terwindt, 1988). Shelly assemblages consist of mainly marine and subordinately brackish molluscan species that roughly reflect the benthic fauna currently inhabiting mud and sandy substrates of the Venice Lagoon. Pebble-sized mud clasts are the product of fragmentation of blocks collapsed from the channel banks (Terwindt, 1988). Bar deposits accumulated as a consequence of lateral shift of the channel, and their localized fining-upward grain size trend, reflects the overall decrease of the bottom shear stress moving from channel

thalweg to bar top in the axial zone of a meander bend (Hooke, 1975; Dietrich et al., 1979; Dietrich and Smith, 1984; Frothingham and Rhoads, 2003). In the lower bar deposits (i.e. lower part of clinostratified sediments), intense bioturbation, and a related paucity of sedimentary structures, is consistent with the permanent presence of water on this part of the bar. In the upper bar deposits (i.e. upper part of clinostratified sediments), the dominance of mud points to the prevalence of flocculation or suspension fallout processes, which were probably dominant during prolonged slack water periods or after storm events (Carniello et al., 2011). Inclined sandy laminae of the upper bar were produced during storms at high tides, when both salt marshes and bar tops were winnowed by waves (Green and Coco, 2007; Carniello et al., 2011; Fruergaard et al., 2011; Choi and Jo, 2015). The decrease in the inclination of laminae reflects the progressive upward flattening of bar slope and heralds the transition into overlying salt-marsh deposits.

5.1.3. Salt-marsh deposits

Salt-marsh sediments commonly cover point-bar bodies, but they can also overlay substrate deposits. Salt-marsh deposits consist of brownish, oxidized mud with 1 – 3 mm thick horizontal well-sorted sandy laminae (Fig 6 A.1, A.2, and B.1). *In situ* roots, wood fragments and bioturbation are common. Along each transect, the thickness of these deposits decreases toward the channel (Fig 8). Maximum thicknesses of salt-marsh deposits are 0.7 and 2 m in the Northern and Southern sites, respectively (s_t in table 1).

Salt-marsh deposits accumulate in the upper part of the intertidal zone, where subaerial exposure is frequent (Silvestri et al., 2005). This is in agreement with widespread oxidation and occurrence of abundant roots. These deposits are mainly accreted through mud settling and organic matter accumulation (Allen, 2000; Mudd et al., 2010; Roner et al., 2016). Various processes can contribute to mud deposition on salt marshes, including baffling effects of the vegetation, suspension settling in ponds after the tidal retreat and

suspension fallout during high water slacks, at the transition between flood and ebb tide. Sorting of sand forming thin laminae suggests their formation during storm events, when the salt-marsh surface was flooded and wave-winnowing suspended mud particles and concentrated coarser sediments (Choi and Jo, 2015).

5.1.4. Channel-fill deposits

These deposits occur only at sites N2, N4 and S1 (Fig 8), are up to 1.5 m thick and overlie point-bar and channel-lag sediments. At the abandoned channel bend of site N4, they are as thick as the adjacent point bar, whereas at sites N2 and S1 they are thinner than the bar. These deposits consist of dark grey, massive mud with dispersed bivalves in life position. At sites N4 and S1 (Fig 8), the transition between these deposits and underlying point-bar sand is transitional.

These muddy deposits settled down from suspension, silting up channels affected by a progressive decrease in water discharge. In the case of site N4, deactivation of the channel followed a neck cut off, which allowed the whole channel to be filled with mud (D'Alpaos et al., 2017). At sites N2 and S1, the increase of fallout processes can be ascribed to a general decrease in the discharge shaping the tidal network in the area, and the gradual transition from underlying bar deposits points out to a progressive deactivation of the channel (cf. Toonen et al., 2012).

5.2. Point-bar brink and channel-thalweg trajectories

The stratigraphic relationship between different sedimentary facies mark the location of the point bar brink (i.e. transition between point-bar and salt-marsh deposits) and thalweg (i.e. base of channel lag deposits) zone in all the study cores. Correlation between adjacent cores defines 2D cross sections, which depict the point bar brink and

channel thalweg trajectories generated during lateral shift of the channel (Fig 7). Brink and thalweg trajectories start from a shared point (i.e. "nucleation point" in Figure 7) and follow specific paths, which are summarized in Figure 8, where the vertical scale has been doubled in order to emphasize different trends.
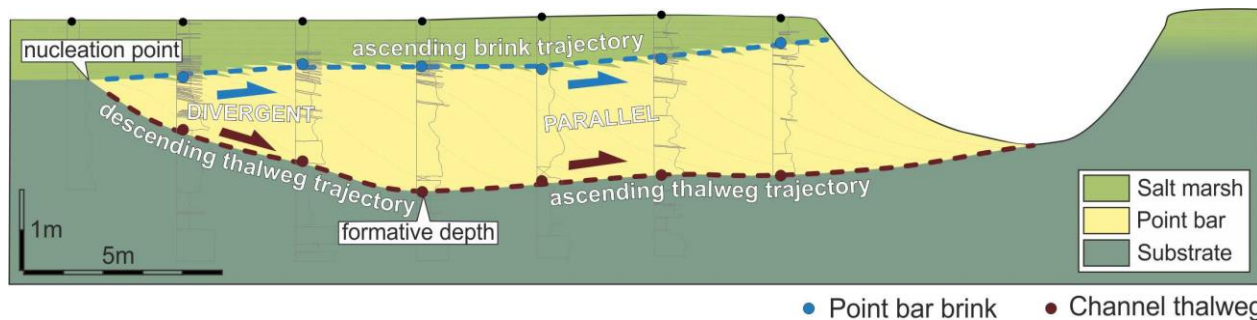
Figure 7. Correlation between cores along the axis of point bar N1. Bar brink and channel thalweg trajectories are highlighted.

All the reconstructed bar brink trajectories show an ascending pattern (Fig 8), although some of them show low steepness (less than 2°) and can be considered sub-horizontal. In sites located in the Northern Lagoon, the trajectories appear to be gentle and linear, with a constant slope ranging between 0.3 and 1.7° (Fig 8 N1-N4). In the Southern Lagoon, a linear and gentle (2.9°) trajectory occurs only at site S4, whereas sites S1 – S3 are characterized by curve and steep trajectories. At sites S2 and S3 (Fig 8), the trajectories show a concave-upward profile, with a slope inclination that changes from sub-horizontal to ca. 41.5° and 9.4°, respectively (Fig 8). At site S1 the brink trajectory defines a convex-upward profile, with the slope decreasing from 16.2° to 6.6°.

The thalweg trajectories appear to be more complex and result from the combination of descending, horizontal and ascending shifts. In all the study cases (Fig 8), with the exceptions of site N2 (where nucleation point has not been detected), the thalweg trajectories show an initial downward shift. The steepness of this descending segment varies from 6.3° to 31.6° and shows a linear or faintly concave-upward geometry (Fig 8). After this first descending reach, the following portion of the trajectories shows either gentle (N1 – N4) or steep (S1 – S4) slopes. In the Northern sites, these trajectories are

commonly sub-horizontal with slightly ascending (N1) or descending (N2-N3) shifts. In the Southern cases, they rise up with inclination ranging between 4.8° and 23.3° (Fig 8). None of the ascending reaches show convex- or concave-upward geometries.
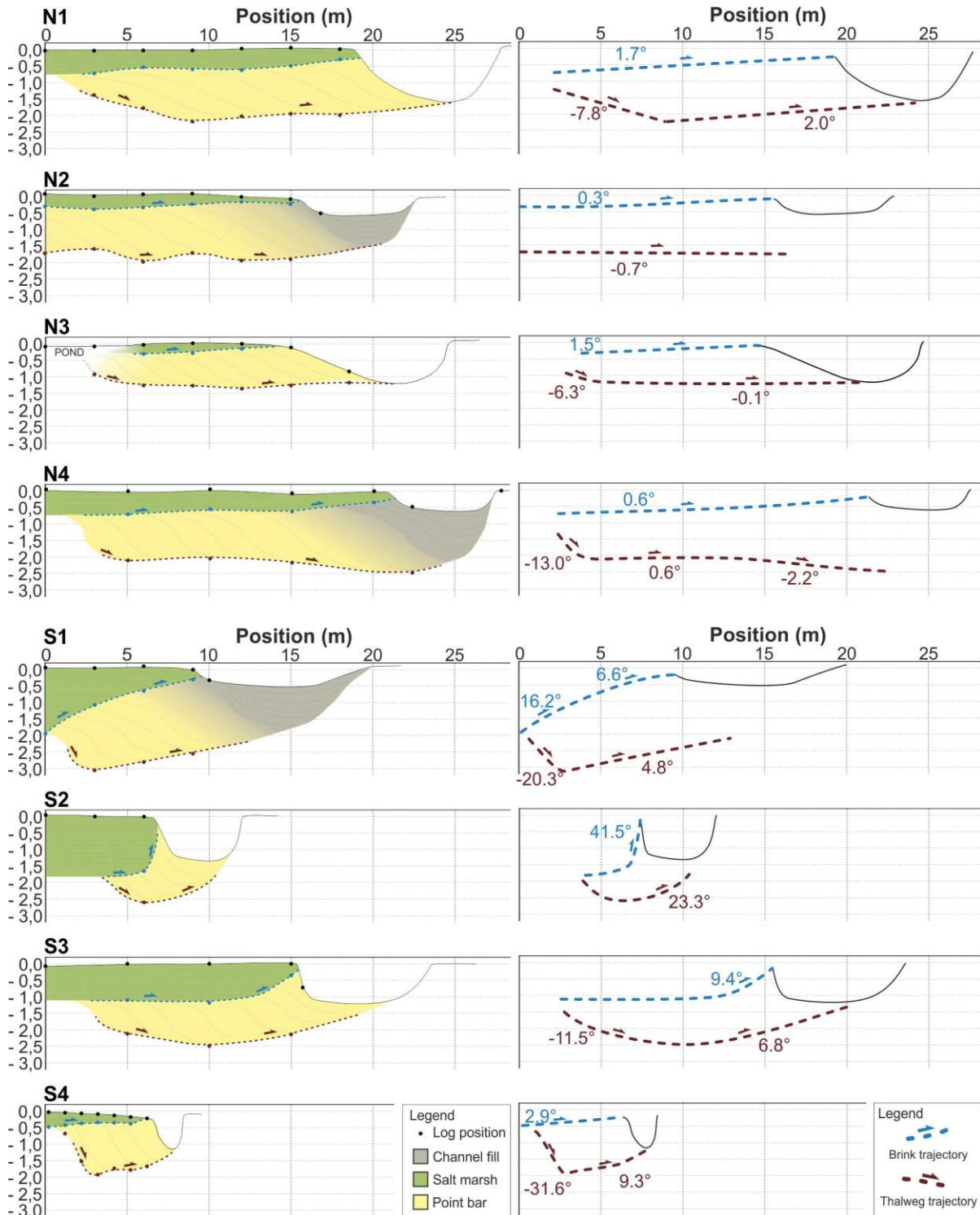
Figure 8. Point bar sections of the northern (N1 – N4) and southern (S1 – S4) study cases. Point bar brink and thalweg trajectories are marked with light blue and red dotted lines, respectively. Slopes of bar brink and channel thalweg trajectories are shown on the right side of the figure. Vertical exaggeration x2.

Different combinations of bar brink and thalweg trajectories occur at different sites (Fig 10), although all the study cases share an early stage where brink and thalweg trajectories diverge (Figs 7 and 8), causing an increase of point bar thickness. This pattern has not been tested at site N2 since deposits of the early channel evolution were not cored (Fig 8). This early stage of divergence occurs over distances spanning between 1 and 7 m, and the angle of divergence ranges between 7.8° (N3) and 36.5° (S1). After the stage of divergence, different patterns of brink and thalweg trajectories are combined. At Northern sites (N1 – N3), gently ascending brink trajectories are combined with similar thalweg trajectories. At site N4, after an initial similar pattern (ascending brink and thalweg) a phase of divergence of brink and thalweg trajectories is recorded. At Southern sites, the stage of divergence is also followed by a stage in which brink and thalweg trajectories show a similar ascending pattern (S1 – S3). Site S4 does not show this trend and, after the stage of divergence, the thalweg trajectory rises converging toward the corresponding brink trajectory.

5.3. Lateral migration rates

The lateral migration rate of each bend has been estimated through a comparison between the maximum thickness of salt-marsh deposits overlying different bars and aggradation rates documented in the study areas (Bellucci et al., 2007; Roner et al., 2017). Table 1 shows that maximum migration rates do not exceed 0.2 m/yr (N2). Minimum migration rates obtained for the Northern and Southern sites are in the range of 0.02-0.04 m/yr and 0.002-0.01 m/yr, respectively; maximum migration rates span between 0.11-0.19 m/yr in the Northern meanders, and between 0.02-0.16 m/yr in the Southern

meanders. These values are consistent with other studies carried out for meandering channels of the Venice Lagoon (McClennen and Housley, 2006; Brivio et al., 2016; D'Alpaos et al., 2017; Donnici et al., 2017; Finotello et al., 2018; Ghinassi et al., 2018) and in other microtidal environments worldwide (Garofalo, 1980; Gabet, 1998).

Site	s_t (m)	d (m)	ζ_{min} (m/yr)	ζ_{max} (m/yr)
N1	0.70	15	0.021	0.107
N2	0.40	15	0.038	0.188
N3	0.30	10	0.033	0.167
N4	0.70	20	0.029	0.143
S1	2.00	9	0.005	0.054
S2	1.65	3	0.002	0.022
S3	1.10	15	0.014	0.164
S4	0.47	6	0.013	0.153

Table 1. Estimation of minimum (ζ_{min}) and maximum (ζ_{max}) lateral migration rates of the different meanders. s_t: maximum thickness of bar top, salt-marsh deposits accumulated during bar migration. d: distance covered by the lateral shift of the channel (Fig 4C).

6. DISCUSSION

Trajectory analysis has been applied here at the point-bar scale, showing the migration patterns of the point bar brink and the channel thalweg along axial cross sections of the study tidal bends. Trajectories are labelled as ascending, descending and horizontal (Fig 9). Ascending and descending trajectories are distinguished in linear and non-linear (Fig 9). While linear trajectories document a constant ratio between vertical and lateral shift rates (d (v/ζ) /dt = 0), non-linear trajectories, which can be concave- or convex-upward, document temporal changes in the ratio between vertical and lateral shift rates (d (v/ζ) /dt ≠ 0).

$$\frac{d}{dt}\left(\frac{v}{\zeta}\right)$$
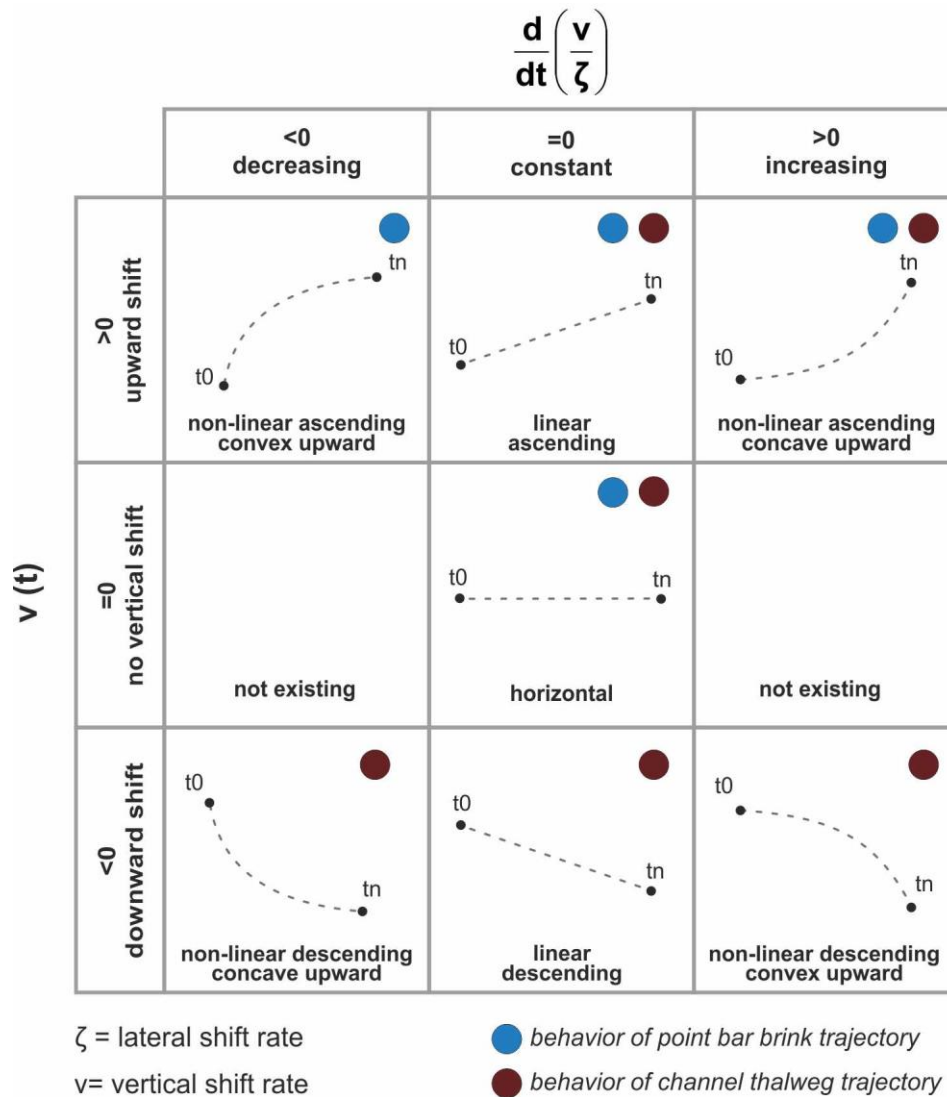
Figure 9. Different types of point bar brink and channel thalweg trajectories.

6.1. Point-bar brink trajectories

Ascending point bar brink trajectories point out that the lateral shift of the brink was influenced by aggradation of surrounding salt-marshes, which kept pace with the progressive sea-level rise by accreting both inorganic and organic sediments (Morris et al., 2002; D'Alpaos et al., 2007; Mudd et al., 2010). Along the study section, steepness of brink trajectories reflects a different ratio between vertical aggradation and lateral

migration, and, where lateral shift rate dominates over that of vertical aggradation, the brink trajectories appear sub-horizontal (i.e. less than 2°). Conversely, where vertical aggradation is higher, it forces the brink to define steep trajectories (i.e. up to 41.5°).

The remarkable difference in the flat and steep trajectories observed in the Northern and Southern Lagoon, respectively, can hardly be ascribed to the slight difference between aggradation rates of these two areas (Bellucci et al., 2007; Roner et al., 2017). Therefore, a further constraint is considered to be responsible for this difference, namely the nature of substrate deposits hosting different bars. Peat deposits, like those hosting S1-S3 bars, are the most compressible of all natural soils (Allen, 1999) and their compaction leads to a substantial increase of local subsidence (Rajchl and Uličný, 2005; Long et al., 2006; Törnqvist et al., 2008; van Asselen et al., 2010; van Asselen, 2011). Peat deposits can be compacted up to 43% within a few centuries (van Asselen et al., 2010), with compaction rates that can exceed 10 mm/yr on decadal to centenary timescales (Törnqvist et al., 2008). The dominant factors influencing peat compaction are the organic matter content and the sediment loading of overlying deposits (Elliott, 1985; van Asselen et al., 2010; van Asselen, 2011). The peat of the Southern Lagoon was progressively compacted by the increasing sediment load due to the growth of the overlying point bars, with a significant increase of local subsidence and related aggradation (Fig 11). The lack of a steep brink trajectory at bar S4, which covers a sandy substrate, supports this hypothesis. Progressive compaction of peat substrate is also consistent with the occurrence of non-linear and concave-upward trajectories (sites S2 and S3; Fig 8), which point to a progressive increase of the ratio between vertical and lateral shift rate. This increase was due to the intensification of local subsidence/aggradation triggered by loading exerted by the growth of bar deposits over peat deposits. The non-linear convex-upward trajectory at site S1 documents a progressive decrease in the ratio between vertical and lateral shift rate. Progressive flattening of this trajectory points to a relative increase in lateral channel shift, which would be caused by the occurrence of

erodible deposits (e.g. sand) along the outer bank of the channel (cf. Smith et al., 2009; Ghinassi et al., 2016). Linear and gently-sloping trajectories of the Northern sites indicate that the ratio between vertical and lateral shift rate remained constant during lateral shift of the channel, and that rate of lateral migration dominated over that of vertical shift. The presence of a sand-prone substrate in the Northern Lagoon nullifies the effects of local substrate compaction, hindering the development of curvilinear trajectories.
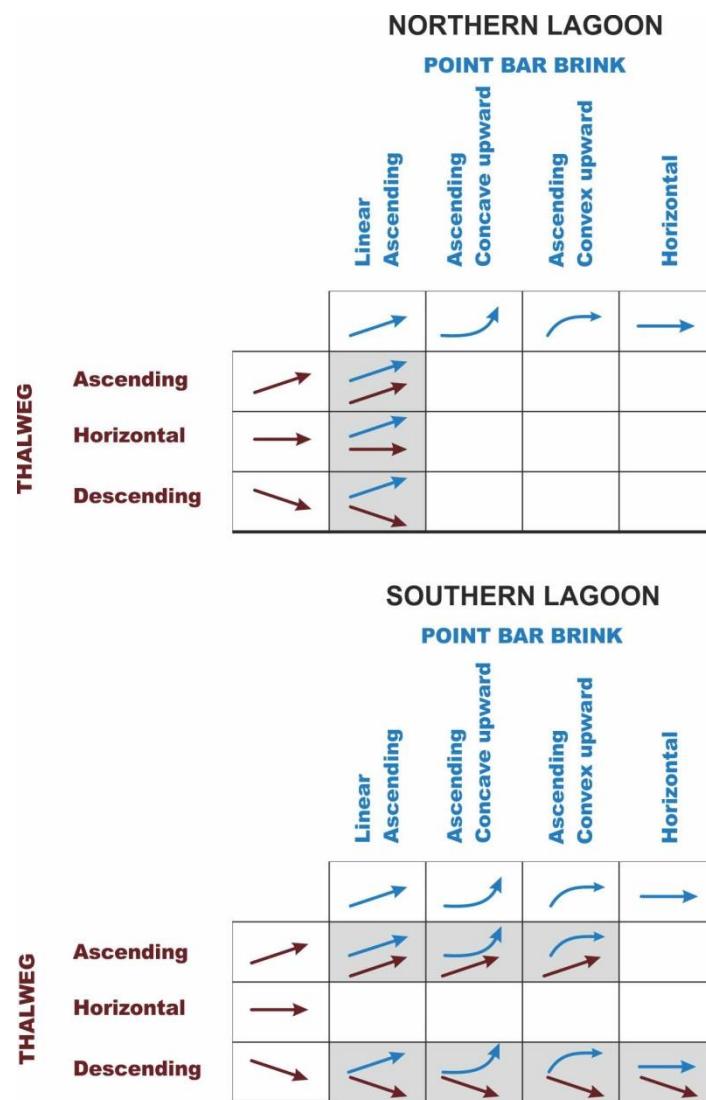
Figure 10. Combinations of point bar brink and channel thalweg trajectories registered in northern and southern study cases.

6.2. Channel thalweg trajectories

Channel thalweg trajectories include ascending, descending and horizontal trends, indicating that the channel base shifted laterally under aggradational, degradational and stable conditions, respectively. The lack of clear convex- or concave-upward profile of ascending and descending trajectories could point to a stable ratio between lateral and vertical shift rates, although the erosive (i.e. irregular) nature of the channel basal surface could prevent a clear detection of these trends.

The descending thalweg trajectories which characterize the early part of all the study trajectories, document the establishment of the channels, which shift laterally and cut down into the substrate in order to reach a cross-sectional depth that is in equilibrium with the local, formative tidal prism. The formative depth in the bend axial zone is a function of the channel discharge and bend geometry. Channel discharge is related to the tidal watershed area, and can vary over temporal scales of decades to centuries as consequence of changes in the tidal prism, watershed area (e.g. due to channel piracies and/or meander cut off) and channel network evolution (Garofalo, 1980; Dalrymple et al., 1991; Allen, 2000; Lanzoni and Seminara, 2002; D'Alpaos et al., 2005; Stefanon et al., 2012). Bend geometry can influence the capability of the channel to cut through its substrate (Hooke, 1984; Nanson and Hickin, 1986; Hudson and Kesel, 2000; Lagasse et al., 2004; Crosato, 2009). Specifically, a progressive increase in bend sinuosity enhances the erosive power of the secondary helical flow, causing a progressive deepening of the pool in the axial zone of the bend (Willis and Tang, 2010). The slope of descending thalweg trajectories indicates the rate of channel incision, which reflects the amount of time required to reach the equilibrium depth.
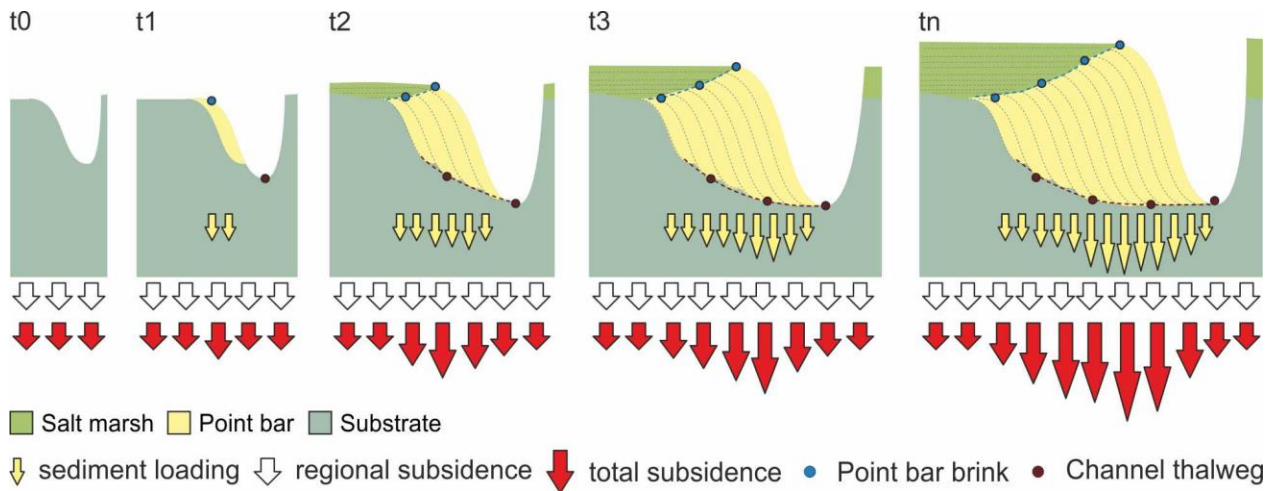
Figure 11. Diagram illustrating the influence of substrate compaction on developing of bar brink and channel thalweg trajectories. The progressive increase in bar sediment loading on the peaty substrate, causes a local increase in subsidence/aggradation, which are both documented by the development of steep brink trajectories.

The thalweg trajectories, which characterize the evolution of the meander after the achievement of the formative depth, show either sub-horizontal (N1 – N4) or steep (S1 – S4) ascending patterns. Sub-horizontal thalweg trajectories (inclination < 2°) indicate that the channel mainly shifted laterally with a minor influence of aggradational or degradational processes. Rising thalweg trajectories indicate that the channel shifted laterally under aggradational conditions, and, as for bar brink trajectories, gently- and steeply-rising trajectories are associated with low and high values of the ratio between vertical and lateral shift rate, respectively. In-channel aggradation can either occur when its transport capability decreases, as in consequence of avulsion or cut-off (Toonen et al., 2012), or when, under aggradational and short-term dynamic equilibrium conditions (*sensu* Allen, 2000), sediments are stored in the channel in order to maintain a constant equilibrium depth. The first scenario is documented at sites N2, N4, and S1 (Fig 8) and implies the progressive decrease of channel cross-sectional area through deposition of fine-grained sediments on the channel floor. The similarity between depth of active channels (N1, N3, and S2 – S4) and thickness of the associated bars indicate that they migrated and deposited sediments at their base in order to maintain equilibrium with the surrounding environment.

6.3. Brink and thalweg trajectory combinations

The study sites document an early stage where brink and thalweg trajectories show an ascending and descending trend, respectively. This stage, named "formative phase" in Figure 12, documents the onset of bar deposition and the achievement of the channel depth equilibrium. The angle between brink and thalweg trajectory controls the increase in point bar thickness and is higher where channels cut rapidly into highly-aggrading marshes. Minor modifications to this process are represented by changes in the climbing angle of the brink trajectory, which can be triggered by changes in the ratio between vertical and lateral shift rate of the channel.

Once the equilibrium depth is reached, six of eight study channels show that thalweg and brink trajectories move following an almost parallel pathway ("equilibrium phase" in Figure 12). It arises that, once the channel reached its equilibrium depth, this was kept constant shifting the thalweg in parallel with the bar brink zone. Minor variations from this overall behaviour are documented at sites N4 and S4. Thalweg trajectory at site N4 slightly cuts down before the onset of the abandonment stage (Fig 8). This downward shift would be consistent either with an increase in water discharge, possibly due to a piracy in the upstream reaches of the tidal network, or with an increase in channel sinuosity due to adjustment of its planform shape. Differently, the rising thalweg trajectory at site S4 suggests that after reaching its formative depth, the channel decreased its discharge, possibly as a consequence of changes in channel network structure.

BRINK TRAJECTORY VARIABILITY

Depending on vertical / lateral shift ratio

Processes

o salt marsh aggradation
o low substrate compaction
o low resistence deposits in the outer bank

o salt marsh aggradation
o high substrate compaction

o salt marsh aggradation
o high substrate compaction
o low resistence deposits in the outer bank

Products

LINEAR & GENTLE
constant ratio in time
predominance of lateral migration

NON-LINEAR (concave) & STEEP
increasing ratio in time
aggradation becomes predominant

NON-LINEAR (convex) & STEEP
decreasing ratio in time
lateral migration becomes predominant

ascending brink trajectory

DIVERGENT   PARALLEL

descending thalweg trajectory   ascending thalweg trajectory

nucleation point   formative depth   present day channel

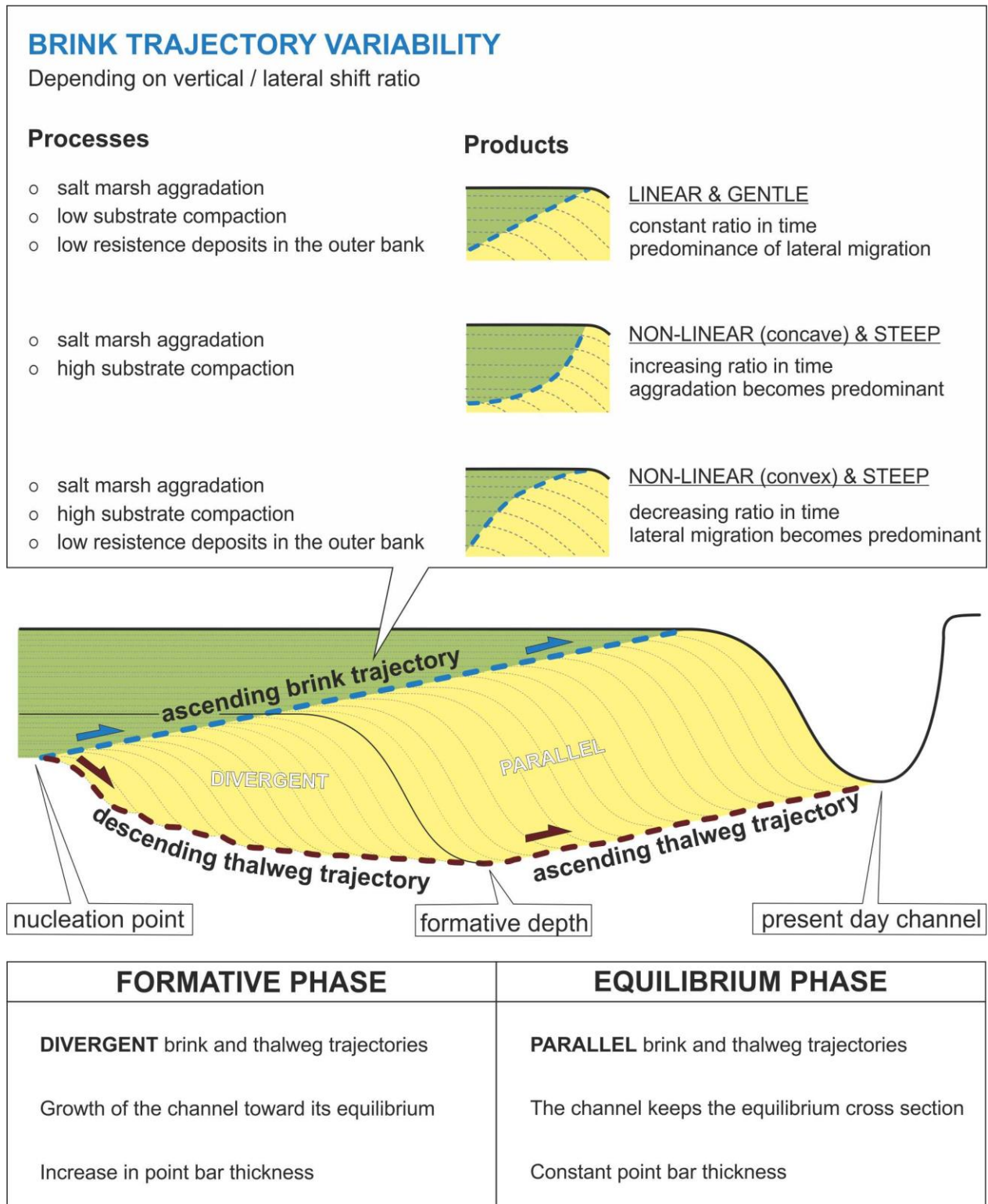| FORMATIVE PHASE	EQUILIBRIUM PHASE
DIVERGENT brink and thalweg trajectories	**PARALLEL** brink and thalweg trajectories
Growth of the channel toward its equilibrium	The channel keeps the equilibrium cross section
Increase in point bar thickness	Constant point bar thickness

Figure 12. Summary of the main architectural features associated with the development and combination of different point bar brink and channel thalweg trajectories.

7. CONCLUSION

The concept of trajectory analysis has been applied at the point bar scale in order to improve our understanding of the behaviour of tidal point bars in microtidal and highly aggradational landscapes.

Along the local vector of bar migration, bar brink trajectories are all ascending and show linear or non-linear trends whether the ratio between vertical and lateral shift rate is constant or not through time. The different shapes and steepness of these trajectories suggest that the bar brinks register different aggradational conditions while shifting laterally. In particular, our results suggest that the differential compaction of sandy and peaty substrates plays a significant role in the creation of local accommodation, which controls the steepness of the trajectory. Thalweg trajectories can be both ascending and descending. Descending thalweg trajectories can be ascribed to the incision rate of the channel while shifting laterally, which is influenced by local tidal prism, bend geometry and evolution of the channel network. Ascending thalweg trajectories suggest that the channel shifts laterally under aggradational conditions.

The combination of brink and thalweg trajectories reveals the variation of point bar thickness during its evolution and allows one to differentiate an early formative phase followed by a late equilibrium phase. During the formative phase, the two trajectories diverge from one another because of the growth of the channel toward its equilibrium depth (formative depth). In the following equilibrium phase, the two trajectories shift in parallel, allowing the channel to keep its equilibrium depth. Variations to this evolution model can be triggered by changes in channel discharge, possibly triggered by piracy events and channel network evolution.

Qualitative models developed in this study provide early insights to investigate the interaction between lateral migration and vertical aggradation in both tidal and fluvial

bends. A comprehensive understanding of this interaction would arise from forthcoming quantitative 3D architectural models, which should also consider the influence of channel planform transformations on developing point-bar geometries.

8. REFERENCES

Allen, J.R.L., 2000. Morphodynamics of Holocene salt marshes: a review sketch from the Atlantic and Southern North Sea coasts of Europe. Quat. Sci. Rev. 19, 1155–1231. https://doi.org/10.1016/S0277-3791(99)00034-7

Allen, J.R.L.L., 1999. Geological impacts on coastal wetland landscapes: Some general effects of sediment autocompaction in the Holocene of northwest Europe. The Holocene 9, 1–12. https://doi.org/10.1191/095968399674929672

Amorosi, A., Fontana, A., Antonioli, F., Primon, S., Bondesan, A., 2008. Post-LGM sedimentation and Holocene shoreline evolution in the NW Adriatic coastal area. GeoActa 7, 41–67.

Barwis, J.H., 1978. Sedimentology of some South Carolina tidal-creek point bars, and a comparison with their fluvial counterparts, in: Miall, A.D. (Ed.), Fluvial Sedimentology. Dallas Geological Society, Calgary, Alberta, Canada, pp. 487–510.

Bellucci, L.G., Frignani, M., Cochran, J.K., Albertazzi, S., Zaggia, L., Cecconi, G., Hopkins, H., 2007. 210Pb and 137Cs as chronometers for salt marsh accretion in the Venice Lagoon - links to flooding frequency and climate change. J. Environ. Radioact. 97, 85–102. https://doi.org/10.1016/j.jenvrad.2007.03.005

Boaga, J., Ghinassi, M., D'Alpaos, A., Deidda, G.P., Rodriguez, G., Cassiani, G., 2018. Geophysical investigations unravel the vestiges of ancient meandering channels and their dynamics in tidal landscapes. Sci. Rep. 8, 1–8. https://doi.org/10.1038/s41598-018-20061-5

Bondesan, A., Meneghel, M., 2004. Geomorfologia della provincia di Venezia. Note illustrative della carta geomorfologica della provincia di Venezia.

Brice, J.C., 1974. Evolution of meander loops. Bull. Geol. Soc. Am. 85, 581–586. https://doi.org/10.1130/0016-7606(1974)85<581:EOML>2.0.CO;2

Bridge, J.S., Alexander, J., Collier, R.E.L.L., Gawthorpe, R.L., Jarvis, J., 1995. Ground-penetrating radar and coring used to study the large-scale structure of point-bar deposits in three dimensions. Sedimentology 42, 839–852.

Bridges, P.H., Leeder, M.R., 1976. Sedimentary model for intertidal mudflat channels, with examples from the Solway Firth, Scotland. Sedimentology 23, 533–552. https://doi.org/10.1111/j.1365-3091.1976.tb00066.x

Brivio, L., Ghinassi, M., D'Alpaos, A., Finotello, A., Fontana, A., Roner, M., Howes, N., 2016. Aggradation and lateral migration shaping geometry of a tidal point bar: An example from salt marshes of the Northern Venice Lagoon (Italy). Sediment. Geol. 343, 141–155. https://doi.org/10.1016/j.sedgeo.2016.08.005

Candel, J.H.J., Makaske, B., Storms, J.E.A., Wallinga, J., 2017. Oblique aggradation: A novel explanation for sinuosity of low-energy streams in peat-filled valley systems. Earth Surf. Process. Landforms 42, 2679–2696. https://doi.org/10.1002/esp.4100

Carniello, L., D'Alpaos, A., Botter, G., Rinaldo, A., 2016. Statistical characterization of spatio-temporal

sediment dynamics in the Venice lagoon. J. Geophys. Res. Earth Surf. 121, 1049–1064. https://doi.org/10.1002/2015JF003793

Carniello, L., D'Alpaos, A., Defina, A., 2011. Modeling wind waves and tidal flows in shallow micro-tidal basins. Estuar. Coast. Shelf Sci. 92, 263–276. https://doi.org/10.1016/j.ecss.2011.01.001

Carniello, L., Defina, A., D'Alpaos, L., 2009. Morphological evolution of the Venice lagoon: Evidence from the past and trend for the future. J. Geophys. Res. Earth Surf. 114, 1–10. https://doi.org/10.1029/2008JF001157

Chen, S., Steel, R.J., Olariu, C., 2015. Palaeo-Orinoco (Pliocene) channels on the tide-dominated Morne L'Enfer delta lobes and estuaries, SW Trinidad, in: Developments in Sedimentology. Elsevier B.V., pp. 227–281. https://doi.org/10.1016/B978-0-444-63529-7.00010-9

Choi, K., Jo, J., 2015. Morphodynamics and stratigraphic architecture of compound dunes on the open-coast macrotidal flat in the northern Gyeonggi Bay, west coast of Korea. Mar. Geol. 366, 34–48. https://doi.org/10.1016/j.margeo.2015.05.002

Colombera, L., Mountney, N.P., Russell, C.E., Shiers, M.N., McCaffrey, W.D., 2017. Geometry and compartmentalization of fluvial meander-belt reservoirs at the bar-form scale: Quantitative insight from outcrop, modern and subsurface analogues. Mar. Pet. Geol. 82, 35–55. https://doi.org/10.1016/j.marpetgeo.2017.01.024

Crosato, A., 2009. Physical explanations of variations in river meander migration rates from model comparison. Earth Surf. Process. Landforms 34, 155–161. https://doi.org/10.1002/esp.1898

D'Alpaos, A., Carniello, L., Rinaldo, A., 2013. Statistical mechanics of wind wave-induced erosion in shallow tidal basins: Inferences from the Venice Lagoon. Geophys. Res. Lett. 40, 3402–3407. https://doi.org/10.1002/grl.50666

D'Alpaos, A., Ghinassi, M., Finotello, A., Brivio, L., Bellucci, L.G., Marani, M., 2017. Tidal meander migration and dynamics: A case study from the Venice Lagoon. Mar. Pet. Geol. 87, 80–90. https://doi.org/10.1016/j.marpetgeo.2017.04.012

D'Alpaos, A., Lanzoni, S., Marani, M., Fagherazzi, S., Rinaldo, A., 2005. Tidal network ontogeny: Channel initiation and early development. J. Geophys. Res. Earth Surf. 110, 1–14. https://doi.org/10.1029/2004JF000182

D'Alpaos, A., Lanzoni, S., Marani, M., Rinaldo, A., 2010. On the tidal prism-channel area relations. J. Geophys. Res. Earth Surf. 115, 1–13. https://doi.org/10.1029/2008JF001243

D'Alpaos, A., Lanzoni, S., Marani, M., Rinaldo, A., 2007. Landscape evolution in tidal embayments: Modeling the interplay of erosion, sedimentation, and vegetation dynamics. J. Geophys. Res. Earth Surf. 112, 1–17. https://doi.org/10.1029/2006JF000537

D'Alpaos, L., 2010. Fatti e misfatti di idraulica lagunare. La laguna di Venezia dalla diversione dei fiumi alle nuove opere delle bocche di porto, Istituto Veneto di Scienze, Lettere e Arti. Istituto Veneto di Scienze, Lettere ed Arti, Venice.

Dalrymple, R.W., Choi, K.S., 2007. Morphologic and facies trends through the fluvial-marine transition in tide-dominated depositional systems: A schematic framework for environmental and sequence-stratigraphic interpretation. Earth-Science Rev. 81, 135–174.

https://doi.org/10.1016/j.earscirev.2006.10.002

Dalrymple, R.W.R.W., Makino, Y., Zaitlin, B.B.A., 1991. Temporal and spatial patterns of rhythmite deposition on mud flats in the macrotidal Cobequid Bay-Salmon River Estuary, Bay of Fundy, Canada. Clastic tidal Sedimentol. 16, 137–160.

Day, J.W., Rismondo, A., Scarton, F., Are, D., Cecconi, G., 1998. Relative sea level rise and Venice lagoon wetlands. J. Coast. Conserv. 4, 27–34. https://doi.org/10.1007/bf02806486

De Mowbray, T., 1983. The genesis of lateral accretion deposits in recent intertidal mudflat channels, Solway Firth, Scotland. Sedimentology 30, 425–435. https://doi.org/10.1111/j.1365-3091.1983.tb00681.x

Dietrich, W.E., Smith, J.D., 1984. Processes controlling the equilibrium bed morphology in river meanders, in: River Meandering: Proceedings of the Conference Rivers '83. pp. 759–769.

Dietrich, W.E., Smith, J.D., Dunne, T., 1979. Flow and Sediment Transport in a Sand Bedded Meander. J. Geol. 87, 305–315. https://doi.org/10.1086/628419

Donnici, S., Madricardo, F., Serandrei-Barbero, R., 2017. Sedimentation rate and lateral migration of tidal channels in the Lagoon of Venice (Northern Italy). Estuar. Coast. Shelf Sci. 198, 354–366. https://doi.org/10.1016/j.ecss.2017.02.016

Durkin, P.R., Hubbard, S.M., Boyd, R.L., Leckie, D.A., 2015. Stratigraphic Expression of Intra-Point-Bar Erosion and Rotation. J. Sediment. Res. 85, 1238–1257. https://doi.org/10.2110/jsr.2015.78

Elliott, R.E., 1985. Quantification of peat to coal compaction stages, based especially on phenomena in the East Pennine Coalfield, England. Proc. Yorksh. Geol. Soc. 45, 163–172. https://doi.org/10.1144/pygs.45.3.163

Faas, R.W., 1991. Rheological boundaries of mud: Where are the limits? Geo-Marine Lett. 11, 143–146. https://doi.org/10.1007/BF02431000

Fagherazzi, S., Gabet, E.J., Furbish, D.J., 2004. The effect of bidirectional flow on tidal channel planforms. Earth Surf. Process. Landforms 29, 295–309. https://doi.org/10.1002/esp.1016

Finotello, A., Lanzoni, S., Ghinassi, M., Marani, M., Rinaldo, A., D'Alpaos, A., 2018. Supporting Information (SI) Appendix. Field migration rates of tidal meanders recapitulate fluvial morphodynamics. Proc. Natl. Acad. Sci. 115, 1463–1468. https://doi.org/10.1073/pnas.1711330115

Fisk, H.N., 1944. Geological Investigation of the Alluvial Valley of the Lower Mississippi River. US Army Corps Eng. Mississippi River Comm. 1–78.

Fontana, A., Mozzi, P., Marchetti, M., 2014. Alluvial fans and megafans along the southern side of the Alps. Sediment. Geol. 301, 150–171. https://doi.org/10.1016/j.sedgeo.2013.09.003

Frothingham, K.M., Rhoads, B.L., 2003. Three-dimensional flow structure and channel change in an asymmetrical compound meander loop, Embarras River, Illinois. Earth Surf. Process. Landforms 28, 625–644. https://doi.org/10.1002/esp.471

Fruergaard, M., Andersen, T.J., Nielsen, L.H., Madsen, A.T., Johannessen, P.N., Murray, A.S., Kirkegaard, L., Pejrup, M., 2011. Punctuated sediment record resulting from channel migration in a shallow

sand-dominated micro-tidal lagoon, Northern Wadden Sea, Denmark. Mar. Geol. 280, 91–104. https://doi.org/10.1016/j.margeo.2010.12.003

Gabet, E.J., 1998. Lateral Migration and Bank Erosion in a Saltmarsh Tidal Channel in San Francisco Bay, California. Estuaries 21, 745–753. https://doi.org/10.2307/1353278

Garofalo, D., 1980. The Influence of Wetland Vegetation on Tidal Stream Channel Migration and Morphology. Estuaries 3, 258–270. https://doi.org/10.2307/1352081

Gatto, P., Carbognin, L., 1981. The Lagoon of Venice: natural environmental trend and man-induced modification. Hydrol. Sci. Bull. 26, 379–391. https://doi.org/10.1080/02626668109490902

Ghinassi, M., Brivio, L., D'Alpaos, A., Finotello, A., Carniello, L., Marani, M., Cantelli, A., 2018. Morphodynamic evolution and sedimentology of a microtidal meander bend of the Venice Lagoon (Italy). Mar. Pet. Geol. 96, 391–404. https://doi.org/10.1016/j.marpetgeo.2018.06.011

Ghinassi, M., Ielpi, A., Aldinucci, M., Fustic, M., 2016. Downstream-migrating fluvial point bars in the rock record. Sediment. Geol. 334, 66–96. https://doi.org/10.1016/j.sedgeo.2016.01.005

Ghinassi, M., Moody, J.A., Martin, D., 2019. Influence of extreme and annual floods on point-bar sedimentation: Inferences from Powder River, Montana, USA. Bull. Geol. Soc. Am. 131, 71–83. https://doi.org/10.1130/B31990.1

Ghinassi, M., Nemec, W., Aldinucci, M., Nehyba, S., Özaksoy, V., Fidolini, F., 2014. Plan-form evolution of ancient meandering rivers reconstructed from longitudinal outcrop sections. Sedimentology 61, 952–977. https://doi.org/10.1111/sed.12081

Gobo, K., Ghinassi, M., Nemec, W., 2015. Gilbert-type deltas recording short-term base-level changes: Delta-brink morphodynamics and related foreset facies. Sedimentology 62, 1923–1949. https://doi.org/10.1111/sed.12212

Green, M.O., Coco, G., 2007. Sediment transport on an estuarine intertidal flat: Measurements and conceptual model of waves, rainfall and exchanges with a tidal creek. Estuar. Coast. Shelf Sci. 72, 553–569. https://doi.org/10.1016/j.ecss.2006.11.006

Helland-Hansen, W., Hampson, G.J., 2009. Trajectory analysis: Concepts and applications. Basin Res. 21, 454–483. https://doi.org/10.1111/j.1365-2117.2009.00425.x

Henriksen, S., Helland-Hansen, W., Bullimore, S., 2011. Relationships between shelf-edge trajectories and sediment dispersal along depositional dip and strike: a different approach to sequence stratigraphy. Basin Res. 23, 3–21. https://doi.org/10.1111/j.1365-2117.2010.00463.x

Hooke, J.M., 1984. Changes in river meanders: a review of techniques and results of analyses. Prog. Phys. Geogr. 8, 473–508. https://doi.org/10.1177/030913338400800401

Hooke, R.L.B., 1975. Distribution of sediment transport and shear stress in a meander bend. J. Geol. 83, 543–565.

Hudson, P.F., Kesel, R.H., 2000. Channel migration and meander-bend curvature in the lower Mississippi River prior to major human modification. Geology 28, 531–534. https://doi.org/10.1130/0091-7613(2000)28<531:CMAMCI>2.0.CO;2

Hughes, Z.J., 2012. Tidal Channels on Tidal Flats and Marshes, in: Davis, R.A., Dalrymple, R.W. (Eds.), Principles of Tidal Sedimentology. Springer, pp. 269–300. https://doi.org/10.1007/978-94-007-0123-6

Ielpi, A., Ghinassi, M., 2014. Planform architecture, stratigraphic signature and morphodynamics of an exhumed Jurassic meander plain (Scalby Formation, Yorkshire, UK). Sedimentology 61, 1923–1960. https://doi.org/10.1111/sed.12122

Ielpi, A., Gibling, M.R., Bashforth, A.R., Dennar, C.I., 2015. Impact of Vegetation on Early Pennsylvanian Fluvial Channels: Insight From the Joggins Formation of Atlantic Canada. J. Sediment. Res. 85, 999–1018. https://doi.org/10.2110/jsr.2015.50

Jackson, R.G.I., 1976. Depositional Model of Point Bars in the Lower Wabash River. J. Sediment. Petrol. 46, 579–594.

Kent, D. V, Rio, D., Massari, F., Kukla, G., Lanci, L., 2002. Emergence of Venice during the Pleistocene. Quat. Sci. Rev. 21, 1719–1727. https://doi.org/10.1016/S0277-3791(01)00153-6

Lagasse, P.F., Spitz, W.J.J., Zevenbergen, L.W.W., 2004. Handbook for predicting stream meander migration, National C. ed. Transportation Research Borard of the National Academies, Fort Collins, CO.

Lanzoni, S., Seminara, G., 2002. Long-term evolution and morphodynamic equilibrium of tidal channels. J. Geophys. Res. 107, 1–13. https://doi.org/10.1029/2000JC000468

Larue, D.K., Martinez, P.A., 1989. Use of bed-form climb models to analyze geometry and preservation potential of clastic facs and erosional surfaces. Am. Assoc. Pet. Geol. Bull. 73, 40–53.

Long, A.J., Waller, M.P., Stupples, P., 2006. Driving mechanisms of coastal change: Peat compaction and the destruction of late Holocene coastal wetlands. Mar. Geol. 225, 63–84. https://doi.org/10.1016/j.margeo.2005.09.004

Makaske, B., 2001. Anastomosing rivers: A review of their classification, origin and sedimentary products. Earth Sci. Rev. 53, 149–196. https://doi.org/10.1016/S0012-8252(00)00038-6

Marani, M., D'Alpaos, A., Lanzoni, S., Carniello, L., Rinaldo, A., Lanzoni, S., Carniello, L., D'Alpaos, A., Marani, M., 2007. Biologically-controlled multiple equilibria of tidal landforms and the fate of the Venice lagoon. Geophys. Res. Lett. 34, 1–5. https://doi.org/10.1029/2007GL030178

Marani, M., Lanzoni, S., Zandolin, D., Seminara, G., Rinaldo, A., Zandolin, D., Lanzoni, S., Marani, M., Rinaldo, A., 2002. Tidal meanders. Water Resour. Res. 38, 7–14. https://doi.org/10.1029/2001WR000404

Massari, F., Grandesso, P., Stefani, C., Jobstraibizer, P., 2009. A small polyhistory foreland basin evolving in a context of oblique convergence: the Venetian basin (Chattian to Recent, Southern Alps, Italy), in: Allen, P.A., Homewood, P. (Eds.), Foreland Basins. Blackwell Scientific, Oxford, pp. 141–168. https://doi.org/10.1002/9781444303810.ch7

Massari, F., Rio, D., Serandrei Barbero, R., Asioli, A., Capraro, L., Fornaciari, E., Vergerio, P.P., 2004. The environment of Venice area in the past two million years. Palaeogeogr. Palaeoclimatol. Palaeoecol. 202, 273–308. https://doi.org/10.1016/S0031-0182(03)00640-0

McClennen, C.E., Housley, R.A., 2006. Late-Holocene Channel Meander Migration and Mudflat Accumulation Rates, Lagoon of Venice, Italy. J. Coast. Res. 224, 930–945.

McGowen, J.H., Garner, L.E., 1970. Physiographic Features and Stratification Types of Coarse-Grained Pointbars: Modern and Ancient Examples. Sedimentology 14, 77–111. https://doi.org/10.1111/j.1365-3091.1970.tb00184.x

Miall, A.D., 1985. Architectural-element analysis: A new method of facies analysis applied to fluvial deposits. Earth-Science Rev. 22, 261–308. https://doi.org/10.1016/0012-8252(85)90001-7

Morris, J.T., Sundareshwar, P.V. V, Nietch, C.T., Kjerfve, B., Cahoon, D.R., 2002. Responses of coastal wetlands to rising sea leve. Ecology 83, 2869–2877. https://doi.org/10.1890/0012-

Mudd, S.M., D'Alpaos, A., Morris, J.T., 2010. How does vegetation affect sedimentation on tidal marshes? Investigating particle capture and hydrodynamic controls on biologically mediated sedimentation. J. Geophys. Res. Earth Surf. 115, F03029. https://doi.org/10.1029/2009JF001566

Nanson, G.C., Croke, J.C., 1992. A genetic classification of floodplains. Geomorphology 4, 459–486. https://doi.org/10.1080/00385417.1971.10770277

Nanson, G.C., Hickin, E.J., 1986. A statistical analysis of bank erosion and channel migration in western Canada. Geol. Soc. Am. Bull. 97, 497–504. https://doi.org/10.1130/0016-7606(1986)97<497:ASAOBE>2.0.CO;2

Pranter, M.J., Ellison, A.I., Cole, R.D., Patterson, P.E., 2007. Analysis and modeling of intermediate-scale reservoir heterogeneity based on a fluvial point-bar outcrop analog, Williams Fork Formation, Piceance Basin, Colorado. Am. Assoc. Pet. Geol. Bull. 91, 1025–1051.

Puigdefabregas, C., 1973. Miocene point bar deposits in the Ebro Basin, Northern Spain. Sedimentology 20, 133–144.

Puigdefabregas, C., Van Vliet, A., 1977. Meandering stream deposits from the Tertiary of the Southern Pyrenees. Fluv. Sedimentol. Mem. 5 5, 469–485.

Rajchl, M., Uličný, D., 2005. Depositional record of an avulsive fluvial system controlled by peat compaction (Neogene, Most Basin, Czech Republic). Sedimentology 52, 601–625.

Rieu, R., van Heteren, S., van der Spek, A.J.F., De Boer, P.L., 2005. Development and preservation of a Mid-Holocene tidal-channel network offshore the Western Netherlands. J. Sediment. Res. 75, 409–419.

Roner, M., D'Alpaos, A., Ghinassi, M., Marani, M., Silvestri, S., Franceschinis, E., Realdon, N., 2016. Spatial variation of salt-marsh organic and inorganic deposition and organic carbon accumulation: Inferences from the Venice lagoon, Italy. Adv. Water Resour. 93, 276–287.

Roner, M., Ghinassi, M., Fedi, M., Liccioli, L., Bellucci, L.G., Brivio, L., D'Alpaos, A., 2017. Latest Holocene depositional history of the southern Venice Lagoon, Italy. The Holocene 27, 1731–1744.

Silvestri, S., Defina, A., Marani, M., 2005. Tidal regime, salinity and salt marsh plant zonation. Estuar. Coast. Shelf Sci. 62, 119–130. https://doi.org/10.1016/j.ecss.2004.08.010

Smith, D.G., 1987. Meandering river point bar lithofacies models: modern and ancient examples

compared, in: Ethridge, F.G., Flores, R.M., Harvey, M.D. (Eds.), Recent Developments in Fluvial Sedimentology: Contributions from the Third International Fluvial Sedimentology Conference. SEPM Society for Sedimentary Geology, pp. 83–91.

Smith, D.G., Hubbard, S.M., Leckie, D.A., Fustic, M., 2009. Counter point bar deposits: lithofacies and reservoir significance in the meandering modern Peace River and ancient McMurray Formation, Alberta, Canada. Sedimentology 56, 1655–1669. https://doi.org/10.1111/j.1365-3091.2009.01050.x

Stefanon, L., Carniello, L., D'Alpaos, A., Rinaldo, A., 2012. Signatures of sea level changes on tidal geomorphology: Experiments on network incision and retreat. Geophys. Res. Lett. 39, 1–6.

Terwindt, J.H.J., 1988. Palaeotidal reconstructions of inshore tidal depositional environments, in: De Boer, P.L., van Gelder, A., Nio, S.-D. (Eds.), Tide-Influenced Sedimentary Environments. pp. 233–263.

Toonen, W.H.J.J., Kleinhans, M.G., Cohen, K.M., 2012. Sedimentary architecture of abandoned channel fills. Earth Surf. Process. Landforms 37, 459–472. https://doi.org/10.1002/esp.3189

Törnqvist, T.E., Wallace, D.J., Storms, J.E.A., Wallinga, J., Van Dam, R.L., Blaauw, M., Derksen, M.S., Klerks, C.J.W., Meijneken, C., Snijders, E.M.A., 2008. Mississippi Delta subsidence primarily caused by compaction of Holocene strata. Nat. Geosci. 1, 173–176. https://doi.org/10.1038/ngeo129

Tosi, L., Rizzetto, F., Bonardi, M., Donnici, S., Serandrei-Barbero, R., Toffoletto, F., 2007. Note Illustrative della Carta Geologica d'Italia alla scala 1:50.000. foglio 148-149, Chioggia-Malamocco.

van Asselen, S., 2011. The contribution of peat compaction to total basin subsidence: Implications for the provision of accommodation space in organic-rich deltas. Basin Res. 23, 239–255.

van Asselen, S., Stouthamer, E., Smith, N.D., 2010. Factors Controlling Peat Compaction in Alluvial Floodplains: A Case Study in the Cold-Temperate Cumberland Marshes, Canada. J. Sediment. Res.

van de Lageweg, W.I., Schuurman, F., Cohen, K.M., van Dijk, W.M., Shimizu, Y., Kleinhans, M.G., 2016. Preservation of meandering river channels in uniformly aggrading channel belts. Sedimentology 63, 586–608. https://doi.org/10.1111/sed.12229

Wightman, D.M., Pemberton, S.G., 1997. The Lower Cretaceous (Aptian) McMurray Formation; an overview of the Fort McMurray area, northeastern Alberta, in: Pemberton, S.G., James, D.P. (Eds.), Petroleum Geology of the Cretaceous Mannville Group, Western Canada. Memoir - Canadian Society of Petroleum Geologists. pp. 312–344.

Willis, B.J., Tang, H., 2010. Three-Dimensional Connectivity of Point-Bar Deposits. J. Sediment. Res. 80, 440–454. https://doi.org/10.2110/jsr.2010.046

Zecchin, M., Baradello, L., Brancolini, G., Donda, F., Rizzetto, F., Tosi, L., 2008. Sequence stratigraphy based on high-resolution seismic profiles in the late Pleistocene and Holocene deposits of the Venice area. Mar. Geol. 253, 185–198. https://doi.org/http://dx.doi.org/10.1016/j.margeo.2008.05.010

Zecchin, M., Brancolini, G., Tosi, L., Rizzetto, F., Caffau, M., Baradello, L., 2009. Anatomy of the Holocene succession of the southern Venice lagoon revealed by very high-resolution seismic data. Cont. Shelf Res. 29, 1343–1359. https://doi.org/10.1016/j.csr.2009.03.006

Zecchin, M., Tosi, L., Caffau, M., Baradello, L., Donnici, S., 2014. Sequence stratigraphic significance of tidal channel systems in a shallow lagoon (Venice, Italy). The Holocene 24, 646–658.

CHAPTER 3

AN INTEGRATED APPROACH TO DETERMINE ACCRETION GEOMETRIES OF TIDAL POINT BARS: EXAMPLES FROM THE VENICE LAGOON

PAPER

Marta Cosma[a], Na Yan[b], Luca Colombera[b], Nigel P. Mountney[b], Andrea D'Alpaos[a] Massimiliano Ghinassi[a]

[a] Department of Geosciences, University of Padova, Padova, Italy

[b] Fluvial & Eolian Research Group, School of Earth & Environment, University of Leeds, Leeds, UK

1. ABSTRACT

Low rates of lateral migration (e.g. cm – dm/year) combined with relatively high rates of vertical accretion (e.g. mm – cm/year) recorded in microtidal channels of the Venice Lagoon (Italy) give rise to point-bar geometries and internal facies arrangements that differ substantially from widely accepted models of point-bar sedimentary architecture. This can affect inter-bar connectivity, with relevant implications for exploitation of water and hydrocarbon reservoirs. In this study, field-derived data from the Venice Lagoon are combined with a three-dimensional forward stratigraphic model – the 'Point-Bar Sedimentary Architecture Numerical Deduction' (PB-SAND) – to predict the stratal geometries of tidal point bars formed in aggradational salt-marsh settings. PB-SAND uses a combined geometric and stochastic modelling approach that can be constrained by field evidence. The model is applied herein to determine the geometry and internal sedimentary facies distribution of four microtidal point bars generated by 9 to 11 m-wide and 0.5 to 1.6 m-deep channels cutting through salt marshes. An iterative best-fit modelling approach is used to obtain multiple simulations for each case-study example, each of which fit the observations derived from the analysis of a time series of historical aerial photos and forty-four sedimentary cores. Modelling results demonstrate how the geometry of the studied bars is determined principally by the development of two key stratal surfaces: bar brink and channel thalweg surfaces. These two surfaces are defined by the progressive translation and vertical shift of the bar brink (i.e. break-of-slope between bar top and bar slope) and the channel thalweg (i.e. deepest part of the channel) at different stages of bar evolution. The approach is used to: (i) reconstruct 3D point-bar geometries; (ii) propose alternative three-dimensional reconstructions; (iii) provide insight to drive the acquisition of additional data to better constrain the proposed models, and (iv) provide insights into the mechanisms of bar growth for slowly migrating channels in settings subject to relatively high rates of aggradation.

Keywords: tidal meanders, aggradation, bar-brink trajectory, channel-thalweg trajectory, Venice Lagoon

2. INTRODUCTION

The influence of vertical aggradation in shaping point-bar bodies is commonly considered to be negligible with respect to lateral migration processes. Hence, point bars are commonly described as purely laterally accreting bodies (e.g., Fisk, 1944; McGowen and Garner, 1970; Bridges and Leeder, 1976; Jackson, 1976; Miall, 1985; Smith, 1987; Durkin et al., 2015; Colombera et al., 2017) with a tabular external geometry, in which the point-bar brink (i.e. the break between bar top and bar slope) and the channel thalweg (i.e. the deepest part of the channel) are considered to shift horizontally and parallel to one another toward the channel outer bank. However, studies that document the lateral and vertical shift of both the bar brink and channel thalweg (De Mowbray, 1983; Nanson and Croke, 1992; Wightman and Pemberton, 1997; Makaske, 2001; Rajchl and Uličný, 2005; Rieu et al., 2005; Ghinassi et al., 2014; Fielding, 2015; Ielpi et al., 2015; Brivio et al., 2016; Candel et al., 2017; Boaga et al., 2018; Finotello et al., 2018; Cosma et al., 2019), suggest that, where the rate of aggradation is high (e.g. mm – cm/year) relative to the rate of lateral channel migration (e.g. cm – dm/year), geometries of resulting point-bar bodies can strongly differ from those of classical tabular sedimentary bodies. Development of point-bar geometries, and their internal stratal architectures, are also influenced by the different styles of bar planform evolution (Willis and Tang, 2010; Ghinassi et al., 2013, 2016; Yan et al., 2017; Willis and Sech, 2019a). However, even though planform transformations of meander bends (i.e. expansion, rotation, translation and combinations thereof) are well known (Daniel, 1971; Brice, 1974; Jackson, 1976; Nicoll and Hickin, 2010), the relationship between these transformations and resulting sediment-body architecture remains relatively under-explored (Fustic et al., 2012;

Ghinassi et al., 2014; Durkin et al., 2015; Johnston and Holbrook, 2019; Russell et al., 2019).

It follows that only a precise understanding of the interplay between planform transformation and vertical shift of the channel system can reveal the effective three-dimensional geometry of point-bar bodies. Prior studies of modern migratory channels and ancient deposits have not yet comprehensively addressed this issue. Scroll patterns of modern meanders provide clear evidence for their planform transformations, but related deposits are usually known only through one- or two-dimensional data from core and geophysical analysis (e.g., Clift et al., 2018). Vice versa: the stratigraphic record provides information on bar architecture, but in most cases the history of channel planform evolution is not evident. Exceptions to this are in cases where 3D seismic data (Smith et al., 2009; Musial et al., 2011) or rare planform exposures of ancient outcropping successions are available (e.g., Ielpi and Ghinassi, 2014; Bhattacharyya et al., 2015; Ghinassi and Ielpi, 2015; Wu et al., 2015; Swan et al., 2019).

Numerical models have contributed to our understanding of point-bar deposits resulting from interaction between planform and vertical styles of channel shifts (e.g., van de Lageweg et al., 2016). Such models demonstrate how vertical aggradation influences whether coarse-grained deposits (i.e. channel lag or lower bar deposits) of adjacent bar bodies are connected (Willis and Tang, 2010; Willis and Sech, 2019b), with notable implications for hydrocarbon recovery. Nevertheless, it is difficult to capture the complex interactions between flow dynamic, sediment transport, bank erosion and bar formation without the need to (i) develop an extremely intricate model, which is highly demanding in computation terms, or (ii) rely on a simplistic model, which has poor applicability to real-case examples.

The Point-Bar Sedimentary Architecture Numerical Deduction (PB-SAND) is a forward stratigraphic model (Yan et al., 2017, 2019a, 2019b; Colombera et al., 2018) that uses

input on channel planform and facies, together with current understanding of relations between meander-bend planform evolution and facies organization, to predict the three-dimensional architecture arising from the evolution of point-bar bodies in response to channel migration. PB-SAND can be constrained by data from ancient deposits and modern systems (e.g. remote sensing imagery, seismic data, cores and well logs). PB-SAND is not process-oriented, and its input cannot be specified in terms of specific controlling factors on sedimentary processes; rather, it employs a primarily geometric-based modelling approach, which produces predictive three-dimensional architectural and facies-distribution models associated with specific planform evolution styles (Yan et al., 2017). Values representative of certain types of point-bars and their deposits are obtained from real-world datasets, typically held in a large database of example types (cf. Colombera et al., 2012, 2013). This modelling approach allows the model to be applied to depict the expected form and behaviour of tidal meander bends and related point bar deposits.

PB-SAND is here parameterized with sedimentological evidence published by a recent study (Cosma et al., 2019) from the Venice Lagoon (Italy), where tidal point bars resulted from a depositional setting where the rate of aggradation (mm – cm/year) is high relative to the rate of lateral channel migration (cm – dm/year).

The aim of this study is to improve current understanding of the mutual role of lateral migration and vertical aggradation on meander dynamics and resultant point-bar stratal architecture. Four case studies of tidal meanders with variable bend geometries are modelled to generate representations of the expected three-dimensional architecture of the accumulated point-bar bodies. Results from the analyses presented herein provide insight with which to better understand bar geometries generated by lateral channel shifts in highly aggradational depositional settings more generally (cf. Candel et al., 2017), and of either tidal or fluvial origin. The specific objectives of this study are as follows: (i) to predict point-bar geometries developed under the active interplay

between aggradation and planform transformation; (ii) to define three-dimensional expression of bar brink and channel thalweg latero-vertical shifts; (iii) to test and discuss the results generated by the model in comparison with field evidence; (iv) to establish typology and amount of data required to confidently determine the 3D architecture of a bar; and (v) to better understand the mechanism of bar growth in relatively high aggradational settings for which current point-bar models are not especially applicable.

3. GEOLOGICAL SETTING

The Venice Lagoon, located along the north-eastern coast of Italy (Fig 1A), represents the largest brackish basin of the Mediterranean Sea, with a longshore length and a width of ~50 km and ~10 km, respectively. It is a shallow microtidal basin, characterized by a mean water depth of tidal flats and subtidal platforms of ~1.5 m and a semidiurnal tidal regime with an average range of ~1.0 m. The lagoon is connected to the sea through three inlets: Lido, Malamocco and Chioggia (Fig 1A).

The Venice Lagoon was formed by the Holocene marine transgression (Amorosi et al., 2008; Zecchin et al., 2008, 2014) in the Venetian plain, a foreland basin comprised between the Apennine and South Alpine chains (Massari et al., 2009). After the Last Glacial Maximum (LGM), the northern Adriatic shelf was a low-gradient alluvial plain, cut through by an extensive network of fluvial channels. During the Holocene, the area was progressively flooded with the formation and drowning of barrier-lagoon systems located in progressively more landward positions (Trincardi et al., 1994; Amorosi et al., 2008; Storms et al., 2008; Ronchi et al., 2018). In this framework, the Venice Lagoon began to form about 7500 yrs BP (Zecchin et al., 2009). The lagoonal deposits are up to 20 m thick and consist of organic-rich mud with isolated sand bodies, which are mainly

tidal or fluvio-tidal in origin (Madricardo et al., 2007, 2012; Zecchin et al., 2009, 2014; Madricardo and Donnici, 2014).
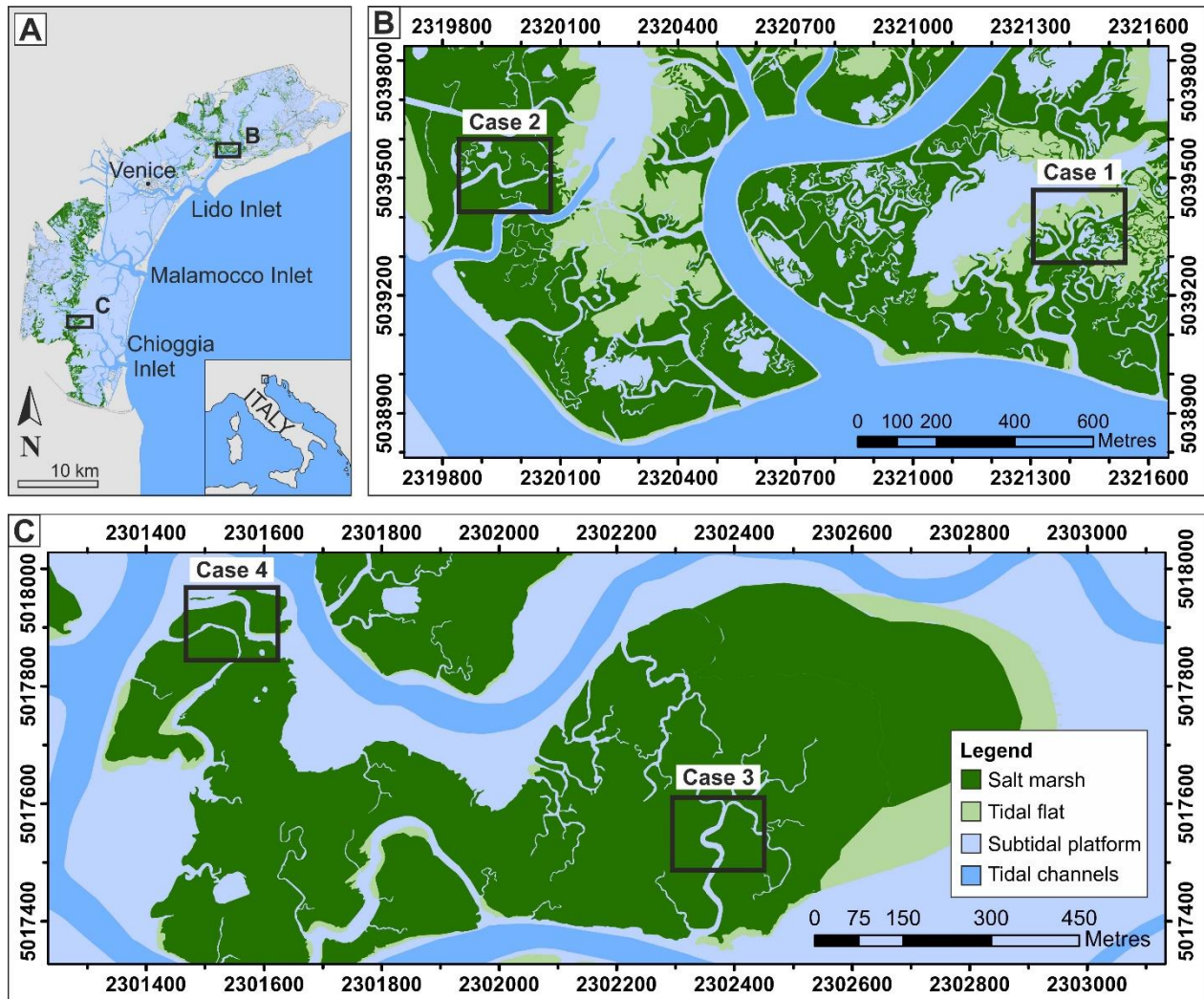
Figure 1. Study sites. (A) Location of the Venice Lagoon along the northeastern coast of Italy. (B and C) Location of the study sites in the northern (Cases 1 and 2) and southern (Cases 3 and 4) Venice Lagoon, respectively.

The present-day configuration of the lagoon is characterized by the presence of sparse salt marshes that have been rapidly eroding in the last two centuries (Tommasini et al., 2019), wide subtidal platforms, and tidal flats that are cut by intertidal and subtidal channels (Fig 1A). Salt marshes, mainly located in the northeastern and southwestern portions of the lagoon, occur at ca. 5 – 50 cm above mean sea level (Silvestri et al., 2005;

Roner et al., 2016, 2017) and their accumulation has kept pace with the increasing rates of relative-sea level rise through organic and inorganic accumulation (e.g. D'Alpaos & Marani, 2016). In the 20th century, salt-marsh accretion rates were about 0.07 - 0.66 cm/yr and 0.03 – 1.50 cm/yr in the northern (Bellucci et al., 2007) and southern (Bellucci et al., 2007; Roner et al., 2017) lagoon, respectively.

The study meander bends occur in the intertidal zone and are located in the northern (Cases 1 and 2, Fig 2C, 2D and 2E) and southern (Cases 3 and 4, Fig 2B, 2F and 2G) Venice Lagoon (Cosma et al., 2019). Channels are 9 to 11 m wide and 0.5 to 1.6 m deep. The radius of curvature ranges between 11 and 21 m, and all the study channels show a "simple symmetric" (*sensu* Brice, 1974) planform geometry. Channel bottoms are covered by 0.1 to 0.3 m of water at the lowest tide, whereas up to 0.5 m of water can cover overbank marshes at the highest tides.

4. DATA & METHODS

4.1. Remote sensing and field data

Morphological characterization and reconstruction of the history of planform evolution of the studied meanders was undertaken by analysing and comparing historical aerial

photographs (1955, 1968 and 1969) with satellite images acquired in 2014 via Google Earth software. Aerial photographs and satellite images were georeferenced using ArcGIS 10.4 (Esri, Redlands, CA, USA) with an accuracy of ~1 m and ~0.5 m, respectively. Superimposition of the different images allowed evaluation of the lateral shifts of the studied channel bends. Radiometrically constrained aggradation rates for the study areas were obtained from published data (Bellucci et al., 2007; Roner et al., 2017).

A total of forty-four sedimentary cores, each up to 3.0 m deep, were recovered from the different point bars (Fig 2). The location and spacing of the cores were limited by the site accessibility. For study case 3, cores were recovered only along the axis of the bar (Fig 2E). For cases 1 and 4, two additional cores were recovered along the inner bank in a seaward and landward position with respect to the bend apex (Fig 2A and 2G). Finally, for case 2, additional cores were also recovered along four radial transects (Fig 2C). The position of the cores was determined using differential GPS TOPCON GR-3 receivers – dual frequency (L1/L2) and dual constellation NavStar/Glonass with integrated Tx/Rx UHF radio. To prevent sediment compaction, cores were recovered using an Eijkelkamp hand auger, with a 1.0 m-long gouge sampler which has a diameter of 30 mm. Core sediment samples were kept humid in PVC liners, and then cut longitudinally, photographed and measured following basic principles of facies analyses. Particular attention was paid to the identification of features that could represent the preserved expression of the point-bar brink and of the channel thalweg zones in the cored sediments. The point-bar brink was placed where the inclination of the laminae changed from horizontal (i.e. bar-top deposits) to inclined (i.e. bar-slope deposits). Uncertainty associated with placement of the brink position was 5 to 10 cm (vertically in the cores), due to the gradual nature of the change in the inclination of the laminae. By contrast, the channel thalweg was precisely placed and corresponded to the bounding surface directly underlying the channel-lag deposits. Lateral correlation between adjacent cores was used to reveal 2D point-bar cross-sections along different transects, and for which bar trajectories were defined based on shifts in position and elevation of bar brink and channel thalweg.
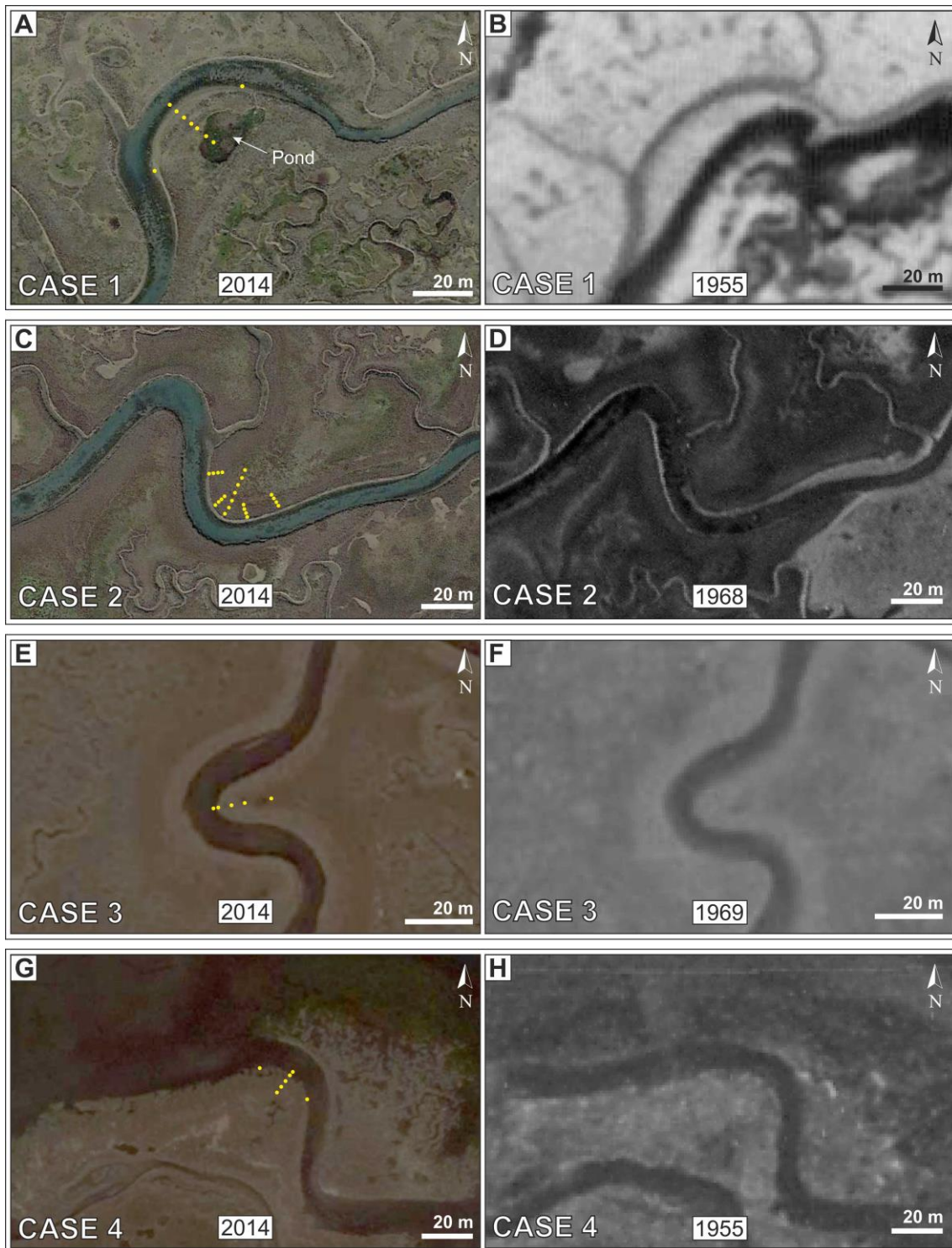
Figure 2. Satellite images (left) and aerial photos (right) used for remote sensing analysis. (A, C, E and G) Satellite images showing the studied meander bends in 2014. (B, D, F and H). Aerial photos showing the bends in 1955 (Cases 1 and 4), 1968 (Case 2) and 1969 (Case 3). The yellow spots indicate the position of the recovered cores for each meander.

4.2. Numerical Modelling

An iterative best-fit modelling approach has been used to create different realizations for each case study, based on comparison with observations derived from the analysis of aerial photos and cores. PB-SAND is a forward numerical model which employs a dominantly geometric-based modelling approach, supported by stochastic- and process-based techniques to model the sedimentary architecture of point bars and meander belts (Yan et al., 2017). The model uses vector-based and grid-free algorithms, and is able to incorporate different meander-bend transformation behaviours (expansion, translation, rotation and combinations thereof) with various sedimentary facies distributions and different aggradational conditions. PB-SAND can be readily applied to tidal meanders and point bars as a product-oriented numerical model. A brief overview of the model is provided below; a more detailed description of the modelling framework is provided by Yan et al. (2017).

The forward stratigraphic modelling of point bars using PB-SAND is performed in two steps (Fig 3A): first, the planform evolution of the study meander is simulated; second, the geometry and distribution of sedimentary facies are modelled along cross sections in any direction. The user controls these two steps through a series of input parameters, summarized in Figure 3A. In particular, the point-bar planform evolution is determined by its evolutionary transformation style, by the positions of the channel centreline at significant time steps during meander evolution (notably, at channel inception and at time steps associated with temporal transition from one planform transformation style to another), and by the number of channel centrelines that are required to simulate accretion between these key time steps. These centrelines, which are used to define accretion surfaces in 3D, are linearly interpolated from the channel centrelines at the key time steps. Changing the number of centrelines being modelled determines the size and geometry of accretion packages in a certain portion of the point-bar body and of the

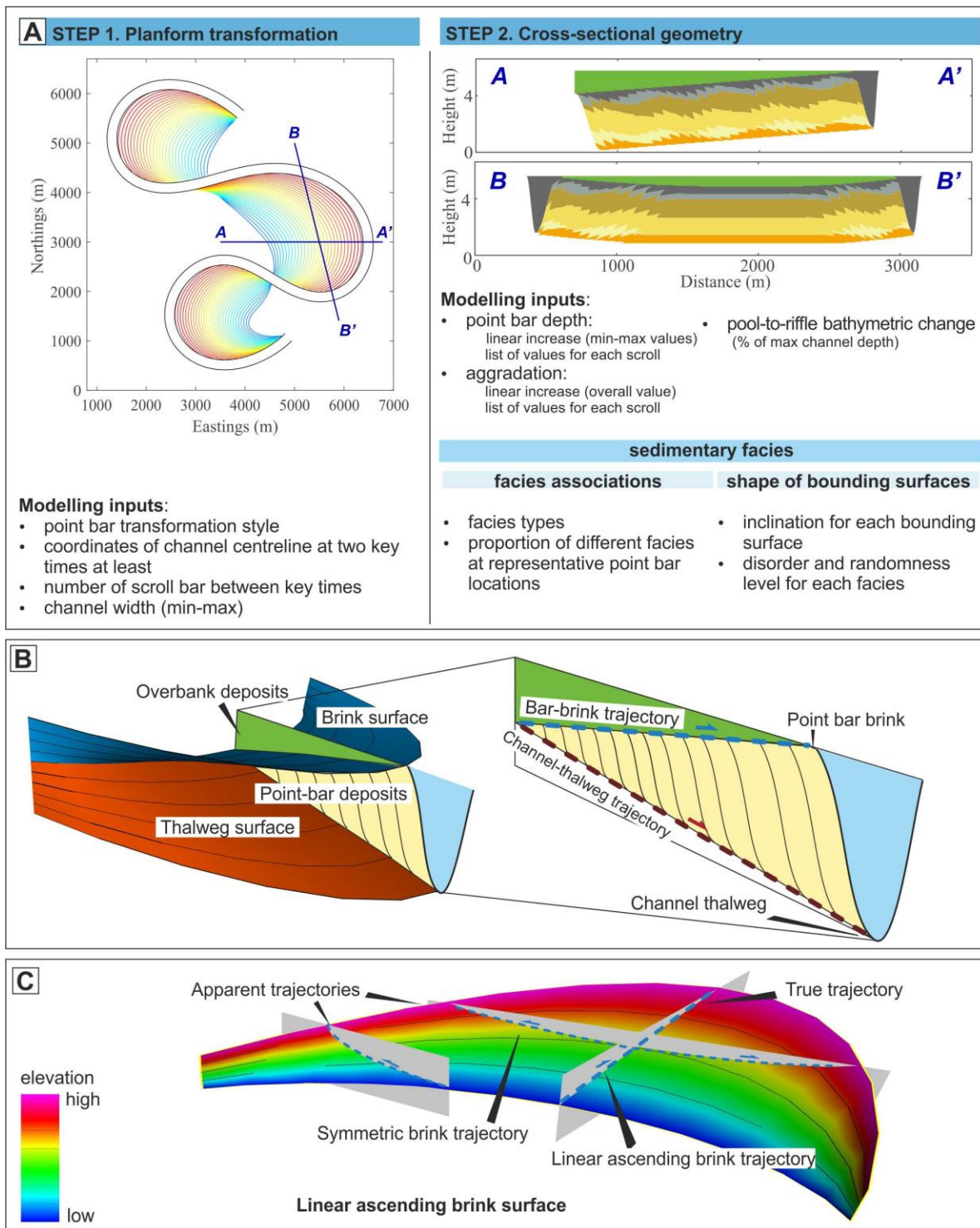Figure 3. PB-SAND workflow and terminology. (A) PB-SAND models the sedimentary architecture of point bars in two steps, reconstructing the planform evolution first, and then the geometry and distribution of sedimentary facies along cross sections (modified after Yan et al., 2019a). (B) Definition diagram for point-bar brink and thalweg surfaces. (C) Example of bar-brink surface and trajectories resulting from point-bar expansion.

sedimentary facies therein, since an accretion package is constrained by two consecutive centrelines. The internal anatomy of point-bar accretion packages is modelled during the follow-on modelling procedure, which constitutes the above-mentioned second step. The spatial distribution of facies is inherently linked to the transformation style of a meander. For example, it is possible to prescribe a transition between sandy point-bar deposits and muddy counter-point-bar deposits (Smith et al., 2009; Ghinassi et al., 2016; Durkin et al., 2019). PB-SAND can also incorporate types of facies variations that are commonly seen in point-bar deposits, such as fining upward, fining outward and fining downstream trends.

Accretion packages are also constrained by the geometry of the channel (width and maximum bankfull depth) and by rate of aggradation (Fig 3A). Temporal variations in channel width and depth can be simulated deterministically, and these give rise to spatial variations in the anatomy of the point-bar body. The model is also capable of accounting for streamwise variations in channel bathymetry, based on specified relative depths of riffle and pool areas, which themselves can vary as a function of channel sinuosity.

Aggradation is modelled through the progressive vertical offset of the channel, which translates to increases in the relative elevation of the point-bar packages at each time step, and can follow a linear behaviour or any other trend chosen by the user (Yan et al., 2019a). Two surfaces can be traced that represent the 3D envelopes of the positions occupied through time by the channel thalweg and the bar brink, respectively; the difference in their vertical elevation corresponds to the thickness of the point bar (Fig 3B). The ratio between rate of lateral shift and vertical aggradation of the brink zone will define geometry of the surface capping the bar, which is herein named the brink surface, and is covered by overbank deposits (Fig 3B). Intersection between this surface and vertical cross sections (Fig 3B) defines the bar-brink trajectory (*sensu* Brivio et al., 2016). Similarly, the ratio between lateral and vertical shift, either upward or downward, of the

thalweg defines the geometry of the thalweg surface (Fig 3B), which corresponds to the effective base of the bar body. Intersection between the thalweg surface and vertical cross sections defines the thalweg trajectory (*sensu* Brivio et al., 2016), which is considered as an apparent trajectory if the section is oblique to the effective direction of channel shift (Fig 3C). Planform evolution of the meander bend will control shape and symmetry of brink and thalweg surfaces (e.g. pure expansion will generate surfaces symmetric to the bar axis, Fig 3C). Modelled point bars are populated with different sedimentary facies. Constraints set by the user include: (i) definition of the different lithofacies (as informed by the sediment cores); (ii) the proportion and vertical succession of facies (again informed by the cores); and (iii) the spatial variation of facies with respect to the different planform transformation types (i.e. expansion, translation, rotation and combinations thereof), and the shape of facies bounding surfaces defined by changes in the trajectories of the bar brink and the thalweg (Fig 3A).

5. RESULTS

5.1. Point-bar deposits

Four main types of deposits have been recognized in the studied successions: substrate, channel-lag, point-bar and salt-marsh deposits. A brief description and interpretation of each deposit can be found in table 1. Because the main focus of this analysis is to quantify point-bar geometry and relate it to the known history of aggradation and planform transformation, the sedimentological analysis has focused mainly on the identification of the bar brink and thalweg, whose trajectories are required for the quantitative reconstruction of the evolution of bar geometries. Further details on the deposits can be found in Cosma et al. (2019).

Name	Description	Interpretation	Photos
Salt Marsh	Overlying point bar and substrate deposits. Brownish, oxidized mud with 1-3 mm thick horizontal well-sorted sandy laminae, in situ roots, wood fragments and bioturbation. Maximum thickness ranges from 1.94 to 0.31 m. Along axial transects, thickness decreases toward the channel.	Oxidation and root presence are indicative of frequent subaerial exposure (*Silvestri et al., 2005*). Mud is deposited by fallout during high slack water. Sandy laminae sorting suggests winnowing of finer particles probably due to wave action during storm events.	
Point Bar	Gradational lower and upper boundaries with channel lag and salt marsh deposits, respectively. From mud to fine sand clinostratified deposits up to 2.30 m thick. Frequently massive toward the base. More clear inclined heterolithic stratification toward the top with well-sorted very fine to fine sand or plant debris laminae dipping channelward between 5° to 25° alternating with mud. Laminae inclination decreases toward the top. Widespread bioturbation often prevents identification of sedimentary structures.	Clinostratification points out the deposition of sediment as a consequence of channel lateral shift. In the heterolithic stratification, abundance of mud reflects the prevalence of fallout processes, probably related to slack water periods (*Carniello et al., 2011*) while the well-sorted laminae are the result of entrainment of finer material probably due to wave-winnowing during storm events (*Choi and Jo, 2015*). Decreasing of laminae inclination toward the top reflects bar slope topography.	
Channel Lag	Erosionally overlying substrate deposits and grading upward toward point bar deposits. 5-20 cm thick massive layer of silt to medium sand. Shells, shell fragments, pebble-sized rounded mud clasts and plant debris are common.	Deepest part of the channel with the erosional surface and the concentration of coarser sediments and shells. Pebble-sized mud clasts are formed by comminution of collapsed bank blocks (*Terwindt, 1988*).	
Substrate	Two different types: 1) alternation of well-sorted medium to very fine sand layers and dark, organic-rich muddy layers with shell and plant debris fragments. Pervasive bioturbation prevents detection of sedimentary structures. 2) comminute dark brown to black plant debris with a minimum amount of dispersed mud with abundant reeds and reed fragments.	1) tidal flat/subtidal environment (Cases 1 and 2). Sandy layer formed because of wave-winnowing during storm events (*Carniello et al., 2009*). Muddy layers settled from suspension during fair weather period. 2) peat deposits (Cases 3 and 4) consistent with wetland setting (*Bondesan and Meneghel, 2004*).	

Table 1. Deposits of the study sites. References for the interpretation (Terwindt, 1988; Bondesan and Meneghel, 2004; Silvestri et al., 2005; Carniello et al., 2009, 2011; Choi and Jo, 2015).

5.2. Case studies

In the following sections, the main results are described for each case study focusing on: (i) channel planform transformations (as revealed by historical aerial and satellite imagery); (ii) bar-brink and channel-thalweg trajectories (i.e. core analyses); and, (iii) PB-SAND realizations. The availability of remote-sensing data and field-derived data used to constrain the models becomes progressively more limited from Case 1 to Case 4.

5.2.1. Case 1

The comparison between aerial photos (Figs 2A, 2B and 4A) shows that the bend expanded during the last six decades, and that the channel width increased from 5 to 10 m. This expansion allowed the inner bank to shift laterally by ca. 14 m. In 1955, the channel cut through a tidal flat (Fig 2A), and in the following decades halophytic vegetation progressively colonized most of the area growing from the channel margins (Fig 2B).

Brink and thalweg trajectories have been reconstructed along the axial cross section (Fig 4B). The brink depth progressively decreases from 0.3 m in the inner part of the bar to zero at the bar edge, portraying a linear ascending trajectory. The thalweg trajectory shows an initial descending section, followed by a sub-horizontal reach (Fig 4B). The point-bar thickness increases channel-ward from 0.60 (core 1) to 1.26 m (core 6) (Fig 4B). The bar thickness is ca 1.26 m in the landward side of the bar (core 8) and at the bar apex (core 6), and ca 1.90 m in the seaward side (core 9). This increase in bar thickness is probably associated with the presence of a confluence in correspondence of the core site in 1955 (Fig 4A).

Historical aerial photos and sedimentary cores provide robust evidence to reconstruct the planform evolution of the bar and geometries of the related brink and thalweg surfaces. Thanks to these constraints, running a single PB-SAND model is sufficient to

successfully simulate the evolution of the bar, via expansion under the influence of a linear rate of aggradation (Fig 4C).

Figure 4. Case 1 results. (A and B) Results from remote sensing and core analysis, showing the planform evolution of the meander bend (A) and bar-brink and channel-thalweg trajectories along the axial cross section (B). (C) PB-SAND modelling results of realization 1, showing the expansional evolution of the meander bend developed under linear aggradational conditions and the resultant three-dimensional geometry of the point bar. Vertical exaggeration: x2.

To match the available core data, the channel depth within the model is set to increase from 0.90 to 1.25 m to simulate the trajectory of the thalweg. This realization accurately reproduced the geometries of the studied bar, along with brink and thalweg surfaces,

which appear to show a symmetric concavity. As a consequence, in a section parallel to the bend axis (sections a, b and c in Figure 4C), the brink trajectory ascends linearly, whereas, in a section transverse to the bend axis, it shows a symmetric concave geometry (sections d and e in Figure 4C). The thalweg trajectory, except for an initial marked descending shift, shows a horizontal trend (Fig 4C).

5.2.2. Case 2

The comparison between the 1968 and 2014 aerial photographs (Figs 2C, 2D and 5A) shows that this channel maintained a constant width while undergoing asymmetric expansion. The amount of channel shift varied along the bend. Along the landward side of the bend, lateral shift ranged between ca. 1.1 m and 2.5 m, whereas in the apex zone it was ca. 3-4 m and decreased to zero at the seaward inflection point (Fig 5A). Cores show that brink depths vary between 0.74 to 0.20 m from bar top. The surface defined by the lateral shift of the bar brink has an asymmetric shape with respect to the bar axis, is deeper and sub-horizontal in the landward part of the bar, and is shallower and with ascending trajectory in the seaward part (Fig 5B). Along the axial cross section, the bar-brink trajectory shows a linear ascending pattern (Fig 5C). Thalweg depths (Fig 5B) vary from 2.20 to 1.38 m from the bar top. In the active channel, the thalweg depth varies from 1.00 to 1.61 m in the riffle and pool areas, respectively. The shallowest thalweg depths are located in the innermost part of the bar. Moving radially away from this point toward the active channel thalweg, a general descending and then ascending trajectory trend is evident (Fig 5B). These trends are also clear on the axial cross section (Fig 5C). Point-bar thickness varies from 0.64 to 1.70 m.

Considering that bend expansion can occur in combination with other planform transformations (Jackson, 1976), three realizations were performed by PB-SAND to represent different transformation scenarios (Fig 5D): (i) pure expansion; (ii) expansion combined with seaward rotation; and (iii) expansion combined with translation. In all
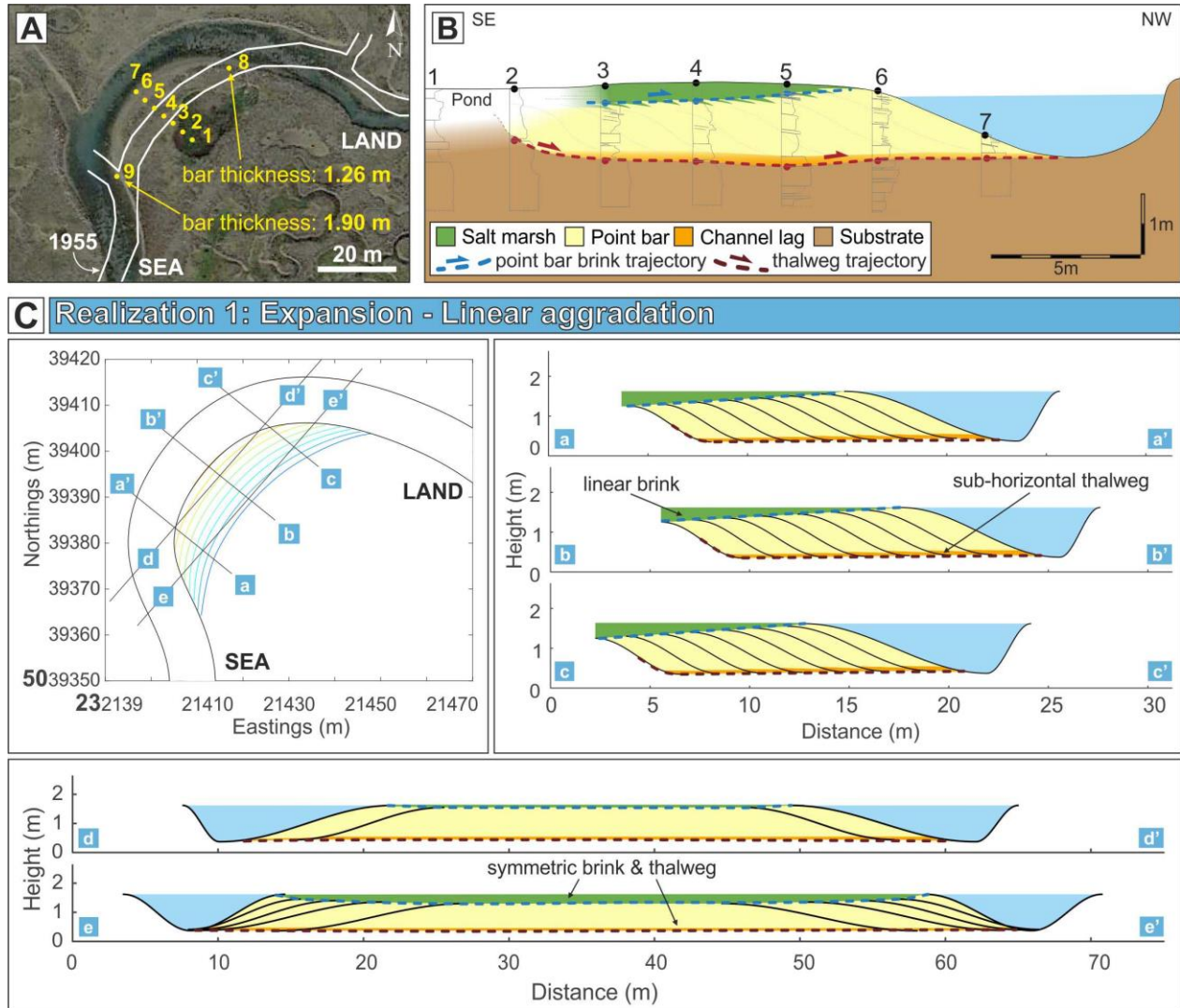
Figure 5. Case 2 results. (A, B and C) Results from remote sensing and core analysis, showing the planform evolution of the meander bend (A), bar-brink and channel-thalweg depths resulting from core analysis (B) and trajectories along the axial cross section (C). (D, E and F) PB-SAND modelling results of realizations 1, 2 and 3, respectively, developed under linear aggradational conditions. (D) Realization 1: expansional evolution of the meander bend and three-dimensional geometry of the point bar. (E) Realization 2: expansional and rotational evolution of the meander bend and resultant three-dimensional geometry of the point bar. →
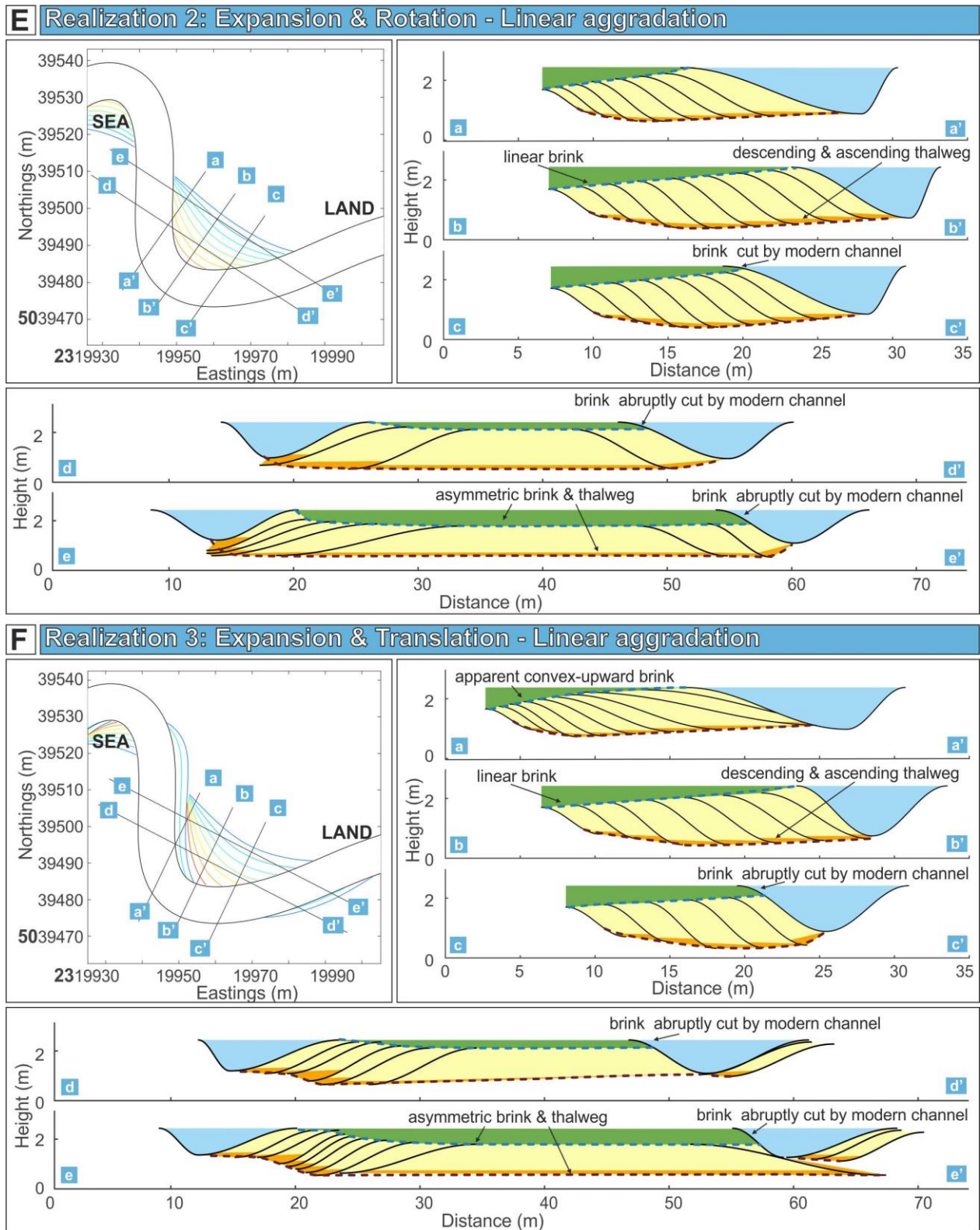
(cont. Fig. 5) (F) Realization 3: expansional and translational evolution of the meander bend and resultant three-dimensional geometry of the point bar. Vertical exaggeration: x2.

three realizations, a linear rate of aggradation is used. Channel depth is increased markedly, from 1.0 to 1.6 m, and then gradually, from 1.6 to 1.7 m, to simulate the trajectory of the thalweg. The resulting point-bar brink and thalweg trajectories are depicted in Figure 5D, E and F (realizations 1-3). In realization 1 (Fig 5D), both brink and thalweg surfaces show symmetric concavity. As a consequence, in sections parallel to the bend axis, brink trajectories rise linearly from the innermost part of the bar toward the channel (sections a – c in Figure 5D), and thalweg trajectories descend slightly and then ascend toward the currently active channel (sections a – c in Figure 5D). Accordingly, in sections that are transverse to the bend axis, both thalweg and brink trajectories show a symmetric concave-upward geometry (sections d – e in Figure 5D). In realization 2 (Fig 5E), the seaward rotational component makes brink and thalweg surfaces asymmetric with respect to the bend axis. In the seaward side of the bar, the brink surface gradually rises toward the present-day bar brink, whereas along the landward side, it is abruptly cut by the modern channel which shifted toward the bar through rotational expansion. In realization 3 (Fig 5F), the combination of expansion with seaward translation produced erosion of the brink surface along the landward side of the bar, whereas in the seaward part of the bar a gradually ascending pattern toward the present-day brink is preserved. Realizations 2 and 3 are considered to be the most realistic, because they better explain the asymmetry of the thalweg surfaces, together with the erosion of the brink surface along the landward side of the bar.

5.2.3. Case 3

The comparison between the 1969 and 2014 aerial photos does not show any substantial variation in either the planform morphology of the bend or of the channel width (Figs 2E, 2F and 6A), indicating an extremely low migration rate.

Brink and thalweg trajectories have been reconstructed along the axial cross section (Fig 6B). The brink depth progressively decreases from 1.10 m in the innermost part of the
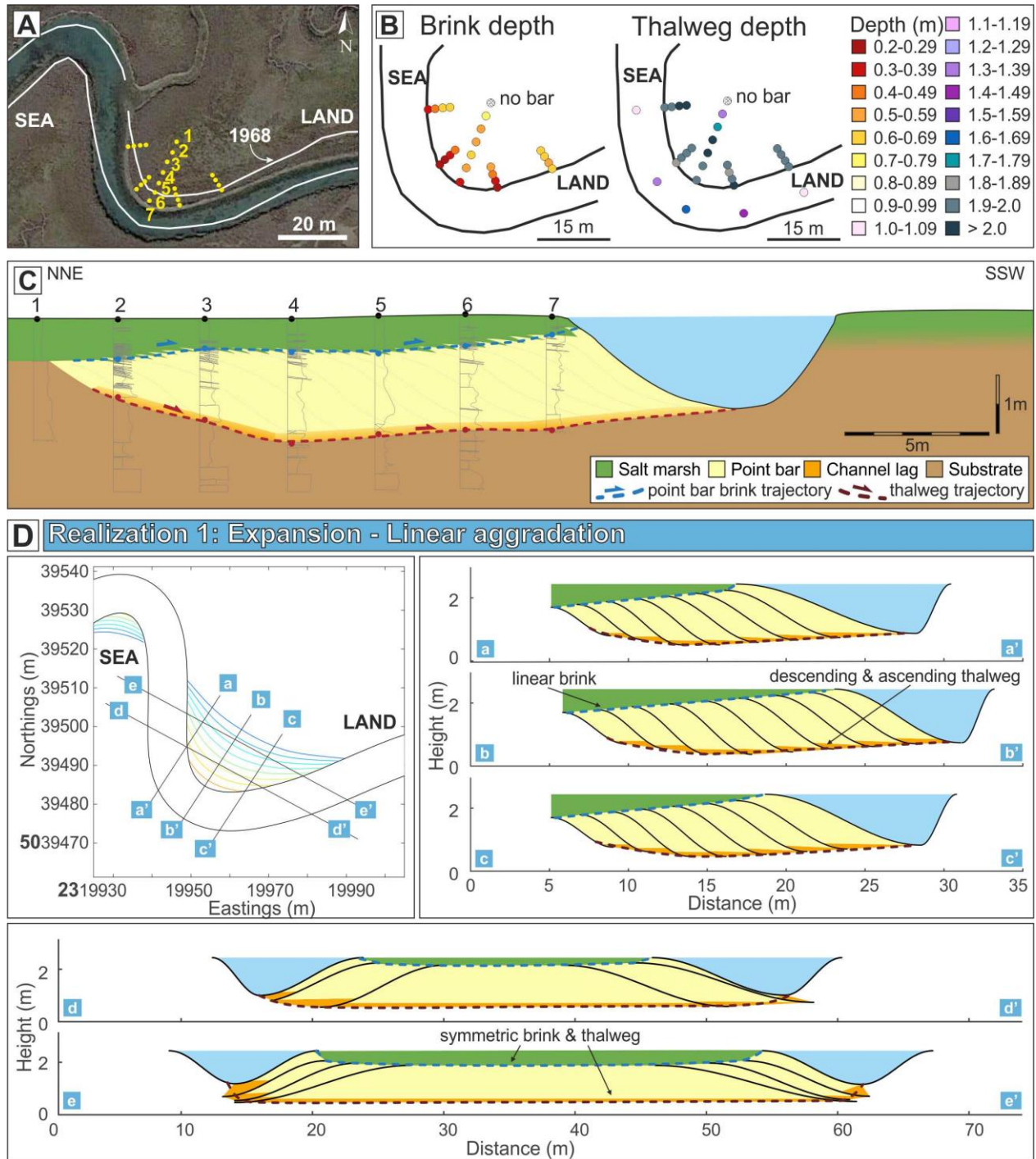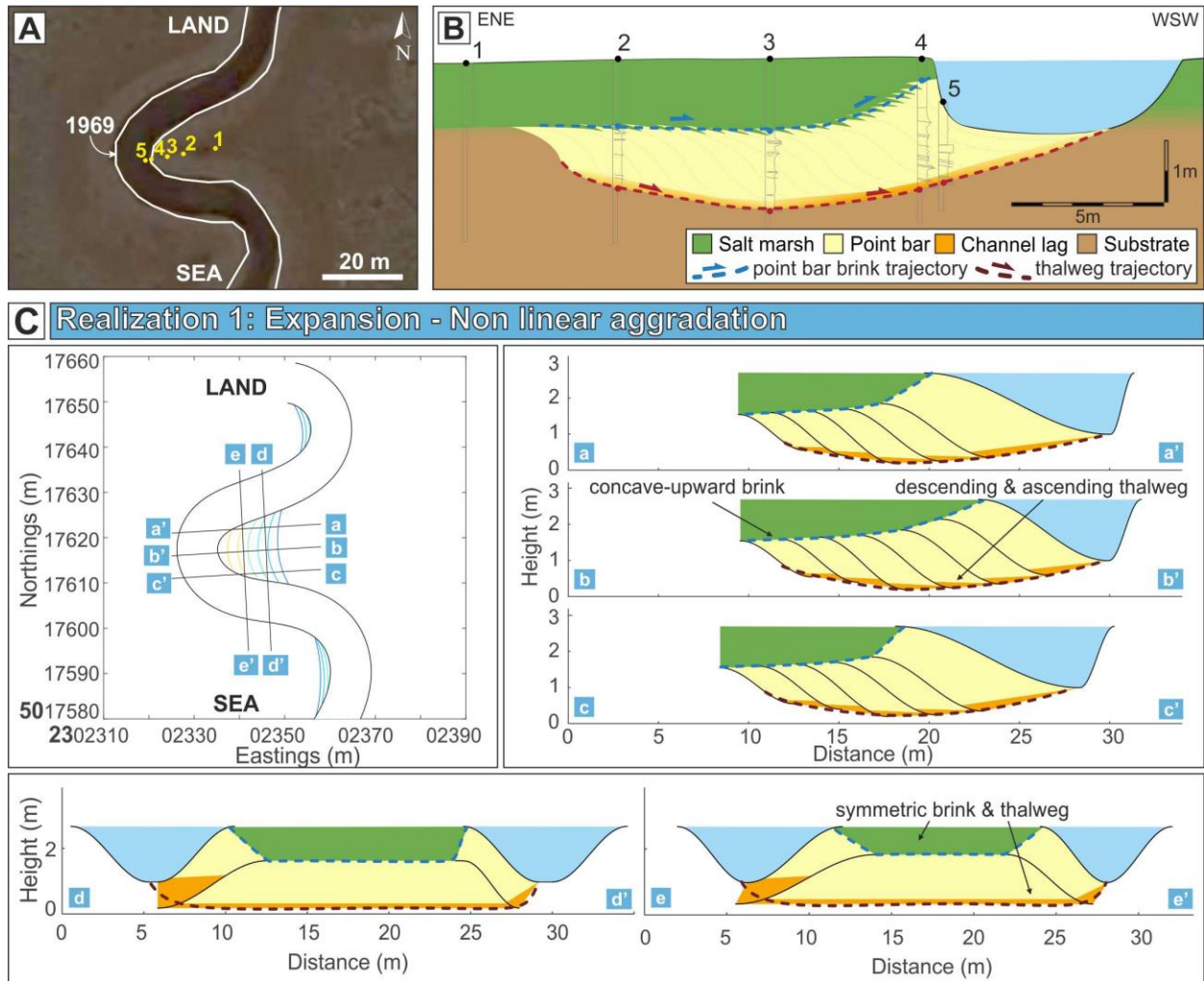
Figure 6. Case 3 results. (A and B) Results from remote sensing and core analysis, showing the planform evolution of the meander bend (A) and bar-brink and channel-thalweg trajectories along the axial cross section (B). (C and D) PB-SAND modelling results of realizations 1 and 2, respectively. (C) Realization 1: expansional evolution of the meander bend developed under non-linear aggradational conditions and resultant three-dimensional geometry of the point bar. (D) Realization 2: translational evolution of the meander bend developed under linear aggradational conditions and resultant three-dimensional geometry of the point bar. Vertical exaggeration: x2.

bar (core 2) to 0.35 m at the bar edge (core 4), creating a concave-upward ascending trajectory. The thalweg trajectory shows an initial descending shift, which is followed by an ascending shift almost parallel to the brink trajectory (Fig 6B). The point-bar thickness ranges between 1.0 and 1.8 m.

Two contrasting PB-SAND realizations (realizations 1 and 2, Fig 6C and D) produced geometries comparable with those documented in the axial section of the study bar.
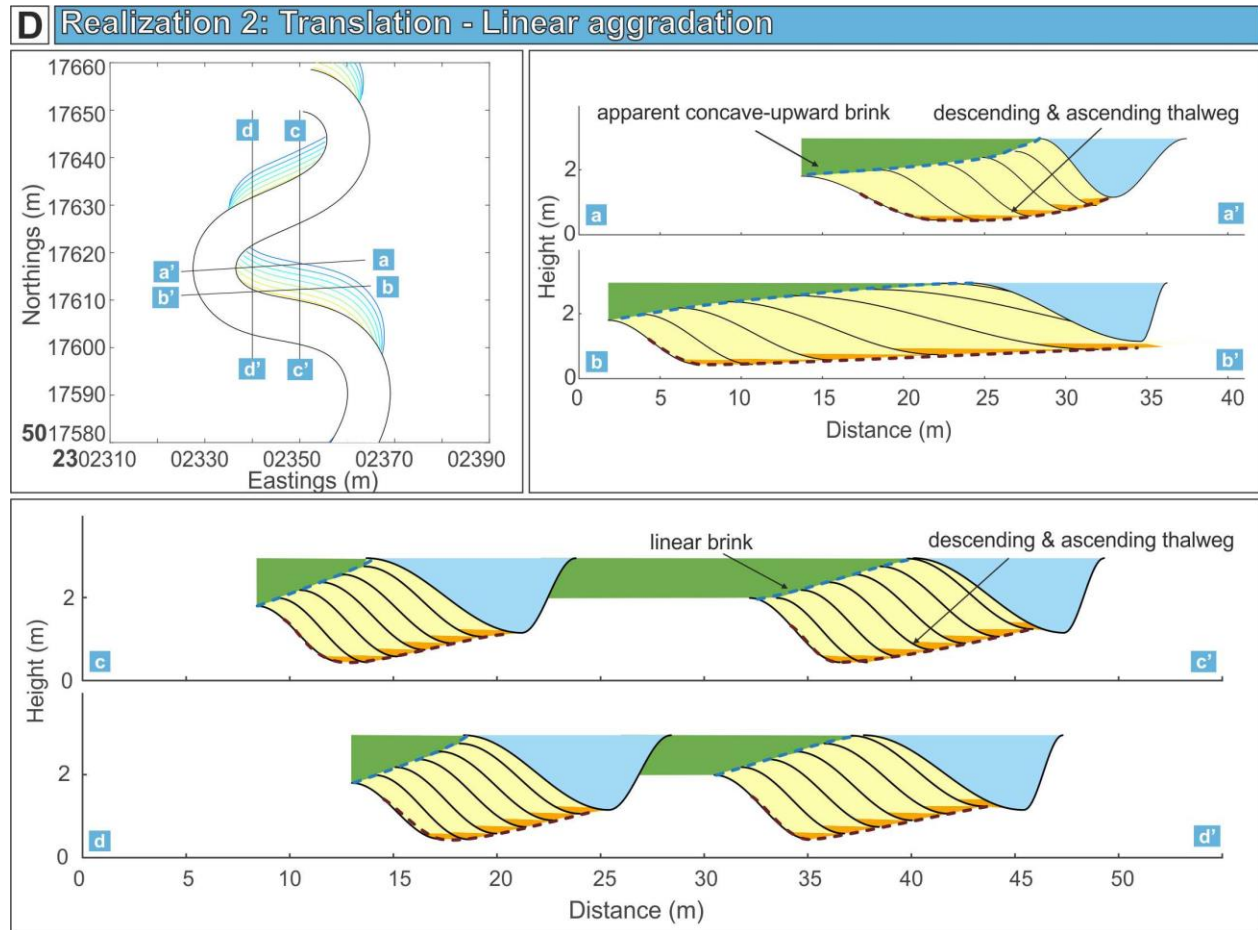
(cont. Fig. 6)

Realization 1 (Fig 6C) was based on point-bar expansion with a non-linear aggradation and channel depth deepening from 1.0 to 1.8 m. The resulting bar brink and thalweg surfaces are symmetric with respect to the bend axis (cross sections d and e in Figure 6C). The bar brink surface shows a rather flat geometry in the inner part of the bar, but rises markedly in proximity to the channel edge (cross sections a – c in Figure 6C). The thalweg surface progressively descends and then ascends from the inner part of the bar toward the channel (cross sections a, b, and c, Fig 6C).

In realization 2 (Fig 6D), bend translation is also modelled assuming linear aggradation. The channel depth is increased through time from 1.35 to 1.80 m, to match closely the results of the core analysis (Fig 6B). The bar-brink trajectory rises linearly, as it emerges from the cross sections c and d (Fig 6D), whereas its upward concavity on the axial cross

section (section a in Figure 6D) is an apparent rather than a true inclination. The thalweg trajectory, in the same direction, sharply descends and then gradually ascends toward the present-day channel (cross sections c and d, Fig 6D). The lack of field evidence does not allow us to point out which of these two realizations is more likely with the study case.

5.2.4. Case 4

The comparison between the point bar and channel depicted in the 1955 aerial photo and that in 2014 image indicates that the channel did not undergo any relevant planform change during that time, and that it maintained a constant width of ca. 11 m (Figs 2G, 2H and 7A). The brink depth progressively diminishes from 1.94 m in the innermost part of the bar (core 1) to 0.30 m at the bar edge (core 4), creating a steep convex-upward ascending trajectory.

The thalweg trajectory records an initial descending shift, which is followed by an ascending shift almost parallel to the brink trajectory (Fig 7B). The point-bar thickness increases from 2.0 to 2.5 m. Three different PB-SAND realizations (realizations 1 – 3 in Figure 7C, D and E) are used to reconstruct possible geometries documented in the axial section, based on the following assumptions: (i) pure expansion under non-linear aggradation; (ii) expansion with rotation under non-linear aggradation; and (iii) expansion followed by translation under linear aggradation. The channel depth has been increased through time from 1.30 to 2.25 m in realizations 1 and 3, and from 1.10 to 2.50 m in realization 2 to simulate the trajectory of the thalweg.

Realization 1 (Fig 7C) produced brink and thalweg surfaces symmetric to the bend axis (cross sections d and e, Fig 7C). Along axial cross-sections, bar brink shows a convex-upward trajectory going from the innermost part of the bar through the channel, whereas thalweg trajectory, after an initial descending shift, rises almost parallel to brink trajectory (cross sections a, b and c, Fig 7C). In realization 2 (Fig 7D), resulting
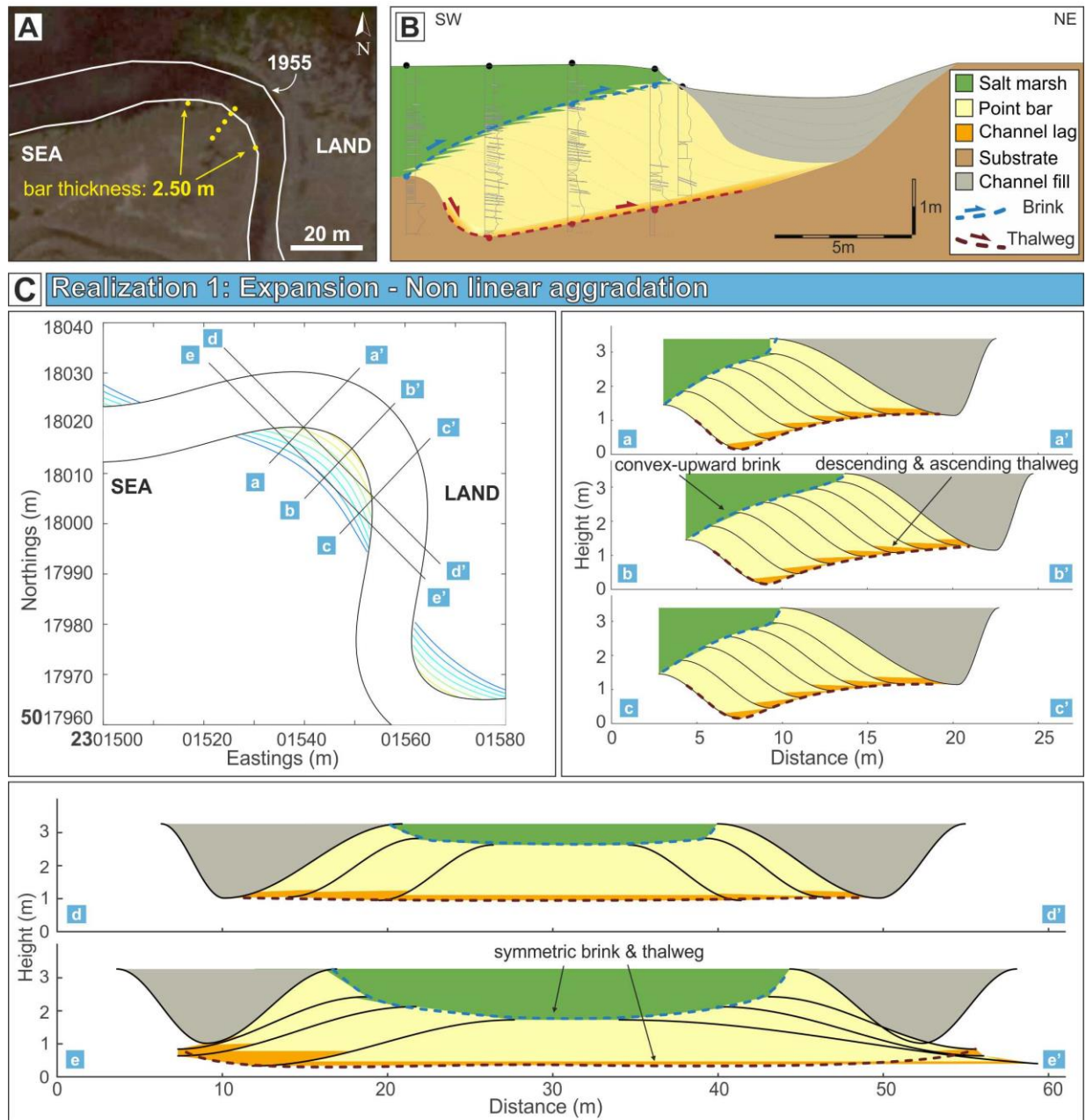
Figure 7. Case 4 results. (A and B) Results from remote sensing and core analysis, showing the planform evolution of the meander bend (A) and bar-brink and channel-thalweg trajectories along the axial cross section (B). (C, D and E) PB-SAND modelling results of realizations 1, 2 and 3, respectively. (C) Realization 1: expansional evolution of the meander bend developed under non-linear aggradation and three-dimensional geometry of the point bar. (D) Realization 2: expansional and rotational evolution of the meander bend developed under non-linear aggradation and resultant three-dimensional geometry of the point bar. (E) Realization 3: expansional and translational evolution of the meander bend developed under linear aggradation and resultant three-dimensional geometry of the point bar. Vertical exaggeration: x2.

(cont. Fig. 7)

surfaces are asymmetric with respect to the bend axis, and are much steeper in the seaward side of the bar (cross sections d and e in Figure 7D) in response to a rotational component during overall planform expansion. In sections parallel to the bend axis, the bar brink shows a convex-upward trajectory, whereas the thalweg trajectory, after an initial descending shift, rises almost parallel to the brink trajectory (cross sections a, b and c, Fig 7D).
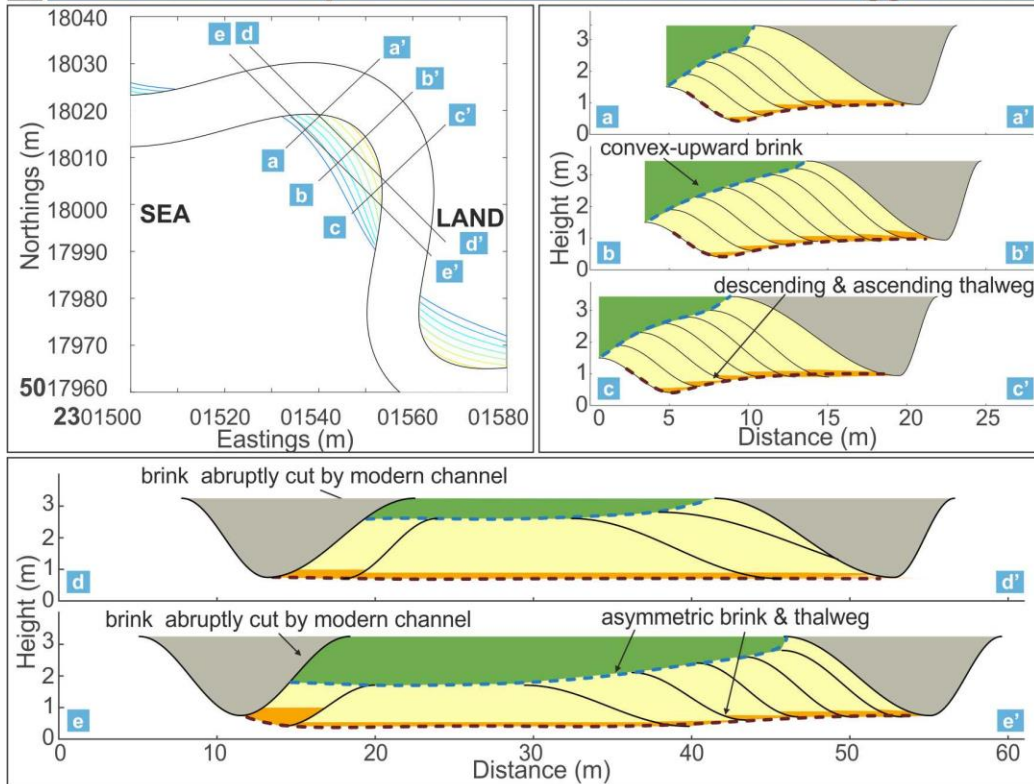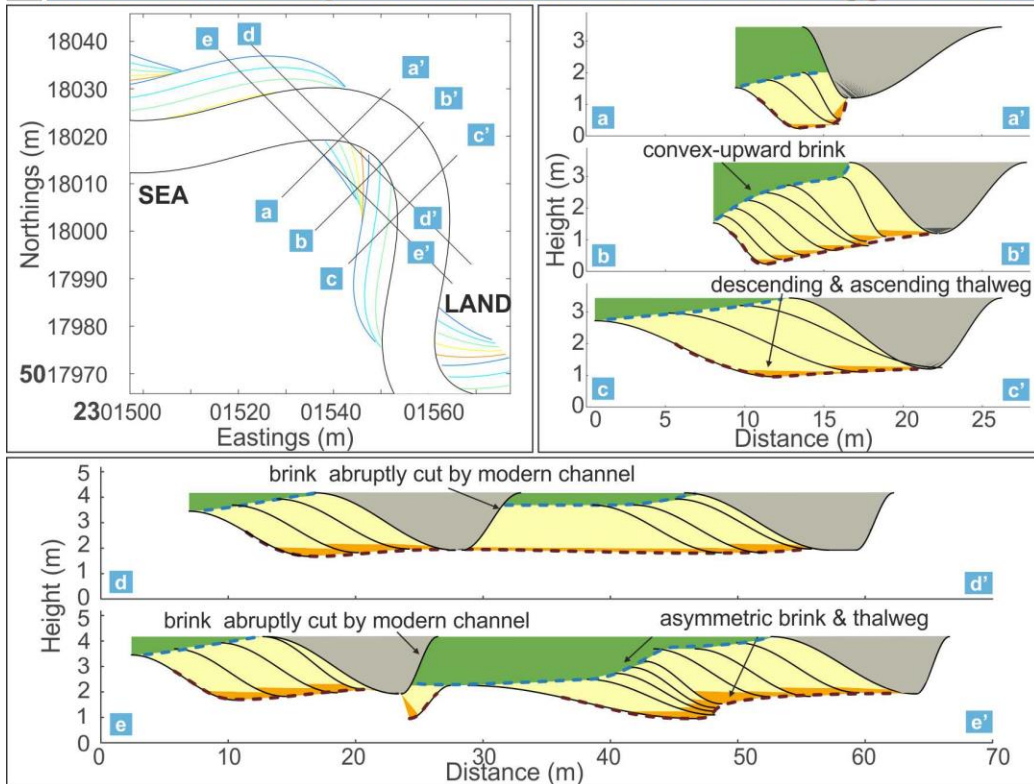
Realization 3 (Fig 7E), produced a strong asymmetry in brink and thalweg surfaces, which are asymmetric with respect to the bend axis (cross sections d and e, Fig 7E). The brink trajectory along the axial cross section (cross section b, Fig 7E) shows a convex-upward trend, whereas the thalweg trajectory shows an initial descending shift followed by an approximately linear ascending shift (cross sections of Figure 7E). The paucity of field evidence for this bar precludes determination of which of these three realizations represents the most likely evolutionary history for this meander.

6. DISCUSSION

The analysis of trajectories is the study of the migratory behaviour of recognizable geomorphological features through space and time (Helland-Hansen and Hampson, 2009). This concept has been widely applied to shelf edges and shorelines to understand the distribution of depositional systems in response to relative sea-level change and variations in sediment supply (Henriksen et al., 2009, and references therein), but it has also provided useful insight when applied to deltas (Gobo et al., 2015; Cosgrove et al., 2018) or fluvial bars (Ghinassi et al., 2014).

A corresponding trajectory analysis is applied here to intertidal point bars to elucidate the possible architecture of deposits produced by slowly meandering tidal channels in relatively high aggradational settings (cf. Candel et al., 2017), highlighting differences

with traditional point-bar models (Fig 8). The significance of the different 2D trajectories is discussed through comparison with 3D data, and results from numerical modelling.
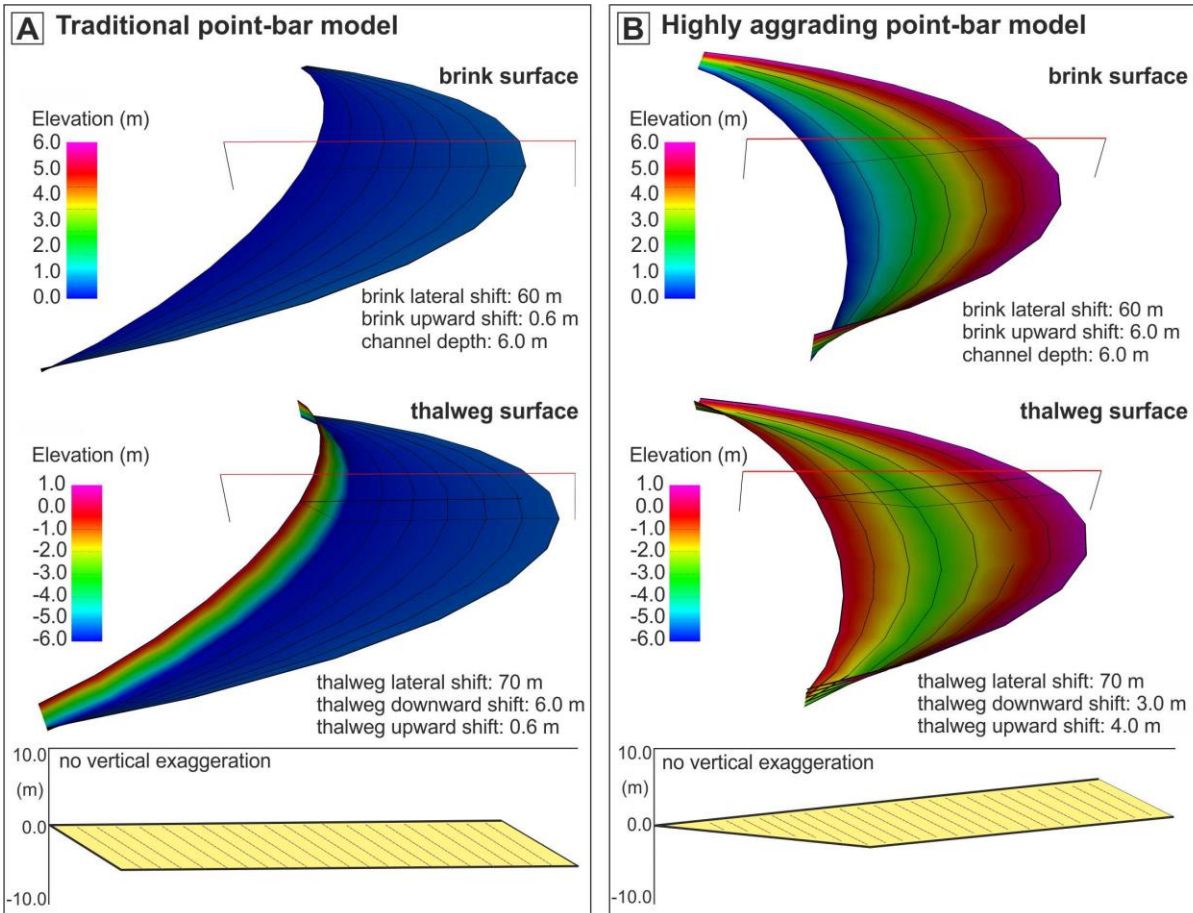
Figure 8. Differences between traditional (A) and highly aggrading (B) point-bar models. (A) Geometries of the brink and thalweg surfaces resulting from an expansional evolution of the meander bend envisaged by traditional models. (B) Geometries of the brink and thalweg surfaces resulting from an expansional evolution of the meander bend developed under aggradational conditions.

6.1. From 2D to 3D trajectory analysis

In case studies 1-4, point-bar brink and channel thalweg trajectories show different slopes and are classified as ascending, descending or horizontal in cross-sections parallel to the meander-bend axis. Point-bar brink trajectories are all ascending (Figs 4B,5C, 6B,

and 7B), pointing out that the lateral shift of the brink is affected by vertical aggradation. Brink trajectories are distinguished between linear (case 1 and 2, Figs 4B and 5C) and non-linear (case 3 and 4, Figs 6B and 7B), on the basis of variations in the ratio between vertical and lateral shift of the brink. This ratio is constant in linear trajectories (Fig 9B), and variable in non-linear ones, which can be concave (case 3) or convex-upward (case 4), when the ratio increases (Fig 9B) and decreases (Fig 9B), respectively. Channel-thalweg trajectories include an initial descending shift, followed by an ascending or horizontal shift (Figs 4B, 5C, 6B, and 7B), indicating that the channel base shifted laterally under degradational, aggradational and stable conditions, respectively (De Mowbray, 1983; Rieu et al., 2005; Cosma et al., 2019). Thalweg trajectories lack any clear concave- or convex-upward pattern, probably because of the erosional, and therefore irregular, nature of the channel basal surface. The channel thalweg follows these trajectories in order to reach and maintain a cross-sectional depth that is in equilibrium with its channel discharge (Allen, 2000; D'Alpaos et al., 2005).

Channel discharge is related to the tidal watershed area, and can vary over temporal scales of decades to centuries as a consequence of changes in the tidal prism, watershed area (e.g. due to channel piracy and/or meander cut-off) and channel-network evolution (Garofalo, 1980; Dalrymple et al., 1991; Allen, 2000; D'Alpaos et al., 2005; Stefanon et al., 2012; Lanzoni and D'Alpaos, 2015; Ghinassi et al., 2018a, 2018b).

Trajectory analyses in cross sections demonstrate how changes in depositional (e.g. aggradation rate) and hydraulic (e.g. discharge) conditions occurred during the evolution of a meander bend, and occurrence of linear and non-linear geometries can be used to demonstrate variations in the ratio between vertical and lateral shifts (Cosma et al., 2019). The numerical modelling realizations provide effective 3D geometries of surfaces generated by brink (i.e. brink surface) and thalweg (i.e. thalweg surface) shifts. Specifically, the numerical modelling exercises undertaken for this study reveal that 2D trajectory analyses are reliable only if sections are oriented parallel to the effective

direction of channel migration (i.e. are true trajectories, Fig 3C and Fig 9C), highlighting the role of planform transformation in controlling geometries of brink and thalweg surfaces (Fig 9A). On the contrary, sections oblique to the direction of channel migration provide only apparent trajectories (Fig 3C), which are not representative of the effective relation between rate of vertical and lateral shifts. For example, the concave-upward geometry of the brink trajectory along the axial cross section in case 3 is obtained both in realization 1 (i.e. expansion with non-linear aggradation) and 2 (i.e. translation with linear aggradation). Nevertheless, the upward concavity of realization 2 is apparent, and arises from oblique orientation of the cross-section in comparison with direction of bar accretion.

Understanding the three-dimensionality of the brink surface can also provide insight into the planform transformation of the meander associated with a bar (Fig 9A). Reconstruction of the brink surface steepness in different parts of the bar (i.e. shape of the brink surface) is crucial to distinguish between symmetric or asymmetric growth of a bend. A steep brink surface is indicative of zones affected by pivoting processes, as commonly seen where bar rotation causes a local minimal lateral shift during vertical aggradation. A sub-vertical brink surface accounts for shift of the channel against the bar, as occurs in cases of translation or strong rotation (Fig 9A). For these reasons, the asymmetric shape of brink surface of case 2 is considered to be consistent with a non-uniform expansion (realization 2 and 3), instead of a pure expansion (realization 1) which generated a symmetric brink surface.

6.2. Model evaluation

Reconstruction of the three-dimensional architecture of modern tidal point-bar bodies is required to produce appropriate facies models. Nevertheless, such a reconstruction is a challenging issue, since understanding the evolution of tidal-bar planform morphology

is commonly hindered by the lack of well-developed scroll-bar morphologies (Hughes, 2012) and by low bend-migration rates (i.e. cm - dm per year; Garofalo, 1980; Gabet, 1998; Allen, 2000; Fagherazzi & Sun, 2004; Hughes, 2012; Finotello et al., 2018). This makes comparison between historical photos unfeasible (e.g. cases 3 and 4). Geophysical investigations are also unsuitable. Ground Penetrating Radar (GPR) is limited by the abundance of muddy sediments and saltwater, which strongly attenuate GPR signal (Neal, 2004). Sub-bottom profilers (McClennen and Housley, 2006; Donnici et al., 2017) require a certain water depth, and cannot be used on salt marshes. By necessity, reconstruction of bar geometries is therefore typically based on sedimentary cores and related 2D reconstructions.

The use of a forward stratigraphic model like PB-SAND allows prediction of the expected 3D internal architecture of these sedimentary bodies and provides an opportunity to consider multiple solutions, which can be used in combination with field-derived and time-series remote-sensing data to constrain the most likely evolutionary history of evolving point bars.

Where there is sufficient constraint to univocally define both the planform evolution (i.e. remote sensing, satellite images) and the cross-sectional geometries (i.e. core data), PB-SAND can predict the three-dimensional architecture of the bar body. This is the case for

point bar 1 in this study, where a wealth of constraints provided by remote-sensing and core data could only be honoured fully by a single unique realization. In cases where field data provides only partial constraint, PB-SAND allows the exploration of alternative competing possible models, and the evaluation of their likelihood, given the available field evidence. This applies in case 2, where two out of the three realizations were selected as potential candidates after verifying their goodness-to-fit with available field data.

A Planform transformation controls point bar geometry – example on the brink surface

Expansion

Expansion & Rotation

channel against the bar:
vertical brink surface

bar apex shift

Expansion followed by Translation

channel against the bar:
vertical brink surface

bar apex shift

B Aggradation controls point bar geometry – example on the brink surface

Increasing aggradation rate

concave-upward brink surface

Constant aggradation rate

linear brink surface

Decreasing aggradation rate

convex-upward brink surface

C Interplay between planform transformation and aggradation – example on the brink surface

Expansion & Non-linear aggradation

section parallel to
direction of channel shift

Translation & Linear aggradation

section oblique
to direction of
channel shift

section parallel
to direction of
channel shift

Cross sections

Elevation (m)

1.2
1.0
0.8
0.6
0.4
0.2
0.0

true trajectory
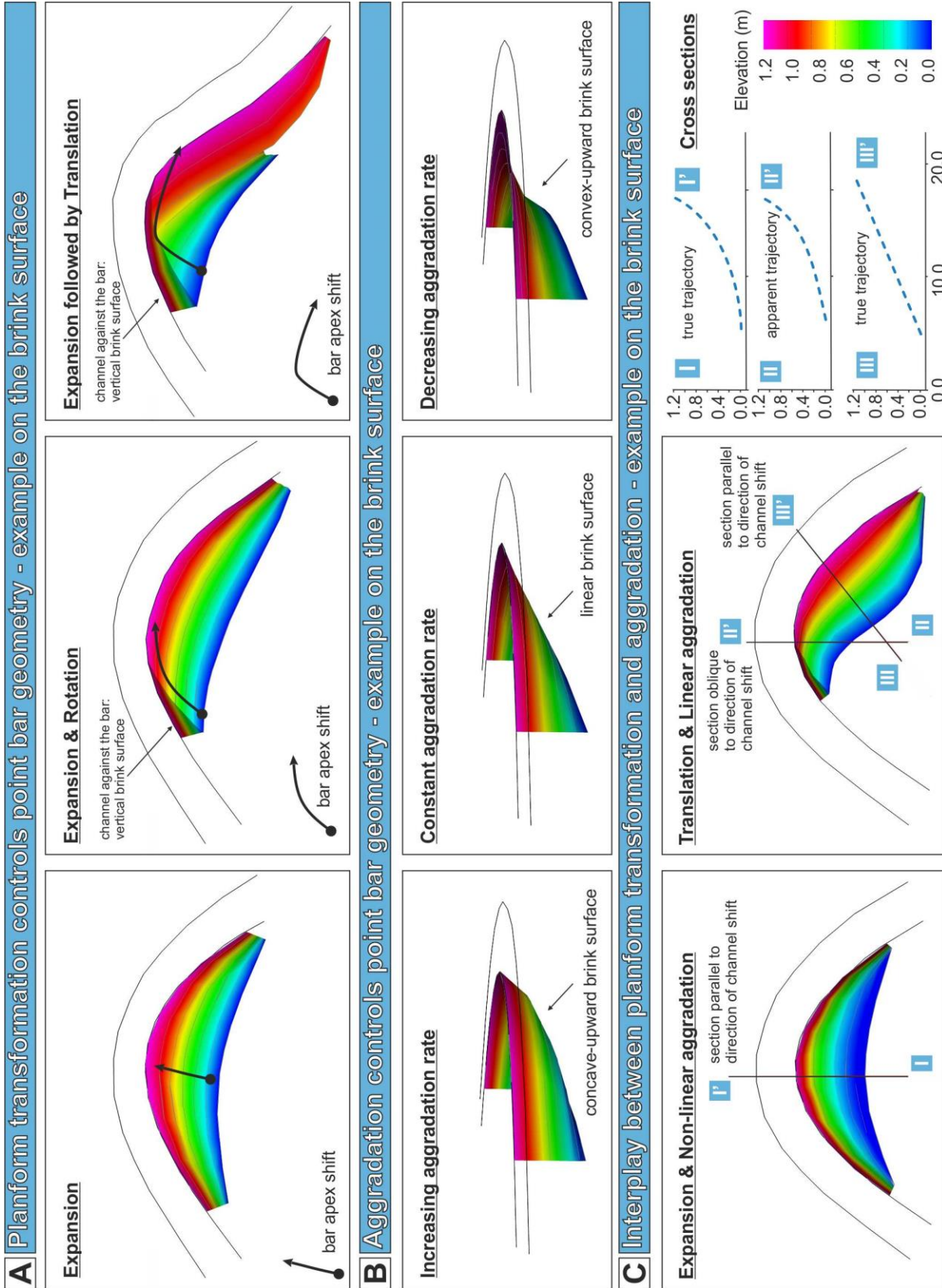
apparent trajectory

true trajectory

Figure 9. Summary of the main factors influencing point-bar geometries. (A) Brink surfaces resulting from different planform transformations. (B) Brink surfaces resulting from different aggradational conditions. (C) Combination of different planform transformations and aggradational conditions (linear vs non-linear) can produce similar cross-sectional configurations. However, only the cross sections parallel to the effective direction of channel migration (I and III) offer a faithful reflection of the relationship between vertical aggradation and lateral migration of the channel system. The examples reported herein are referred to the brink surface, but the same considerations can be made for the thalweg surface. Vertical exaggeration: x5.

Where constraints are more limited (e.g. case 3 and 4), different alternative models show how contrasting styles of bar evolution can produce similar cross-sectional configurations (Fig 9C). These models, in turn, provide information that can be used to plan further investigations (i.e. defining coring sites) to constrain the bar geometry more effectively.

7. CONCLUSION

Data derived from remote-sensing and core analyses have been combined with the 'Point-Bar Sedimentary Architecture Numerical Deduction' (PB-SAND), a three-dimensional forward stratigraphic model, to predict the stratal geometries of point bars formed by different meander bends in the aggradational marshes of the Venice Lagoon (Italy).

Field data reveal how the geometries of four studied bars, which differ from that envisaged in traditional point-bar models, can be shaped in different ways by progressive lateral and vertical shifts of the bar brink and channel thalweg zone. Integration between field data and numerical modelling demonstrates how cross sections parallel to shift direction of the channels can show different shapes and steepness of bar-brink and channel-thalweg trajectories. Ascending bar-brink trajectories (i.e. linear, concave- and convex-upward) record different aggradational conditions in

response to lateral channel shift. Descending and ascending thalweg trajectories document incision and maintenance of the channel cross section.

The employment of PB-SAND has been crucial to reconstruct the three-dimensional architecture of the studied bars. PB-SAND can unequivocally reconstruct the three-dimensional architecture of a point bar body where the planform evolution of the bend and the bar brink and thalweg trajectories are known. Moreover, PB-SAND simulations can demonstrate what combinations of different planform transformations and vertical aggradation can produce defined point-bar geometries along two-dimensional cross sections. Finally, where field data are insufficient to constrain a single 3D model, PB-SAND can render a series of possible alternative solutions, which can be used to plan further investigations.

8. REFERENCES

Allen, J.R.L., 2000. Morphodynamics of Holocene salt marshes: a review sketch from the Atlantic and Southern North Sea coasts of Europe. Quat. Sci. Rev. 19, 1155–1231. https://doi.org/10.1016/S0277-3791(99)00034-7

Amorosi, A., Fontana, A., Antonioli, F., Primon, S., Bondesan, A., 2008. Post-LGM sedimentation and Holocene shoreline evolution in the NW Adriatic coastal area. GeoActa 7, 41–67.

Bellucci, L.G., Frignani, M., Cochran, J.K., Albertazzi, S., Zaggia, L., Cecconi, G., Hopkins, H., 2007. 210Pb and 137Cs as chronometers for salt marsh accretion in the Venice Lagoon - links to flooding frequency and climate change. J. Environ. Radioact. 97, 85–102. https://doi.org/10.1016/j.jenvrad.2007.03.005

Bhattacharyya, P., Bhattacharya, J.P., Khan, S.D., 2015. Paleo-channel reconstruction and grain size variability in fluvial deposits, Ferron Sandstone, Notom Delta, Hanksville, Utah. Sediment. Geol. 325, 17–25. https://doi.org/10.1016/j.sedgeo.2015.05.001

Boaga, J., Ghinassi, M., D'Alpaos, A., Deidda, G.P., Rodriguez, G., Cassiani, G., 2018. Geophysical investigations unravel the vestiges of ancient meandering channels and their dynamics in tidal landscapes. Sci. Rep. 8, 1–8. https://doi.org/10.1038/s41598-018-20061-5

Bondesan, A., Meneghel, M., 2004. Geomorfologia della provincia di Venezia. Note illustrative della carta geomorfologica della provincia di Venezia.

Brice, J.C., 1974. Evolution of meander loops. Bull. Geol. Soc. Am. 85, 581–586. https://doi.org/10.1130/0016-7606(1974)85<581:EOML>2.0.CO;2

Bridges, P.H., Leeder, M.R., 1976. Sedimentary model for intertidal mudflat channels, with examples from the Solway Firth, Scotland. Sedimentology 23, 533–552. https://doi.org/10.1111/j.1365-3091.1976.tb00066.x

Brivio, L., Ghinassi, M., D'Alpaos, A., Finotello, A., Fontana, A., Roner, M., Howes, N., 2016. Aggradation and lateral migration shaping geometry of a tidal point bar: An example from salt marshes of the Northern Venice Lagoon (Italy). Sediment. Geol. 343, 141–155. https://doi.org/10.1016/j.sedgeo.2016.08.005

Candel, J.H.J., Makaske, B., Storms, J.E.A., Wallinga, J., 2017. Oblique aggradation: A novel explanation for sinuosity of low-energy streams in peat-filled valley systems. Earth Surf. Process. Landforms 42, 2679–2696. https://doi.org/10.1002/esp.4100

Carniello, L., D'Alpaos, A., Defina, A., 2011. Modeling wind waves and tidal flows in shallow micro-tidal basins. Estuar. Coast. Shelf Sci. 92, 263–276. https://doi.org/10.1016/j.ecss.2011.01.001

Carniello, L., Defina, A., D'Alpaos, L., 2009. Morphological evolution of the Venice lagoon: Evidence from the past and trend for the future. J. Geophys. Res. Earth Surf. 114, 1–10. https://doi.org/10.1029/2008JF001157

Choi, K.S., Jo, J.H., 2015. Morphodynamics of Tidal Channels in the Open Coast Macrotidal Flat, Southern Ganghwa Island in Gyeonggi Bay, West Coast of Korea. J. Sediment. Res. 85, 582–595. https://doi.org/10.2110/jsr.2015.44

Clift, P.D., Olson, E.D., Lechnowskyj, A., Moran, M.G., Barbato, A., Lorenzo, J.M., 2018. Grain-size variability within a mega-scale point-bar system, False River, Louisiana. Sedimentology 66, 408–434. https://doi.org/10.1111/sed.12528

Colombera, L., Mountney, N.P., McCaffrey, W.D., 2013. A quantitative approach to fluvial facies models: Methods and example results. Sedimentology 60, 1526–1558. https://doi.org/10.1111/sed.12050

Colombera, L., Mountney, N.P., McCaffrey, W.D., 2012. A relational database for the digitization of fluvial architecture. Pet. Geosci. 18, 129–140. https://doi.org/10.1144/1354-079311-021

Colombera, L., Mountney, N.P., Russell, C.E., Shiers, M.N., McCaffrey, W.D., 2017. Geometry and compartmentalization of fluvial meander-belt reservoirs at the bar-form scale: Quantitative insight from outcrop, modern and subsurface analogues. Mar. Pet. Geol. 82, 35–55. https://doi.org/10.1016/j.marpetgeo.2017.01.024

Colombera, L., Yan, N., McCormick-Cox, T., Mountney, N.P., 2018. Seismic-driven geocellular modeling of fluvial meander-belt reservoirs using a rule-based method. Mar. Pet. Geol. 93, 553–569. https://doi.org/10.1016/j.marpetgeo.2018.03.042

Cosgrove, G.I.E.E., Hodgson, D.M., Poyatos-Moré, M., Mountney, N.P., McCaffrey, W.D., 2018. Filter Or Conveyor? Establishing Relationships Between Clinoform Rollover Trajectory, Sedimentary Process Regime, and Grain Character Within Intrashelf Clinothems, Offshore New Jersey, U.S.A. J. Sediment. Res. 88, 917–941. https://doi.org/10.2110/jsr.2018.44

Cosma, M., Ghinassi, M., D'Alpaos, A., Roner, M., Finotello, A., Tommasini, L., Gatto, R., 2019. Point-bar brink and channel thalweg trajectories depicting interaction between vertical and lateral shifts of microtidal channels in the Venice Lagoon (Italy). Geomorphology 342, 37–50. https://doi.org/10.1016/j.geomorph.2019.06.009

D'Alpaos, A., Lanzoni, S., Marani, M., Fagherazzi, S., Rinaldo, A., 2005. Tidal network ontogeny: Channel initiation and early development. J. Geophys. Res. Earth Surf. 110, 1–14. https://doi.org/10.1029/2004JF000182

D'Alpaos, A., Marani, M., 2016. Reading the signatures of biologic-geomorphic feedbacks in salt-marsh landscapes. Adv. Water Resour. 93, 265–275. https://doi.org/10.1016/j.advwatres.2015.09.004

Dalrymple, R.W., Makino, Y., Zaitlin, Brian A., 1991. Temporal and Spatial Patterns of Rhythmite Deposition on Mud Flats in the Macrotidal Cobequid Bay-Salmon River Estuary, Bay of Fundy, Canada, in: Smith, D.G., Reinson, G.E., Zaitlin, B. A., Rahmani, R.A. (Eds.), Clastic Tidal Sedimentology. pp. 137–160.

Daniel, J.F., 1971. Channel movement of meandering Indiana streams. U.S. Geol. Surv. Prof. Pap. 732-A, 1–18.

De Mowbray, T., 1983. The genesis of lateral accretion deposits in recent intertidal mudflat channels, Solway Firth, Scotland. Sedimentology 30, 425–435. https://doi.org/10.1111/j.1365-3091.1983.tb00681.x

Donnici, S., Madricardo, F., Serandrei-Barbero, R., 2017. Sedimentation rate and lateral migration of tidal channels in the Lagoon of Venice (Northern Italy). Estuar. Coast. Shelf Sci. 198, 354–366. https://doi.org/10.1016/j.ecss.2017.02.016

Durkin, P.R., Hubbard, S.M., Boyd, R.L., Leckie, D.A., 2015. Stratigraphic Expression of Intra-Point-Bar Erosion and Rotation. J. Sediment. Res. 85, 1238–1257. https://doi.org/10.2110/jsr.2015.78

Durkin, P.R., Hubbard, S.M., Smith, D.G., Leckie, D.A., 2019. Predicting heterogeneity in meandering fluvial and tidal-fluvial deposits: The point bar to counter point bar transition, in: Ghinassi, M., Colombera, L., Mountney, N.P., Reesink, A.J., Bateman, M. (Eds.), Fluvial Meanders and Their Sedimentary Products in the Rock Record. John Wiley & Sons, Ltd, pp. 231–249. https://doi.org/10.1002/9781119424437.ch9

Fagherazzi, S., Sun, T., 2004. A stochastic model for the formation of channel networks in tidal marshes. Geophys. Res. Lett. 31, 1–4. https://doi.org/10.1029/2004GL020965

Fielding, C.R., 2015. A reappraisal of large, heterolithic channel fills in the upper Permian Rangal Coal Measures of the Bowen Basin, Queensland, Australia: The case for tidal influence, in: Ashworth, P.J., Best, J.L., Parsons, D.R. (Eds.), Fluvial-Tidal Sedimentology, Developments in Sedimentology. Elsevier B.V., pp. 323–351. https://doi.org/10.1016/B978-0-444-63529-7.00012-2

Finotello, A., Lanzoni, S., Ghinassi, M., Marani, M., Rinaldo, A., D'Alpaos, A., 2018. Supporting Information (SI) Appendix. Field migration rates of tidal meanders recapitulate fluvial morphodynamics. Proc. Natl. Acad. Sci. 115, 1463–1468. https://doi.org/10.1073/pnas.1711330115

Fisk, H.N., 1944. Geological Investigation of the Alluvial Valley of the Lower Mississippi River. US Army Corps Eng. Mississippi River Comm. 1–78.

Fustic, M., Hubbard, S.M., Spencer, R., Smith, D.G., Leckie, D.A., Bennett, B., Larter, S., 2012. Recognition of down-valley translation in tidally influenced meandering fluvial deposits, Athabasca Oil Sands (Cretaceous), Alberta, Canada. Mar. Pet. Geol. 29, 219–232. https://doi.org/10.1016/j.marpetgeo.2011.08.004

Gabet, E.J., 1998. Lateral Migration and Bank Erosion in a Saltmarsh. Estuaries 21, 745–753.

Garofalo, D., 1980. The Influence of Wetland Vegetation on Tidal Stream Channel Migration and Morphology. Estuaries 3, 258–270. https://doi.org/10.2307/1352081

Ghinassi, M., Billi, P., Libsekal, Y., Papini, M., Rook, L., 2013. Inferring Fluvial Morphodynamics and Overbank Flow Control From 3D Outcrop Sections of A Pleistocene Point Bar, Dandiero Basin, Eritrea. J. Sediment. Res. 83, 1065–1083. https://doi.org/10.2110/jsr.2013.80

Ghinassi, M., Brivio, L., D'Alpaos, A., Finotello, A., Carniello, L., Marani, M., Cantelli, A., 2018a. Morphodynamic evolution and sedimentology of a microtidal meander bend of the Venice Lagoon (Italy). Mar. Pet. Geol. 96, 391–404. https://doi.org/10.1016/j.marpetgeo.2018.06.011

Ghinassi, M., D'alpaos, A., Gasparotto, A., Carniello, L., Brivio, L., Finotello, A., Roner, M., Franceschinis, E., Realdon, N., Howes, N., Cantelli, A., 2018b. Morphodynamic evolution and stratal architecture of translating tidal point bars: Inferences from the northern Venice Lagoon (Italy). Sedimentology 65, 1354–1377. https://doi.org/10.1111/sed.12425

Ghinassi, M., Ielpi, A., 2015. Stratal Architecture and Morphodynamics of Downstream-Migrating Fluvial Point Bars (Jurassic Scalby Formation, U.K.). J. Sediment. Res. 85, 1123–1137. https://doi.org/10.2110/jsr.2015.74

Ghinassi, M., Ielpi, A., Aldinucci, M., Fustic, M., 2016. Downstream-migrating fluvial point bars in the rock record. Sediment. Geol. 334, 66–96. https://doi.org/10.1016/j.sedgeo.2016.01.005

Ghinassi, M., Nemec, W., Aldinucci, M., Nehyba, S., Özaksoy, V., Fidolini, F., 2014. Plan-form evolution of ancient meandering rivers reconstructed from longitudinal outcrop sections. Sedimentology 61, 952–977. https://doi.org/10.1111/sed.12081

Gobo, K., Ghinassi, M., Nemec, W., 2015. Gilbert-type deltas recording short-term base-level changes: Delta-brink morphodynamics and related foreset facies. Sedimentology 62, 1923–1949. https://doi.org/10.1111/sed.12212

Helland-Hansen, W., Hampson, G.J., 2009. Trajectory analysis: Concepts and applications. Basin Res. 21, 454–483. https://doi.org/10.1111/j.1365-2117.2009.00425.x

Henriksen, S., Hampson, G.J., Helland-Hansen, W., Johannessen, E.P., Steel, R.J., 2009. Shelf edge and shoreline trajectories, a dynamic approach to stratigraphic analysis. Basin Res. 21, 445–453. https://doi.org/10.1111/j.1365-2117.2009.00432.x

Hughes, Z.J., 2012. Tidal Channels on Tidal Flats and Marshes, in: Davis, R.A., Dalrymple, R.W. (Eds.), Principles of Tidal Sedimentology. Springer, pp. 269–300. https://doi.org/10.1007/978-94-007-0123-6

Ielpi, A., Ghinassi, M., 2014. Planform architecture, stratigraphic signature and morphodynamics of an exhumed Jurassic meander plain (Scalby Formation, Yorkshire, UK). Sedimentology 61, 1923–1960. https://doi.org/10.1111/sed.12122

Ielpi, A., Gibling, M.R., Bashforth, A.R., Dennar, C.I., 2015. Impact of Vegetation on Early Pennsylvanian Fluvial Channels: Insight From the Joggins Formation of Atlantic Canada. J. Sediment. Res. 85, 999–1018. https://doi.org/10.2110/jsr.2015.50

Jackson, R.G.I., 1976. Depositional Model of Point Bars in the Lower Wabash River. J. Sediment. Petrol. 46, 579–594.

Johnston, S., Holbrook, J., 2019. Toggling between expansion and translation, in: Ghinassi, M., Colombera, L., Mountney, N.P., Reesink, A.J., Bateman, M. (Eds.), Fluvial Meanders and

Their Sedimentary Products in the Rock Record. John Wiley & Sons, Ltd, pp. 47–80. https://doi.org/10.1002/9781119424437.ch3

Lanzoni, S., D'Alpaos, A., 2015. On funneling of tidal channels. J. Geophys. Res. Earth Surf. 120, 433–452. https://doi.org/10.1002/2014JF003203

Madricardo, F., Donnici, S., 2014. Mapping past and recent landscape modifications in the Lagoon of Venice through geophysical surveys and historical maps. Anthropocene 6, 86–96. https://doi.org/10.1016/j.ancene.2014.11.001

Madricardo, F., Donnici, S., Lezziero, A., De Carli, F., Buogo, S., Calicchia, P., Boccardi, E., 2007. Palaeoenvironment reconstruction in the Lagoon of Venice through wide-area acoustic surveys and core sampling. Estuar. Coast. Shelf Sci. 75, 205–213. https://doi.org/10.1016/j.ecss.2007.02.031

Madricardo, F., Tegowski, J., Donnici, S., 2012. Automated detection of sedimentary features using wavelet analysis and neural networks on single beam echosounder data: A case study from the Venice Lagoon, Italy. Cont. Shelf Res. 43, 43–54. https://doi.org/10.1016/j.csr.2012.04.018

Makaske, B., 2001. Anastomosing rivers: A review of their classification, origin and sedimentary products. Earth Sci. Rev. 53, 149–196. https://doi.org/10.1016/S0012-8252(00)00038-6

Massari, F., Grandesso, P., Stefani, C., Jobstraibizer, P., 2009. A small polyhistory foreland basin evolving in a context of oblique convergence: the Venetian basin (Chattian to Recent, Southern Alps, Italy), in: Allen, P.A., Homewood, P. (Eds.), Foreland Basins. Blackwell Scientific, Oxford, pp. 141–168. https://doi.org/10.1002/9781444303810.ch7

McClennen, C.E., Housley, R.A., 2006. Late-Holocene Channel Meander Migration and Mudflat Accumulation Rates, Lagoon of Venice, Italy. J. Coast. Res. 224, 930–945. https://doi.org/10.2112/03-0113.1

McGowen, J.H., Garner, L.E., 1970. Physiographic Features and Stratification Types of Coarse-Grained Pointbars: Modern and Ancient Examples. Sedimentology 14, 77–111. https://doi.org/10.1111/j.1365-3091.1970.tb00184.x

Miall, A.D., 1985. Architectural-element analysis: A new method of facies analysis applied to fluvial deposits. Earth-Science Rev. 22, 261–308. https://doi.org/10.1016/0012-8252(85)90001-7

Musial, G., Reynaud, J.-Y., Gingras, M.K., Féniès, H., K.Labourdette, R., Parize, O., 2011. Subsurface and outcrop characterization of large tidally influenced point bars of the Cretaceous McMurray Formation (Alberta, Canada). Sediment. Geol. 279, 156–172. https://doi.org/10.1016/j.sedgeo.2011.04.020

Nanson, G.C., Croke, J.C., 1992. A genetic classification of floodplains. Geomorphology 4, 459–486. https://doi.org/10.1080/00385417.1971.10770277

Neal, A., 2004. Ground-penetrating radar and its use in sedimentology: principles, problems and progress. Earth Sci. Rev. 66. https://doi.org/10.1016/j.earscirev.2004.01.004

Nicoll, T.J., Hickin, E.J., 2010. Planform geometry and channel migration of confined meandering rivers on the Canadian prairies. Geomorphology 116, 37–47. https://doi.org/10.1016/j.geomorph.2009.10.005

Rajchl, M., Uličný, D., 2005. Depositional record of an avulsive fluvial system controlled by peat compaction (Neogene, Most Basin, Czech Republic). Sedimentology 52, 601–625. https://doi.org/10.1111/j.1365-3091.2005.00691.x

Rieu, R., van Heteren, S., van der Spek, A.J.F., De Boer, P.L., 2005. Development and preservation of a Mid-Holocene tidal-channel network offshore the Western Netherlands. J. Sediment. Res. 75, 409–419. https://doi.org/10.21110/jsr.2005.032

Ronchi, L., Fontana, A., Correggiari, A., Asioli, A., 2018. Late Quaternary incised and infilled landforms in the shelf of the northern Adriatic Sea (Italy). Mar. Geol. 405, 47–67. https://doi.org/10.1016/j.margeo.2018.08.004

Roner, M., D'Alpaos, A., Ghinassi, M., Marani, M., Silvestri, S., Franceschinis, E., Realdon, N., 2016. Spatial variation of salt-marsh organic and inorganic deposition and organic carbon accumulation: Inferences from the Venice lagoon, Italy. Adv. Water Resour. 93, 276–287. https://doi.org/http://dx.doi.org/10.1016/j.advwatres.2015.11.011

Roner, M., Ghinassi, M., Fedi, M., Liccioli, L., Bellucci, L.G., Brivio, L., D'Alpaos, A., 2017. Latest Holocene depositional history of the southern Venice Lagoon, Italy. The Holocene 27, 1731–1744. https://doi.org/10.1177/0959683617708450

Russell, C.E., Mountney, Nigel P, Hodgson, D.M., Colombera, Luca, 2019. A novel approach for prediction of lithological heterogeneity in fluvial point-bar deposits from analysis of meander morphology and scroll-bar pattern, in: Ghinassi, M., Colombera, L., Mountney, N. P., Reesink, A.J., Bateman, M. (Eds.), Fluvial Meanders and Their Sedimentary Products in the Rock Record. John Wiley & Sons, Ltd, pp. 385–417. https://doi.org/10.1002/9781119424437.ch15

Silvestri, S., Defina, A., Marani, M., 2005. Tidal regime, salinity and salt marsh plant zonation. Estuar. Coast. Shelf Sci. 62, 119–130. https://doi.org/10.1016/j.ecss.2004.08.010

Smith, D.G., 1987. Meandering river point bar lithofacies models: modern and ancient examples compared, in: Ethridge, F.G., Flores, R.M., Harvey, M.D. (Eds.), Recent Developments in Fluvial Sedimentology: Contributions from the Third International Fluvial Sedimentology Conference. SEPM Society for Sedimentary Geology, pp. 83–91.

Smith, D.G., Hubbard, S.M., Leckie, D.A., Fustic, M., 2009. Counter point bar deposits: lithofacies and reservoir significance in the meandering modern Peace River and ancient McMurray Formation, Alberta, Canada. Sedimentology 56, 1655–1669. https://doi.org/10.1111/j.1365-3091.2009.01050.x

Stefanon, L., Carniello, L., D'Alpaos, A., Rinaldo, A., 2012. Signatures of sea level changes on tidal geomorphology: Experiments on network incision and retreat. Geophys. Res. Lett. 39, 1–6. https://doi.org/10.1029/2012GL051953

Storms, J.E.A., Weltje, G.J., Terra, G.J., Cattaneo, A., Trincardi, F., 2008. Coastal dynamics under

conditions of rapid sea-level rise: Late Pleistocene to Early Holocene evolution of barrier–lagoon systems on the northern Adriatic shelf (Italy). Quat. Sci. Rev. 27, 1107–1123. https://doi.org/https://doi.org/10.1016/j.quascirev.2008.02.009

Swan, A., Hartley, A.J., Owen, A., Howell, J., 2019. Reconstruction of a sandy point-bar deposit: implications for fluvial facies analysis, in: Ghinassi, M., Colombera, L., Mountney, N.P., Reesink, A.J., Bateman, M. (Eds.), Fluvial Meanders and Their Sedimentary Products in the Rock Record. John Wiley & Sons, Ltd, pp. 445–474. https://doi.org/10.1002/9781119424437.ch17

Terwindt, J.H.J., 1988. Palaeotidal reconstructions of inshore tidal depositional environments, in: De Boer, P.L., van Gelder, A., Nio, S.-D. (Eds.), Tide-Influenced Sedimentary Environments. pp. 233–263.

Tommasini, L., Carniello, L., Ghinassi, M., Roner, M., D'Alpaos, A., 2019. Changes in the wind-wave field and related salt-marsh lateral erosion: inferences from the evolution of the Venice Lagoon in the last four centuries. Earth Surf. Process. Landforms. https://doi.org/10.1002/esp.4599

Trincardi, F., Correggiari, A., Roveri, M., 1994. Late Quaternary transgressive erosion and deposition in a modern epicontinental shelf: The Adriatic semienclosed basin. Geo-Marine Lett. 14, 41–51. https://doi.org/10.1007/BF01204470

van de Lageweg, W.I., Schuurman, F., Cohen, K.M., van Dijk, W.M., Shimizu, Y., Kleinhans, M.G., 2016. Preservation of meandering river channels in uniformly aggrading channel belts. Sedimentology 63, 586–608. https://doi.org/10.1111/sed.12229

Wightman, D.M., Pemberton, S.G., 1997. The Lower Cretaceous (Aptian) McMurray Formation; an overview of the Fort McMurray area, northeastern Alberta, in: Pemberton, S.G., James, D.P. (Eds.), Petroleum Geology of the Cretaceous Mannville Group, Western Canada. Memoir - Canadian Society of Petroleum Geologists. pp. 312–344.

Willis, B.J., Sech, R.P., 2019a. Emergent facies patterns within fluvial channel belts, in: Ghinassi, M., Colombera, L., Mountney, N.P., Reesink, A.J., Bateman, M. (Eds.), Fluvial Meanders and Their Sedimentary Products in the Rock Record. John Wiley & Sons, Ltd, pp. 509–542. https://doi.org/10.1002/9781119424437.ch19

Willis, B.J., Sech, R.P., 2019b. Quantifying impacts of fluvial intra-channel-belt heterogeneity on reservoir behaviour, in: Ghinassi, M., Colombera, L., Mountney, N.P., Reesink, A.J., Bateman, M. (Eds.), Fluvial Meanders and Their Sedimentary Products in the Rock Record. John Wiley & Sons, Ltd, pp. 543–572. https://doi.org/10.1002/9781119424437.ch20

Willis, B.J., Tang, H., 2010. Three-Dimensional Connectivity of Point-Bar Deposits. J. Sediment. Res. 80, 440–454. https://doi.org/10.2110/jsr.2010.046

Wu, C., Bhattacharya, J.P., Ullah, M.S., 2015. Paleohydrology and 3D Facies Architecture of Ancient Point Bars, Ferron Sandstone, Notom Delta, South-Central Utah, U.S.A. J. Sediment. Res. 85, 399–418. https://doi.org/10.2110/jsr.2015.29

Yan, N., Colombera, L., Mountney, N.P., 2019a. Three-dimensional forward stratigraphic

modelling of the sedimentary architecture of meandering-river successions in evolving half-graben rift basins. Basin Res. published. https://doi.org/10.1111/bre.12367

Yan, N., Colombera, L., Mountney, N.P., Dorrell, R.M., 2019b. Fluvial point-bar architecture and facies heterogeneity and their influence on intra-bar static connectivity in humid coastal-plain and dryland fan systems, in: Ghinassi, M., Colombera, L., Mountney, N.P., Reesink, A.J., Bateman, M. (Eds.), Fluvial Meanders and Their Sedimentary Products in the Rock Record. John Wiley & Sons, Ltd, pp. 475–508. https://doi.org/10.1002/9781119424437.ch18

Yan, N., Mountney, N.P., Colombera, L., Dorrell, R.M., 2017. A 3D forward stratigraphic model of fluvial meander-bend evolution for prediction of point-bar lithofacies architecture. Comput. Geosci. 105, 65–80. https://doi.org/10.1016/j.cageo.2017.04.012

Zecchin, M., Baradello, L., Brancolini, G., Donda, F., Rizzetto, F., Tosi, L., 2008. Sequence stratigraphy based on high-resolution seismic profiles in the late Pleistocene and Holocene deposits of the Venice area. Mar. Geol. 253, 185–198. https://doi.org/http://dx.doi.org/10.1016/j.margeo.2008.05.010

Zecchin, M., Brancolini, G., Tosi, L., Rizzetto, F., Caffau, M., Baradello, L., 2009. Anatomy of the Holocene succession of the southern Venice lagoon revealed by very high-resolution seismic data. Cont. Shelf Res. 29, 1343–1359. https://doi.org/10.1016/j.csr.2009.03.006

Zecchin, M., Tosi, L., Caffau, M., Baradello, L., Donnici, S., 2014. Sequence stratigraphic significance of tidal channel systems in a shallow lagoon (Venice, Italy). The Holocene 24, 646–658. https://doi.org/10.1177/0959683614526903

SEDIMENTOLOGY OF A MACROTIDAL POINT-BAR (MONT-SAINT-MICHEL BAY, NW FRANCE) REVEALED BY COMBINING LIDAR TIME-SERIES AND SEDIMENTARY CORE DATA

PAPER

To be submitted to *Sedimentology*

Marta Cosma[a], Dimitri Lague[b], Andrea D'alpaos[a], Jerome Leroux[b], Baptiste Feldmann[c], Massimiliano Ghinassi[a]

[a] Department of Geosciences, University of Padova, Padova, Italy

[b] Université de Rennes, CNRS, Géosciences Rennes, Rennes, France

[c] Université de Rennes, CNRS, Observatoire des Sciences de l'Univers, Rennes, France

1. ABSTRACT

Intertidal meanders developed on saltmarshes are known to progressively expand and produce inclined heterolithic strata which tend to bear evidence for rhythmic deposition in the upper part of the bar, since the lower bar deposits are commonly washed by strong currents which are able to remove mud and develop discontinuous record of tidal cycles. Although these criteria are widely accepted, facies models for tidal point bars still lack a 3D perspective and overlook along-bend variability of sediment distribution and sedimentary processes. This can have a direct impact on intra-point bar heterogeneities and connectivity, with remarkable implications on development of oil reservoirs. The present study focuses on a macrotidal point-bar of the Mont Saint Michel Bay (France), and analyses sedimentology of a time-framed accretionary package by means of Lidar topographic data, geomorphological field surveys and sedimentological core data. Study deposits were accreted along the bar between 28/03/2012 and 29/11/2012. Integration between Lidar and sedimentary core data shows that over this time the bar expanded alternating deposition along its seaward and landward side. The maximum thickness of deposits was accumulated in the bar apex zone, and just landward of it, where the largest amount of mud was also stored. High sediment accretion in the bend apex zone is ascribed to development of ebb and flood recirculation zones, and related slough water conditions. High accretion rate of the bar apex zone promoted also higher preservation of rhythmites, which are almost missing from deposits accumulated along the bar sides.

Keywords: tidal meander, rhythmites, tidal cycles, recirculation zone, mutually-evasive currents, bidirectional flow

2. INTRODUCTION

Tidal meandering channels and related point bar deposits have mainly been studied in modern coastal plains, both in microtidal (Smith, 1987; Fruergaard et al., 2011; Brivio et al., 2016; Ghinassi et al., 2018), mesotidal (Barwis, 1978; Smith, 1987; Fenies and Faugères, 1998; Sisulak and Dashtgard, 2012; Johnson and Dashtgard, 2014) and macrotidal setting (Bridges and Leeder, 1976; De Mowbray, 1983; Pearson and Gingras, 2006; Choi, 2010, 2011; Choi and Jo, 2015). Migration and planform evolution of tidal bends are governed by a complex interaction between hydrodynamics, changes of tidal prism, tidal asymmetry, bidirectionality of tidal currents, pattern of mutually evasive tidal-current, sediment grain size, substrate composition and morphology and vegetation cover (Gabet, 1998; Cleveringa and Oost, 1999; Zeff, 1999; Marani et al., 2002; Solari et al., 2002; Fagherazzi et al., 2004; Garotta et al., 2007; Li et al., 2008; Carling et al., 2015; D'Alpaos et al., 2017; Finotello et al., 2018). However, despite these complex interactions occurring at different spatial and temporal scales, most accepted models link evolution of tidal meanders with a progressive increase in sinuosity (Bridges and Leeder, 1976; De Mowbray, 1983) pointing out that the morphodynamics of tidal bends is still poorly understood.

Detection of tidal point bars in the stratigraphic record (Nio and Yang, 1991; Santos and Rossetti, 2006; Legler et al., 2013; Díez-Canseco et al., 2014; Pelletier et al., 2016), and discrimination from their fluvial counterparts (Allen, 1963; McGowen and Garner, 1970; Brice, 1974; Jackson, 1976; Nanson, 1980), is based on a number of features including: abundance of mud, high degree of bioturbation (brackish-to-marine trace fossil), rhythmic deposition, reactivation surfaces, and bidirectional flows (Allen, 1982; Smith, 1987; Cuevas Gonzalo and De Boer, 1991; Gingras et al., 2016). Abundance of mud and rhythmic deposition are commonly considered as crucial evidence to detect tidal signature in the stratigraphic record (Bridges and Leeder, 1976; Barwis, 1978; De

Mowbray, 1983; Pearson and Gingras, 2006; Santos and Rossetti, 2006; Dalrymple and Choi, 2007), and also in bar deposits (Choi et al., 2004; Hubbard et al., 2011; Fustic et al., 2012; La Croix and Dashtgard, 2014, 2015).

In tidal environments, mud occurs at different scales: i) as laminae within sedimentary structures (Dalrymple et al., 1991; Tessier, 1993; Choi, 2010, 2011); ii) as thick layers (e.g. fluid mud – Harris et al., 2004; Ichaso and Dalrymple, 2009; Longhitano et al., 2012; Chen et al., 2015) and iii) as intervals within the inclined heterolithic stratification (IHS – Bridges and Leeder, 1976; Barwis, 1978; De Mowbray, 1983; Thomas et al., 1987; Choi et al., 2004, 2013; Fagherazzi et al., 2004; Rebata-H. et al., 2006; Hovikoski et al., 2008; Kleinhans et al., 2009; Sisulak and Dashtgard, 2012; Johnson and Dashtgard, 2014; La Croix and Dashtgard, 2014). In tidal point bars, mud is thought to be dominant in the upper bar zone, where it commonly promotes development of sliding surfaces, with collapses of the bar top deposits and development of mud clast breccias (Musial et al., 2011; Sisulak and Dashtgard, 2012; Broughton, 2018). However, a lack of knowledge still remains on its spatial and vertical distribution which strongly depends on the peculiar hydrodynamics of ebb and flood tidal currents.

Rhythmites are the most reliable evidence for tidal processes (Choi and Park, 2000; Choi and Dalrymple, 2004). However, with the exception of some uniquely preserved examples (Pelletier et al., 2016), distribution and preservation of these structures within tidal point bars are not ubiquitous (Choi, 2010, 2011; Choi et al., 2013). Their occurrence has been investigated mainly in a vertical frame and it is thought to depends on the relative elevation of the point bar with respect to Mean Sea Level (MSL). Rhythmites are commonly documented in the middle part of point bar deposits, where major number of submergence events can be recorded (Tessier, 1993; Archer, 1998). Differently, dominance of subaerial exposure (Dalrymple et al., 1991) and of high-energy conditions (Choi et al., 2004), prevents recording of a rhythmic deposition in upper and lower bar

deposits, respectively. The along bend distribution and preservation of tidal rhythmites have not received the same attention.

Understanding sedimentology of tidal point-bars has remarkable implications in pointing out how tidal currents can modulate fluvial deposition along channel bends, with remarkable implication for development of oil reservoirs (Hubbard et al., 2011; Musial et al., 2011; Fustic et al., 2012; Martinius et al., 2015). Accordingly, great efforts have been put to understand the role of tidal currents in modulating fluvial sedimentation and to establish criteria for their relative identification in the fossil record (Hovikoski et al., 2008; Dashtgard et al., 2012; Johnson and Dashtgard, 2014; Carling et al., 2015; Dalrymple et al., 2015; Gugliotta et al., 2016; Jablonski and Dalrymple, 2016; Mclean and Wilson, 2017). Nevertheless, tidal point bars are simplistically depicted as "expansional bars" (i.e. characterized by a progressive increase in sinuosity; cg. Jackson, 1976), which preserve tidal rhythmites in their middle part and contain muddy bar top deposits. These facies models still lack a 3D perspective, do not consider the effects of tidal currents in planform evolution of mender bends, and overlook along-bend variability of sedimentary processes.

The present study focuses on a macrotidal point-bar formed by a tidal bend of the Mont Saint Michel Bay (France), and aims at better understanding the mechanisms of tidal point bar growth and distribution of sediments along the bend. Sedimentary features and depositional dynamics of a time-framed accretionary package are analysed here in a 3D perspective, by means of integration between: i) Lidar topographic data, ii) geomorphological field surveys and iii) sedimentological core data. The along-bend distribution of sedimentary features, including grain size, thickness and preservation of tidal signature are illustrated and discussed.

3. GEOLOGICAL SETTING

3.1. The Bay of Mont-Saint-Michel

The Bay of Mont-Saint-Michel (MSMB) is located in the north-western coast of France along the English Channel (Fig 1A). It is one of the world's most well-known hypertidal environments, with a tidal range reaching up to 15.3 m during the highest spring tides (Tessier, 1993). The tidal regime is semi-diurnal. The MSMB is a wide (500 km^2) and shallow (< 20 m) embayment gently dipping toward the northwest, and incised into a Precambrian substrate. As most coastal landscapes around the English Channel, the morphology of the MSMB is a heritage of the Plio-Pleistocene glacio-eustatic fluctuations. Since the regional subsidence is negligible, only the last post-glacial transgression is recorded into the infilling of the MSMB, the previous sea-level fall having reworked almost all older marine sediments (Larsonneur et al., 1994; L'Homer et al., 1999). As a consequence, the coastal sedimentary wedge of the bay consists almost entirely of Holocene deposits, with only few remnants of Pleistocene fluvial terraces.

Protected from offshore wave action, the bay is almost entirely submitted to tidal dynamics. Tidal current speeds show highly spatio-temporal variations, with maximum flood current at the entrance of the bay of about 1 m/s (for mean high spring tides), which decreases toward the inner part of the bay to 0.3 – 0.7 m/s on the tidal flats. The highest speeds are recorded in intertidal channels, where currents can reach up to 2.5 m/s (Larsonneur, 1989). Three rivers (Sée, Sélune, and Couesnon) flow into the eastern bay (Fig 1A) and are characterized by low mean annual discharge, which is less than 20 m^3/s for the Sélune and the Couesnon, and only 8 m^3/s for the Sée (Larsonneur, 1989). Their annual sediment supply can be considered as almost negligible and does not exceed half of the sediment volume reworked during a single tidal cycle (Bonnot-Courtois, 2002). Sediment grain size progressively decreases from the outer to the inner

part of the estuarine domain. In the upper intertidal zone, mean grain size ranges from very-fine sand (0.09 mm) to silt (0.03 mm - Bourcart & Charlier, 1959; Larsonneur, 1975, 1989) and consists of both a bioclastic (up to 50%) and a mineral fraction (Larsonneur, 1989; Tessier, 1993).

3.2. The study site

The study site is located at the fringe of the salt marshes in the surrounding of MSM and about 500 m east of the Couesnon mouth (Fig 1A). The study channel, draining 2.2 km² of salt marshes, shows a radius of curvature of about 85 m, a sinuosity of ~ 1.26 and is almost 3 m deep at bankfull stage.

Data derived from Lidar surveys acquired between 2011 and 2017 (Fig 1B, C, and D - see relative high tide elevation in Fig 2A) show that elevation in the study area ranges between 3.5 (in the channel thalweg) to 7.5 (in the bar top zone) m asl IGN69 (vertical reference is implied henceforth). The study bend is located in the upper intertidal domain, implying that during spring tides, the channel empties out twice per day, while during neap tides, the bar is subjected to periods of emersion of about one week. The bar top zone site exhibits a clear vegetation zonation typical of the MSMB (Tessier et al., 2000; Bonnot-Courtois, 2002; Langlois et al., 2003; Détriché et al., 2011), with a permanent vegetation cover of *Halimione portulacoides* and *Festuca rubra* in the middle (~ 6.2 – 7.0 m asl, in the study site) and high (> 7.0 m asl ca, in the study site) marsh (Fig 1B), and a progressively less dense cover in the low marsh going from ~6.2 to 4.5 m asl ca, with the presence of *Suaeda maritima, Salicornia fragilis, Pulcinella maritima* and *Spartina anglica*. These species progressively colonized the bar top. Specifically, between 2011 to 2017 vegetation cover mainly expanded toward NE, whereas between 2013 and 2017 it grew mainly

toward W (dashed lines in Figure 1B and C). Growth pattern of vegetation also reflects the overall expansion of the bar (Fig 1B, C, and D), which alternatively accreted both landward and seaward between 2011 and 2017.
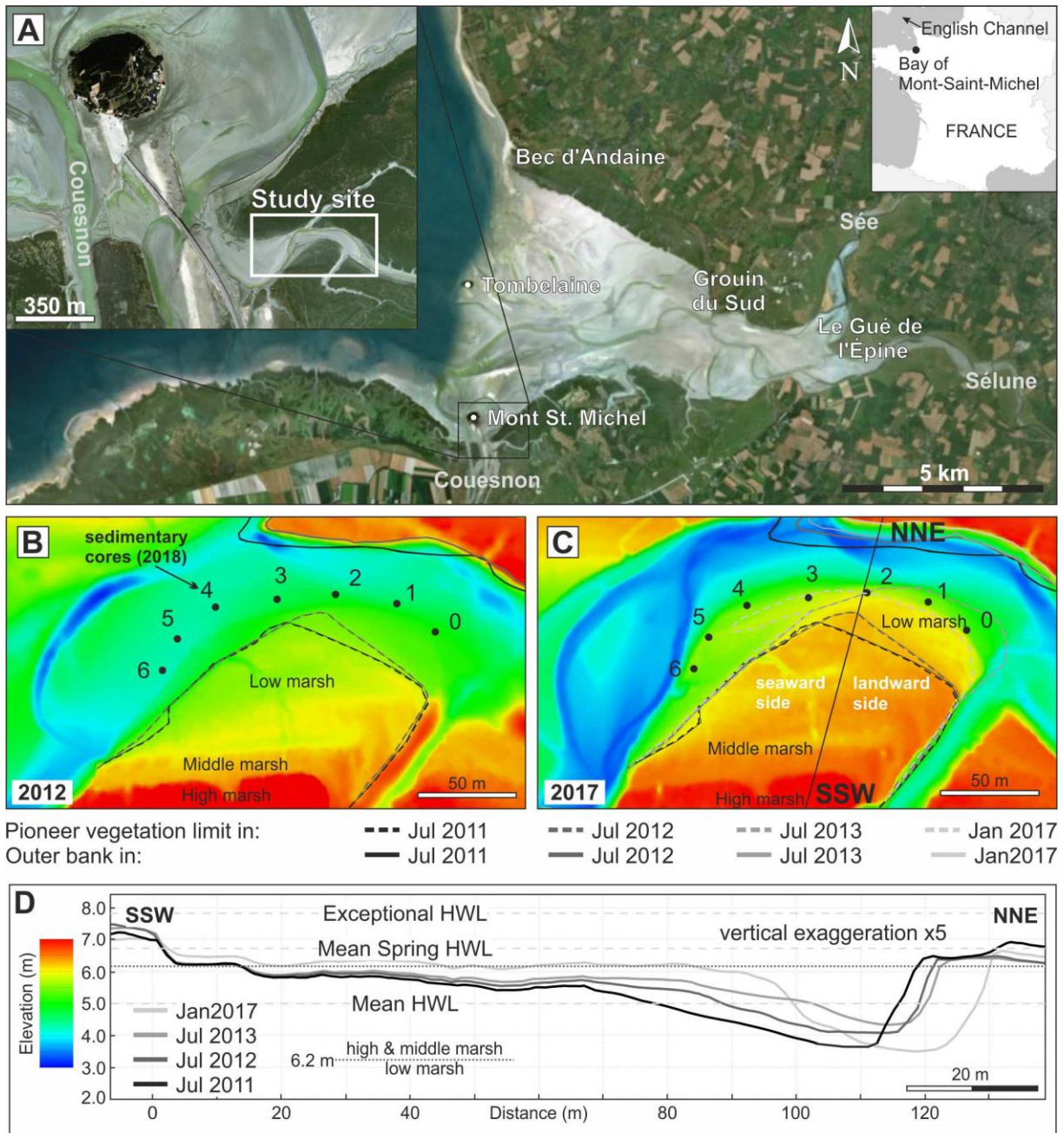

Figure 1. The study site. (A) Geographic location of the studied meander bend within the estuarine domain of the Mont Saint Michel Bay. (B and C) Lidar images showing bar topography in 2012 (B) and 2017 (C), with the location of the vegetation limit (dashed lines) and the outer bank (solid lines) between 2011 and 2017. (D) Changes in bar elevation along the bend axis between 2011 and 2017.

The overall retreat of the outer bank (mainly toward NE) in this period ranges between 7 and 15 m ca (solid lines in Figure 1B and C).

Velocities of tidal currents in the study meander have been analysed by Leroux (2013) with data acquisition performed by the Université de Rennes 1 between 2010 and 2013. During overmarsh tides, the seaward side of the bar is dominated by flood flow (directed toward ENE across the bar), with almost null velocity recorded during ebb flow; vice-versa, at the landward side, ebb flow (~1.00 m/s) is two times larger than flood flow and is directed toward NW (parallel to the vegetation limit). In the apex zone, flood and ebb flows are weaker (~0.75 m/s). In the channel thalweg, the highest velocities are registered for the ebb flow, exceeding 1.50 m/s (toward W); while flood current exceeds 0.50 m/s.

4. METHODS

Morphodynamic evolution and sedimentology of the bar have been characterized by means of integration between Lidar surveys, ground-checking and recovery of sedimentary cores. Specifically, a bar accretionary package accumulated between 28/03/2012 and 29/11/2012 (hereinafter 2012 accretionary package) has been spatially defined and cored in order to compare sedimentary products with corresponding styles of bar accretion and recorded variations of tidal excursion. This time interval has been selected because of the availability of nearly regularly-distributed Terrestrial Laser Scanner (TLS) surveys (acquired by Université de Rennes 1 – Leroux, 2013), which capture changes in bar morphology during both neap and spring tides (Fig 2A). This integrated approach aims at characterize morphodynamics and sedimentological processes occurring along the seaward and landward side (Fig 1C) of the bar (*sensu*

Brivio *et al.*, 2016). Different methods used in this work are concisely described in the next paragraphs.

4.1. Morphodynamic evolution of the bar: topographic data sources and point-cloud processing

The topographic data, kindly provided by the Université de Rennes, consist of thirteen short-range Terrestrial Laser Scanner (TLS) surveys and one long-range airborne Lidar survey (Fig 2A). This last survey was acquired in January 2017 using a Teledyne Optech Titan Lidar resulting in a point cloud density of 10 pts/m², with a vertical uncertainty of +-10 cm. The TLS surveys were conducted at low tide using a Leica® Scanstation 2 mounted on a survey tripod. Detailed characteristics of this scanner can be found in (Lague et al., 2013). For each survey, 3 to 8 different scanning stations were used, depending on the time available between tides, and were co-registered both for intra-survey registration and for local geo-referencing using both fixed and mobile targets. Registration errors vary between 1.5 and 3.4 mm. As typical of TLS data, large variations in point density occurred, ranging between 1 to 10 pts/cm² in the pioneer vegetation area, and around 1 pt/cm² in the outer bank. The targets were also surveyed with differential GPS at ± 2 cm vertical precision to link the TLS surveys to the IGN69 reference elevation.

All the processing of Lidar data, described hereinafter, were performed using CloudCompare, a 3D point cloud editing and processing software (EDF R&D, 2011). In this research, an initial treating of the raw data has been necessary to obtain well suitable data for the creation of the synthetic stratigraphy. In this phase, Lidar data were processed for the removal of vegetation and for the reconstruction of the channel thalweg, where data points were missing because of the presence of water during the

scanning period. For the vegetation removal and to homogenise point density, the lowest point of the raw data for each pixel of 20 cm grid was kept. Manual validation ensured that no vegetation points remained. This process is particularly effective where sparse patches of vegetation occur, whereas densely vegetated areas were not included in the following analyses (i.e. above 6.2 m asl) as the ground cannot be detected below vegetation. For the interpolation on the missing data of thalweg zone due stagnant low tide water (i.e., below 3.75 – 4.10 m asl), the grid of ground point cloud was transformed into a tin via the Poisson Surface Reconstruction algorithm (Kazhdan et al., 2006; Kazhdan and Hoppe, 2013), as implemented in CloudCompare (set parameters: octree cell size of 0.0003 m², octree depth of 10 and radius of 3 m to compute the surface normal orientation). Using a multiscale approach and accounting for surface normal orientation, the Poisson Surface Reconstruction provided a visually realistic interpolation of the thalweg. Because of this interpolation process of the channel thalweg, we do not interpret quantitatively this part of the results. The obtained surfaces are sampled at a regular grid (1 m resolution), and the resulting point clouds are used for the creation of the synthetic stratigraphy.

4.2. Identification of the 2012 accretionary package: the synthetic stratigraphy approach

The Lidar data have been used to create a synthetic stratigraphy of the study bar, in order to define spatial distribution of the deposits forming the 2012 accretionary package, along with their internal architecture. Multi-temporal lidar topographic data have been widely used to create point bar synthetic stratigraphy and assess patterns of erosion and deposition in laboratory experiments (Van de Lageweg et al., 2013), nevertheless this is a first attempt to integrate a synthetic stratigraphic model with related real core data.

The synthetic stratigraphy was obtained by means of a python™ script, selecting from the oldest (1st-iteration) to the youngest (n-iteration) survey, each point cloud has been lowered wherever a younger survey shows a lower elevation (i.e. where erosion occurred). At the (n-1)-iteration the synthetic stratigraphy was created (Fig 2C). Measuring the vertical distances between the obtained point clouds reflect the thickness of the preserved deposits in the bar. An estimation of the resulting volumes has been performed using a CloudCompare tool ('Compute 2.5 volume' which realizes a vertical difference of digital elevation model interpolated from the point clouds and sum up the difference and accounts for pixel size). This procedure allowed us to identify the overall volume of sediments forming the 2012 accretionary package and also to discriminate seven preserved sub-volumes accreted between successive surveys (hereafter "internal increments"). In order to provide a simple nomenclature of the increments, each one is going to be called with the date of the older survey: for example, the internal increment of sediments deposited between 03/05/12 and 11/06/12 and preserved in the synthetic stratigraphy is going to be called "03/05/12 internal increment".

4.3. Bar-deposits: surface and core data

An initial investigation of the study bar was performed in September 2017 in order to document surface sediment distribution and sedimentary processes (Fig 3), whereas seven sedimentary cores were collected in June 2018. Cores were recovered along the bar brink (Fig 1C), and coring sites were georeferenced using a differential GPS with a maximum position uncertainty of 6 cm. Coring aimed at picking up sediments from different parts of the bar (landward and seaward sides) and, above all, at recovering deposits forming the 2012 accretionary package. Sedimentary cores, each up to 3.0 m deep, were recovered using an Eijkelkamp hand auger, with a 1.0 m-long gouge sampler which has a diameter of 30 mm. Core sediment samples were kept humid in PVC liners

and then cut longitudinally, photographed and stored as sedimentary peels produced using epoxy resins. Cores were measured following basic principles of facies analyses, to understand the overall distribution of sedimentary facies in different parts of the bar (Fig 3). Deposits from the 2012 accretionary package (Figs 4 and 5) have been analysed in order to provide a quantitative classification of different sedimentary features. Cores from these deposits have been subdivided into 1 cm-thick intervals, and each interval has been characterized on the basis of the: i) percentage of sand/mud fraction (5 classes on the basis of the sand %: 100%, more than 60%, between 30 and 60%, less than 30%, and 0%); ii) sedimentary structures (e.g. cross laminations, plane-parallel laminations); iii) occurrence of roots, oxidation, mud cracks and mud clasts. Pie charts have been created to summarized data on grain size and sedimentary structures of each core (Figs 7 and 8). Grain size data have also been plotted as pie charts for the different internal increments in order to investigate possible correlations between grain size changes and tidal excursion (Fig 9).

In order to investigate preservation of the tidal signature in the 2012 accretionary package, attention has been paid on the rhythmic alternation of sandy and muddy laminae and progressive changes of related thickness. Following (Tessier, 1993), each couplet of sandy/mud laminae represents one elementary tidal cycle (TC), while their progressive thickening and thinning (with a total of 10 – 12 successive TCs) represents the neap/spring tidal cycle, or tidal cycle sequence (TC sequence). Progressive increase or decrease of thickness of TCs, within a single or adjacent 1 cm-thick intervals, has been ascribed to variations of tidal discharge (i.e. alternation between neap and spring tides), and therefore interpreted as signature of tidal processes (Fig 2D). Progressive changes in thickness of TCs can define different TC sequence trends (Fig 2D): i) thickening- to thinning-upward trends (i.e. a complete TC sequence) ii) thickening- or thinning-upward trend (i.e. partially preserved TC sequence) and iii) no trend (i.e. no tidal signature preserved).
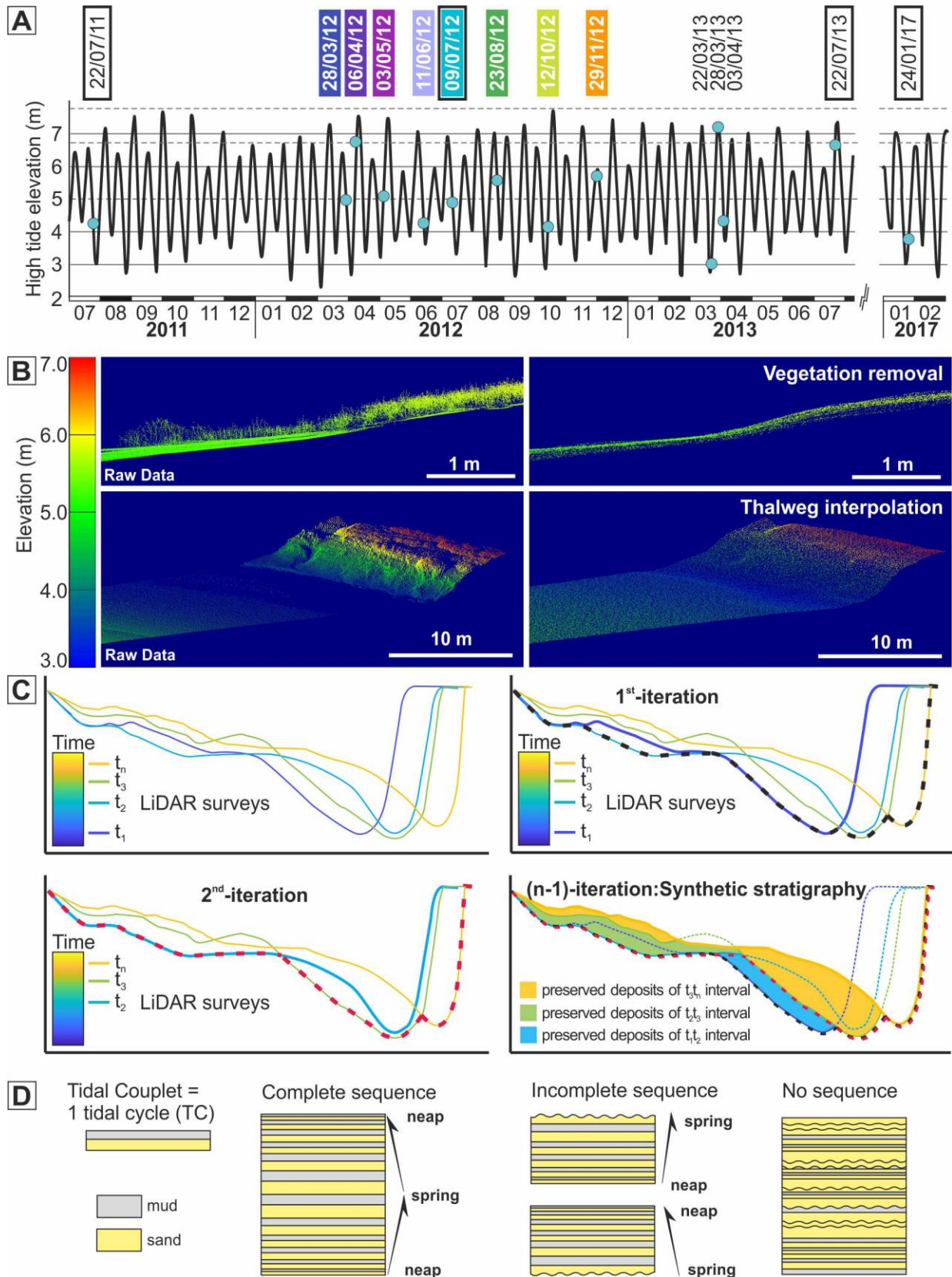
Figure 2. Methodologies used to define and analyse the 2012 accretionary package. (A) Date of the Lidar surveys between 2011 and 2017 relative to the high tide elevation. (B) Example of the raw data processing for the vegetation removal and for the reconstruction of the thalweg zone. (C) Simplified diagram showing the synthetic stratigraphy approach, which allow to define the effectively preserved accretionary units. See text for explanation. (D) Sketch illustrating criteria to define different amount of preservation for tidal rhythmites.

4.4. Tide data sources

Tide data series for the study time interval (Fig 2A) were supplied by the Service Hydrographique et Océanographique de la Marine (http://refmar.shom.fr). Measurements related to Saint-Malo gauge are transposed to MSM subtracting 5.7 m to the tide elevation (Roux, 1998). Tide data allowed to establish how many times the study channel was drained either during spring or neap tides.

5. RESULTS

5.1. Bar morphology and deposits

Different deposits accumulated by specific depositional processes in three main zones of the studied bend: bar top, bar slope and channel thalweg (Fig 3).

The bar top zone is characterized by a flat topography (Fig 3A and B) and by the presence of a sparse vegetation cover (Fig 3C). Polygonal mud cracks are also common in this zone. Bar top deposits consists of plane-parallel laminated mud with silt and very-fine sand concentrated in 1-2 mm thick laminae (Fig 3D). Oxidation and sand-filled crack are common (Fig 3N).

The bar slope connects the bar top with the channel thalweg zone, and dips up to 20°. Inclination decreases from the upper (10-15°) to the lower (5-10°) slope (Fig 3A and B).
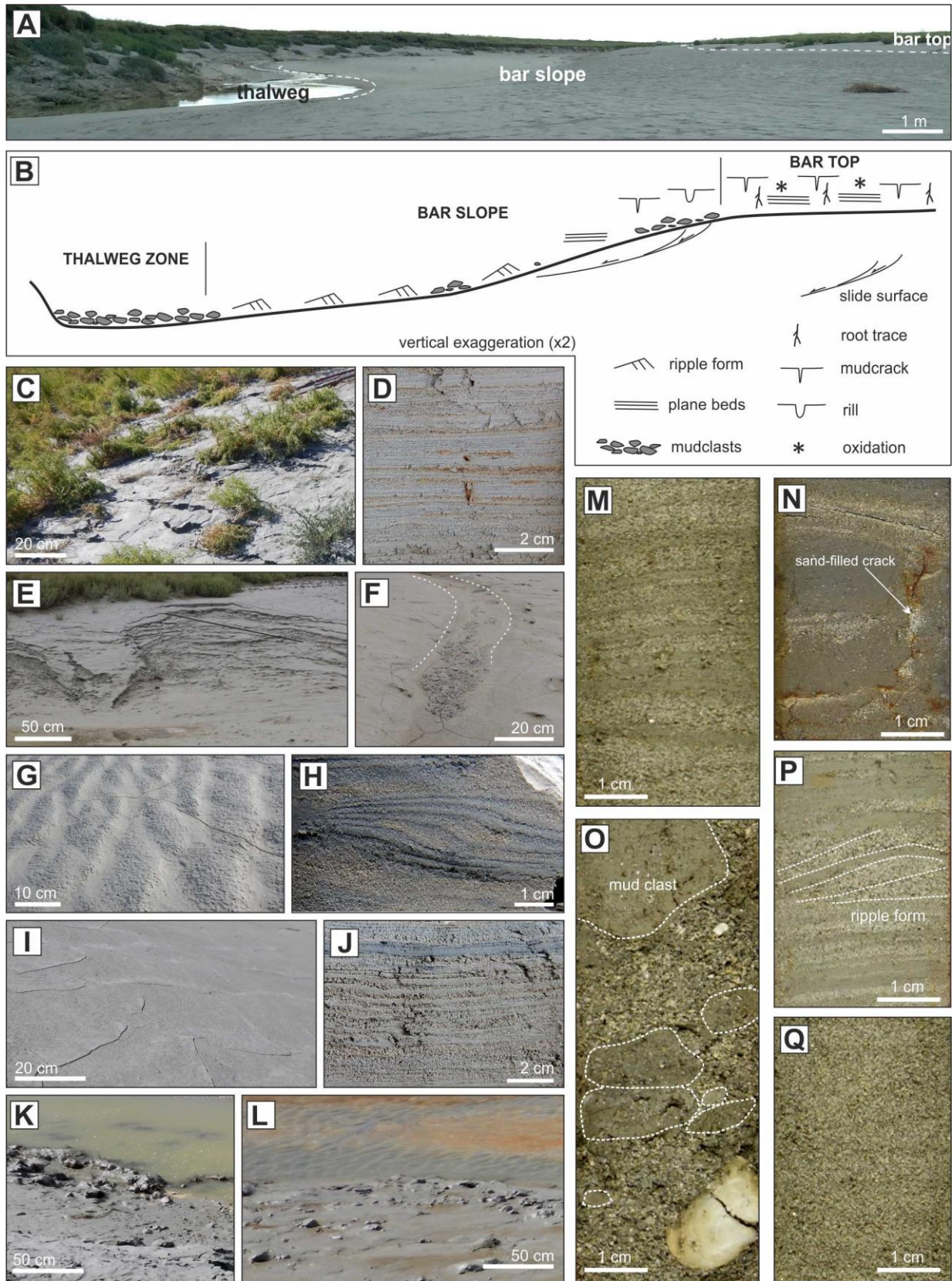
Figure 3. Morphological and sedimentological feature of the study site obtained from the 2017 field survey (A and C – L) and sedimentary cores (M – Q). The axial zone of the study bend (A) and relative sketch (B) showing spatial distribution of different sedimentary features. (C) Sporadically vegetated bar top deposits. (D) Plane-parallel laminated and oxidized bar top deposits showing clear tidal couplets. (E) Bank collapses affecting the landward side of the bar. (F) Mud clasts at the outlet of a minor rill cut in the upper part of the bar. (G) Current ripple forms in the central part of the bar slope. (H) Rhythmic lamination within a climbing ripple form. (I) Mud cracks in the upper part of the bar slope. (J) Rhythmic lamination in plane-parallel laminated bar deposits accumulated in the upper slope. (K) Cobble to pebble-sized mud clasts in the lower part channel thalweg zone, where current ripples develop (L). (M) Plane-parallel stratified bar sand with muddy laminae developed during slack water stages. (N) Bar top mud showing a sand-filled desiccation fracture. (O) Channel lag medium sand with scattered mud clasts and shell fragments. (P) Ripple-cross laminated sand with mud drapes. (Q) Mud-free sand from the lowermost part of the bar.

Bar slope is characterized by the presence of current ripple and plane beds (Fig 3G, H and J), polygonal mud cracks (Fig 3I), rills (Fig 3F) and local accumulation of flat mud clasts (Fig 3F). Slides commonly occur in this zone (Fig 3E). The related deposits consist of sediments ranging in grain size between mud to fine sand (Fig 3M and Q). These deposits are plane-parallel and ripple-cross laminated, and laminae are commonly marked by mud (Fig 3M and P). Moving from the upper to the lower bar slope, sand content increases and mud laminae become progressively less common.

The channel thalweg zone shows an irregular topography (Fig 3A, B, K, and L). Mud clasts are spherical, and are up to 10-15 cm in size (Fig 3K). They occur individually or in clusters over a sandy bed, which contains shell fragments and is locally characterized by the occurrence of current ripples (Fig 3L). Thalweg deposits are mainly massive (Fig 3O) and characterized by the common occurrence of mud clasts and shell fragments.

5.2. The 2012 accretionary package

5.2.1. Synthetic stratigraphy

Synthetic stratigraphy shows that the 2012 accretionary package consists of ca. 3300 m^3 of deposits, which were accumulated mainly in the bar slope zone (Fig 4). The substrate of the 2012 accretionary package sloped from bar top (~5.5 – 6.0 m asl) to the channel

thalweg (~3.5 m asl) (Fig 5). The 2012 accretionary package forms an arcuate sedimentary body, that follows the pre-existing bar morphology, and reaches the maximum thickness in the bar apex zone (Fig 4A). This sedimentary body pinches out toward the bar top and channel thalweg (Figs 4B, C and 5C).
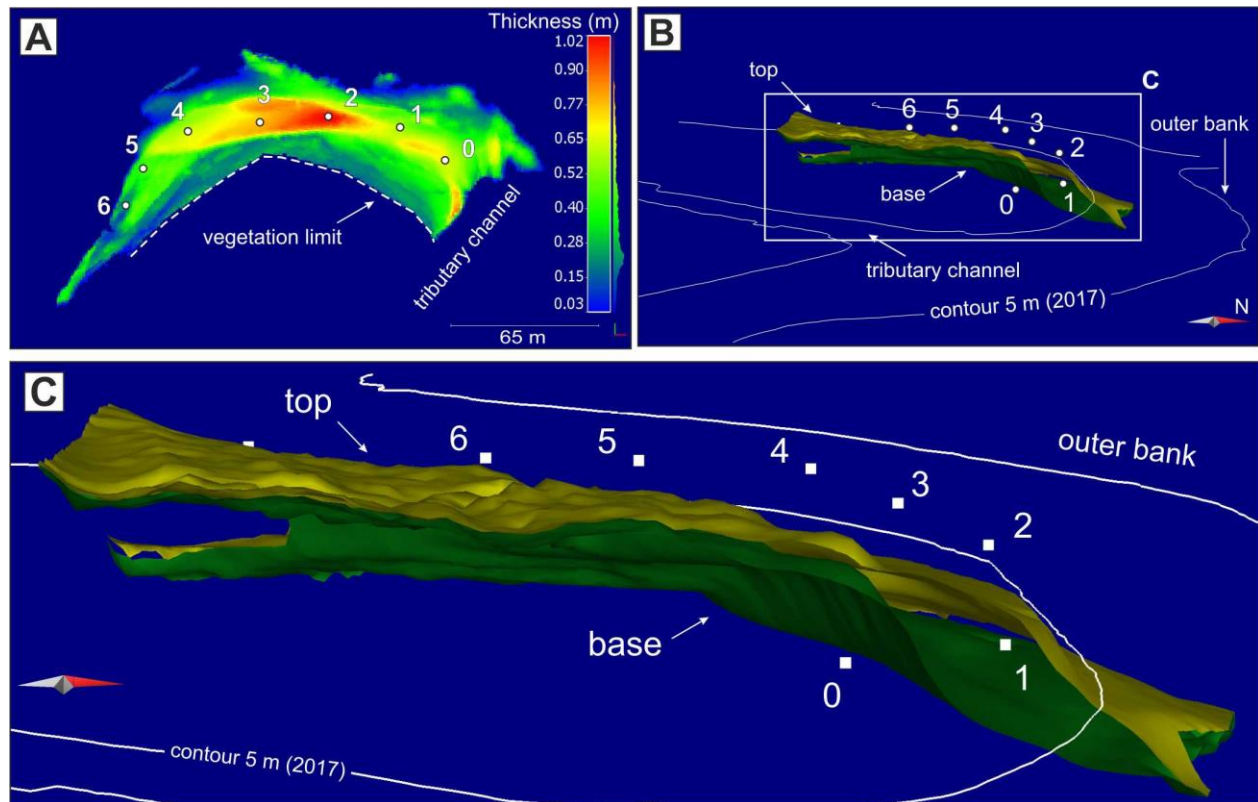

Figure 4. The 2012 accretionary package. (A) Thickness distribution within the accretionary package. (B) 3D reconstruction showing the upper and lower surface bounding the study package. (C) Close view of B (Vertical exaggeration: x10).

A cross-section along the bar axis (Fig 5A and C), shows that ca. 20 cm of deposits accreted on the bar top, with single internal increment accumulation of few centimetres (Fig 5C). In contrast, few deposits accumulated in the thalweg zone, with evident cross-cutting relations between the different internal increments (Fig 5C). Thicker deposits are recorded on the bar slope zone (Fig 5C), and they form a rim along the bar (Fig 4A). The maximum thickness is ca 1 m (Fig 4A) and is recorded in the bend apex zone (i.e. cores 2 – 3), although 70 cm thick deposits occur along the landward side of the accretionary package (cores 0 – 1).
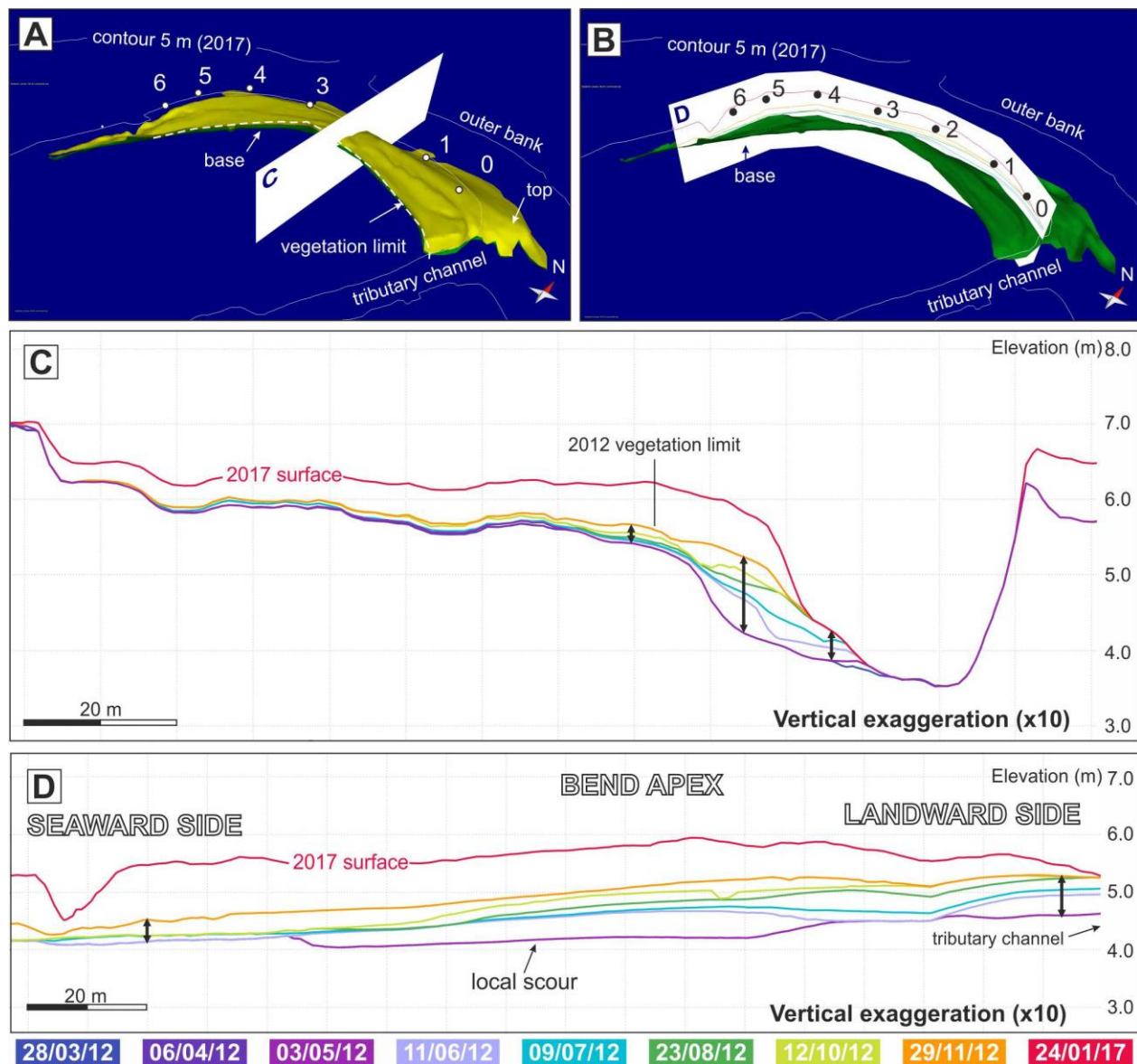
Figure 5. Synthetic stratigraphy of the 2012 accretionary package. (A) Location of a cross section cutting the accretionary package along the bend axis (A) and along the 2017 bar brink (B). Position of the study cores is also shown. Axial (C) and along-bend (D) cross sections showing the internal increments within the study accretionary package. Dark-grey arrows indicate 2012 accretionary package thickness variations.

An along-bend cross section (Fig 5B and D) shows that the 2012 accretionary package thins toward the seaward side of the bar, whereas along the landward side it is abruptly cut (Fig 5D) by a secondary tributary channel (Fig 1).

The analysis of the spatial distribution of these increments suggests that the overall expansion of the bar (Fig 1B and C) was achieved by an irregular storage of sediments along the bar, that occurred through localized accretionary episodes, which affected: i) the seaward side (11/06/12, 23/08/12, and 12/10/12); ii) the landward side (03/05/12, 11/06/12, 09/07/12, and 23/08/12); iii) both sides (11/06/12 and 23/08/12); and iv) the bar apex zone (03/05/12, 11/06/12, 09/07/12, 23/08/12, and 12/10/12). Sedimentation in a local scour is also evident in one case: the 03/05/12 internal increment shows in the along-bend cross section a concave-upward basal surface, which is lower with respect to the overall elevation (Fig 5D).

Preservation of internal increments changes from the seaward to the landward side of the bar, and is highest in the bar apex zone, where 5 increments (03/05/12, 11/06/12, 09/07/12, 23/08/12, and 12/10/12) are preserved, and lowest along the seaward side of the bar, where only two or three increments are recorded.
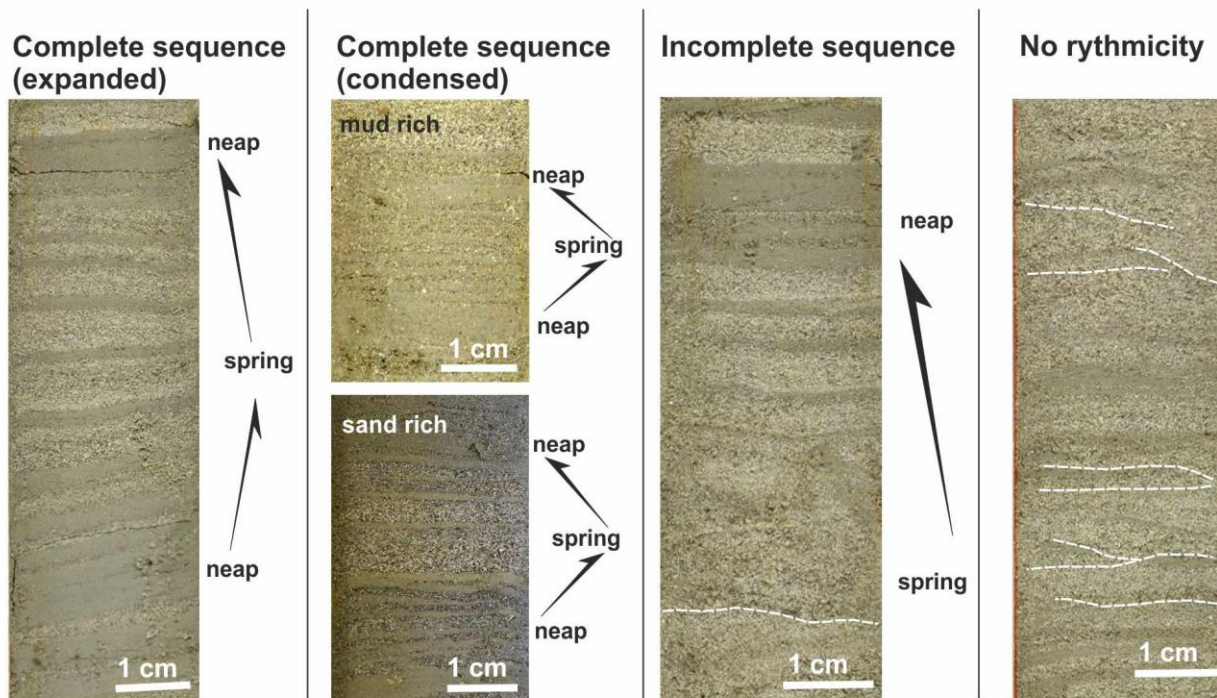

Figure 6. Different expression of rhythmites within the 2012 accretionary package.
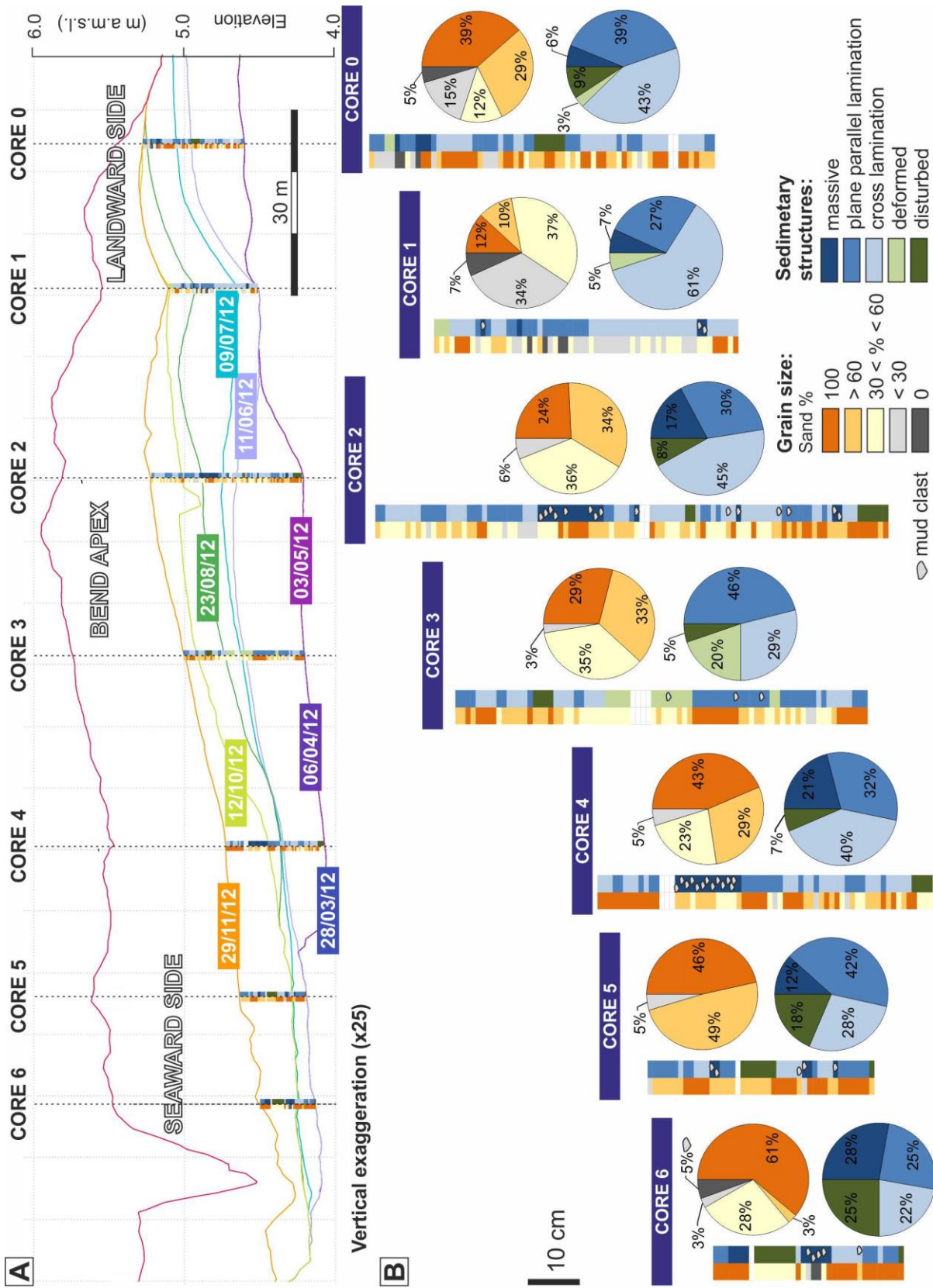
Figure 7. Along-bend distribution of grain size and sedimentary structures within the 2012 accretionary package. (A) Location of the study cores along the bend and synthetic stratigraphy of the 2012 accretionary package. (B) Anatomy of the 2012 accretionary package. Pie charts show distribution of grain size and sedimentary structures for different cores.

5.2.2. Sedimentology

Grain-size distribution varies both vertically and laterally within the 2012 accretionary package, but the along-bend distribution of grain size is not influenced by elevation above the thalweg zone, being the accretionary package sites at a similar elevation (i.e. between 30 cm and 1 m above the channel thalweg) along the inner bank. Specifically, sand content increases both downward and seaward within the accretionary package (Fig 7B). The lowest sand content occurs in the central bar zone (cores 1 – 3), where the accretionary package reaches its maximum thickness, and the minimum amount of sand is in core 1, just landward of the bend apex (Fig 7B). Mud content is complementary to sand distribution, and the highest mud content is recorded between core 1 and 3. Accretionary deposits along the seaward side of the bar are mud free, since all the mud in core 6 occurs as pebble-sized intraclasts. These mud clasts are locally oxidized and contain plant debris, suggesting that they were sourced through collapses from either the upper bar zone or outer banks. In most of the cores, mud clasts are scattered and millimetric in size. They show both rounded or flat shapes, and commonly oriented according with the main stratification.

Sedimentary structures in the 2012 accretionary package consists of plane-parallel stratification and current ripple-cross laminations, and their spatial distribution does not show any specific trend, neither vertically nor along the bend (Fig 7B). Deposits accumulated on the bar slope show local evidence of deformation, which could be ascribed to gravitational collapses, although the limited diameter of cores prevents detailed observations. Integration between synthetic stratigraphy and grain-size data (Fig 8), show that the smallest amount of clean sand (i.e. 25%) occurs in 09/07/12 and
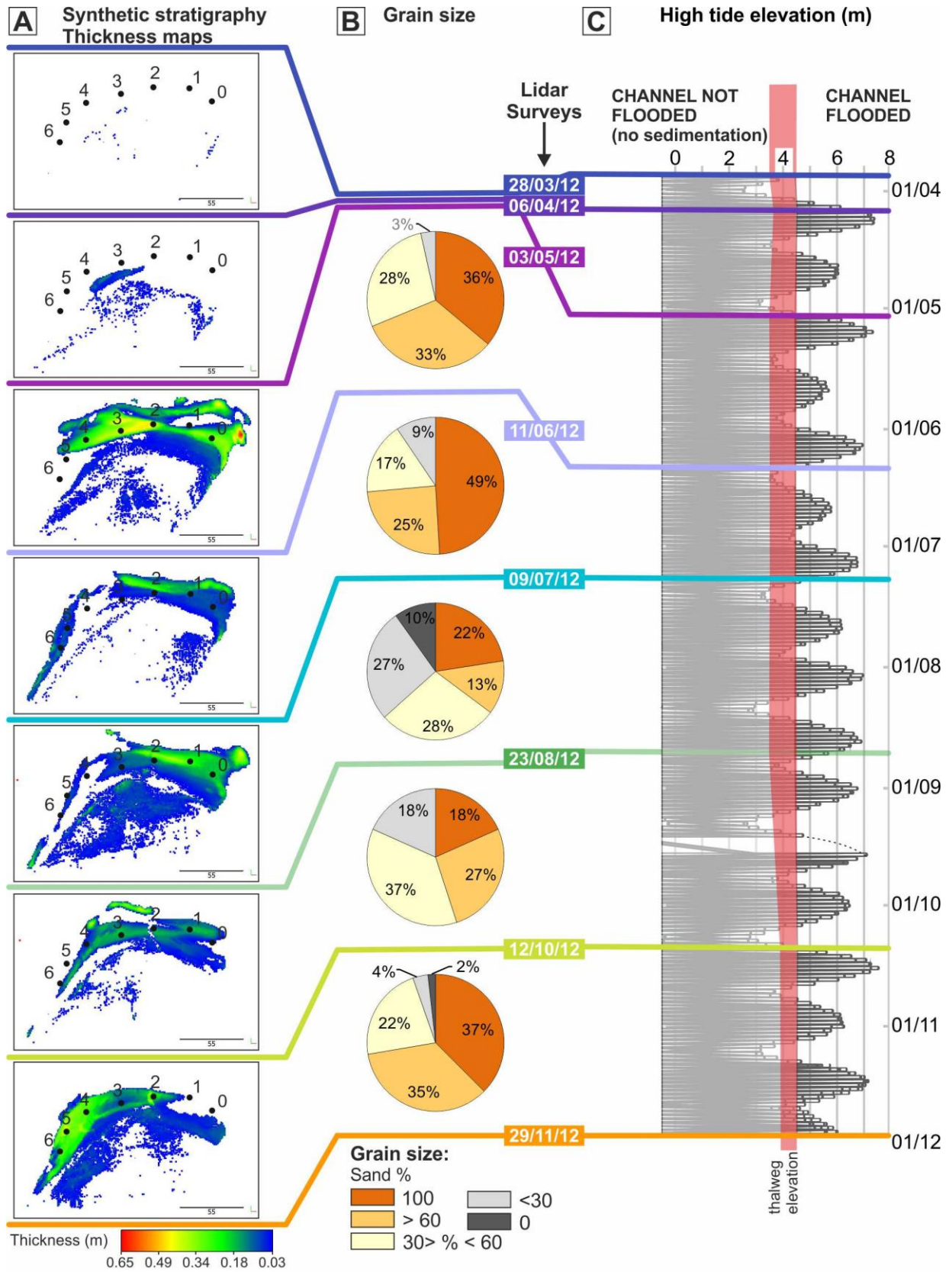
A Synthetic stratigraphy Thickness maps

B Grain size

C High tide elevation (m)

Lidar Surveys

CHANNEL NOT FLOODED (no sedimentation)

CHANNEL FLOODED

Grain size:
Sand %
- 100
- > 60
- 30> % < 60
- <30
- 0

Thickness (m)
0.65 0.49 0.34 0.18 0.03

23/08/12 internal increments (Fig 8B), which accumulated when sediment was mainly stored along the landward side of the bar (Fig 8A).

Tidal signatures in the 2012 accretionary package were analysed to quantify the spatial distribution of fully- or partially-preserved TC sequences (Fig 2D). A complete TC sequence (Fig 6) can vary in thickness between 1 (i.e. condensed sequences) and 7 cm (i.e. expanded sequences), and can be made up of 9 – 12 TCs (in accordance to the results of Tessier, 1993). Single tidal couplets are commonly only a few millimetres thick, but their thickness can range from 1 mm to 2 cm in condensed and expanded sequences, respectively (Fig 6). Expanded sequences commonly contain abundant sand, whereas condenses sequences can be either mud- or sand-rich. Abundance of complete TC sequences varies along the bend (Fig 9) from 0 to 26% of the 2012 accretionary package thickness. They are more common (i.e. > 10% of 2012 accretionary package thickness) in the central part of the bar (i.e. cores 1 to 4), and reach the maximum abundance in core 1 (i.e. immediately landward of the bend apex). In cores 1 to 4, TC sequences are not distributed at any specific elevation within the 2012 accretionary package, and can occur randomly (e.g. core 1 and 3) in the accretionary package or in its higher (e.g. core 2) or lower (e.g. core 4) portion. Partially-preserved TC sequences are spatially distributed along the bend and represent the 5 to 18% of the accretionary package thickness of interest, except for core 6 (i.e. the most seaward core), where neither complete nor partially-preserved sequences are recorded (Fig 9). Partially-preserved TC sequences are located in proximity of complete ones. As a whole, the spatial distribution of fully- and partially-preserved TC sequences show that rhythmic signal on sedimentation is mainly preserved in the central bar zone, where rhythmites (i.e. fully- and partially-preserved
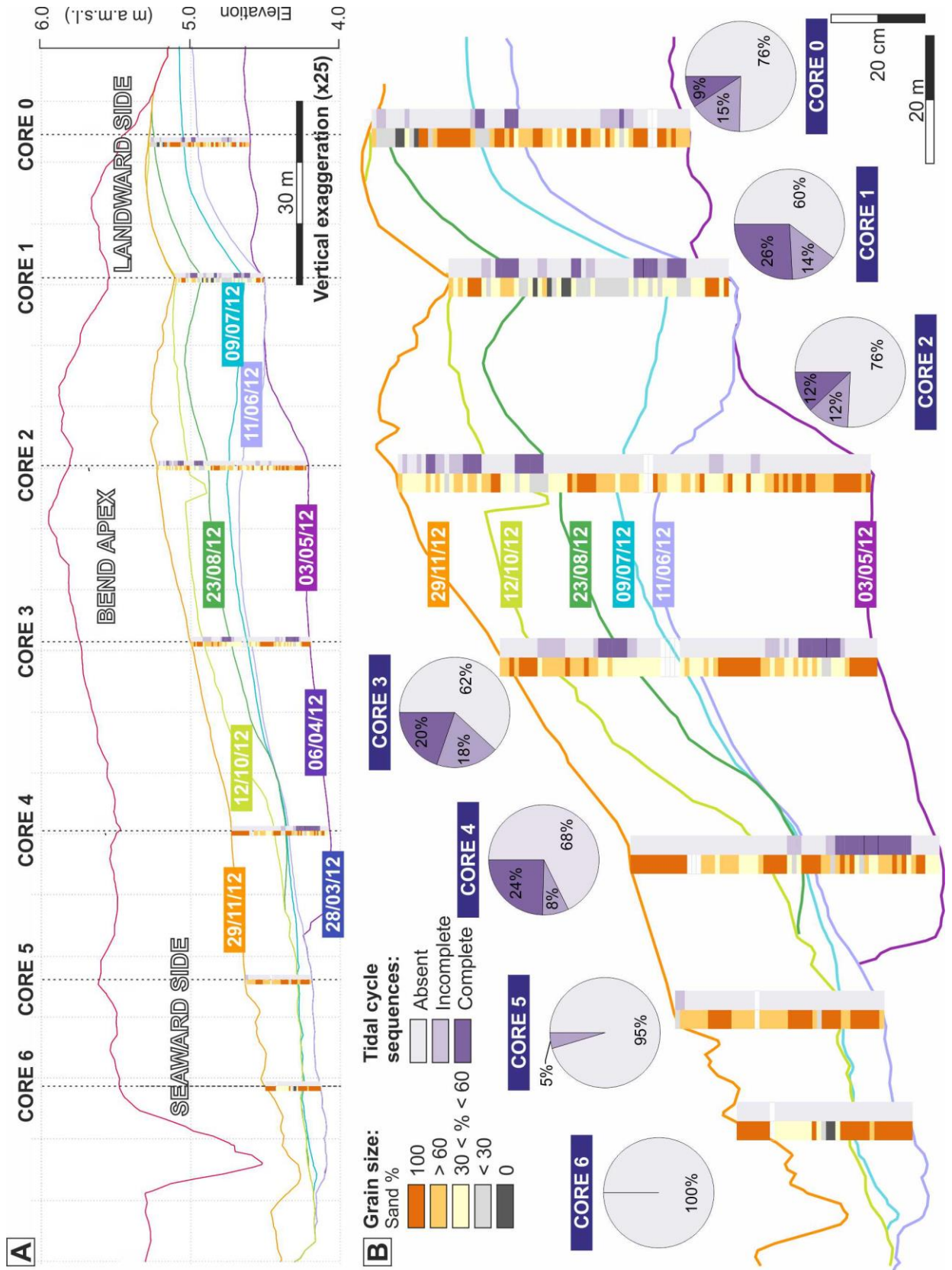
Figure 9. Along-bend distribution of rhythmites and grain size within the 2012 accretionary package. (A) Location of the study cores along the bend. Synthetic stratigraphy of the 2012 accretionary package is shown along with distribution of grain size and sediments bearing different amount of rhythmites. (B) Anatomy of the 2012 accretionary package. Distribution of deposits recording complete and incomplete TCs is shown by pie charts.

TC sequences) are preserved at different elevations and form up to 40% of the 2012 accretionary package.

6. DISCUSSION

6.1. Bar growth and sediment distribution

Lidar survey analysis shows that planform changes of the study channel bend caused the bend apex to moves away from the belt axis (Fig 1B and C), pointing to an overall expansion of the bar and increase of channel sinuosity. Although this would fit with morphodynamic models for tidal point bars, comparison between different surveys and reconstructed synthetic stratigraphy highlights that increasing bend sinuosity is not achieved through a progressive bend expansion, but by alternating storage of sediments along the landward and seaward side of the bar (Fig 8A). This morphodynamic evolution reflects the presence of ebb and flood formative currents, which shaped alternatively, and contrast with planform transformations described for bends developed under unidirectional flow conditions (Ielpi and Ghinassi, 2014; Yan et al., 2017).

The occurrence of the thickest deposits in the bar apex zone (Fig 4A and 5D) suggests that accumulation and preservation of deposits are more pronounced here than anywhere else in the bar. This trend is confirmed by a comparison between 2012 and 2017 LIDAR surveys, that highlight that the occurrence of the thickest deposits still occurs in the bar apex zone (Fig 5D). Sediment storage and preservation in this area can be explained by the flow configuration and development of recirculation eddies. This process is well-documented in river bends, where the apex zone is characterized by flow

separation which generates a main recirculation eddy sited just downstream of the bend apex along the inner bank (Leopold and Wolman, 1960; Leeder and Bridges, 1975; Ferguson et al., 2003; Frothingham and Rhoads, 2003; Blanckaert, 2009). This eddy is characterized by a weak reverse flow that produces a slough-water zone (i.e. dead zone), where deposition is enhanced (Leeder and Bridges, 1975; Riley and Taylor, 1978; Woodyer et al., 1979; Thoms and Sheldon, 1996; Changxing et al., 1999; Ferguson et al., 2003). In purely tidal channels, such as those analysed herein, recirculation eddies develop during flood and ebb stages allowing establishment of a dead zone which is much wider than those formed in fluvial bends and covers most of the bar apex zone. Occurrence of such a large dead zone explains the scarce abundance of clean sand in the bar apex zone (cores 1 – 3 in Figure 7), where mud settling was promoted by cyclically recurrent slough water conditions. In this frame, mud accumulation appears also to be enhanced when subsequent spring tides show a similar amplitude (e.g. internal increments 09/07/12 and 23/08/12, and related tide elevation - Fig 8). Similar abundance of mud in tidal rhythmites deposited during phase flip periods (i.e. periods in which spring tides show similar amplitude as an effect of the anomalistic month – Kvale, 2012), are visible in a macrotidal estuarine channel, in the Gomso Bay, west coast of Korea (Choi, 2011; its Figure 8) and in the Mississippian Tar Springs Formation, Indiana, USA (Kvale, 2012; its Figure 1.5c).

Mud-free sand is more common along the seaward and landward sides of the bar (cores 0, 5 and 6 in Figure 7), where high-flow velocity occurs on the bar during flood and ebb stages, respectively. In this frame, the occurrence of large amounts of clean sand (> 40%) with large mud clasts along the seaward side of the bar (core 5 and 6, Fig 7B), suggests that flood currents strongly shape this area, removing most of the mud drapes accumulated during slough water stages. The reduced thickness of the 2012 accretionary package in this area fits with the dominance of erosion-bypass processes.

The intensity of flood currents along the seaward side, fits with significant mud accumulation just landward of the bar apex, where the flood-related recirculation eddy develops (core 1 and 2, Fig 7B). Although the strongest currents are recorded during the ebb phase of overmarsh tides, it arises that bar sedimentation is mainly controlled by flood flows. Such a counterintuitive relationship (cf. Dalrymple & Choi, 2007) has also been highlighted by Choi et al. (2004) in a tidal point bar of the Han River Delta (Korea), where the mutually evasive nature of the ebb and flood currents causes the point-bar surface to be flood dominated even though the channel as a whole is ebb dominated. Similarly, (Ghinassi et al., 2018) described an ebb-dominated translating tidal point bar in the Venice Lagoon (Italy), where sedimentation is mainly ascribed to flood flows.

The 2012 accretionary package shows that accumulation is higher in the bar slope (Fig 5A), whereas limited thickness of sediment is accreted in the upper bar and channel thalweg zone, which are affected by limited accumulation and scarce preservation of deposits, respectively. Limited preservation of thalweg deposits is confirmed by the more frequent cross-cutting relationships between subsequent increments, as highlighted by comparison between Lidar surveys. The occurrence of bypass/erosive processes in the channel thalweg zone can also be considered to play a key role in triggering bar collapses (Fig 10). In fact, sediment removal from the thalweg zone during low flow stages (i.e. late ebb phase) causes undercutting and destabilization of the aggradational bar slope (Fig 10).
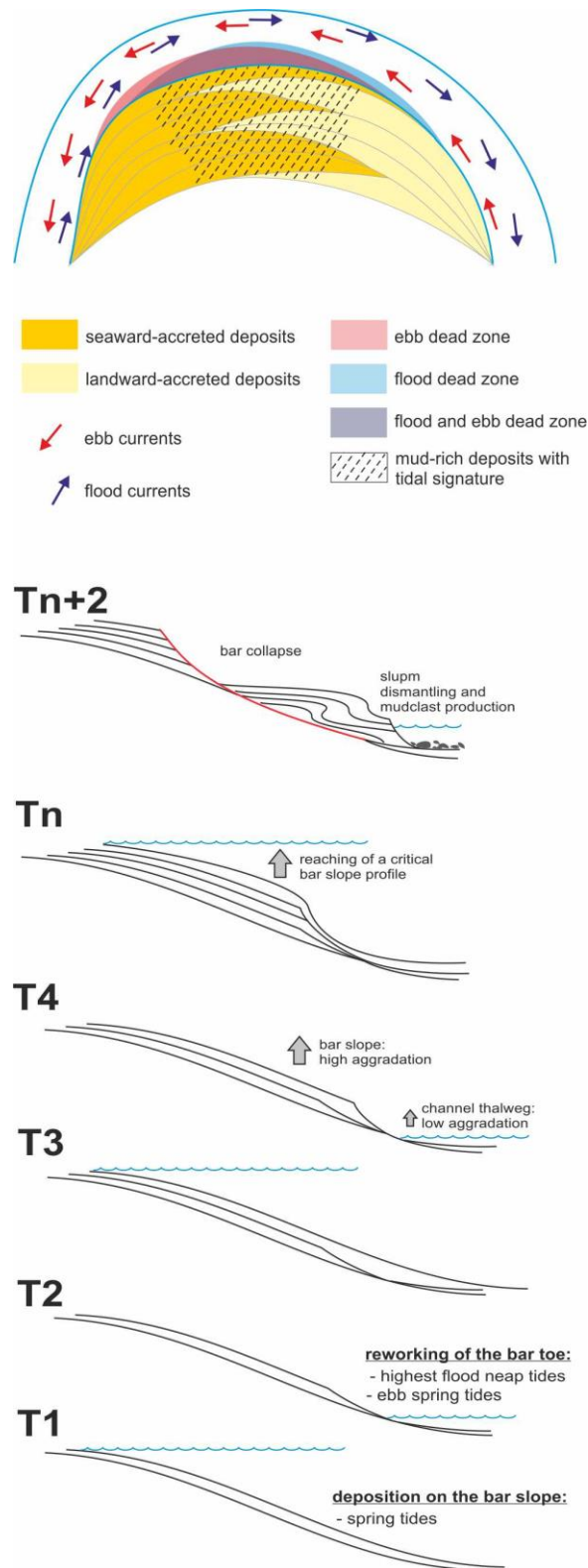
Figure 10. Conceptual model showing flow and sediment distribution within the study bend, along with the mechanisms for triggering bar collapses.

6.2. Preservation of the tidal signal

The characteristics of the best developed tidal rhythmites registered in the studied bar strongly reflect the relationship between the elevation of the channel thalweg and related bar with respect to the tidal range (Figs 1D and 8C). Lying in the upper intertidal zone, the channel can host water only during flood phases, and will not experience the ebb slough waters (Fig 8C), making the record of semidiurnal tides intermittent. Additionally, flood tides hardly reach the channels during neap tides (Fig 8C), making the neap/spring cycles to be recorded by 9 to 12 TCs at the best, out of the 28 possible in a semidiurnal regime. Similar results for tidal deposits of the Mont Saint Michel Bay were shown by Tessier (1993), and highlight that elevation of the depositional site in comparison with tidal range plays a key role in preserving the number of tidal couplets forming a tidal sequence.

The limited occurrence of TC sequences, either complete or incomplete, indicates that preservation of the tidal signal is not straightforward in such a dynamic environment, although tides are the only effective forcing driving sedimentation. Tidal rhythmites are considered to be well expressed in meandering tidal channel, since their morphology provides a good protection to wave reworking (Tessier, 1993; Choi, 2011). Preservation of the tidal signal is commonly discussed as a function of elevation within tidal channels (Choi et al., 2004; Choi, 2010, 2011), and upper point bar deposits are commonly considered the most prone to preserve tidal rhythmicity (Choi, 2010, 2011; Sisulak and Dashtgard, 2012; La Croix and Dashtgard, 2015; Pelletier et al., 2016). The occurrence of complete TC sequences in the lower portion of cores 3 and 4 and their absence in cores 2, 5 and 6 at the same elevation (Fig 9B), suggests that preservation of tidal rhythmites is not just a matter of elevation but also depends on their position along the meander bend, along with local morphology of the depositional surface. In particular, their occurrence in cores 3 and 4 is associated with the presence of a local scour (Figs 5D and

9B), which allows their preservation in the lower point bar, where generally high-energy conditions occur. More commonly, however, tidal rhythmites are preserved in the central part of the bar (e.g. core 2) and immediately landward of the bend apex (i.e. core 1), where point bar deposits reach their maximum thickness and a zone of weak reverse flow due to the recirculation eddy occurs.

7. CONCLUSION

A macrotidal point bar of the Mont Saint Michel Bay (France) is analysed by means of an integrated approach, which focused on bar deposits accreted between 28/03/2012 and 29/11/2012. We integrated Lidar topographic data, geomorphological field surveys and sedimentological cores and we conclude the following:

- the study bar expanded through alternating stages of sediment storage along the seaward and landward side of the inner bank;

- maximum sediment accumulation occurred in the bar apex zone and just landward of it, where maximum mud deposition is documented;

- development of ebb and flood recirculation zones, and related slough water conditions, is considered to play a key role in accumulation of mud in the central bar zone;

- the central bar zone is prone to increase preservation of tidal rhythmites, which can also be recorded in protected sites, such as localized erosive scours.

8. REFERENCES

Allen, J.R.L., 1982. Sedimentary Structures. Their Character and Physical Basis. Volume II, Elsevier. ed, Developments in Sedimentology.

Allen, J.R.L., 1963. The classification of cross-stratified units. With notes on thier origin. Sedimentology 2, 93–114. https://doi.org/10.1111/j.1365-3091.1963.tb01204.x

Archer, A.W., 1998. Hierarchy of Controls on Cyclic Rhythmite Deposition: Carboniferous Basins of Eastern and Mid-Continental U.S.A., in: Tidalites: Processes and Products. SEPM Society for Sedimentary Geology, pp. 59–68. https://doi.org/10.2110/pec.98.61.0059

Barwis, J.H., 1978. Sedimentology of some South Carolina tidal-creek point bars, and a comparison with their fluvial counterparts, in: Miall, A.D. (Ed.), Fluvial Sedimentology. Dallas Geological Society, Calgary, Alberta, Canada, pp. 487–510.

Blanckaert, K., 2009. Saturation of curvature-induced secondary flow, energy losses, and turbulence in sharp open-channel bends: Laboratory experiments, analysis, and modeling. J. Geophys. Res. Solid Earth 114, 1–23. https://doi.org/10.1029/2008JF001137

Bonnot-Courtois, C., 2002. Bay of Mont-Saint-Michel and the Rance Estuary: Recent Development and Evolution of the Depositional Environments. Editions Technip.

Bourcart, J., Charlier, R., 1959. The tangue: A "nonconforming" sediment. Geol. Soc. Am. Bull. 70, 565–568.

Brice, J.C., 1974. Evolution of meander loops. Bull. Geol. Soc. Am. 85, 581–586. https://doi.org/10.1130/0016-7606(1974)85<581:EOML>2.0.CO;2

Bridges, P.H., Leeder, M.R., 1976. Sedimentary model for intertidal mudflat channels, with examples from the Solway Firth, Scotland. Sedimentology 23, 533–552. https://doi.org/10.1111/j.1365-3091.1976.tb00066.x

Brivio, L., Ghinassi, M., D'Alpaos, A., Finotello, A., Fontana, A., Roner, M., Howes, N., 2016. Aggradation and lateral migration shaping geometry of a tidal point bar: An example from salt marshes of the Northern Venice Lagoon (Italy). Sediment. Geol. 343, 141–155. https://doi.org/10.1016/j.sedgeo.2016.08.005

Broughton, P.L., 2018. Mudstone Clast Breccia in the Cretaceous Athabasca Oil Sands, Western Canada: Fluvial Debris-Flow Transitions into Traction Carpets. J. Geol. 126, 63–97. https://doi.org/10.1086/694747

Carling, P.A., Chateau, C.C., Leckie, D.A., Langdon, C.T., Scaife, R.G., Parsons, D.R., 2015. Sedimentology of a tidal point-bar within the fluvial–tidal transition:River Severn Estuary, UK, 1st ed, Fluvial-Tidal Sedimentology. Elsevier B.V. https://doi.org/10.1016/b978-0-444-63529-7.00008-0

Changxing, S., Petts, G., Gurnell, A., 1999. Bench development along the regulated, lower river Dee, UK. Earth Surf. Process. Landforms 24, 135–149. https://doi.org/10.1002/(SICI)1096-9837(199902)24:2<135::AID-ESP946>3.0.CO;2-2

Chen, S., Steel, R.J., Olariu, C., 2015. Palaeo-Orinoco (Pliocene) channels on the tide-dominated Morne L'Enfer delta lobes and estuaries, SW Trinidad, in: Developments in Sedimentology. Elsevier B.V., pp. 227–281. https://doi.org/10.1016/B978-0-444-63529-7.00010-9

Choi, K., 2011. Tidal rhythmites in a mixed-energy, macrotidal estuarine channel, Gomso Bay, west coast of Korea. Mar. Geol. 280, 105–115. https://doi.org/10.1016/j.margeo.2010.12.004

Choi, K., 2010. Rhythmic Climbing-Ripple Cross-Lamination in Inclined Heterolithic Stratification (IHS) of a Macrotidal Estuarine Channel, Gomso Bay, West Coast of Korea. J. Sediment. Res. 80, 550–561. https://doi.org/10.2110/jsr.2010.054

Choi, K.S., Dalrymple, R.W., 2004. Recurring tide-dominated sedimentation in Kyonggi Bay (west coast of Korea): similarity of tidal deposits in late Pleistocene and Holocene sequences. Mar. Geol. 212, 81–96. https://doi.org/https://doi.org/10.1016/j.margeo.2004.07.008

Choi, K.S., Dalrymple, R.W., Chun, S.S., Kim, S.-P.S.-P., 2004. Sedimentology of modern, Inclined Heterolithic Stratification (IHS) in the macrotidal Han River Delta, Korea. J. Sediment. Res. 74, 677–689. https://doi.org/10.1306/030804740677

Choi, K.S., Hong, C.M., Kim, M.H., Oh, C.R., Jung, J.H., 2013. Morphologic evolution of macrotidal estuarine channels in Gomso Bay, west coast of Korea: Implications for the architectural development of inclined heterolithic stratification. Mar. Geol. 346, 343–354. https://doi.org/10.1016/j.margeo.2013.10.005

Choi, K.S., Jo, J.H., 2015. Morphodynamics of Tidal Channels in the Open Coast Macrotidal Flat, Southern Ganghwa Island in Gyeonggi Bay, West Coast of Korea. J. Sediment. Res. 85, 582–595. https://doi.org/10.2110/jsr.2015.44

Choi, K.S., Park, Y.A., 2000. Late Pleistocene silty tidal rhythmites in the macrotidal flat between Youngjong and Yongyou Islands, west coast of Korea. Mar. Geol. 167, 231–241. https://doi.org/https://doi.org/10.1016/S0025-3227(00)00037-2

Cleveringa, J., Oost, A.P., 1999. The fractal geometry of tidal-channel systems in the Dutch Wadden Sea. Geol. en Mijnbouw/Netherlands J. Geosci. 78, 21–30. https://doi.org/10.1023/A:1003779015372

Cuevas Gonzalo, M., De Boer, P.L., 1991. Tide-influenced fluvial deposits; Examples from the Eocene of the Southern Pyrenees, Spain, 4th International Conference on Fluvial Sedimantology.

D'Alpaos, A., Ghinassi, M., Finotello, A., Brivio, L., Bellucci, L.G., Marani, M., 2017. Tidal meander migration and dynamics: A case study from the Venice Lagoon. Mar. Pet. Geol. 87, 80–90. https://doi.org/10.1016/j.marpetgeo.2017.04.012

Dalrymple, R.W., Choi, K.S., 2007. Morphologic and facies trends through the fluvial-marine transition in tide-dominated depositional systems: A schematic framework for environmental and sequence-stratigraphic interpretation. Earth-Science Rev. 81, 135–174. https://doi.org/10.1016/j.earscirev.2006.10.002

Dalrymple, R.W., Kurcinka, C.E., Jablonski, B.V.J., Ichaso, A.A., Mackay, D.A., 2015. Deciphering the relative importance of fluvial and tidal processes in the fluvial-marine transition, 1st ed, Developments in Sedimentology. Elsevier B.V. https://doi.org/10.1016/B978-0-444-63529-7.00002-X

Dalrymple, R.W.R.W., Makino, Y., Zaitlin, B.B.A., 1991. Temporal and spatial patterns of rhythmite deposition on mud flats in the macrotidal Cobequid Bay-Salmon River Estuary, Bay of Fundy, Canada. Clastic tidal Sedimentol. 16, 137–160.

Dashtgard, S.E., Venditti, J.G., Hill, P.R., Sisulak, C.F., Johnson, S.M., LaCroix, A.D., 2012. Sedimentation across the Tidal-Fluvial Transition in the Lower Fraser River, Canada. Sediment. Rec. 10, 4–9. https://doi.org/10.2110/sedred.2012.4.4

De Mowbray, T., 1983. The genesis of lateral accretion deposits in recent intertidal mudflat channels, Solway Firth, Scotland. Sedimentology 30, 425–435. https://doi.org/10.1111/j.1365-3091.1983.tb00681.x

Détriché, S., Susperregui, A.-S., Feunteun, E., Lefeuvre, J.-C., Jigorel, A., 2011. Interannual (1999–2005) morphodynamic evolution of macro-tidal salt marshes in Mont-Saint-Michel Bay (France). Cont. Shelf Res. 31, 611–630. https://doi.org/https://doi.org/10.1016/j.csr.2010.12.015

Díez-Canseco, D., Arz, J.A., Benito, J.I., Díaz-Molina, M., Arenillas, I., 2014. Tidal influence in redbeds: A palaeoenvironmental and biochronostratigraphic reconstruction of the Lower Tremp Formation (South-Central Pyrenees, Spain) around the Cretaceous/Paleogene boundary. Sediment. Geol. 312, 31–49. https://doi.org/http://dx.doi.org/10.1016/j.sedgeo.2014.06.008

EDF R&D, T.P., 2011. Cloud Compare (version 2.4) [GPL software] http://www.danielgm.net/cc/.

Fagherazzi, S., Gabet, E.J., Furbish, D.J., 2004. The effect of bidirectional flow on tidal channel planforms. Earth Surf. Process. Landforms 29, 295–309. https://doi.org/10.1002/esp.1016

Fenies, H., Faugères, J.C., 1998. Facies and geometry of tidal channel-fill deposits (Arcachon Lagoon, SW France). Mar. Geol. 150, 131–148. https://doi.org/10.1016/S0025-3227(98)00049-8

Ferguson, R.I., Parsons, D.R., Lane, S.N., Hardy, R.J., 2003. Flow in meander bends with recirculation at the inner bank. Water Resour. Res. 39, n/a--n/a. https://doi.org/10.1029/2003WR001965

Finotello, A., Lanzoni, S., Ghinassi, M., Marani, M., Rinaldo, A., D'Alpaos, A., 2018. Supporting

Information (SI) Appendix. Field migration rates of tidal meanders recapitulate fluvial morphodynamics. Proc. Natl. Acad. Sci. 115, 1463–1468. https://doi.org/10.1073/pnas.1711330115

Frothingham, K.M., Rhoads, B.L., 2003. Three-dimensional flow structure and channel change in an asymmetrical compound meander loop, Embarras River, Illinois. Earth Surf. Process. Landforms 28, 625–644. https://doi.org/10.1002/esp.471

Fruergaard, M., Andersen, T.J., Nielsen, L.H., Madsen, A.T., Johannessen, P.N., Murray, A.S., Kirkegaard, L., Pejrup, M., 2011. Punctuated sediment record resulting from channel migration in a shallow sand-dominated micro-tidal lagoon, Northern Wadden Sea, Denmark. Mar. Geol. 280, 91–104. https://doi.org/10.1016/j.margeo.2010.12.003

Fustic, M., Hubbard, S.M., Spencer, R., Smith, D.G., Leckie, D.A., Bennett, B., Larter, S., 2012. Recognition of down-valley translation in tidally influenced meandering fluvial deposits, Athabasca Oil Sands (Cretaceous), Alberta, Canada. Mar. Pet. Geol. 29, 219–232. https://doi.org/10.1016/j.marpetgeo.2011.08.004

Gabet, E.J., 1998. Lateral Migration and Bank Erosion in a Saltmarsh. Estuaries 21, 745–753.

Garotta, V., Rummel, A.C., Seminara, G., 2007. Long-term morphodynamics and hydrodynamics of tidal meandering channels, in: River, Coastal and Estuarine Morphodynamics: RCEM 2007 - Proceedings of the 5th IAHR Symposium on River, Coastal and Estuarine Morphodynamics. pp. 163–168.

Ghinassi, M., Brivio, L., D'Alpaos, A., Finotello, A., Carniello, L., Marani, M., Cantelli, A., 2018. Morphodynamic evolution and sedimentology of a microtidal meander bend of the Venice Lagoon (Italy). Mar. Pet. Geol. 96, 391–404. https://doi.org/10.1016/j.marpetgeo.2018.06.011

Gingras, M.K., Maceachern, J.A., Dashtgard, S.E., Ranger, Mi.J., Pemberton, G.S., 2016. The significance of trace fossils in the McMurray Formation , Résumé. Bull. cana 64, 233–250.

Gugliotta, M., Flint, S.S., Hodgson, D.M., Veiga, G.D., 2016. Recognition criteria, characteristics and implications of the fluvial to marine transition zone in ancient deltaic deposits (Lajas Formation, Argentina). Sedimentology 63, 1971–2001. https://doi.org/10.1111/sed.12291

Harris, P.T., Hughes, M.G., Baker, E.K., Dalrymple, R.W., Keene, J.B., 2004. Sediment transport in distributary channels and its export to the pro-deltaic environment in a tidally dominated delta: Fly River, Papua New Guinea. Cont. Shelf Res. 24, 2431–2454. https://doi.org/10.1016/j.csr.2004.07.017

Hovikoski, J., Räsänen, M., Gingras, M., Ranzi, A., Melo, J., 2008. Tidal and seasonal controls in the formation of Late Miocene inclined heterolithic stratification deposits, western Amazonian foreland basin. Sedimentology 55, 499–530. https://doi.org/10.1111/j.1365-3091.2007.00907.x

Hubbard, S.M., Smith, D.G., Nielsen, H., Leckie, D.A., Fustic, M., Spencer, R.J., Bloom, L., 2011.

Seismic geomorphology and sedimentology of a tidally influenced river deposit, Lower Cretaceous Athabasca oil sands, Alberta, Canada. Am. Assoc. Pet. Geol. Bull. 95, 1123–1145. https://doi.org/10.1306/12131010111

Ichaso, A.A., Dalrymple, R.W., 2009. Tide- and wave-generated fluid mud deposits in the Tilje Formation (Jurassic), offshore Norway. Geology 37, 539–542. https://doi.org/10.1130/G25481A.1

Ielpi, A., Ghinassi, M., 2014. Planform architecture, stratigraphic signature and morphodynamics of an exhumed Jurassic meander plain (Scalby Formation, Yorkshire, UK). Sedimentology 61, 1923–1960. https://doi.org/10.1111/sed.12122

Jablonski, B.V.J.J., Dalrymple, R.W., 2016. Recognition of strong seasonality and climatic cyclicity in an ancient, fluvially dominated, tidally influenced point bar: Middle McMurray Formation, Lower Steepbank River, north-eastern Alberta, Canada. Sedimentology 63, 552–585. https://doi.org/10.1111/sed.12228

Jackson, R.G.I., 1976. Depositional Model of Point Bars in the Lower Wabash River. J. Sediment. Petrol. 46, 579–594.

Johnson, S.M., Dashtgard, S.E., 2014. Inclined heterolithic stratification in a mixed tidal-fluvial channel: Differentiating tidal versus fluvial controls on sedimentation. Sediment. Geol. 301, 41–53. https://doi.org/10.1016/j.sedgeo.2013.12.004

Kazhdan, M., Bolitho, M., Hoppe, H., 2006. Poisson Surface Reconstruction, in: Polthier, K., Sheffer, A. (Eds.), Eurographics Symposium on Geometry Processing.

Kazhdan, M., Hoppe, H., 2013. Screened Poisson Surface Reconstruction. ACM Trans. Graph. 32, 1–13. https://doi.org/10.1145/2487228.2487237

Kleinhans, M.G., Schuurman, F., Bakx, W., Markies, H., 2009. Meandering channel dynamics in highly cohesive sediment on an intertidal mud flat in the Westerschelde estuary, the Netherlands. Geomorphology 105, 261–276. https://doi.org/10.1016/j.geomorph.2008.10.005

Kvale, E.P., 2012. Tidal Constituents of Modern and Ancient Tidal Rhythmites: Criteria for Recognition and Analyses, in: Davis, R.A., Dalrymple, R.W. (Eds.), Principles of Tidal Sedimentology. pp. 1–621. https://doi.org/10.1007/978-94-007-0123-6

L'Homer, A., Courbouleix, S., Chantraine, J., Deroin, J.P., Bonnot-Courtois, C., Caline, B., Ehrhold, A., Lautridou, J.P., Morzadec-Kerfourn, M.T., 1999. Notice Explicative, Carte Géol. France (1/50 000), Feuille Baie Du Mont-Saint-Michel (208). BRGM, Orléans.

La Croix, A.D., Dashtgard, S.E., 2015. A Synthesis of Depositional Trends In Intertidal and Upper Subtidal Sediments Across the Tidal–Fluvial Transition In the Fraser River, Canada. J. Sediment. Res. 85, 683–698. https://doi.org/10.2110/jsr.2015.47

La Croix, A.D., Dashtgard, S.E., 2014. Of sand and mud: Sedimentological criteria for identifying

the turbidity maximum zone in a tidally influenced river. Sedimentology 61, 1961–1981. https://doi.org/10.1111/sed.12126

Lague, D., Brodu, N., Leroux, J., 2013. Accurate 3D comparison of complex topography with terrestrial laser scanner: Application to the Rangitikei canyon (N-Z). ISPRS J. Photogramm. Remote Sens. 82, 10–26. https://doi.org/10.1016/j.isprsjprs.2013.04.009

Langlois, E., Bonis, A., Bouzillé, J.B., 2003. Sediment and plant dynamics in saltmarshes pioneer zone: Puccinellia maritima as a key species? Estuar. Coast. Shelf Sci. 56, 239–249. https://doi.org/https://doi.org/10.1016/S0272-7714(02)00185-3

Larsonneur, C., 1989. La Baie du Mont-Saint-Michel. Bull. lnst. Géol. Bassin Aquit 46, 5–74.

Larsonneur, C., 1975. Tidal Deposits, Mont Saint-Michel Bay, France., in: Ginsburg, R.N. (Ed.), Tidal Deposits. Springer, Berlin, Heidelberg.

Larsonneur, C., Auffret, J.-P., Caline, B., Gruet, Y., Lautridou, J.-P., 1994. The Bay of Mont-Saint-Michel: A sedimentation model in a temperate macrotidal environment. Senckenbergiana maritima. Frankfurt/Main 24, 3–63.

Leeder, M.R., Bridges, P.H., 1975. Flow separation in meander bends. Nature 253, 338–339. https://doi.org/doi:10.1038/253338a0

Legler, B., Johnson, H.D., Hampson, G.J., Massart, B.Y.G., Jackson, C.A.L., Jackson, M.D., El-Barkooky, A., Ravnas, R., 2013. Facies model of a fine-grained, tide-dominated delta: Lower Dir Abu Lifa Member (Eocene), Western Desert, Egypt. Sedimentology 60, 1313–1356. https://doi.org/10.1111/sed.12037

Leopold, L.B., Wolman, G.M., 1960. River Meanders. Geol. Soc. Am. Bull. 71, 769–793. https://doi.org/10.1130/0016-7606(1960)71

Leroux, J., 2013. Chenaux tidaux et dynamique des prés-salés en régime méga-tidal: Approche Multi-Temporelle du Siècle à L'événement de Marée. Université Rennes 1.

Li, C., Chen, C., Guadagnoli, D., Georgiou, I.Y., 2008. Geometry-induced residual eddies in estuaries with curved channels: Observations and modeling studies. J. Geophys. Res. Ocean. 113, 1–14. https://doi.org/10.1029/2006JC004031

Longhitano, S.G., Mellere, D., Steel, R.J., Ainsworth, R.B., 2012. Tidal depositional systems in the rock record: A review and new insights. Sediment. Geol. 279, 2–22. https://doi.org/10.1016/j.sedgeo.2012.03.024

Marani, M., Lanzoni, S., Zandolin, D., Seminara, G., Rinaldo, A., Zandolin, D., Lanzoni, S., Marani, M., Rinaldo, A., 2002. Tidal meanders. Water Resour. Res. 38, 7–14. https://doi.org/10.1029/2001WR000404

Martinius, A.W., Jablonski, B.V.J., Fustic, M., Strobl, R., den Berg, J.H. Van, 2015. Fluvial to tidal transition zone facies in the McMurray Formation (Christina River, Alberta, Canada), with

emphasis on the reflection of flow intensity in bottomset architecture, in: Ashworth, P.J., Best, J.L., Parsons, D.R. (Eds.), Fluvial-Tidal Sedimentology, Developments in Sedimentology. Elsevier, pp. 445–480. https://doi.org/https://doi.org/10.1016/B978-0-444-63529-7.00019-5

McGowen, J.H., Garner, L.E., 1970. Physiographic Features and Stratification Types of Coarse-Grained Pointbars: Modern and Ancient Examples. Sedimentology 14, 77–111. https://doi.org/10.1111/j.1365-3091.1970.tb00184.x

Mclean, A.Q., Wilson, B., 2017. Recognizing seasonal fluvial influence in ancient tidal deposits. Geol. Soc. Spec. Publ. 444, 287–303. https://doi.org/10.1144/SP444.6

Musial, G., Reynaud, J.-Y., Gingras, M.K., Féniès, H., K.Labourdette, R., Parize, O., 2011. Subsurface and outcrop characterization of large tidally influenced point bars of the Cretaceous McMurray Formation (Alberta, Canada). Sediment. Geol. 279, 156–172. https://doi.org/10.1016/j.sedgeo.2011.04.020

Nanson, G.C., 1980. Point bar and floodplain formation of the meandering Beatton River, northeastern British Columbia, Canada. Sedimentology 27, 3–29. https://doi.org/https://doi.org/10.1111/j.1365-3091.1980.tb01155.x|

Nio, S.D., Yang, C.S., 1991. Sea-level fluctuations and the geometric variability of tide-dominated sandbodies. Sediment. Geol. 70. https://doi.org/10.1016/0037-0738(91)90140-9

Pearson, N.J., Gingras, M.K., 2006. An Ichnological and Sedimentological Facies Model for Muddy Point-Bar Deposits. J. Sediment. Res. 76, 771–782. https://doi.org/10.2110/jsr.2006.070

Pelletier, J., Abouessa, A., Schuster, M., 2016. Hierarchy of tidal rhythmites from semidiurnal to solstitial cycles : Origin of inclined heterolithic stratifications (IHS) in tidal channels from the Dur At Talah Formation (upper Eocene , Sirte Basin , Libya) and a facies comparison with modern Mont. Contrib. to Mod. Anc. Tidal Sedimentol. Proc. Tidalites 2012 Conf. 203–216.

Rebata-H., L.A., Gingras, M.K., Räsänen, M.E., Barberi, M., 2006. Tidal-channel deposits on a delta plain from the upper miocene nauta formation, Marañón Foreland Sub-basin, Peru. Sedimentology 53, 971–1018. https://doi.org/10.1111/j.1365-3091.2006.00795.x

Riley, S.J., Taylor, G., 1978. The geomorphology of the upper Darling River system with special reference to the present fluvial system. Proc. R. Soc. Victoria 90, 89–102.

Roux, P., 1998. Rapport sur les niveaux de la mer aux abords du Mont-Saint-Michel. Données de 1884 à 1998.

Santos, A.E.D.A., Rossetti, D.D.F., 2006. Depositional model of the Ipixuna Formation (late cretaceous-?early tertiary), Rio Capim Area, northern Brazil. Lat. Am. J. Sedimentol. Basin Anal. 13, 101–117.

Sisulak, C.F., Dashtgard, S.E., 2012. Seasonal Controls On the Development And Character of Inclined Heterolithic Stratification In A Tide-Influenced, Fluvially Dominated Channel: Fraser River, Canada. J. Sediment. Res. 82, 244–257. https://doi.org/10.2110/jsr.2012.21

Smith, D.G., 1987. Meandering river point bar lithofacies models: modern and ancient examples compared, in: Ethridge, F.G., Flores, R.M., Harvey, M.D. (Eds.), Recent Developments in Fluvial Sedimentology: Contributions from the Third International Fluvial Sedimentology Conference. SEPM Society for Sedimentary Geology, pp. 83–91.

Solari, L., Seminara, G., Lanzoni, S., Marani, M., Rinaldo, A., 2002. Sand bars in tidal channels Part 2. Tidal meanders. J. Fluid Mech. 451, 203–238. https://doi.org/10.1017/S0022112001006565

Tessier, B., 1993. Upper intertidal rhythmites in the Mont-Saint-Michel Bay (NW France): Perspectives for paleoreconstruction. Mar. Geol. 110, 355–367. https://doi.org/10.1016/0025-3227(93)90093-B

Tessier, M., Gloaguen, J.C., Lefeuvre, J.C., 2000. Factors affecting the population dynamics of Suaeda maritima at initial stages of development. Plant Ecol. 147, 193–203.

Thomas, R.G., Smith, D.G., Wood, J.M., Visser, M.J., Calverley-Range, E.A., Koster, E.H., Visser, J., Calverley-Range, E.A., Koster, E.H., 1987. Inclined heterolithic stratification - terminology, description, interpretation and significance. Sediment. Geol. 53, 123–179. https://doi.org/10.1016/S0037-0738(87)80006-4

Thoms, M.C., Sheldon, F., 1996. The importance of channel complexity for ecosystem processing: An example of the Barwon-Darling River. Stream Manag. Aust. 111–118.

Van de Lageweg, W.I., van Dijk, W.M., Kleinhans, M.G., Utrecht, U., 2013. Channel belt architecture formed by a meandering river. Sedimentology 60, 840–859. https://doi.org/10.1111/j.1365-3091.2012.01365.x

Woodyer, K.D., Taylor, G., Crook, K.A.W., 1979. Depositional processes along a very low-gradient, suspended-load stream: the Barwon River, New South Wales. Sediment. Geol. 22, 97–120. https://doi.org/https://doi.org/10.1016/0037-0738(79)90023-X

Yan, N., Mountney, N.P., Colombera, L., Dorrell, R.M., 2017. A 3D forward stratigraphic model of fluvial meander-bend evolution for prediction of point-bar lithofacies architecture. Comput. Geosci. 105, 65–80. https://doi.org/10.1016/j.cageo.2017.04.012

Zeff, M.L., 1999. Salt marsh tidal channel morphometry: Applications for wetland creation and restoration. Restor. Ecol. 7, 205–211. https://doi.org/10.1046/j.1526-100X.1999.72013.x

CHAPTER 5

PIRACY-CONTROLLED GEOMETRY OF TIDAL POINT BARS: EXAMPLES FROM MODERN AND ANCIENT CHANNEL NETWORKS

PAPER

In preparation for *Frontiers in Earth Science. Sedimentology, Stratigraphy and Diagenesis*

Marta Cosma[a], Alvise Finotello[a], Alessandro Ielpi[b], Dario Ventra[c], Oriol Oms[d], Andrea D'alpaos[a], Massimiliano Ghinassi[a]

[a] Department of Geosciences, University of Padova, Padova, Italy

[b] Harquail School of Earth Sciences, Laurentian University, Sudbury, ON, Canada

[c] Department of Earth and Environmental Sciences, Université de Genéve, Genéve, Switzerland

[d] Department of Geology, Universitat Autònoma de Barcelona, Bellaterra, Spain

1. ABSTRACT

Freely migrating meandering rivers are known to produce extensive sand bodies, which can exhibit width:thickness ratios of up to 300. Meandering channels are also widespread in tidal networks draining intertidal plains, where they exhibit planform dynamics similar to their fluvial analogues. However, owing to the high channel density that characterizes intertidal areas, tidal meandering channels can hardly migrate laterally for long distances without interact with other channels. In order to better understand how the interaction between adjacent meandering channels can control the development of tidal-point bars, two ancient point-bar bodies from the Castigaleu Formation (Eocene of Spain) are investigated and compared with deposits arising from the evolution of a tidal-meander bend of the northern Venice Lagoon (Italy). The two study tidal-point bars are characterized by a low width:thickness ratio (<30), which is interpreted as a result of abrupt deactivation of their migrating parent channels. Such abrupt deactivations are likely related to avulsive piracy operated by an adjoining channel in the tidal network, and prevented the bar from generating a laterally extensive tabular sand body. This is corroborated with direct time-lapse observations of similar dynamics in the modern tidal meanders of the Venice Lagoon. In densely-drained tidal networks, channel bends cannot meander freely without interacting with adjacent channels, and thus triggering channel piracy. In summary, we present a morphodynamic model to justify a recurring architectural dissimilarity between the deposits of fluvial- and tidal-meandering channels.

2. INTRODUCTION

Tidal channel networks are ubiquitous features of tidal landscapes and play a key role in the evolution of coastal environments by controlling water, sediment, and nutrient fluxes therein (Rinaldo et al., 1999a; Hughes, 2012; Coco et al., 2013). Their planform morphologies can exhibit a wide range of patterns (Rinaldo et al., 1999b; Kearney and Fagherazzi, 2016), with both dead-end and interconnected channels, whose individual morphology may range from straight to meandering, and further to convoluted (Hughes, 2012). Within such a complex set of planforms, the shape and characteristics of a given channel network, much as its initial growth and later development, are the results of complex biogeomorphic feedbacks (Perillo and Iribarne, 2003a, 2003b; Hughes et al., 2009; D'Alpaos, 2011; Belliard et al., 2015). Although the latter have been widely investigated using different approaches, spanning remote sensing (Fagherazzi et al., 1999; Chirol et al., 2018), field analyses (D'Alpaos et al., 2007; Vandenbruwaene et al., 2012), numerical modelling (D'Alpaos et al., 2005; Kirwan and Murray, 2007; van Maanen et al., 2015), and laboratory experiments (Stefanon et al., 2010; Vlaswinkel and Cantelli, 2011; Finotello, 2017; Geng et al., 2019), the ontogeny and late-stage evolution of tidal channel networks still remains only partially understood.

A distinctive key features of tidal plains incised by channel networks is represented by the higher drainage density (*sensu* Marani et al., 2003, i.e., defined as the mean unchanneled path length from any salt marsh location to the nearest channel) they exhibit compared to alluvial plains (Pallard et al., 2009; Trigg et al., 2012). Particularly, it has been noted that only fully-developed fluvial anabranching systems can be characterized by drainage densities comparable to those found in tidal settings (e.g., Schumm et al., 1996; Jones and Harper, 1998). Such a high drainage density implies that when adjacent sinuous channels migrate, they easily come into contact, thus leading to piracy and reorganization of the local channel network (e.g., Letzsch and Frey, 1980;

Rizzetto and Tosi, 2012; Litwin et al., 2013). Following piracy-induced modification of the drainage network, a single channel can experience either a dramatic reduction of the flowing discharge (i.e., channel deactivation) or a relevant increase in the discharge (Fig 1). Where piracy deactivates part of the drainage network, planform evolution of related channels is hindered, such in case of sinuous channels which cannot develop a fully meandering pattern (Finotello et al., 2018).
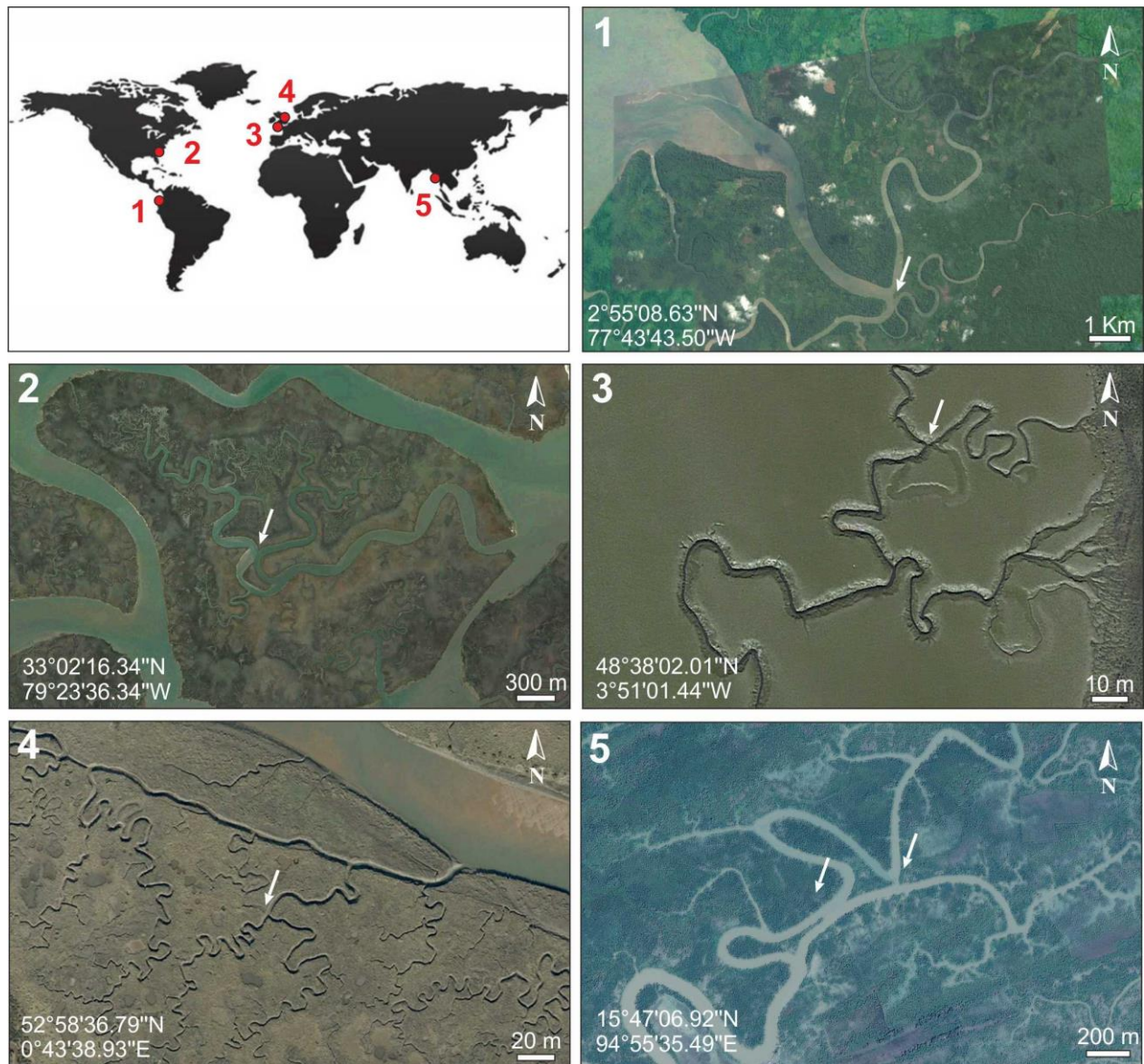

Figure 1. Piracies in tidal channel networks from different coastal areas. Piracy sites are indicated by white arrows, and geographic coordinates are reported in each image.

Hindering planform evolution of sinuous channels might have relevant impacts on the geometries of point bar bodies developed in tidal networks, and, although the occurrence of piracy events is documented in tidal landscapes (Letzsch and Frey, 1980; Rizzetto and Tosi, 2012), the sedimentary products following these processes are poorly known. Relevant insights on this issue would, therefore, derive from studies on the evolution of tidal networks and related sedimentary products both in modern and ancient systems.

In this context, the present study focuses on the geometries of two tidal point-bar bodies of the Eocene Castigaleu Formation (South Pyrenean Foreland Basin, Spain) and discusses their origin through a comparison with the evolution of a modern pirated tidal meander bend located in the Northern Venice Lagoon (Italy).

3. GEOLOGICAL SETTING

3.1. The Tremp-Graus Basin and the Castigaleu Fm.

The Eocene Castigaleu Formation forms the lower part of the Montanyana Group, that was deposited during Ypresian time in the Tremp-Graus Basin (Fig 2A, B and C). The Tremp-Graus Basin, located in the south-central segment of the Southern Pyrenean Foreland Basin, is one of a set of piggyback basins of Mesozoic and Cenozoic age developed upon and in front of three major thrusts: Bóixols, Montsec and Sierras Marginales thrusts (Muñoz, 1992; Puigdefàbregas et al., 1992). The Bóixols and Montsec thrusts form the northern and southern margins of the Tremp-Graus Basin, respectively. The eastern boundary of the basin is formed by the lateral ramp system of the Segre Fault (Vergés, 2003), while the western boundary of the Tremp-Graus sub-basin is usually placed at the Mediano Anticline and the Ainsa sub-basin (Nijman and Nio, 1975; Mutti et al., 1988; Soto et al., 2002; Fernández et al., 2012; Muñoz et al., 2013).

During deposition of the Montanyana Group the Tremp-Graus Basin was an east-west elongated depression, where continental to shallow marine sedimentary systems evolved westward into slope (Ainsa Basin) and deep marine (Jaca Basin) deposits (Nijman and Nio, 1975; Cuevas Gozalo, 1989; Cuevas Gonzalo and De Boer, 1991; Puigdefàbregas et al., 1992). The Lower Montanyana Group unconformably overlies shallow marine deposits of the Ager Group (Fig 2D) and represents a tide-dominated deltaic complex (Castigaleu Fm – Galloway, 1975; Martinius, 2012; Chanvry et al., 2018) whose major clastic feeder were a fluvial system (Montllobat Fm) and alluvial fan systems (San Esteban Fm), which were sourced from the central-southern and northern parts of the basin, respectively (Nijman and Nio, 1975; Van Der Meulen, 1983; Mutti et al., 1988; Nijman, 1998). Equivalent facies of the Upper Montanyana Group are mapped as the Capella and Perrarua Fms, respectively (Fig 2D – Nijman and Nio, 1975; Van Der Meulen, 1983; Cuevas Gozalo, 1989; Cuevas Gonzalo and De Boer, 1991; Puigdefàbregas et al., 1992; Martinius, 2012); while the Middle Montanyana, which unconformably overlies the Lower Montanyana Group, is an incised fluvial sheet sandstone that prograded rapidly westwards across the basin (the Castissent Fm - Marzo et al., 1988; Nijman, 1998).

The delta plain brackish facies of the Castigaleu Fm consist of channelized and mouth-bar sandstone bodies interbedded within organic-rich interdistributary bay mudstones (Nijman and Nio, 1975; Van Der Meulen, 1983; Cuevas Gozalo, 1989; Martinius, 2012; Chanvry et al., 2018). Laterally-accreting bars are widespread, and their tidal origin is inferred by the common occurrence of tidal bundles, tidal rhythmites, mud drapes, reactivation surfaces, brackish-water to normal marine trace fossil assemblages and oyster beds, alongside evidences of bidirectional flows (Nijman and Nio, 1975; Van Der Meulen, 1983; Cuevas Gozalo, 1989; Martinius, 2012; Chanvry et al., 2018).
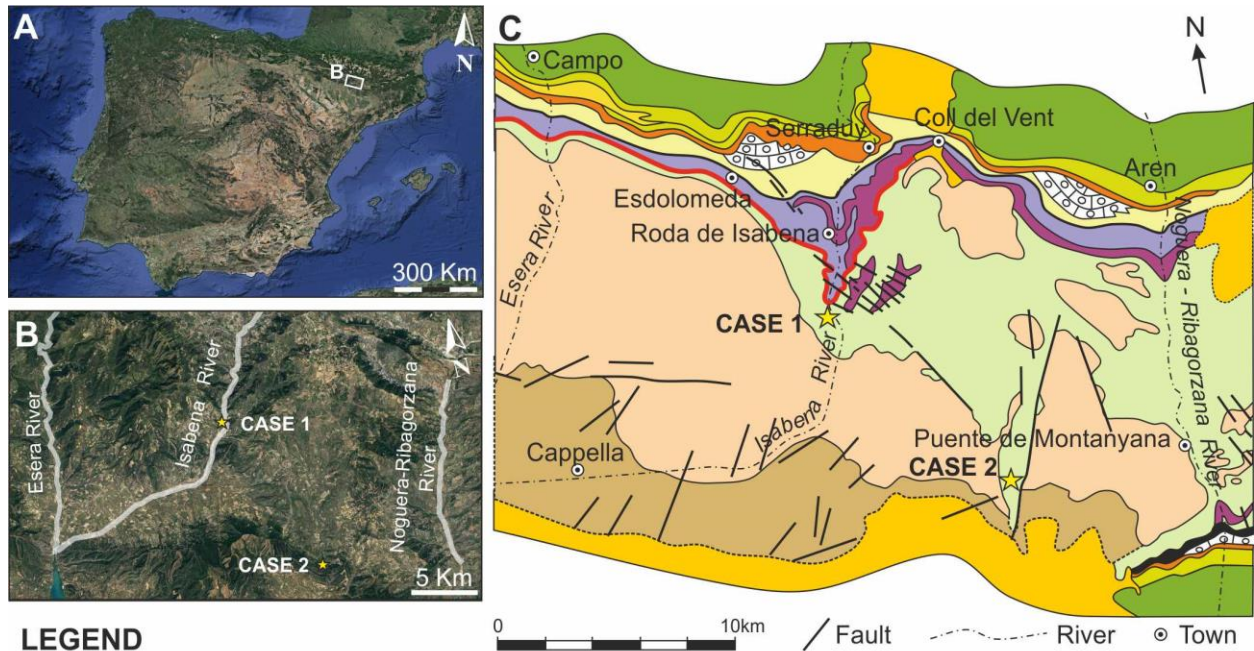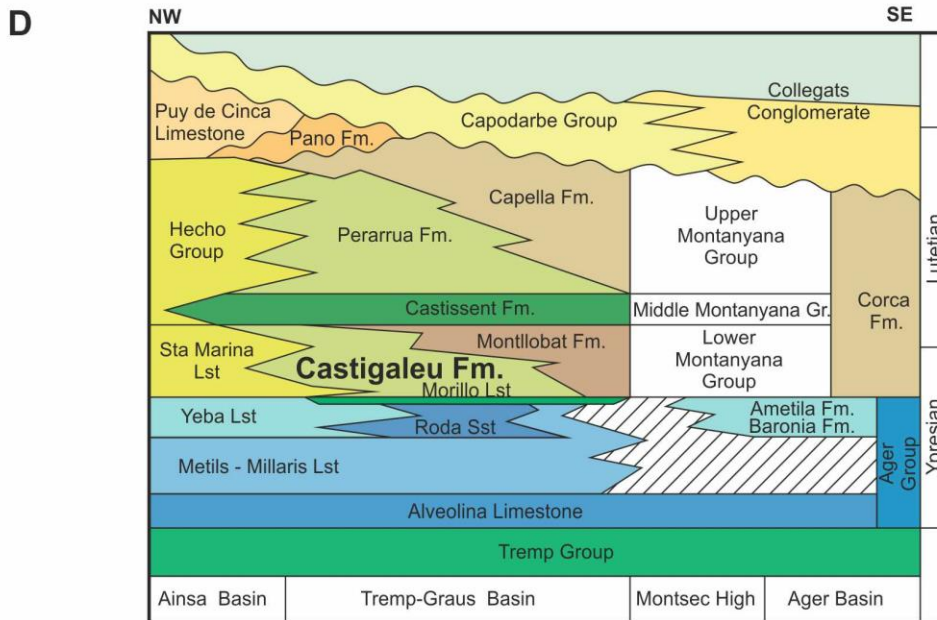
Figure 2. Location of the studied bars and geological setting of the Castigaleu Fm (A) Location of the study area in Spain. (B) Location of the study cases between the Isabena and Nougera Ribagorzana Valleys. (C) Simplified geological map of the present-day Tremp-Graus Basin (modifeid after Martinius,2012; who used data from Serra-Kiel et al. 1994, Fonnesu 1984, Samsó 1988 and Tosquella 1988, and Cuevas Gozalo 1989). (D) Summary correlation diagram of Ypresian and Lutetian stratigraphy of the present-day Tremp-Graus and Ager Basins with a focus on the Montanyana Group (modified after Martinius, 2012 and Nijman 1998).

3.2. The Venice Lagoon and the study site

The Venice Lagoon, which formed as a consequence of the Holocene transgression on the Last Glacial Maximum alluvial deposits of the Northern epicontinental Adriatic shelf (Trincardi et al., 1994; Amorosi et al., 2008; Storms et al., 2008; Zecchin et al., 2008, 2014; Ronchi et al., 2018), is located along the north-eastern coast of Italy and represents the largest brackish-water body of the Mediterranean Sea. The lagoon, characterized by a total surface area of about 550 km², is connected to the Adriatic Sea through three inlets (Lido, Malamocco and Chioggia – Fig 3A). The tidal regime is semidiurnal, with an average tidal range of about 1.0 m and maximum astronomical tidal excursions of about 0.75 m (D'Alpaos et al., 2013) around mean sea level (msl). The present-day configuration of the lagoon is characterized by the presence of sparse salt marshes, which have been rapidly eroding during the last two centuries (Tommasini et al., 2019), wide subtidal platforms, and tidal flats that are cut by intertidal and subtidal channels (Fig 3A). The study site is located in the San Felice salt marsh (Fig 3B), which is colonized by dense halophytic vegetation species (such as *Spartina maritima, Limonium narbonense, Sarcocornia fruticosa* and *Juncus maritimum* – Silvestri et al., 2005) and represents one of the most naturally preserved portions of the Venice Lagoon (Marani et al., 2003; Roner et al., 2016). The salt marsh is drained by a dense network of tidal channels which show a standard Hortonian drainage density (i.e., total channelled length divided be watershed area) of about 0.02 m/m² and a mean unchanneled length on the order of ℓ = 12 m (Marani et al., 2003).

The present study focuses on point bar deposits associated with an abandoned meander (Fig 3F) formed by an 8 m wide channel. The meander shows a "simple symmetric" (*sensu* Brice, 1974) planform geometry and has a radius of curvature of about 15 m. The analysis of historical photos (Fig 3C – F) reveals that at the end of 60's the bend was abandoned as consequence of a piracy involving two adjacent channels. This piracy caused a significant reorganization of the local drainage system. Some channel reaches, such as that containing our study bend, were deactivated and rapidly infilled (see channels "d" in Figure 3E and F), whereas other reaches widened significantly, suggesting increasing cross-sectional areas and flow discharges (see channels "i" in Figure 3E and F).
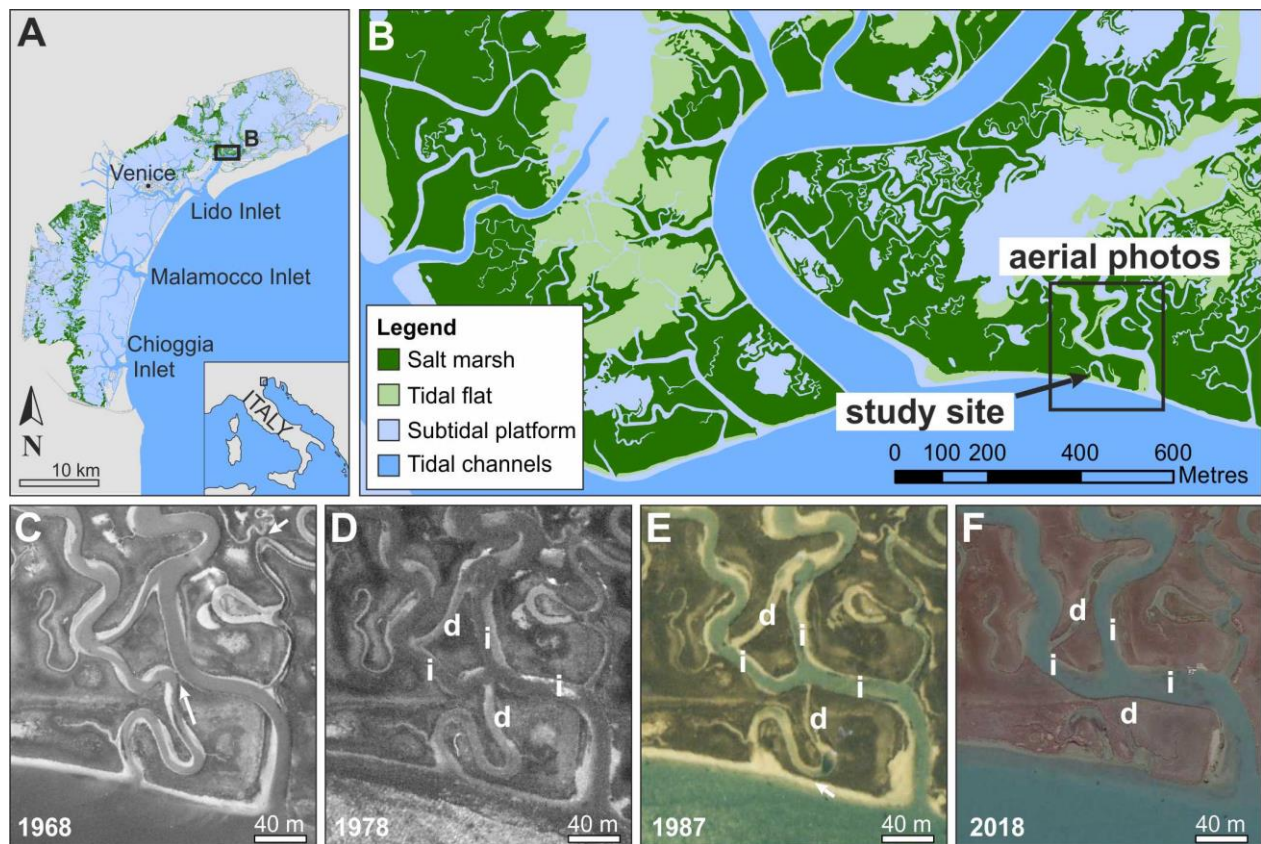

Figure 3. Abandoned channel deposits of the Northern Venice Lagoon (Italy). (A - B) geographic location of the study site. (C – F) Sequential aerial photos showing evolution of the study area since 1968. See text for detailed explanation. Piracy sites are indicated by white arrows (in addition to the study piracy event, two other piracies occurred in this channel network in the last decades).

4. METHODS

4.1. Data acquisition in ancient deposits

The two studied bar bodies of the Castigaleu Fm were analysed through classical outcrop sedimentology approach, which included line-drawing of photomosaics and bed-by-bed logging. Line-drawing was performed on photographic panels obtained by merging high-resolution digital images (16 megapixel). Bar top and basal surfaces were traced to define the 2D cross-sectional geometry of the bar bodies, and bedding surfaces were defined to detect accretionary increments within the bar. Sedimentological logs were acquired following basic principles of facies analyses and aimed at defining the main changes in grain size of sediments and distribution of sedimentary structures. A total of 8 sedimentological logs were measured across the two point-bar bodies. Sedimentological logs and line-drawings were further augmented with the collection of paleo-flow indicators, using the vector of migration of bedforms, inferred from current-ripple cross lamina and from cross-stratification.

4.2. Data acquisition in modern deposits

Geometry of the modern bar was defined by acquiring four sedimentary cores (2 – 2.5 m deep) along the bar axis. Soft mud made the abandoned channel inaccessible for recovery of a core from channel-fill deposits. Position of the cores was determined using differential GPS TOPCON GR-3 receivers – dual frequency (L1/L2) and dual constellation NavStar/Glonass with integrated Tx/Rx UHF radio. To prevent sediment compaction, cores were recovered using an Eijkelkamp hand auger, with a 1.0 m-long gouge sampler which has a diameter of 30 mm. Core sediment samples were kept humid in PVC liners, and then cut longitudinally, photographed and measured

following principles of facies analyses. Lateral correlation between adjacent cores was used to reveal 2D point-bar cross sections along the bend axis. Top and basal surfaces of the bar bodies were defined in cores by detecting the bar brink and channel thalweg zone following the approach proposed by Cosma et al. (2019). The point bar brink is defined as the bar rim, developed where flat bar top turns into the bar slope, and in cores it is pointed out where lamination changed from horizontal (i.e., bar top deposits) to inclined (i.e., bar slope deposits). The channel thalweg is the deepest part of a channel, and, in cores, it corresponds to the surface flooring the channel lag deposits.

5. RESULTS

5.1. Point-bar bodies of the Eocene Castigaleu Fm (Spain)

The two point bars of the Castigaleu Fm. form lensoidal sandstone bodies embedded within flat-bedded muddy deposits containing abundant brackish malacofaunas.

5.1.1. Study deposits

5.1.1.1. Substrate deposits

Substrate deposits mainly consist of a massive, dark clay-rich mudstone with abundant bioclastic debris and black coaly fragments (Fig 4A). Locally, they contain tabular sandstone and siltstone beds up to 5 cm thick. Flaser bedding is also common. These beds are characterized by plane-parallel and current ripple-cross lamination, commonly marked by thin muddy laminae. Substrate mud is emplaced by suspension fall-out or flocculation processes in a tidal flat environment mainly during slack water phases (van den Berg et al., 2007; Davis and Dalrymple, 2012), whereas tabular sandy layers probably accumulated during exceptional tides or as wind-induced storm layers.

5.1.1.2.   Point-bar deposits

Point-bar deposits show a sharp erosive basal surface floored by ~ 10 cm thick medium to coarse massive sandstone with abundant granule-sized mud chips, shells fragments and plant debris (Fig 4B). These sandstones are covered by large-scale inclined bedsets, which consist of decimetre- to meter-thick coarse to fine cross-bedded sandstone with sigmoidal cross-stratification (Fig 4C) and few decimetre-thick heterolithic intervals, and lenticular to flaser laminations (Fig 4D). These deposits grade upward into medium to very-fine sandstone with smaller scale planar cross- and plane-parallel stratified heterolithic beds. Millimetre- to centimetre-thick mud drapes are abundant and accumulate on sigmoidal cross-stratification foresets (Fig 4E), locally defining a rhythmic organization (Fig 4F and G). Palaeocurrent directions from cross strata are perpendicular to the dip azimuth of the large-scale inclined beds, and small paleoflow indicators (i.e., ripple cross lamination) show some evidence of reverse flow. These deposits are interpreted as bank-attached bars, which accreted transverse to the main channel (Bridge, 2003). Abundance of mud drapes, likely deposited by flocculation or suspension fallout during slack water (Thomas et al., 1987; Burban et al., 1989; Davis and Dalrymple, 2012), together with the occurrence of tidal rhythmites and reverse flows, suggest a tide-controlled point bar sedimentation (Barwis, 1978; De Mowbray, 1983; Choi, 2011; Choi et al., 2013), as indeed pointed out by other previous interpretations (Cuevas Gonzalo and De Boer, 1991; Martinius, 2012; Chanvry et al., 2018).

5.1.1.3.   Channel-fill deposits

Although these deposits occur at both sites, they have been closely observed only at site 2. Channel-fill deposits show a concave-upward geometry, with beds that drape the basal surface, thus producing a concentric infill (Fig 4H and I). They consist mainly of an
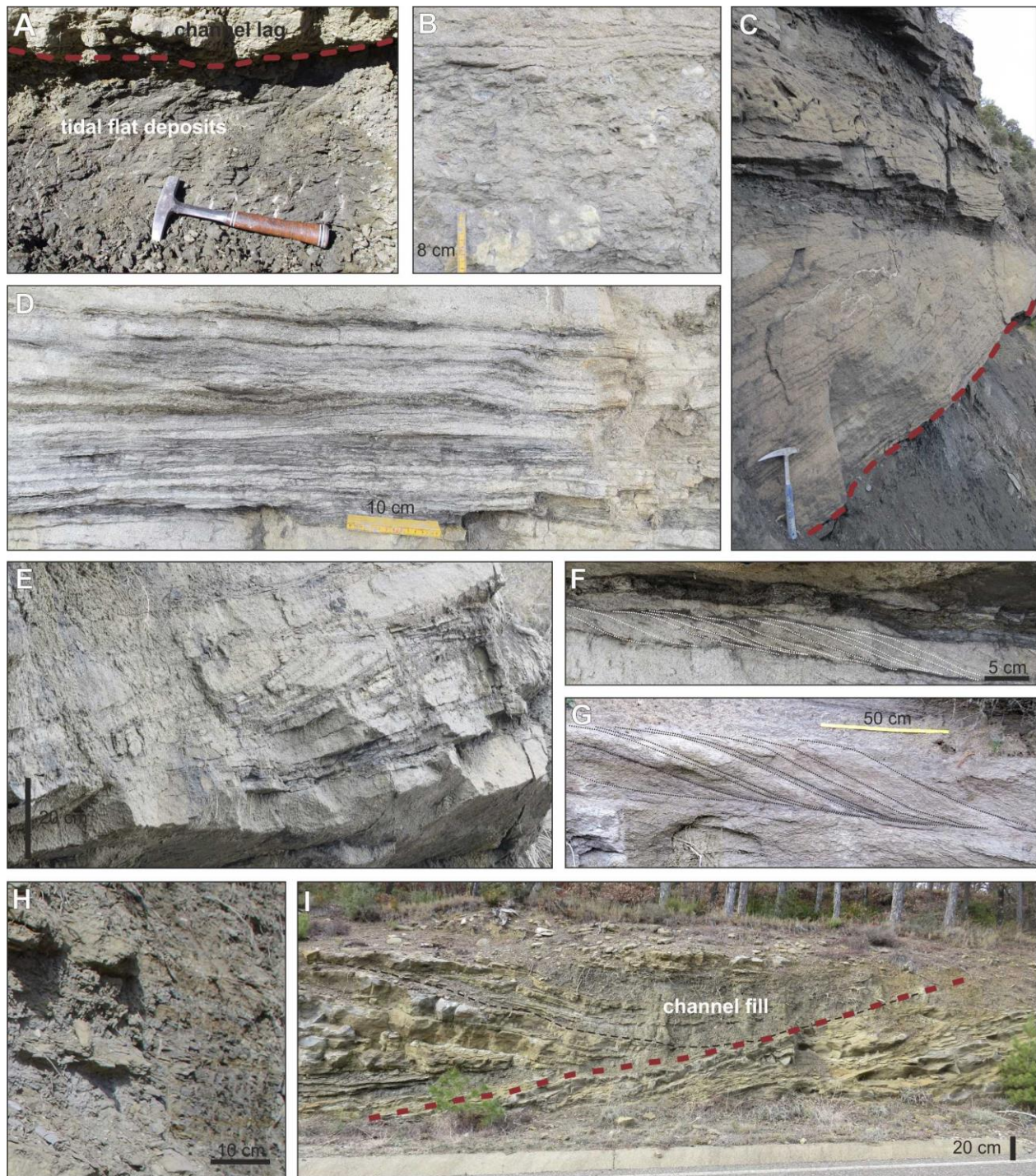
Figure 4. Sedimentary facies of the studied point bars of the Castigaleu Fm. (A) Overbank muddy deposits (tidal flat) abruptly overlain by point bar sandstone. (B) Shell-rich sandstone forming the channel lag layer at the base of point bar bodies. (C) Inclined point-bar beds erosively overlain by tidal flat mudstone. (D) Wavy-laminated fine sandstone with muddy laminae. (E - G) Cross stratified sandstone showing rhythmic distribution of mud drapes. Note sigmoidal geometries of foreset laminae. (H - I) Concentric channel-fill deposits consisting of laminated mud with rare sandy layers. Red-dashed lines indicate the channel base.

alternation of centimetre- to decimetre-thick silty claystone beds and sandy siltstone beds with some very fine to medium sandy beds up to 15 cm-thick with faintly plane

parallel lamination. Locally the silty claystone intervals are slightly oxidized and contain bioclastic debris. Channel-fill deposits represent the abandonment phase of the channel (Toonen et al., 2012). The presence of isolated sandy beds at different elevations in the channel-fill succession suggests that the channel was not abruptly deactivated, and occasionally received coarser deposits. The occurrence of oxidized intervals potentially indicates episodes of subaerial exposure, although post-depositional oxidation can also be invoked as the causing mechanism.

5.1.2. Geometries of bar bodies

Depicting point bar brink and channel thalweg trajectories, allows us to define changes in thickness of the two studied bar bodies. Brink and thalweg trajectories originate from a shared point (Fig 5B and D) and follow specific paths. In case study 1 (Fig 5A and B), the bar brink trajectory shows a sub-horizontal pattern, while the thalweg trajectory indicates a progressively downward shift. Brink and thalweg trajectories diverge from one another for the whole point bar width, causing a progressive increase in point bar thickness which grows up to ten meters just before the abandonment and accumulation of the channel fill (Fig 5B). The lateral extent of the point bar is ca 200 meters, and the width:thickness ratio is 20. In case study 2 (Fig 5C and D), the bar brink shows, once restored, a sub-horizontal trajectory parallel to tidal flat beds, whereas the channel thalweg trajectory points to a progressive downward shift, which allows the bar to reach 4 m in thickness just before the abandonment phase (Fig 5D). The lateral extent of the point bar is around 40 m, and the width:thickness ratio is 10.

Although they are characterized by different sizes, the studied point-bar bodies show similar architectures, displaying a wedge-shaped geometry defined by diverging thalweg and brink trajectories. Such a geometry documents the onset of bar formation

and later accretion under progressively increasing channel depth (cf. Cosma et al., 2019), which is in turn likely related to increasing tidal prism, and channel discharge. The diverging trajectories end up in the channel fill deposits documenting that the increase in channel depth stopped just before the deactivation of the channel (Dalrymple et al., 1991; Allen, 2000; D'Alpaos et al., 2005; Stefanon et al., 2012; Lanzoni and D'Alpaos, 2015).
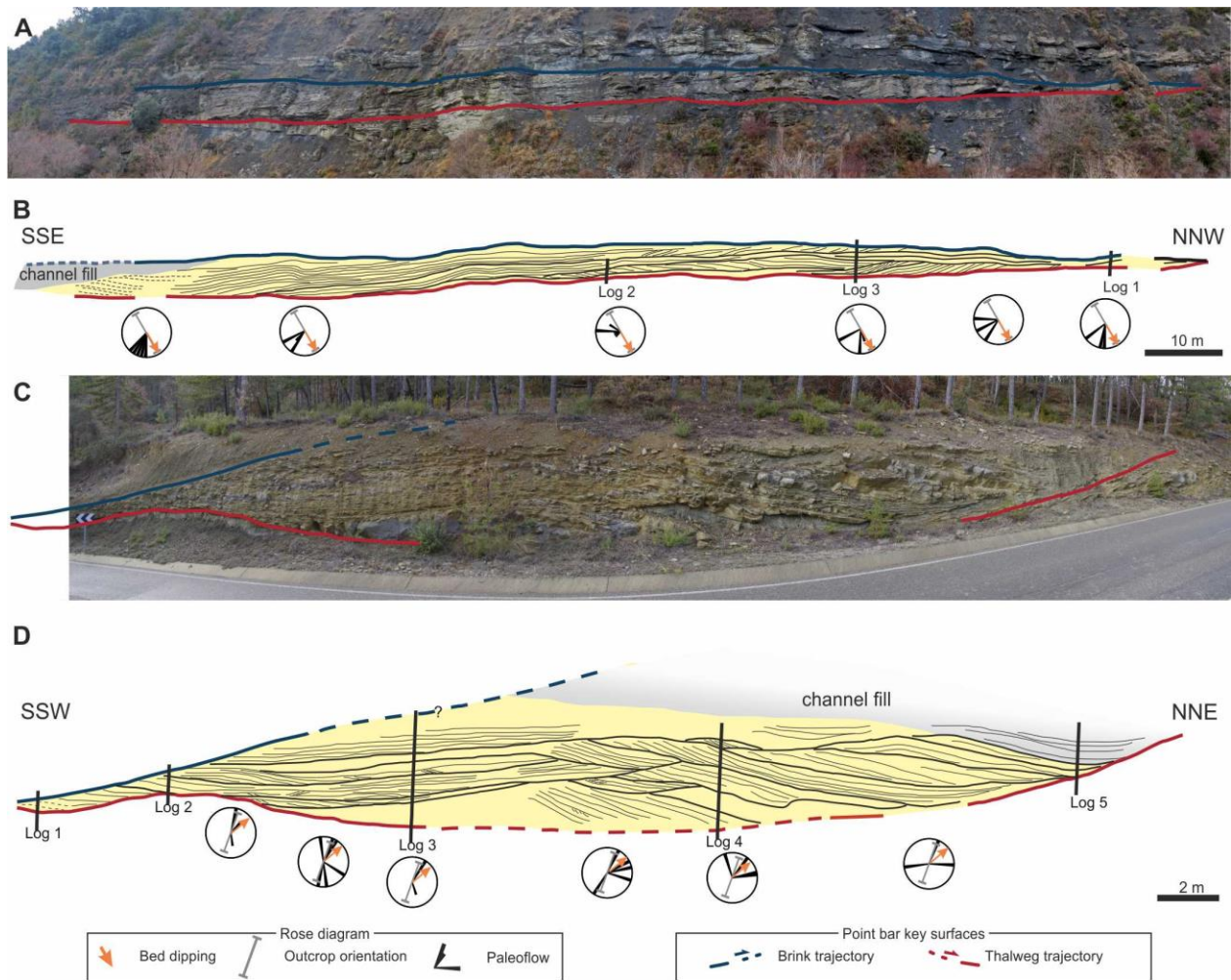

Figure 5. Architectural features of the studied point bars of the Castigaleu Fm (A and B) Outcrop panorama and related interpretation of study case 1. (C and D) Outcrop panorama and related interpretation of study case 2.

In both cases the channel was deactivated when the thalweg was still shifting downward, indicating that abandonment occurred before formative discharge reached a

steady state, that would have been indicated by flattening of the thalweg trajectory (Cosma et al., 2019). Although the 3D control on the point-bar deposit is limited, these two sections are interpreted to dissect the bars close to their axis, since: i) they contain abundant percentage of mud, which is commonly preserved in the central bar zone (see previous chapter); and, ii) a steep downward shift of the thalweg is promoted in the pool (i.e. axial) zone, where helical flow is more efficient (Willis and Tang, 2010).

5.2. The point-bar body of the Northern Venice Lagoon (Italy)

The studied bar is a sandy body embedded within muddy deposits containing abundant brackish malacofaunas and capped by channel fill mud. Core from the bar axis (Fig 6A) allows us to distinguish different types of deposits and to depict a 2D cross-sectional bar geometry.

5.2.1. Study deposits

5.2.1.1.   Substrate deposits

These deposits represent the lowermost stratigraphic unit and consist of alternating of well-sorted, dark grey, very-fine to fine sand layers (Fig 6B) and dark mud with shell and plant debris (Fig 6C). Pervasive bioturbation prevents detection of sedimentary structures. These deposits are interpreted to be formed in a tidal flat/subtidal platform environment. Sandy deposits probably originated during wind-induced storm events, when wave winnowing entrained fine-grained sediments and sand concentrated on the lagoon floor (Carniello et al., 2009). Muddy deposits settled down from suspension or by flocculation processes during the waning stage of storm events.

5.2.1.2.   Point-bar deposits

These deposits are up to 1.8 m thick, erosionally overlie substrate deposits, and are covered by salt marsh or channel fill deposits, through a gradational transition. From the bottom to the top, they consist of: i) a 5-15 cm thick massive layer of very-fine to fine sand, with abundant millimetric rounded mud clasts, shells, shell fragments, and plant debris (Fig 6D); and, ii) a fine sand to mud clinostratified interval up to 1.7 m thick. The clinostratified interval shows an heterolithic alternation of sandier (Fig 6E) and muddier (Fig 6F) deposits at the decimetre scale, and the occurrence of channelward-inclined millimetric laminae of well-sorted very fine to fine sand or plant debris (Fig 6E and F). Inclination of the laminae decreases from 25° to 5° moving upward in the clinostratified deposits. Widespread bioturbation often prevents identification of sedimentary structures. These deposits were accreted during lateral shift of the channel. In heterolithic deposits, abundance of mud reflects the prevalence of fallout or flocculation processes, probably related to slack water periods (Thomas et al., 1987) while the well-sorted laminae are the result of entrainment of finer material probably due to wave-winnowing during storm events (Choi and Jo, 2015). The deepest part of the channel is related to the erosional surface and the concentration of coarser sediments and shells. Mud clasts are formed by comminution of collapsed bank blocks (Terwindt, 1988; Sisulak and Dashtgard, 2012). The decrease in the inclination of laminae reflects the progressive upward flattening of bar slope and heralds the transition into overlying salt-marsh deposits.

5.2.1.3.   Salt-marsh deposits

These deposits cover point bar and substrate deposits. They consist of brownish, oxidized mud with 1-3 mm thick horizontal well-sorted sandy laminae (Fig 6H), *in situ* roots, wood fragments and bioturbation (Fig 6G). Thickness decreases toward the channel from 0.85 to 0.10 m. Oxidation, indicative of frequent subaerial exposure, and

roots, generated by halophytic vegetation, are related to salt-marsh deposition in the intertidal zone (Silvestri et al., 2005). These deposits mainly accreted through mud settling and organic matter accumulation (Allen, 2000; Mudd et al., 2010; Roner et al., 2016). Mud is deposited both by fallout during high slack water, and by the salt marsh vegetation baffling effect. Sandy laminae sorting suggests winnowing of finer particles probably due to wave action during storm events (Choi and Jo, 2015).
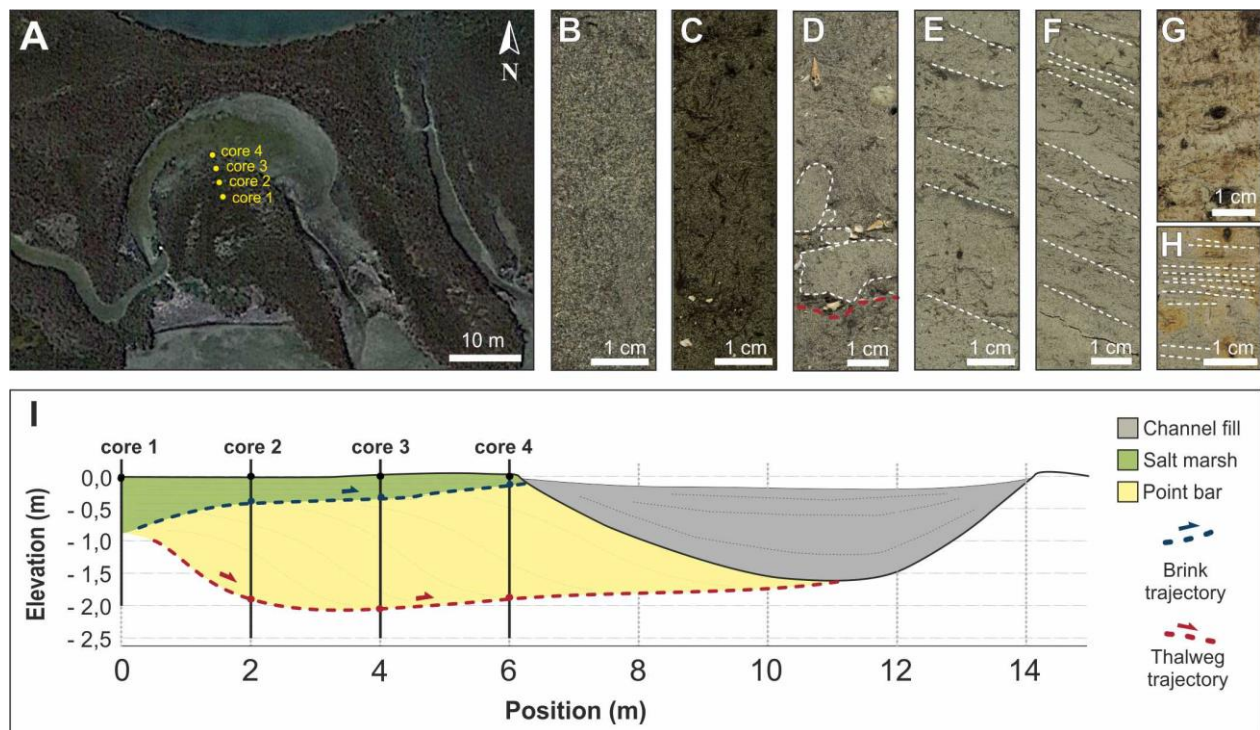

Figure 6. Sedimentary features of the bar from the Northern Venice Lagoon (Italy). (A) Location of the cores along the axis of the abandoned bend. (B) Substrate dark-gray sand, medium to very fine in grain size. (C) Substrate organic-rich mud with shells and plant fragments. (D) Pebble-sized mud clast in massive channel-lag sand with abundant shells. (E and F) Heterolithic bar deposits consisting of sandier and muddier intervals with inclined sandy laminae. (G) Oxidized salt-marsh mud with roots. (H) Salt-marsh mud with horizontal sandy laminae. (I) Reconstructed cross-sectional geometry of the point bar.

5.2.2. Geometries of the bar body

Correlation between adjacent cores depicts the point bar brink and channel thalweg trajectories, which are generated during lateral shift of the channel and accumulation of the related point-bar body. Both the brink and thalweg trajectories initiate from the

same point (Fig 6I) and then diverge following specific paths. Bar brink trajectory shows an ascending, slightly convex upward shift. Thalweg trajectory shows a gradually descending shift, followed by a slightly ascending shift. Combination of the bar brink and thalweg trajectories reveals the geometry of the point bar, as well as its depositional evolution. Brink and thalweg trajectories diverge along the four-meter-long point bar deposit, causing increase of the point bar thickness up to 1.80 m. After this stage, bar brink and channel thalweg trajectories rise almost parallel to each other maintaining a constant point bar thickness for the remaining six meters before the bar is covered by channel fill mud.

Similar to point bars of the Castigaleu Fm, diverging trajectories document the onset of bar formation and later accretion under progressively increasing channel depth (cf. Cosma et al., 2019). In this case, once the formative discharge reached a steady-state, the thalweg and brink trajectories shifted laterally together, keeping the channel depth constant until the bend was abandoned and mud deposition began.

6. DISCUSSION

Architectural features of the point bars of the Castigaleu Fm. reveal that they are characterized by an aspect ratio of 20 and 10, respectively. These values point out that their thickness is disproportionally high with respect to their lateral extent. Such a disproportion is evident after a comparison with tabular point-bar bodies generated by freely-meandering channels, which show a mean width:thickness ratio of about 200, with a range of 70 to 300 (Blum et al., 2013). Although these values can fall to 30 – 40 for river channels within the backwater zone (Blum et al., 2013), the bars of the Castigaleu Fm still represent peculiar bodies, even applying the more conservative empirical power-law equation derived by Colombera et al. (2017) to describe relationships

between bar-form width and thickness. The basal surface of both bars depicts a descending trajectory of the channel lag, that points to a progressive deepening of the channel during the phase of bar lateral accretion (Cosma et al., 2019). This geometry indicates a progressive increase in channel discharge, that is typically documented in tidal channels either during the early stage of development (Cosma et al., 2019) or following an increase of local tidal prism (Rieu et al., 2005). Occurrence of channel-fill deposits on one side of the thickest bar deposits, suggests that the channel was abruptly deactivated at a certain stage of bar accretion and thalweg deepening, thus promoting mud settling processes. Point bar bodies with similar geometries (Fig 7) are frequently documented by high-resolution shallow-seismic data from Early- to Mid-Holocene tidal channel deposits (Missiaen et al., 2008; Zecchin et al., 2008, 2014), highlighting that genetic mechanisms leading to premature abandonment of meander bends would commonly occur in tidal networks.
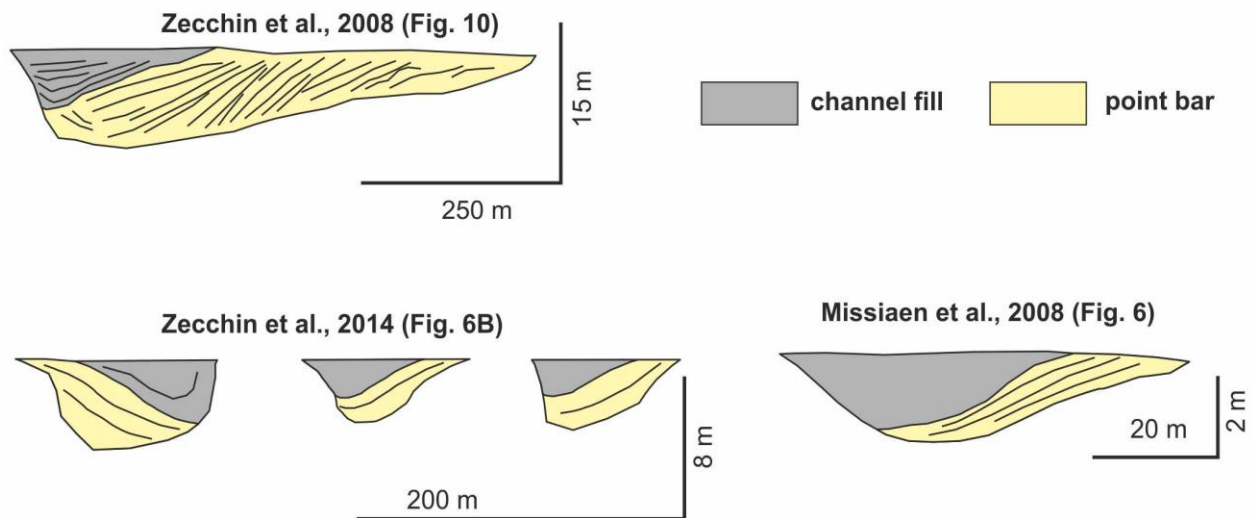

Figure 7. Examples of immature tidal point bars from tidal successions of the Venice Lagoon (Zecchin et al., 2008 and 2014) and Wadden Sea (Missiaen et al., 2008).

Processes leading to abandonment of channel bends are essentially know from fluvial realm, and include: i) chute cut-off, where a chute channel cut through the whole bar connecting the upstream riffle with the downstream one (Hooke, 1984; Gay et al., 1998;

Ghinassi, 2011); ii) neck cut-off, where the inner banks of the up- and down-stream sides of the bend connect as consequence of meander bend tightening (Allen, 1965; Mosley, 1976); and (iii) avulsion, where the whole meandering reach of a river shifts laterally from a specific node (Allen, 1965; Erskine et al., 1992). Tidal meander bends evolve under conditions which are comparable with their fluvial counterparts, although some differences can be highlighted (Solari et al., 2002; Fagherazzi et al., 2004; Kleinhans et al., 2009; Finotello et al., 2018). Neck-cut offs are widely documented in tidal networks (Brivio et al., 2016; D'Alpaos et al., 2017), whereas chute cut-offs are less common (Choi et al., 2013), particularly within vegetated intertidal marshes. Since chute cut-offs processes require that a relevant amount of flowing water overpasses the bar top zone, their paucity in the tidal realm is ascribed to the fact that bar top areas are flooded mainly at slough water flood conditions, when flow velocity is small and the flow is unable to cut chute channels across the bar. Deactivation of entire meandering reaches (i.e., channel avulsion) is a common process in tidal networks, but the triggering processes cannot fully correspond to those acting in fluvial systems. In fact, classic channel avulsions, whereby the rapid abandonment of one channel is associated to the formation of a new channel reach, are not typically observed in tidal settings. This is more than likely due to the high channel density which characterizes intertidal plains. In fact: i) the dendritic character and the spatial extent of channel networks, which favour spatially homogeneous accretion rates throughout the whole tidal basin, prevent the formation of significant topographic gradients, which are necessary drivers for channel avulsion (e.g., Slingerland and Smith, 1998); and, ii) the density of the channels in intertidal plains favours the accommodation of water excess, whenever a channel is abandoned, by the existing adjoining channels rather than causing the incision of brand-new ones. Moreover, even in tidal channels developed within distributary networks (Goodbred and Saito, 2012; Hoitink et al., 2017; Finotello et al., 2019), where topographic-driven avulsions are more likely to occur compared to purely tidal networks, the periodic action of tides stabilizes the existing channels and hinders

avulsion by maintaining tidal channels in a flushed condition, enhancing sediment bypass through the delta plain, and preventing the growth of mouth-bars at the channel outlets (Rossi et al., 2016; Lentsch et al., 2018).Deactivation of the channel bends forming the two study point bars can barely be caused by either chute- or neck-cut off processes. In fact, in both of these cases the newly formed channel should be cut onto the bar deposits, which, on the contrary, are made of conformable laterally-accreting beds. Deactivation of these two channel bends documents, therefore, an avulsive piracy event, that caused premature abandonment of meander bends and formation of immature point bars, which find remarkable geometrical similarities (i.e., aspect ratio) with that documented in the modern Venice Lagoon (Fig 4). Differently from most alluvial systems, meander bends in tidal channel networks cannot freely meander without interacting with adjacent channels, thereby triggering piracies (Fig 8). These processes cause deactivation of sinuous channel reaches, which cannot develop a fully meandering pattern (Finotello et al., 2018) and form immature point bars defined by a low width:thickness ratio (Fig 8).
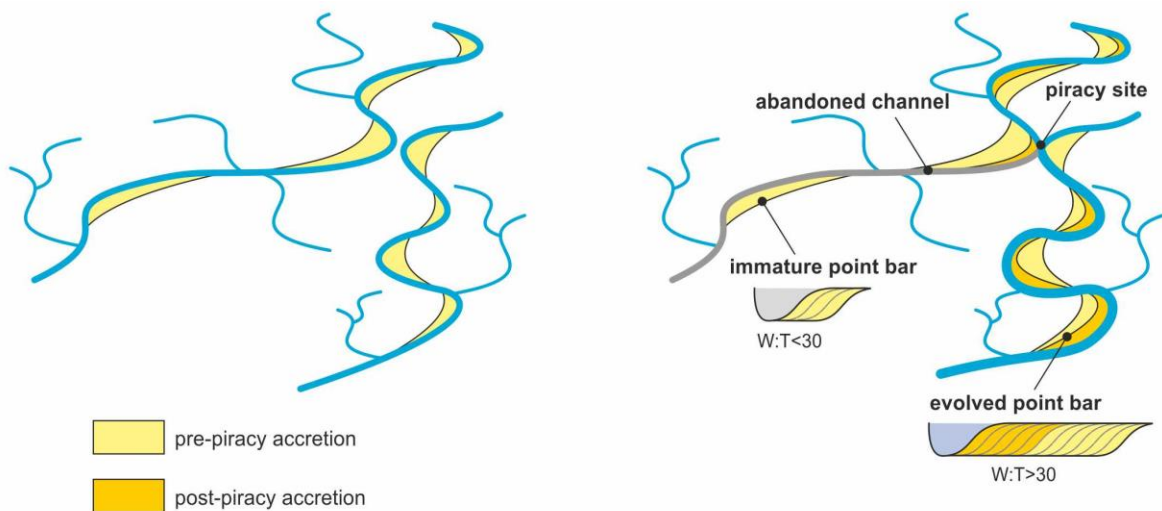

Figure 8. Conceptual model explaining formation of immature and evolved point bars in tidal realms.

7. CONCLUSION

The study of two tidal point bars of the Eocene Castigaleu Fm allowed us to define geometries of immature point bars, which are characterized by a ratio between bar width and thickness lower than 30. These bars grew through lateral accretion processes, but their evolution is abruptly interrupted by deactivation of the related channel bend, which prevents them from generating laterally extensive tabular sand bodies. Although different processes can explain abandonment of meander bends, morphodynamic evidence and comparison with modern analogue deposits of the Northern Venice Lagoon (Italy) suggest there is a link between development of immature point bars and avulsive processes generated by piracy events. These events are commonly triggered in tidal drainages because of the high density of the channel network. In these systems channel bends cannot freely meander without interacting with adjacent channels triggering piracies, which, in turn, cause premature deactivation of sinuous channel reaches. This process hinders development of a fully meandering pattern and forms immature point bars with a low width:thickness ratio.

8. REFERENCES

Allen, J.R.L., 2000. Morphodynamics of Holocene salt marshes: a review sketch from the Atlantic and Southern North Sea coasts of Europe. Quat. Sci. Rev. 19, 1155–1231. https://doi.org/10.1016/S0277-3791(99)00034-7

Allen, J.R.L., 1965. A review of the origin and characteristics of recent alluvial sediments. Sedimentology 5, 89–191. https://doi.org/10.1111/j.1365-3091.1965.tb01561.x

Amorosi, A., Fontana, A., Antonioli, F., Primon, S., Bondesan, A., 2008. Post-LGM sedimentation and Holocene shoreline evolution in the NW Adriatic coastal area. GeoActa 7, 41–67.

Barwis, J.H., 1978. Sedimentology of some South Carolina tidal-creek point bars, and a comparison with their fluvial counterparts, in: Miall, A.D. (Ed.), Fluvial Sedimentology. Dallas Geological Society, Calgary, Alberta, Canada, pp. 487–510.

Belliard, J.-P., Toffolon, M., Carniello, L., D'Alpaos, A., 2015. An ecogeomorphic model of tidal channel initiation and elaboration in progressive marsh accretional contexts. J. Geophys. Res. Earth Surf. 120, 1040–1064. https://doi.org/10.1002/2015JF003445

Blum, M., Martin, J., Milliken, K., Garvin, M., 2013. Paleovalley systems: Insights from Quaternary analogs and experiments. Earth-Science Rev. 116, 128–169. https://doi.org/10.1016/j.earscirev.2012.09.003

Brice, J.C., 1974. Evolution of meander loops. Bull. Geol. Soc. Am. 85, 581–586. https://doi.org/10.1130/0016-7606(1974)85<581:EOML>2.0.CO;2

Bridge, J.S., 2003. Rivers and Floodplains: Forms, Processes, and Sedimentary Record. Blackwell Science, oxford.

Brivio, L., Ghinassi, M., D'Alpaos, A., Finotello, A., Fontana, A., Roner, M., Howes, N., 2016. Aggradation and lateral migration shaping geometry of a tidal point bar: An example from salt marshes of the Northern Venice Lagoon (Italy). Sediment. Geol. 343, 141–155. https://doi.org/10.1016/j.sedgeo.2016.08.005

Burban, P.-Y., Lick, W., Lick, J., 1989. The flocculation of fine-grained sediments in estuarine waters. J. Geophys. Res. 94, 8323–8330.

Carniello, L., Defina, A., D'Alpaos, L., 2009. Morphological evolution of the Venice lagoon: Evidence from the past and trend for the future. J. Geophys. Res. Earth Surf. 114, 1–10. https://doi.org/10.1029/2008JF001157

Chanvry, E., Teinturier, S., Garcia, D., Deschamps, R., Puigdefàbregas, C., Joseph, P., Poyatos-Moré, M., Serra-Kiel, J., 2018. The influence of intrabasinal tectonics in the stratigraphic evolution of piggyback basin fills: Towards a model from the Tremp-Graus-Ainsa Basin (South-Pyrenean Zone, Spain). Sediment. Geol. 377, 34–62. https://doi.org/10.1016/j.sedgeo.2018.09.007

Chirol, C., Haigh, I.D., Pontee, N., Thompson, C.E., Gallop, S.L., 2018. Parametrizing tidal creek morphology in mature saltmarshes using semi-automated extraction from lidar. Remote Sens. Environ. 209, 291–311. https://doi.org/10.1016/j.rse.2017.11.012

Choi, K., 2011. Tidal rhythmites in a mixed-energy, macrotidal estuarine channel, Gomso Bay, west coast

of Korea. Mar. Geol. 280, 105–115. https://doi.org/10.1016/j.margeo.2010.12.004

Choi, K.S., Hong, C.M., Kim, M.H., Oh, C.R., Jung, J.H., 2013. Morphologic evolution of macrotidal estuarine channels in Gomso Bay, west coast of Korea: Implications for the architectural development of inclined heterolithic stratification. Mar. Geol. 346, 343–354. https://doi.org/10.1016/j.margeo.2013.10.005

Choi, K.S., Jo, J.H., 2015. Morphodynamics of Tidal Channels in the Open Coast Macrotidal Flat, Southern Ganghwa Island in Gyeonggi Bay, West Coast of Korea. J. Sediment. Res. 85, 582–595. https://doi.org/10.2110/jsr.2015.44

Coco, G., Zhou, Z., van Maanen, B., Olabarrieta, M., Tinoco, R., Townend, I.H., 2013. Morphodynamics of tidal networks: Advances and challenges. Mar. Geol. 346, 1–16. https://doi.org/10.1016/j.margeo.2013.08.005

Colombera, L., Mountney, N.P., Russell, C.E., Shiers, M.N., McCaffrey, W.D., 2017. Geometry and compartmentalization of fluvial meander-belt reservoirs at the bar-form scale: Quantitative insight from outcrop, modern and subsurface analogues. Mar. Pet. Geol. 82, 35–55. https://doi.org/10.1016/j.marpetgeo.2017.01.024

Cosma, M., Ghinassi, M., D'Alpaos, A., Roner, M., Finotello, A., Tommasini, L., Gatto, R., 2019. Point-bar brink and channel thalweg trajectories depicting interaction between vertical and lateral shifts of microtidal channels in the Venice Lagoon (Italy). Geomorphology 342, 37–50. https://doi.org/10.1016/j.geomorph.2019.06.009

Cuevas Gonzalo, M., De Boer, P.L., 1991. Tide-influenced fluvial deposits; Examples from the Eocene of the Southern Pyrenees, Spain, 4th International Conference on Fluvial Sedimantology.

Cuevas Gozalo, M., 1989. Sedimentary facies and sequential architecture of tide-influenced alluvial deposits. An example from the Middle Eocene Capella Fm; South-Central Pyrenees; Spain, Geologica Ultraiectina.

D'Alpaos, A., 2011. The mutual influence of biotic and abiotic components on the long-term ecomorphodynamic evolution of salt-marsh ecosystems. Geomorphology 126, 269–278. https://doi.org/10.1016/j.geomorph.2010.04.027

D'Alpaos, A., Carniello, L., Rinaldo, A., 2013. Statistical mechanics of wind wave-induced erosion in shallow tidal basins: Inferences from the Venice Lagoon. Geophys. Res. Lett. 40, 3402–3407. https://doi.org/10.1002/grl.50666

D'Alpaos, A., Ghinassi, M., Finotello, A., Brivio, L., Bellucci, L.G., Marani, M., 2017. Tidal meander migration and dynamics: A case study from the Venice Lagoon. Mar. Pet. Geol. 87, 80–90. https://doi.org/10.1016/j.marpetgeo.2017.04.012

D'Alpaos, A., Lanzoni, S., Marani, M., Bonometto, A., Cecconi, G., Rinaldo, A., 2007. Spontaneous tidal network formation within a constructed salt marsh: Observations and morphodynamic modelling. Geomorphology 91, 186–197. https://doi.org/10.1016/j.geomorph.2007.04.013

D'Alpaos, A., Lanzoni, S., Marani, M., Fagherazzi, S., Rinaldo, A., 2005. Tidal network ontogeny: Channel initiation and early development. J. Geophys. Res. Earth Surf. 110, 1–14. https://doi.org/10.1029/2004JF000182

Dalrymple, R.W.R.W., Makino, Y., Zaitlin, B.B.A., 1991. Temporal and spatial patterns of rhythmite deposition on mud flats in the macrotidal Cobequid Bay-Salmon River Estuary, Bay of Fundy, Canada. Clastic tidal Sedimentol. 16, 137–160.

Davis, R.A., Dalrymple, R.W., 2012. Principles of tidal sedimentology, Springer. ed, Principles of Tidal Sedimentology. Springer Netherlands, Dordrecht. https://doi.org/10.1007/978-94-007-0123-6

De Mowbray, T., 1983. The genesis of lateral accretion deposits in recent intertidal mudflat channels, Solway Firth, Scotland. Sedimentology 30, 425–435. https://doi.org/10.1111/j.1365-3091.1983.tb00681.x

Erskine, W., McFadden, C., Bishop, P., 1992. Alluvial cutoffs as indicators of former channel conditions. Earth Surf. Process. Landforms 17, 23–37. https://doi.org/10.1002/esp.3290170103

Fagherazzi, S., Bortoluzzi, A., Dietrich, W.E., Adami, A., Lanzoni, S., Marani, M., Rinaldo, A., 1999. Tidal networks 1. Automatic network extraction and preliminary scaling features from digital terrain maps. Water Resour. Res. 35, 3891–3904. https://doi.org/10.1029/1999WR900236

Fagherazzi, S., Gabet, E.J., Furbish, D.J., 2004. The effect of bidirectional flow on tidal channel planforms. Earth Surf. Process. Landforms 29, 295–309. https://doi.org/10.1002/esp.1016

Fernández, O., Muñoz, J.A., Arbués, P., Falivene, O., 2012. 3D structure and evolution of an oblique system of relaying folds: The Ainsa basin (Spanish Pyrenees). J. Geol. Soc. London. 169, 545–559. https://doi.org/10.1144/0016-76492011-068

Finotello, A., 2017. Tidal channel patterns: field investigations, numerical modelling and laboratory experiments. University of Padova.

Finotello, A., Lanzoni, S., Ghinassi, M., Marani, M., Rinaldo, A., D'Alpaos, A., 2018. Field migration rates of tidal meanders recapitulate fluvial morphodynamics. Proc. Natl. Acad. Sci. 201711330. https://doi.org/10.1073/pnas.1711330115

Finotello, A., Lentsch, N., Paola, C., 2019. Experimental delta evolution in tidal environments: Morphologic response to relative sea-level rise and net deposition. Earth Surf. Process. Landforms. https://doi.org/10.1002/esp.4627

Galloway, W.E., 1975. Process framework for describing the morphological and stratigraphic evolution of deltaic depositional systems. Deltas Model. Explor. 87–98.

Gay, G.R., Gay, H.H., Gay, W.H., Martinson, H.A., Meade, R.H., Moody, J.A., 1998. Evolution of cutoffs across meander necks in Powder River, Montana, USA. Earth Surf. Process. Landforms 23, 651–662. https://doi.org/10.1002/(SICI)1096-9837(199807)23:7<651::AID-ESP891>3.0.CO;2-V

Geng, L., Gong, Z., Zhou, Z., Lanzoni, S., D'Alpaos, A., 2019. Assessing the relative contributions of the flood tide and the ebb tide to tidal channel network dynamics. Earth Surf. Process. Landforms 0–3. https://doi.org/10.1002/esp.4727

Ghinassi, M., 2011. Chute channels in the Holocene high-sinuosity river deposits of the Firenze plain, Tuscany, Italy. Sedimentology 58, 618–642. https://doi.org/10.1111/j.1365-3091.2010.01176.x

Goodbred, S.L., Saito, Y., 2012. Tide-Dominated Deltas, in: Davis, R.A., Dalrymple, R.W. (Eds.), Principles of Tidal Sedimentology. pp. 1–621. https://doi.org/10.1007/978-94-007-0123-6

Hoitink, A.J.F.F., Wang, Z.B., Vermeulen, B., Huismans, Y., Kästner, K., 2017. Tidal controls on river delta morphology. Nat. Geosci. 10, 637–645. https://doi.org/10.1038/ngeo3000

Hooke, J.M., 1984. Changes in river meanders: a review of techniques and results of analyses. Prog. Phys. Geogr. 8, 473–508. https://doi.org/10.1177/030913338400800401

Hughes, Z.J., 2012. Tidal Channles on Tidal Flats and Marshes, in: Davis, R.A., Dalrymple, R.W. (Eds.), Principles of Tidal Sedimentology. Springer, pp. 269–300. https://doi.org/10.1007/978-94-007-0123-6_11

Hughes, Z.J., FitzGerald, D.M., Wilson, C.A., Pennings, S.C., Wiçski, K., Mahadevan, A., 2009. Rapid headward erosion of marsh creeks in response to relative sea level rise. Geophys. Res. Lett. 36, 1–5. https://doi.org/10.1029/2008GL036000

Jones, L.S., Harper, J.T., 1998. Channel avulsions and related processes, and large-scale sedimentation patterns since 1875, Rio Grande, San Luis Valley, Colorado. Bull. Geol. Soc. Am. 110, 411–421. https://doi.org/10.1130/0016-7606(1998)110<0411:CAARPA>2.3.CO;2

Kearney, W.S., Fagherazzi, S., 2016. Salt marsh vegetation promotes efficient tidal channel networks. Nat. Commun. 7, 1–7. https://doi.org/10.1038/ncomms12287

Kirwan, M.L., Murray, A.B., 2007. A coupled geomorphic and ecological model of tidal marsh evolution. Proc. Natl. Acad. Sci. U. S. A. 104, 6118–6122. https://doi.org/10.1073/pnas.0700958104

Kleinhans, M.G., Schuurman, F., Bakx, W., Markies, H., 2009. Meandering channel dynamics in highly cohesive sediment on an intertidal mud flat in the Westerschelde estuary, the Netherlands. Geomorphology 105, 261–276. https://doi.org/10.1016/j.geomorph.2008.10.005

Lanzoni, S., D'Alpaos, A., 2015. On funneling of tidal channels. J. Geophys. Res. Earth Surf. 120, 433–452. https://doi.org/10.1002/2014JF003203

Lentsch, N., Finotello, A., Paola, C., 2018. Reduction of deltaic channel mobility by tidal action under rising relative sea level. Geology 46, 599–602. https://doi.org/10.1130/G45087.1

Letzsch, W.S., Frey, R.W., 1980. Deposition and erosion in a Holocene salt marsh, Sapelo Island, Georgia. J. Sediment. Petrol. 50, 529–542. https://doi.org/10.1306/212F7A45-2B24-11D7-8648000102C1865D

Litwin, R.J., Smoot, J.P., Pavich, M.J., Oberg, E., Steury, B., Helwig, B., Markewich, H.W., Santucci, V.L., Sanders, G., 2013. Rates and probable causes of freshwater tidal marsh failure, Potomac River estuary, Northern Virginia, USA. Wetlands 33, 1037–1061. https://doi.org/10.1007/s13157-013-0461-6

Marani, M., Belluco, E., D'Alpaos, A., Defina, A., Lanzoni, S., Rinaldo, A., 2003. On the drainage density of tidal networks. Water Resour. Res. 39, 1–11. https://doi.org/10.1029/2001WR001051

Martinius, A.W., 2012. Contrasting Styles of Siliciclastic Tidal Deposits in a Developing Thrust-Sheet-Top Basins – The Lower Eocene of the Central Pyrenees (Spain), in: Davis, R.A., Dalrymple, R.W. (Eds.), Principles of Tidal Sedimentology. pp. 1–621. https://doi.org/10.1007/978-94-007-0123-6

Marzo, M., Nijman, W., Puigdefabregas, C., 1988. Architecture of the Castissent fluvial sheet sandstones, Eocene, south Pyrenees, Spain. Sedimentology 35, 719–738.

Missiaen, T., Slob, E., Donselaar, M.E., 2008. Comparing different shallow geophysical methods in a tidal estuary, Verdronken Land van Saeftinge, western Scheldt, the Netherlands. Geol. en Mijnbouw/Netherlands J. Geosci. 87, 151–164. https://doi.org/10.1017/S0016774600023192

Mosley, M.P., 1976. An experimental study of channel confluences. J. Geol. 84, 535–562.

Mudd, S.M., D'Alpaos, A., Morris, J.T., 2010. How does vegetation affect sedimentation on tidal marshes? Investigating particle capture and hydrodynamic controls on biologically mediated sedimentation. J. Geophys. Res. Earth Surf. 115, F03029. https://doi.org/10.1029/2009JF001566

Muñoz, J.A., 1992. Evolution of a continental collision belt: ECORS-Pyrenees crustal balanced cross-section, in: Mc Clay, K. (Ed.), Thrust Tectonics. Springer, pp. 235–246. https://doi.org/10.1007/978-94-011-3066-0

Muñoz, J.A., Beamud, E., Fernández, O., Arbués, P., Dinarès-Turell, J., Poblet, J., 2013. The Ainsa Fold and thrust oblique zone of the central Pyrenees: Kinematics of a curved contractional system from paleomagnetic and structural data. Tectonics 32, 1142–1175. https://doi.org/10.1002/tect.20070

Mutti, E., Séguret, M., Sgavetti, M., 1988. Sedimentation and deformation in the Tertiary Sequences of the Southern Pyrenees: Field trip 7. University of Parma.

Nijman, W., 1998. Cyclicity and basin axis shift in a piggy-back basin - Modelling the Tremp Ager Basin (Eocene) South Pyrenees, in: MASCLE, A., PUIGDEFABREGAS, C., LUTERBACHER, H. P. 8z FERNANDEZ, M. (eds) (Ed.), Cenozoic Foreland Basins of Western Europe. pp. 135–162. https://doi.org/10.3997/2214-4609.201410293

Nijman, W., Nio, S., 1975. The Eocene Montañana delta (Tremp-Graus Basin, provinces of Lerida and Huesca, Southern Pyrenees, N. Spain), in: Rosell, J., Puigdefabregas, C. (Eds.), Sedimentarv Evolution of the Paleogene South Pyrenean Basin, Part B, IAS 9th International Congress. Nice.

Pallard, B., Castellarin, A., Montanari, A., 2009. A look at the links between drainage density and flood statistics. Hydrol. Earth Syst. Sci. 13, 1019–1029. https://doi.org/10.5194/hess-13-1019-2009

Perillo, G.M.E., Iribarne, O.O., 2003a. Processes of tidal channel development in salt and freshwater marshes. Earth Surf. Process. Landforms 28, 1473–1482. https://doi.org/10.1002/esp.1018

Perillo, G.M.E., Iribarne, O.O., 2003b. New mechanisms studied for creek formation in tidal flats: From crabs to tidal channels. Eos (Washington. DC). 84, 1–3. https://doi.org/10.1029/2003EO010001

Puigdefàbregas, C., Muñoz, J.A., Vergés, J., 1992. Thrusting and foreland basin evolution in the Southern Pyrenees, in: Mc Clay, K. (Ed.), Thrust Tectonics. Springer, pp. 247–254. https://doi.org/10.1007/978-94-011-3066-0_22

Rieu, R., van Heteren, S., van der Spek, A.J.F., De Boer, P.L., 2005. Development and preservation of a Mid-Holocene tidal-channel network offshore the Western Netherlands. J. Sediment. Res. 75, 409–419. https://doi.org/10.21110/jsr.2005.032

Rinaldo, A., Fagherazzi, S., Lanzoni, S., Marani, M., Dietrich, W.E., 1999a. Tidal networks 3. Landscape-forming discharges and studies in empirical geomorphic relationships. Water Resour. Res. 35, 3919–3929. https://doi.org/10.1029/1999WR900238

Rinaldo, A., Fagherazzi, S., Lanzoni, S., Marani, M., Dietrich, W.E., 1999b. Tidal networks 2. Watershed

delineation and comparative network morphology. Water Resour. Res. 35, 3905–3917. https://doi.org/10.1029/1999WR900237

Rizzetto, F., Tosi, L., 2012. Rapid response of tidal channel networks to sea-level variations (Venice Lagoon, Italy). Glob. Planet. Change 92–93, 191–197. https://doi.org/10.1016/j.gloplacha.2012.05.022

Ronchi, L., Fontana, A., Correggiari, A., Asioli, A., 2018. Late Quaternary incised and infilled landforms in the shelf of the northern Adriatic Sea (Italy). Mar. Geol. 405, 47–67. https://doi.org/10.1016/j.margeo.2018.08.004

Roner, M., D'Alpaos, A., Ghinassi, M., Marani, M., Silvestri, S., Franceschinis, E., Realdon, N., 2016. Spatial variation of salt-marsh organic and inorganic deposition and organic carbon accumulation: Inferences from the Venice lagoon, Italy. Adv. Water Resour. 93, 276–287.

Rossi, V.M., Kim, W., López, J.L., Edmonds, D., Geleynse, N., Olariu, C., Steel, R.J., Hiatt, M., Passalacqua, P., 2016. Impact of tidal currents on delta-channel deepening, stratigraphic architecture, and sediment bypass beyond the shoreline. Geology 44, 927–930. https://doi.org/10.1130/G38334.1

Schumm, S.A., Erskine, W.D., Tilleard, J.W., 1996. Morphology, hydrology, and evolution of the anastomosing Ovens and King Rivers, Victoria, Australia. Bull. Geol. Soc. Am. 108, 1212–1224. https://doi.org/10.1130/0016-7606(1996)108<1212:MHAEOT>2.3.CO;2

Silvestri, S., Defina, A., Marani, M., 2005. Tidal regime, salinity and salt marsh plant zonation. Estuar. Coast. Shelf Sci. 62, 119–130. https://doi.org/10.1016/j.ecss.2004.08.010

Sisulak, C.F., Dashtgard, S.E., 2012. Seasonal Controls On the Development And Character of Inclined Heterolithic Stratification In A Tide-Influenced, Fluvially Dominated Channel: Fraser River, Canada. J. Sediment. Res. 82, 244–257. https://doi.org/10.2110/jsr.2012.21

Slingerland, R., Smith, N.D., 1998. Necessary conditions for a meandering-river avulsion. Geology 26, 435–438. https://doi.org/10.1130/0091-7613(1998)026<0435:NCFAMR>2.3.CO

Solari, L., Seminara, G., Lanzoni, S., Marani, M., Rinaldo, A., 2002. Sand bars in tidal channels Part 2. Tidal meanders. J. Fluid Mech. 451, 203–238. https://doi.org/10.1017/S0022112001006565

Soto, R., Casas, A.M., Storti, F., Faccenna, C., 2002. Role of lateral thickness variations on the development of oblique structures at the Western end of the South Pyrenean Central Unit. Tectonophysics 350, 215–235. https://doi.org/10.1016/S0040-1951(02)00116-6

Stefanon, L., Carniello, L., D'Alpaos, A., Lanzoni, S., 2010. Experimental analysis of tidal network growth and development. Cont. Shelf Res. 30, 950–962. https://doi.org/10.1016/j.csr.2009.08.018

Stefanon, L., Carniello, L., D'Alpaos, A., Rinaldo, A., 2012. Signatures of sea level changes on tidal geomorphology: Experiments on network incision and retreat. Geophys. Res. Lett. 39, 1–6. https://doi.org/10.1029/2012GL051953

Storms, J.E.A., Weltje, G.J., Terra, G.J., Cattaneo, A., Trincardi, F., 2008. Coastal dynamics under conditions of rapid sea-level rise: Late Pleistocene to Early Holocene evolution of barrier–lagoon systems on the northern Adriatic shelf (Italy). Quat. Sci. Rev. 27, 1107–1123. Terwindt, J.H.J., 1988. Palaeotidal reconstructions of inshore tidal depositional environments, in: De Boer, P.L., van Gelder, A., Nio, S.-D. (Eds.), Tide-Influenced Sedimentary Environments. pp. 233–263.

Thomas, R.G., Smith, D.G., Wood, J.M., Visser, M.J., Calverley-Range, E.A., Koster, E.H., Visser, J., Calverley-Range, E.A., Koster, E.H., 1987. Inclined heterolithic stratification - terminology, description, interpretation and significance. Sediment. Geol. 53, 123–179. https://doi.org/10.1016/S0037-0738(87)80006-4

Tommasini, L., Carniello, L., Ghinassi, M., Roner, M., D'Alpaos, A., 2019. Changes in the wind-wave field and related salt-marsh lateral erosion: inferences from the evolution of the Venice Lagoon in the last four centuries. Earth Surf. Process. Landforms. https://doi.org/10.1002/esp.4599

Toonen, W.H.J.J., Kleinhans, M.G., Cohen, K.M., 2012. Sedimentary architecture of abandoned channel fills. Earth Surf. Process. Landforms 37, 459–472. https://doi.org/10.1002/esp.3189

Trigg, M.A., Bates, P.D., Wilson, M.D., Schumann, G., Baugh, C., 2012. Floodplain channel morphology and networks of the middle Amazon River. Water Resour. Res. 48, 1–17. https://doi.org/10.1029/2012WR011888

Trincardi, F., Correggiari, A., Roveri, M., 1994. Late Quaternary transgressive erosion and deposition in a modern epicontinental shelf: The Adriatic semienclosed basin. Geo-Marine Lett. 14, 41–51. https://doi.org/10.1007/BF01204470

van den Berg, J.H., Boersma, J.R., van Gelder, A., 2007. Diagnostic sedimentary structures of the fluvial-tidal transition zone—evidence from deposits of the Rhine and Meuse. Netherlands J. Geosci. 86, 287–306.

Van Der Meulen, S., 1983. Internal structure and environmental reconstruction of eocene transitional fan-delta deposits, monllobat-castigaleu formations, Southern Pyrenees, Spain. Sediment. Geol. 37, 85–112.

van Maanen, B., Coco, G., Bryan, K.R., 2015. On the ecogeomorphological feedbacks that control tidal channel network evolution in a sandy mangrove setting. Proc. R. Soc. A Math. Phys. Eng. Sci. 471, 20150115. https://doi.org/10.1098/rspa.2015.0115

Vandenbruwaene, W., Meire, P., Temmerman, S., 2012. Formation and evolution of a tidal channel network within a constructed tidal marsh. Geomorphology 151–152, 114–125. https://doi.org/10.1016/j.geomorph.2012.01.022

Vergés, J., 2003. Evolución de los sistemas de rampas oblicuas de los Pirineos meridionales: fallas del Segre y Pamplona. Bol. Geol. Min 114, 87–101.

Vlaswinkel, B.M., Cantelli, A., 2011. Geometric characteristics and evolution of a tidal channel network in experimental setting. Earth Surf. Process. Landforms 36, 739–752. https://doi.org/10.1002/esp.2099

Willis, B.J., Tang, H., 2010. Three-Dimensional Connectivity of Point-Bar Deposits. J. Sediment. Res. 80, 440–454. https://doi.org/10.2110/jsr.2010.046

Zecchin, M., Baradello, L., Brancolini, G., Donda, F., Rizzetto, F., Tosi, L., 2008. Sequence stratigraphy based on high-resolution seismic profiles in the late Pleistocene and Holocene deposits of the Venice area. Mar. Geol. 253, 185–198. https://doi.org/http://dx.doi.org/10.1016/j.margeo.2008.05.010

Zecchin, M., Tosi, L., Caffau, M., Baradello, L., Donnici, S., 2014. Sequence stratigraphic significance of tidal channel systems in a shallow lagoon (Venice, Italy). The Holocene 24, 646–658.

CHAPTER 6

CONCLUSIONS

Using a multidisciplinary approach, that couples remote sensing, sedimentological and forward stratigraphic modelling analysis, the present study focused on the sedimentology of tidal point-bars and addresses four main topics: i) the influence of vertical aggradation and substrate compaction in shaping bar geometries; ii) the reconstruction of three-dimensional architecture of point bars developed under different aggradational conditions and planform transformation styles; iii) the relationship between mechanism of bar growth and the internal sedimentary facies distribution; and iv) the analysis of piracy-controlled geometries of point bar bodies.

The main results derived from this research can be summarized as follows:

I.   Geometry of tidal point bars evolving under the effects of aggradational marshes and substrate compaction is shaped by the interaction between the rate of lateral shifting of the channel, and rate of vertical aggradation of the overbank areas. In axial cross sections, these geometries are captured by the trajectories of the bar brink and channel thalweg.

II. Three dimensional geometries of tidal point bars are strongly influenced by: i) the interaction between lateral and vertical shift of the channel; and ii) different styles of planform transformations. Geometries and stratal architecture of the point bars developing under these conditions can strongly differ from those predicted for classical laterally accreted bars.

III.   Tidal bends can expand and increase their sinuosity alternating storage of sediments along the seaward and landward side of the related point bar. Within this frame, the development of superimposed ebb and flood recirculation zones allows the bend apex zone to be the area of maximum accretion, where tidal signature is better preserved and the maximum amount of mud accumulates.

IV.   The high drainage of tidal networks prevents tidal bends from freely meandering without interacting with adjacent channels and triggering piracy processes. Piracy hinders lateral migration of tidal channels and prevents the development of laterally-extensive point bar bodies, leading to frequent formation of immature point bars, which are characterized by a low width:thickness ratio.